NOTICE

The quality of this microform is heavily dependent upon the quality of the original thesis submitted for microfilming. Every effort has been made to ensure the highest quality of reproduction possible.

If pages are missing, contact the university which granted the degree.

Some pages may have indistinct print especially if the original pages were typed with a poor typewriter ribbon or if the university sent us an inferior photocopy.

Reproduction in full or in part of this microform is governed by the Canadian Copyright Act, R.S.C. 1970, c. C-30, and subsequent amendments.

AVIS

La qualité de cette microforme dépend grandement de la qualité de la thèse soumise au microfilmage. Nous avons tout fait pour assurer une qualité supérieure de reproduction.

S'il manque des pages, veuillez communiquer avec l'université qui a conféré le grade.

La qualité d'impression de certaines pages peut laisser à désirer, surtout si les pages originales ont été dactylographiées à l'aide d'un ruban usé ou si l'université nous a fait parvenir une photocopie de qualité inférieure.

La reproduction, même partielle, de cette microforme est soumise à la Loi canadienne sur le droit d'auteur, SRC 1970, c. C-30, et ses amendements subséquents.

THE ROLE OF HEAT TRANSFER AND VARYING PHYSICAL PROPERTIES IN THE LAMINAR FLOW TUBULAR REACTOR FOR HOMOGENEOUS LIQUID PHASE REACTIONS: A NUMERICAL STUDY

A THESIS
SUBMITTED TO THE DEPARTMENT OF CHEMICAL ENGINEERING
AND THE SCHOOL OF GRADUATE STUDIES
OF THE UNIVERSITY OF OTTAWA
IN PARTIAL FULFILLMENT OF THE REQUIREMENTS
FOR THE DEGREE OF
DOCTOR OF PHILOSOPHY

By
John S. Hopkins
June 1991

ISBN 0-315-70506-X

UNIVERSITÉ D'OTTAWA
UNIVERSITY OF OTTAWA

Abstract

A numerical model was developed to examine the behaviour of a vertical laminar flow tubular reactor subject to varying physical properties. Analysis of the results of the model using factorial design techniques indicated that the characteristics of the reactor were closely tied to the heat transfer occurring in the reactor.

Three regimes of heat transfer behaviour were identified. These three regimes were instrumental in the effect that varying physical properties had upon reactor performance. In the high heat transfer regime it was found that varying properties were only important when there were appreciable changes in the thermal conductivity and density due to changes in composition. The medium heat transfer regime gave similar results; however, under some conditions changes in heat capacity were found to be significant. In the low heat transfer regime physical property variations had the largest effect. Under these conditions temperature dependent properties were capable of affecting reactor performance when large temperature rises occurred. Concentration dependence was also significant. With respect to concentration dependence of the physical properties, density and heat capacity variations were found to be the most significant in this regime.

An experimental program was carried out to verify the more obvious effects determined in the theoretical program. Although the experimental results could not completely be modelled through the developed numerical model, some of the major findings of the numerical study were verified. In the experimental investigation the reaction was carried out in an adiabatic reactor. Some of the differences between theoretical and experimental conversions were directly attributable to the sensitivity of the system to the dimensionless heat of reaction and to free convection. To a

smaller extent the effect of a varying heat capacity was observed.

The correspondence between numerical and experimental results could be improved if the following modifications were made:

1. Modify the numerical model to allow for the possibility of negative or stagnant flows.

2. In conjunction with the above recommendation the range of values for the buoyancy term that are solvable by the numerical model should be increased. Convergence difficulties were encountered for larger values of β_{ij}. These were quite likely due to the manner in which the system pressure was solved. A different formulation of the momentum equation may be necessary.

3. Investigate a reaction in which all of the pertinent information regarding the kinetics and physical property data are readily available. Some of the error between the numerical and experimental results could be attributed to the contradictory literature on the hydrolysis of acetic anhydride. The experimental results also indicated that the heat of reaction, heat capacity and density should be as accurate as possible.

Acknowledgements

The author wishes to express his gratitude to NSERC for the one year of support that they provided. A similar expression of gratitude is extended to the University of Ottawa. Thanks also are extended to the departmental chairmen who gave me extra marking assignments to supplement my income when times were bad. Special thanks are given to Professor J. A. Golding for his unbounded understanding, compassion, and sympathy. Of course no work whatsoever could be performed at all without the superb talents of our technical staff, particularly Joe Gasparetti and Louis Tremblay.

Thanks to my family for making me stick with it. Particular thanks are extended to my brother Donald and his wife Michelle for allowing me into their home to use their computer. I don't know what else I could have done to perform the numerical aspects of this study.

The most important person in this endeavor was my wife, Carol. Her courage through this project was the glue that held everything together through some difficult times. I'll love you always, Precious.

Contents

List of Tables

List of Figures

Nomenclature

a	Reactor aspect ratio, R/L, dimensionless
A	Frequency factor, s^{-1} (for a first order reaction)
$\mathbf{A}_y$	Banded matrix generated by finite difference equations, dimensionless
Bi	Biot Number, $h_c R/k_{c_o}$, dimensionless
c_A	Concentration of acetic anhydride, mol/cm^3
c_B	Concentration of water, mol/cm^3
c_C	Concentration of acetic acid, mol/cm^3
c_i	Concentration of component i, mol/m^3
$\hat{C}_p$	Constant pressure heat capacity, J/kgK
$\hat{C}'_p$	Dimensionless heat capacity, $\hat{C}_p/\hat{C}_{p_o}$
$\mathcal{D}$	Diffusivity, m^2/s
D_{ij}	Multicomponent diffusivity of the pair i, j, m^2/s
E	Activation energy, J/mol
f_y	Dimensionless function of physical property derivatives
$F_{\nu_1,\nu 2}$	Value of F distribution with ν_1 and ν_2 degrees of freedom
$\mathbf{g}$	Gravitational acceleration vector, m/s^2
$\bar{G}_j$	partial molal Gibbs free energy for component j, J/mol
g_y	Dimensionless function of physical property derivatives
g_z	Gravitational acceleration in z direction, m/s^2
$\bar{H}_i$	Partial molal enthalpy of component i, J/mol
ΔH_r	Heat of reaction, J/mol
h_c	Outside heat transfer coefficient, J/m^2sK
$\mathbf{j}_i$	Mass flux vector for component i, kg/m^2s

j_i, Mass flux of component i in the radial direction, kg/m^2s

$\mathbf{J}_i$ Molar flux vector of component i, mol/m^2s

J_i, Molar flux of component i in the radial direction, mol/m^2s

k_1 Activation energy for acetic anhydride hydrolysis model, $cm^3/(mol\ acetic\ acid)(s)$

k_2 Correction of activation energy in acetic anhydride hydrolysis model due to presence of acetic anhydride, $(cm^3)^2/(mol\ acetic\ acid)(mol\ acetic\ anhydride)(s)$

k_3 E/R_g in acetic anhydride hydrolysis model, K

k_4 Correction in E/R_g due to presence of acetic anhydride, $Kcm^3/mol\ acetic\ acid$

k_5 Reaction order of acetic acid in acetic anhydride hydrolysis model, dimensionless

k_c Thermal conductivity, W/mK

k_c' Dimensionless thermal conductivity, k_c/k_{c_o}

k_m Rate constant for mechanism proposed by Rao et. al., $(cm^3)^{1.7}/(mol)^{1.7}(min)$

k_R First order reaction rate constant, s^{-1}

k_R' Reduced rate constant, $k_m c_{C_o}$, $cm^3/(mol)(min)$

L Reactor length, m

M_i Molecular weight of component i, $kg/kgmol$

N Number of interior grid points in the finite difference method

N_{i_r} Molar flux of component i in the radial direction, mol/m^2s

p Pressure, Pa

p' Dimensionless pressure drop, $(p-p_o)k_{R_o}R^2/4\langle v_z\rangle_o^2\mu_o$

P' Dimensionless pressure, $(pR^2)/(2\langle v_z\rangle_o\mu_o L)$

$\mathbf{q}$ Heat flux vector, J/m^2s

Q Ratio used to determine quantitative lack of fit, dimensionless

r radius, m

r_i Mass rate of reaction of component i, kg/m^3s

r'	Dimensionless radius, r/R
R	Reactor radius, m
R_g	Gas constant, $J/mol\ K$
R_i	Molar rate of reaction of component i, $mol/m^3 s$
$\mathbf{R_y}$	Matrix of nonlinear generation terms, dimensionless
R_y	Dimensionless general generation term
R^2	Coefficient of determination
Re	Reynolds number, $(2R\langle v_z\rangle_o \rho_o)/\mu_o$, dimensionless
t	Time, s
t_o	Residence time of reactor centerline, s
T	Temperature, K
U	Dimensionless axial velocity, $v_z/2\langle v_z\rangle_o$
$\mathbf{U}$	Diagonal matrix composed of system axial velocities
$\mathbf{v}$	Velocity vector, m/s
v_r	Radial velocity component, m/s
v_z	Axial velocity component, m/s
$\hat{V}$	Volume per unit mass, m^3/kg
V^*	Dimensionless radial velocity, $(v_r L)/(2\langle v_z\rangle_o R)$
V	Dimensionless radial velocity, v_r/Rk_{R_o}
w_i	Mass fraction of component i
w_j	Weighting factor for point j in Simpson's and Trapezoidal Rules
x_i	Dimensionless concentration of component i, c_i/c_{i_o}
x_j	Mole fraction of component j
y	Ratio of variable property concentration to constant property concentration, $\langle x\rangle_{nc}/.1$
$\mathbf{y}$	Vector of system state variables
z	Axial distance, m
z^*	Normalized reactor length, z/L, dimensionless
z'	Dimensionless axial distance, $k_{R_o} z/2\langle v_z\rangle_o$

Greek Letters

α_T	Dimensionless radial heat dispersion term, $k_{r_o}/R^2\rho_o\hat{C}_{P_o}k_{R_o}$
α_x	Dimensionless radial mass dispersion term, $\mathcal{D}_{im_o}/R^2k_{R_o}$
α_y	General dimensionless radial dispersion term for variable y
$\hat{\beta}_i$	Estimates of regression coefficients
β_T	Dimensionless heat of reaction, $-\Delta H_R c_{i_o}/\rho_o C_{p_o} T_o$
β_U	Dimensionless buoyancy term, $\pm\rho_o g_z R^2/2\langle v_z\rangle_o\mu_o$
β_y	General dimensionless generation term for variable y
γ	Dimensionless activation energy, E/R_gT_o
ϵ_y	General dimensionless constant for component y
θ	Dimensionless temperature, $(T-T_o)/T_o$
μ	Viscosity, $Pa\cdot s$
μ'	Dimensionless viscosity, μ/μ_o
$\nu_{1,2}$	Degrees of freedom
ρ	Density, kg/m^3
ρ_i	Mass concentration of component i, kg/m^3
ρ'	Dimensionless density, ρ/ρ_o
$\hat{\sigma}$	Estimate of variance
τ	Viscous stress tensor, N/m^2
τ_{rz}	Shear stress exerted in the z-direction on a fluid surface of constant r by the fluid in the region of lesser r, N/m^2

Operators, Superscripts, Subscripts

$\langle\ \rangle$	Cup-mixed or average
∇	Gradient operator
$'$	Dimensionless quantity
$\hat{}$	Per unit mass or estimated value
cal	Calculated from numerical model
E	Effective value
exp	Experimental value
n	Reaction order
$n.c.$	Non-constant
i	Component i
j	Component j
j	Jacket
o	Initial value
r	Radial direction
T	Energy balance parameter
U	Momentum balance parameter
x	Species balance parameter
y	Arbitrary state variable parameter
z	Axial direction

Chapter 1

Introduction

In the field of chemical engineering the mass, energy and momentum balance equations are widely employed to model processes. Depending upon the goal of a particular application, the use of these equations may lead to simple or extremely difficult formulations. The degree of complexity employed is determined by the type of problem to be solved and the assumptions used to set up the problem.

The microscopic equations of change have often been used to model tubular flow reactors. Initially, if the reactor under study was assumed to be operating under isothermal, plug flow conditions the mass balance could be reduced to a single ordinary differential equation which could be solved analytically.

Unfortunately most problems can rarely be modelled by simple ordinary differential equations. The assumptions used to reduce a system to such a simple set of equations are often in error. More realistically, in the case of a tubular flow reactor, at the very least both mass and energy balances must be considered, and heat transfer with the surroundings may be of importance. In this latter case the radial transfer of heat would require the solution of a partial differential equation. These more complicated systems have to be solved numerically using computers.

With advances in the field of numerical methods the capability to solve more complicated systems exists. In this regard much recent work in the area of laminar flow tubular reactors has centered around the velocity profile distortion caused by large radial viscosity gradients in polymerization reactors. Free convection has

also been considered. Calculation of the velocity profile distortions has required including the momentum balance in the solution of the system. The velocity profile distortions mentioned above were the result of changes in physical properties within the reactor. To date the inclusion of variable viscosity in polymerization systems and variable density in free convection have been the only varying properties studied in detail. In this study heat capacity and thermal conductivity have also been included in the analysis.

The primary goal of this study was to determine the circumstances under which the inclusion of variable physical properties in a laminar flow reactor model would be appropriate. The analysis was applied to a homogeneous liquid system in a vertical flow reactor. This was accomplished through the use of a rigorous numerical model. In order to examine the effect that variable physical properties had upon reactor performance a theoretical study was undertaken. Both temperature dependent and composition dependent physical properties were considered. The influence of heat transfer with the surroundings using a wall heat transfer boundary condition was also investigated.

The results of the numerical study were compared with the data of previous studies reported in the literature. In these studies physical properties were essentially constant since very dilute solutions were employed. Laboratory experiments were carried out in this study under conditions where physical properties could be expected to vary significantly.

Chapter 2

Literature Review

2.1 Introduction

Models describing laminar flow tubular reactors have evolved through the years from the simple study of an isothermal reaction to more complex cases of non-isothermal reactors. It has been recognized that the presence of the laminar velocity profile and subsequent residence time distribution within the reactor may result in complex radial concentration and temperature profiles. Different types of behaviour are possible when laminar flow is accompanied by reaction. Of particular interest has been the distortion experienced by the velocity profile due to free convection and viscosity changes in the reactor fluid. These velocity profile distortions are known to affect the degree of conversion in the reactor. Through the years, with the growing capabilities of computers and numerical methods, more rigorous models have been developed to take into account these velocity profile distortions.

For the most part, the study of laminar flow reactors has involved the study of relatively simple chemical systems. Sophistication has come about through the addition of the energy balance and, subsequently, consideration of the momentum balance. Much of the work has concentrated upon the solution of the pertinent partial differential equations considering only the temperature dependence of the viscosity and density. An area of special interest to polymer scientists has been the potential for highly distorted velocity profiles to occur in polymerizing systems due

to the large differences in viscosity between monomer and polymer solutions.

Another aspect of the problem that has acquired special consideration has been the adaptation of the isothermal situation to the axial dispersion model often employed in plug flow reactor studies. Numerous papers have been written on this approach to the problem. Although this particular technique has been shown to be useful for isothermal reactors, extension of the method to a non-isothermal reactor would be difficult since the temperature profile and concentration profiles interact in a complex manner. Much of the foundation upon which the axial dispersion model has been based would not apply to the non-isothermal reactor because of the extra complexity.

2.2 General Studies of Laminar Flow Reactor Systems

Bosworth [1] and Denbigh [2] examined the effect that residence time distribution had upon conversions for a first and second order reaction respectively. Through simplifying assumptions, the reactors under study were described by differential equations having analytical solutions. These analyses were performed primarily to compare the conversions in a laminar flow reactor with those in a plug flow reactor. Radial composition effects were not considered by Denbigh, but Bosworth attempted to establish the significance of radial diffusion upon the conversion. By calculating the deviation in the concentration profile from that due to residence time effects alone, he concluded that radial diffusion was significant only if:

$$\mathcal{D}_{im} t_o / R^2 \geq 3.1 \times 10^{-3} \tag{2.1}$$

where

$\mathcal{D}_{im}$ = mixture diffusivity of component i, m^2/s

t_o = residence time of the reactor centerline, s

R = reactor radius, m

Lauwerier [3] derived an expression for determining the radial and axial concentration profiles for a first order isothermal reaction. By incorporating a parabolic velocity profile within the species continuity equation, a series solution was obtained that involved calculation of a set of eigenvalues and the corresponding eigenfunctions. However, near the entrance of the reactor, a large number of terms was required. As a result, application of the solution was difficult.

Cleland and Wilhelm [4] were the first researchers to employ a digital computer to assist in carrying out their calculations. Both theoretical and experimental studies were performed. In the theoretical work, an isothermal first order reaction with constant physical properties and fully developed laminar flow was studied. Radial diffusion was included. Analytical solutions for the limiting cases of no radial diffusion and infinite radial diffusion (which was identical to a plug flow solution) were presented. Dimensionless parameters were incorporated into the resultant species continuity equation. Axial concentration profiles were presented in graphical form for differing values of the parameter characterizing radial diffusion. In an analysis similar to that of Bosworth, Cleland and Wilhelm determined that radial diffusion could be neglected if:

$$\mathcal{D}_{im} t_o / R^2 \leq 1.95 \times 10^{-3} \tag{2.2}$$

The above criterion was determined by assuming that radial diffusion could be neglected when its effect upon the conversion was less than one percent.

The theoretical work was compared with experimental data for the hydrolysis of acetic anhydride. Deviations between the theoretical and experimental studies were attributed to heat generated during the reaction and free convection caused by radial concentration and temperature gradients. An effective diffusivity rather than the true molecular diffusivity was used to predict the experimental values using the numerical model. The effective diffusivity was a function of both temperature changes in the reactor and free convection. Rather than including these effects in a more complete model, Cleland and Wilhelm concluded that replacing the molecular diffusivity with an effective diffusivity was sufficient for describing the system.

A theoretical and experimental study of a second order isothermal reaction was

performed by Vignes and Trambouze [5]. A theoretical model similar to that presented by Cleland and Wilhelm was derived. The species continuity equation was suitably changed to reflect second order rather than first order kinetics. The system studied was the saponification of ethyl acetate. In the subsequent comparisons of theoretical and experimental results, a mixture diffusivity, defined as the arithmetical average of the diffusivities of sodium hydroxide and ethyl acetate, was employed. It was found that the experimental results could adequately be described if an effective diffusivity ten times greater than the mixture diffusivity was employed in the theoretical model.

By transforming the species continuity equation into a form represented by the extent of reaction and employing a general enthalpy balance, Chambré [6] derived a general analytical solution for a non-isothermal laminar flow reactor. Again, physical properties were assumed to be constant. The Lewis number, a dimensionless number reflecting the ratio of mass to heat diffusivities, was set to 1 for the derivation. A perturbation technique was used to solve the mass and energy equations. Due to the high Lewis number involved, the results and conclusions were most applicable to a gas phase reactor.

Trombetta and Happel [7] studied hydrocarbon pyrolysis. They used a Polhausen technique to solve numerically the momentum, energy, and species conservation equations. A first order gas phase reaction for which the ideal gas law was applicable was tested. The usual balance equations were integrated in the radial direction to obtain ordinary differential equations in the axial direction. Incorporation of polynomial trial functions for the state variables simplified the equations. Multi-component diffusion was considered in the analysis and later compared to a simpler binary diffusion analog. The simplified binary system yielded results similar to the multi-component system. Results were presented graphically in the form of correction factors (i.e. the length of the reactor needed for laminar flow divided by the length needed for a plug flow reactor to obtain the same conversion). The results were compared with the theoretical data of Cleland and Wilhelm. Agreement was good for Damköhler numbers ($k_R R^2/\mathcal{D}_{AB}$) less than 10.

Rothenberg and Smith [8,9] studied the enhancement of wall heat transfer caused

by the diffusion of the reacting species in a non-isothermal reactor. Because they assumed stoichiometric diffusion, the influence of molecular diffusion did not appear explicitly in the energy conservation equation. Incorporation of a diffusional term within a Nusselt number illustrated the presence of a heat transfer enhancement. Both an irreversible first order [8] and an equilibrium dissociation reaction [9] were studied. Both reactions were run at high Lewis numbers, suggesting that the results were again primarily applicable to gas phase reactions. One set of radial concentration profiles was presented for a Lewis number (10^{-3}) approaching a value that could be expected for a liquid phase reaction. Comparison of these profiles with those at higher Lewis numbers clearly indicated that concentration gradients near the wall were larger at low Lewis numbers. This suggested that heat transfer enhancement at the wall could occur in reacting liquid systems. Rothenberg and Smith demonstrated that, for a non-isothermal reaction, the criteria determined by Bosworth and by Cleland and Wilhelm were not necessarily applicable. The interdependence of the concentration and temperature profiles illustrated the complex roles of all of the terms appearing in the conservation equations.

Andersen and Coull [10] compared the solutions of Rothenberg and Smith and of Trombetta and Happel. Equimolar counter-diffusion was assumed which eliminated the radial velocity included earlier by Trombetta and Happel. A temperature dependent diffusion coefficient was included along with a temperature dependent molar density derived from the ideal gas law. The equations derived by Rothenberg and Smith were limited to systems in which the number of moles did not change during the reaction. Andersen and Coull extended the work of Rothenberg and Smith to examine a change in the number of moles. The equations were solved for a gas phase reaction and were compared with the results of Rothenberg and Smith. The temperature dependent diffusivity and molar densities did not significantly affect the results. Calculated correction factors agreed favorably with those reported by Trombetta and Happel. Radial profiles calculated by the two methods were compared. Although the approach taken by Trombetta and Happel accurately predicted the axial profiles, it was found that the approximations that were employed did not adequately describe the radial profiles.

Merrill and Hamrin [11] studied the demethylation of toluene as an example of a complex reaction. The reaction rate was first order with respect to toluene and half order with respect to H_2. Temperature dependent viscosity, diffusivity and heat of reaction were included. Comparisons were made among different types of reactor models. It was concluded that for this particular reaction, an adiabatic plug flow reactor would provide the best performance followed by adiabatic or constant wall temperature in laminar flow, and constant wall temperature in plug flow. The least desirable was isothermal laminar flow.

Shinohara [12] studied the saponification of ethyl acetate in both a theoretical and experimental analysis of a laminar flow tubular reactor. Of primary interest was the effect that the hydrodynamic properties would have upon conversion. Among the subjects studied were free convection, the effect of flow index in a power law fluid, and a developing velocity profile at the reactor entrance. Constant wall temperature was employed throughout the work. The viscosity and diffusivity were assumed to be temperature dependent. Heating and cooling at the wall in both downward and upward flow were considered. In the theoretical results the heat of reaction was found to have considerable influence; however, the experimental work was performed at such low concentrations there was minimal influence of the heat of reaction (i.e. the dimensionless heat of reaction term was too small). Since the reaction rate expression depended on both sodium hydroxide and ethyl acetate concentrations, a species continuity equation was solved for both components. Different diffusivities were used for the two reactants. Stoichiometric diffusion was not assumed, which necessitated the inclusion of a radial velocity in the model. However, although the radial velocity was included in the analysis, its influence upon the results was not discussed.

In his theoretical work, Shinohara determined that, for an exothermic reaction, free convection in an upward flow reactor decreased conversion. Increased conversion was observed in a downward flow reactor. The opposite effects were found to hold for endothermic reactions. The temperature dependence of viscosity decreased conversion in exothermic reactions but, as the flow index of a power law fluid was increased, the magnitude of this effect was observed to decrease. Inclusion of a

developing velocity profile at the entrance of the reactor increased the conversion. In the case of developing flow at the inlet, the system was initially operating under plug flow. A greater level of conversion could be expected to occur near the entrance of the reactor because of the uniform radial mixing inherent in plug flow.

Santarelli and Foraboschi [13] studied the effect of free convection upon the conversion in an analysis similar to that of Shinohara. The effect of the concentration gradient on free convection was included in the developed equations although not exploited in the ensuing study. Essentially the same conclusions that were made by Shinohara were made by the above researchers.

Gray and Kostin [14] also studied free convection in a vertical flow reactor. The purpose of their work was to compare two methods of representing the momentum balance equation. The first method considered the use of the stream function. It was assumed that this representation was rigorous enough to yield the exact solution. In the second method, a simplified momentum equation was employed. The assumptions employed in the simplified equation included a negligible radial pressure gradient, and negligible inertial terms. Comparisons of the two methods indicated that the simplified momentum balance yielded results comparable to the more rigorous method.

Golding *et al* [15,16,17,18,19] have performed experimental and theoretical work on a homogeneous liquid reaction: the hydrolysis of acetic anhydride. Heat transfer at the wall was considered but primarily an adiabatic reactor was investigated. In one instance, the possibility of natural convection heat transfer at the wall was considered to explain differences between experimental and theoretical results in the reactor [19]. In the experimental work, radial temperature profiles within the reactor were measured by the use of thermocouples attached to traversing mechanisms. For the most part, the experimental and theoretical temperature profiles had similar characteristics although the numerical values differed.

Lin [20] examined the effect of a temperature dependent viscosity for a power law fluid and n^{th} order kinetics in a laminar flow reactor. The theoretical species and energy balance equations were solved numerically. The results showed that conversion for a given set of circumstances was affected by the flow index of the

fluid and the order of the reaction. The theoretical conversion decreased with an increase in the flow index. The temperature dependence of viscosity was also shown to affect conversion. In these cases, a velocity profile different from the typical parabolic profile associated with the laminar flow of a Newtonian fluid was shown to yield different conversions.

Houzelot and Villermaux [21] investigated an annular reactor in which a catalytic heterogeneous reaction occurred at either the inside, outside or both walls. An isothermal reaction was investigated. It was found that the annular reactors were more efficient than the simple tubular reactor. The efficiency criterion was based on the equivalent reactor lengths needed to provide a given conversion.

Chang and Chern [22] performed a theoretical study of an isothermal tubular reactor in non-Newtonian flow (power law) with arbitrary order heterogeneous and homogeneous reactions occurring. The heterogeneous cases were examples of catalysis occurring at the wall. It was found that, upon increasing the flow index, the reactant wall concentration increased while the bulk reactant concentration decreased.

To summarize, a number of different aspects of the laminar flow reactor have been examined. Most of the studies have emphasized the modelling of the reactor based on the underlying balance equations. The experimental work has not entirely been reconciled with the theoretical models. Much of the differences could be attributed to the overall complexity of the system. Compromises in the representation of some of the properties of the system, particularly diffusion, have sometimes been used to yield better correspondence between the numerical and experimental results. In the limited experimental work that has been performed to date, the concentrations of reactants have been low enough that the assumption of temperature dependent properties only has been valid. It seems to have been overlooked however, that these concentrations have been so low that very little heat was generated so that the inclusion of these effects was trivial. Although in some instances the temperature dependence of physical properties has been used to explain the deviation between experimental and theoretical results, it was more likely that other factors were creating these deviations. One of the greatest areas of uncertainty could be the

calculation of the initial values of the properties in a liquid mixture and establishing the kinetics of the reaction. The properties of liquid mixtures have been difficult to estimate accurately. With higher concentrations of given species, the estimation of these properties has become more difficult. Coupled with this problem has been the difficulty in adequately establishing the kinetics of some of the reactions that have been employed in laminar flow reactor studies. These reactions have been found to be very sensitive to the medium in which they occur.

2.3 Polymerization and Laminar Flow

Of particular interest are polymerization reactions taking place and these have been studied extensively. The viscous nature of polymer solutions has led to the use of the laminar flow conditions in polymerization models for many systems. A unique feature of polymerization systems is the potential for the creation of extremely high radial viscosity gradients due to the large difference between monomer and polymer viscosities. These large gradients can result in highly distorted velocity profiles [23,24,25,26,27,28,29,30].

Cintron-Cordero *et al* [31] recognized that the laminar flow in a polymerization reactor could create a molecular weight distribution across the radius of the reactor. They also surmised that the non-uniform temperature profiles within the reactor could contribute to the polydispersity. Primarily, the type of polymerization mechanism was found to play a role. Condensation reactions were influenced by both the residence time distribution and the thermal gradients. Molecular weight distributions in a chain polymerization were determined by the thermal gradients. Of interest was the effect of flow index in a power law fluid model. An interesting result, based upon theory and substantiated by their model, was that in an isothermal reactor the molecular weight dispersion for condensation polymerization was not as great as was encountered in a stirred tank reactor undergoing non-ideal mixing.

Wallis *et al* [32,33] examined the feasibility of performing a bulk styrene polymerization in a tubular reactor. A reasonably complex reaction mechanism was

employed and a parabolic velocity profile was assumed in their reactor model. Surprisingly good agreement was attained between the model conversions and molecular weight distributions and those found experimentally, despite the lack of a varying viscosity in the model. Comparisons between a laminar flow model and plug flow model demonstrated that the laminar flow model gave better results.

Lynn and Huff [23] derived a numerical model for studying a polymerization reaction in a tubular reactor. The main purpose of the work was to evaluate the effect of variable viscosity upon the reaction. Newtonian flow was assumed and the viscosity was represented by a complex function of both temperature and degree of polymerization. The resultant velocity, temperature, and concentration profiles were highly distorted. As a result of the distortions, a large variation in the number average molecular weight was predicted from the model. This was consistent with observations made from experimental studies. The numerical model was also employed to examine different strategies to narrow the molecular weight distribution.

In a study similar to that of Wallis *et al*, Baillagou and Soong [27,28] studied methylmethacrylate polymerization in a tubular reactor. They suggested that the agreement found by Wallis *et al* with their simple model may have been a result of not allowing the reaction to reach steady state. Much theoretical evidence has shown that the large viscosity gradients experienced in the tubular polymerization reactor can have a great influence upon conversion and molecular weight dispersion. In the study, it was found that by operating a tubular reactor above the glass transition temperature, many of the problems associated with the viscosity gradients could be avoided. At higher temperatures the product molecular weight was smaller than that for colder reactors.

Most of the previously mentioned polymerization studies have included a velocity profile distortion in their analyses. Because the viscosity of polymer solutions could change by several orders of magnitude with conversion, the degree of axial velocity profile distortion was large. The presence and importance of a radial velocity has only recently been considered in these systems [29,30]. McLaughlin *et al.* [29] demonstrated that, although the radial velocity term may not be required

in the momentum equation. exclusion of this term from the heat and mass balances resulted in a 30 percent difference in conversions. Vrentas and Huang [30] showed that the error in excluding the radial velocity term from the mass balance was a strong function of the product to reactant viscosity ratio. The radial velocity became more important for larger viscosity ratios.

2.4 The Axial Dispersion Model

The plug flow reactor model has been the basis for tubular reactor design. The simplicity of the plug flow equation allowed analytical solutions to be developed for a number of different reaction mechanisms. The axial dispersion model was developed as an extension of the plug flow model to account for deviations of a true reactor from the ideal plug flow condition. An additional term was added to the plug flow model based on the concept of axial diffusion of material. This was accomplished by employing an effective diffusion, $\mathcal{D}^E$ such that for a first order reaction:

$$\mathcal{D}^E \frac{d^2 c_i}{dz^2} - \langle v_z \rangle \frac{dc_i}{dz} - k_R c_i = 0 \tag{2.3}$$

By employing different values of the effective diffusivity, $\mathcal{D}^E$, the model could be used to describe many types of reactor. If the effective diffusivity was high then the model approached the stirred tank reactor equation. For a diffusivity approaching 0, the equation reduced to the ideal plug flow equation.

Analytical derivations performed by Taylor [34] and Aris [35] demonstrated that an effective diffusivity could be calculated for laminar flow situations. In other words, the laminar flow model could be reduced to the axial dispersion model by the use of an appropriate value of the effective diffusivity. The value required was shown to be a function of the molecular diffusivity and the centerline velocity. In the case of the Taylor analysis, the effective diffusivity was defined as:

$$\mathcal{D}^E = \frac{R^2 \langle v_z \rangle^2}{48 \mathcal{D}_i} \tag{2.4}$$

subject to the constraint;

$$\frac{\langle v_z \rangle L}{\mathcal{D}^E} > 6.65 \tag{2.5}$$

Aris extended the analysis to remove the constraint and developed the following definition for effective diffusivity:

$$\mathcal{D}^E = \mathcal{D}_i + \frac{R^2 \langle v_z \rangle^2}{\mathcal{D}_i} \tag{2.6}$$

Wan and Ziegler [36] tested the applicability of the Taylor dispersion coefficient to laminar flow reactors. Comparison of analytical data for the full laminar flow model, first and second order reactions, and the solutions yielded by the axial dispersion model showed good agreement. It was shown that for a reactive system the restrictions upon the applicability of the axial dispersion model differed. The axial dispersion model was shown to yield good results for:

$$\frac{\mathcal{D}_i}{k_R R^2 c_{i_o}^{n-1}} \geq \frac{1}{2} \tag{2.7}$$

Other extensions to the Taylor analysis have been considered. Among these were the studies performed by Nigam and Vasudeva [37,38]. In the first study, the analysis was extended to a power law fluid. Empirical correlations were developed to estimate the best value of dispersion coefficient to use for a given flow index and reaction rate. Expressions were developed for both dilatant and pseudoplastic fluids. In the second study [38] consecutive reactions in laminar flow were examined. In this instance, two dispersion coefficients were required. Again the coefficients were given in terms of empirical relationships.

All of the above analyses were carried out assuming isothermal flow. The axial dispersion model for plug flow conditions has been extended to non-isothermal conditions. Of particular interest have been situations involving multiple steady states around which a vast literature has developed [39]. Adapting the axial dispersion model to a non-isothermal laminar flow reactor has not been attempted. Sundaram and Froment [40] have pointed out that, in order to accurately predict the reactor characteristics using a one dimensional model, the wall heat transfer characteristics of the corresponding two dimensional model must be known. They examined the simulation results from a two dimensional model for both turbulent and laminar velocity profiles. They derived empirical equations for predicting the wall heat

transfer characteristics of the reactor to be incorporated into the one dimensional model.

Further derivations to include the effect of free convection and other situations involving changing physical properties in terms of a one dimensional model would seem to create more complications rather than making the problem simpler.

Chapter 3

Theoretical and Numerical Development

The feature that distinguishes the laminar flow reactor from the plug flow reactor is the inclusion of a velocity profile. In the simplest case, the inclusion of a velocity profile in a tubular reactor model requires the incorporation of this profile in the mass and energy balance equations. Because of the subsequent residence time distribution, radial concentration and temperature profiles will develop. With more complex situations in which it is suspected that the velocity profile will change within the reactor, it is necessary to include a momentum balance as part of the model. Additionally, a microscopic and macroscopic mass balance are required to insure that the momentum balance yields a physically meaningful result.

3.1 Equations and General Assumptions

The following equations from Bird, Stewart, and Lightfoot [41] were employed to model the reactor performance:

- Species Balance

$$\frac{\partial \rho_i}{\partial t} + \nabla \cdot (\rho_i \mathbf{v}) = -\nabla \cdot \mathbf{j}_i + r_i \tag{3.1}$$

- Energy Balance

$$\rho\hat{C}_p\left[\frac{\partial T}{\partial t}+\mathbf{v}\cdot\nabla T\right] = -\nabla\cdot\mathbf{q}+\sum_{i=1}^{n}\bar{H}_i[\nabla\cdot\mathbf{J}_i-R_i]+\sum_{i=1}^{n}(\mathbf{j}_i\cdot\mathbf{g}_i) + \left(\frac{\partial\ln\hat{V}}{\partial\ln T}\right)_{p,x_i}\frac{Dp}{Dt}-\boldsymbol{\tau}:\nabla\mathbf{v} \tag{3.2}$$

- Momentum Balance

$$\rho\left(\frac{\partial\mathbf{v}}{\partial t}+\mathbf{v}\cdot\nabla\mathbf{v}\right)=-\nabla p-\nabla\cdot\boldsymbol{\tau}+\rho\mathbf{g} \tag{3.3}$$

- Microscopic Continuity

$$\frac{\partial\rho}{\partial t}+\nabla\cdot(\rho\mathbf{v})=0 \tag{3.4}$$

- Macroscopic Continuity

$$\rho_o\langle v_z\rangle_o R^2=2\int_0^R\rho v_z r\,dr \tag{3.5}$$

The primary purpose of the computer simulation was to determine how temperature and composition dependent physical properties affected the performance in a laminar flow reactor operating under steady state conditions. The inclusion of axial dispersion terms in the equations would create a system of equations more difficult than necessary to achieve this purpose. Estimation of the boundary conditions at the outlet would be difficult for the full elliptic model. Typically, the outlet boundary conditions have been defined so that the respective axial gradients were set equal to 0 [24,42]. Assuming that the axial derivatives vanished at the outlet could lead to some contradictory information with respect to the overall continuity of the system. The inclusion of this particular set of boundary conditions would require that all of the radial gradients be set to 0 also. This would not necessarily be true, for example, if the reaction had not reached completion at the outlet.

By modelling a vertical reactor the momentum balance may be simplified since the angular component would not apply. Also axial symmetry would be maintained so that the boundary conditions would not be complicated in the other balance equations, in particular at the reactor centerline.

Equation 3.4 contained radial and axial density gradients when expanded. It was felt that although density was changing in this study that the variations in density provided by this equation were minor. The equation itself was used only to estimate the radial velocity. It was therefore felt that little error would be created by asssuming that these gradients were negligible. This assumption also had the advantage of reducing the number of terms in the radial and axial components of the momentum balance. The removal of these gradients from Equation 3.4 did not imply that density changes in the reactor were negligible. As will be seen, a variable density appeared in other terms. In this respect, the equations were similar to those in previous investigations [12,13,14].

The reaction mechanisms in this study have been kept simple. Most of the work has been performed for a first order reaction. Some work has also been done using a second order reaction. The majority of investigations reported in the literature have also assumed first or second order reactions.

The above comments led to the following assumptions.

1. The system was at steady state.
2. The axial dispersion effects were negligible compared to convective effects.
3. The reactor was vertical and flow was axisymmetric.
4. Fully developed Newtonian flow was present at the inlet.
5. The kinetic rate constant was described by the Arrhenius equation.
6. The liquid was incompressible with respect to the microscopic continuity equation.

Application of the assumptions reduced the equations to the following:

- Species Equation

$$v_z \frac{\partial \rho_i}{\partial z} + v_r \frac{\partial \rho_i}{\partial r} = -\frac{1}{r}\frac{\partial}{\partial r}(r j_{i_r}) + r_i \tag{3.6}$$

- Temperature Equation

$$\rho\hat{C}_p\left(v_z\frac{\partial T}{\partial z}+v_r\frac{\partial T}{\partial r}\right) = -\frac{1}{r}\frac{\partial}{\partial r}(rq_r)+\sum_{i=1}^{n}\bar{H}_i\left[\frac{1}{r}\frac{\partial}{\partial r}(rJ_{i_r})-R_i\right]+\sum_{i=1}^{n}j_{i_z}g_{i_z} + \left(\frac{\partial \ln \hat{V}}{\partial \ln T}\right)_{p,x_i}\left(v_z\frac{\partial p}{\partial z}+v_r\frac{\partial p}{\partial r}\right)-\boldsymbol{\tau}:\nabla\mathbf{v} \qquad (3.7)$$

- Momentum Equation

z-component

$$\rho\left(v_z\frac{\partial v_z}{\partial z}+v_r\frac{\partial v_z}{\partial r}\right) = -\left(\frac{1}{r}\frac{\partial}{\partial r}(r\tau_{rz})+\frac{\partial \tau_{zz}}{\partial z}\right)-\frac{\partial p}{\partial z}\pm\rho g_z \qquad (3.8)$$

r-component

$$\rho\left(v_r\frac{\partial v_r}{\partial r}+v_z\frac{\partial v_r}{\partial z}\right) = -\left(\frac{1}{r}\frac{\partial}{\partial r}(r\tau_{rr})+\frac{\partial \tau_{rz}}{\partial z}\right)-\frac{\partial p}{\partial r} \qquad (3.9)$$

- Microscopic Continuity Equation

$$\frac{\partial v_z}{\partial z}+\frac{1}{r}\frac{\partial}{\partial r}(rv_r)=0 \qquad (3.10)$$

The macroscopic continuity equation was not affected.

The following initial and boundary conditions applied:

At $z=0$, for all r;

$$T = T_o \qquad (3.11)$$

$$\rho_i = \rho_{i_o} \qquad (3.12)$$

$$v_{z_o} = 2\langle v_z\rangle_o\left(1-(r/R)^2\right) \qquad (3.13)$$

$$v_r = 0 \qquad (3.14)$$

$$p = p_o \qquad (3.15)$$

At $r=0$, for all z:

$$\frac{\partial \rho_i}{\partial r}=\frac{\partial T}{\partial r}=\frac{\partial v_z}{\partial r}=v_r=0 \qquad (3.16)$$

At $r=R$, for all z:

$$\frac{\partial \rho_i}{\partial r}=v_z=v_r=0 \qquad (3.17)$$

$$-k_c\frac{\partial T}{\partial r} = h_c(T_w - T_j) \tag{3.18}$$

Any further assumptions required to reduce the above equations have been applied in the ensuing sections.

3.2 The Species Equation

The systems examined in this study were generally considered to be composed of a reactant, solvent, and product. The solvent was either a co-reactant in excess or was an inert substance. A minimum of three components formed the basis of the hypothetical system. Ideally, a component balance such as that given by Equation 3.6 was required for every component. If each component was to be included in the model, a complex multi-component diffusion problem could be developed. In this situation the flux, $\mathbf{j}_i$ could be composed of several terms. These terms included the regular diffusional flux and thermal, pressure and forced diffusional fluxes. Assuming that the regular diffusional flux was the only one of importance, it could be written as [41]:

$$\mathbf{j}_i^{(x)} = \frac{c^2}{\rho RT}\sum_{j=1}^{n} M_i M_j D_{ij}\left[x_j \sum_{\substack{k=1\\k\neq j}}^{n}\left(\frac{\partial \bar{G}_j}{\partial x_k}\right)_{\substack{T,p,x_s\\s\neq j,k}} \nabla x_k\right] \tag{3.19}$$

Through the above equation it would be possible to establish a complex interaction among the species of the system. In most previous studies only the concentration of the reactant has been followed using Equation 3.6. If required the concentrations of other components were evaluated from the stoichiometry of the reaction. This was the approach taken in this study also. Using this approach and suitable assumptions the complexity represented by Equation 3.19 was avoided.

A mixture diffusivity was derived for the system consistent with that of previous studies. It was defined by employing:

$$N_{i_r} = -c\mathcal{D}_{im}\frac{\partial x_i}{\partial r} + x_i\sum_{j=1}^{n} N_{j_r} \tag{3.20}$$

For the purposes of the present study, it was assumed that the mixture diffusivities given by Equation 3.20 were equivalent to the regular binary diffusivities. Previous studies have determined that the diffusion rate was important only at higher mass transfer rates [1,4]. This study was concerned with liquid systems in which the diffusion rates were low. It was therefore felt that as long as the diffusivity was estimated within an order of magnitude, no appreciable errors would arise.

Because of the above assumption, the mixture diffusivity $\mathcal{D}_{im}$ was employed in the species balance such that:

$$j_{i_r} = -\rho \mathcal{D}_{im} \frac{\partial w_i}{\partial r} \tag{3.21}$$

Insertion of Equation 3.21 into the species balance yielded:

$$v_z \frac{\partial \rho_i}{\partial z} + v_r \frac{\partial \rho_i}{\partial r} = \frac{1}{r} \frac{\partial}{\partial r} \left(r \rho \mathcal{D}_{im} \frac{\partial w_i}{\partial r} \right) + r_i \tag{3.22}$$

By dividing Equation 3.22 by the species molecular weight, the species i was written in terms of molar concentrations rather than mass concentrations;

$$v_z \frac{\partial c_i}{\partial z} + v_r \frac{\partial c_i}{\partial r} = \frac{1}{r} \frac{\partial}{\partial r} \left(r \rho \mathcal{D}_{im} \frac{\partial}{\partial r} \left(\frac{c_i}{\rho} \right) \right) + R_i \tag{3.23}$$

For a first order reaction the last term on the right hand side of Equation 3.23 became, for reactant i;

$$v_z \frac{\partial c_i}{\partial z} + v_r \frac{\partial c_i}{\partial r} = \frac{1}{r} \frac{\partial}{\partial r} \left(r \rho \mathcal{D}_{im} \frac{\partial}{\partial r} \left(\frac{c_i}{\rho} \right) \right) - k_R c_i \tag{3.24}$$

By employing Assumption 5, the rate constant was written as:

$$k_R = A \exp \left(\frac{-E}{R_g T} \right) \tag{3.25}$$

Substitution of Equation 3.25 into Equation 3.24 yielded:

$$v_z \frac{\partial c_i}{\partial z} + v_r \frac{\partial c_i}{\partial r} = \frac{1}{r} \frac{\partial}{\partial r} \left(r \rho \mathcal{D}_{im} \frac{\partial}{\partial r} \left(\frac{c_i}{\rho} \right) \right) - A \exp \left(\frac{-E}{R_g T} \right) c_i \tag{3.26}$$

The above equation was further reduced by assuming constant physical properties for some of the runs. Doing this yielded the species equation used by other investigators. In the majority of runs in this study the properties were assumed to vary as functions of concentration and temperature and were therefore functions of the radius. They could not be removed from the Laplacian term in the above equation.

3.3 The Energy Equation

Initially, it was assumed that the viscous dissipation, pressure work, and potential energy terms were negligible. This reduced the energy equation to:

$$\rho\hat{C}_p\left(v_z\frac{\partial T}{\partial z}+v_r\frac{\partial T}{\partial r}\right)=-\frac{1}{r}\frac{\partial}{\partial r}(rq_r)+\sum_{i=1}^{n}\bar{H}_i\left[\frac{1}{r}\frac{\partial}{\partial r}(rJ_{i_r})-R_i\right] \tag{3.27}$$

Similar to j_{i_r} of the previous section, the radial heat flux term q_r for a multi-component situation consisted of more than a conductive heat flux. The heat flux was:

$$q_r=-k_c\frac{\partial T}{\partial r}+\sum_{i=1}^{n}\bar{H}_iJ_{i_r} \tag{3.28}$$

Insertion of Equation 3.28 into Equation 3.27 yielded:

$$\begin{aligned}\rho\hat{C}_p\left(v_z\frac{\partial T}{\partial z}+v_r\frac{\partial T}{\partial r}\right) &= \frac{1}{r}\frac{\partial}{\partial r}\left(rk_c\frac{\partial T}{\partial r}\right)-\frac{1}{r}\frac{\partial}{\partial r}\left(r\sum_{i=1}^{n}\bar{H}_iJ_{i_r}\right)\\ &\quad+\sum_{i=1}^{n}\bar{H}_i\left[\frac{1}{r}\frac{\partial}{\partial r}(rJ_{i_r})-R_i\right]\end{aligned} \tag{3.29}$$

Upon rearrangement and application of the chain rule,

$$\rho\hat{C}_p\left(v_z\frac{\partial T}{\partial z}+v_r\frac{\partial T}{\partial r}\right)=\frac{1}{r}\frac{\partial}{\partial r}\left(rk_c\frac{\partial T}{\partial r}\right)-\sum_{i=1}^{n}\frac{J_{i_r}}{r}\frac{\partial}{\partial r}\left(r\bar{H}_i\right)-\sum_{i=1}^{n}\bar{H}_iR_i \tag{3.30}$$

The second term on the right hand side of Equation 3.30 contained a summation of the product of molecular fluxes and their respective molar enthalpies. It has been previously shown [12] that when the heat capacities of each of the components were equal, then this term would disappear. Although the heat capacities in the present study varied it was assumed that this term would be negligible compared to the convective and conductive processes since each of the species present in the system would be carrying its enthalpy with it. Since the various species of the system were diffusing in opposite directions, it was felt that the components of the summation would cancel each other.

The last term on the right hand side of Equation 3.30 represented the heat of reaction term and could be written for a single reaction as:

$$\sum_{i=1}^{n}\bar{H}_iR_i=\Delta H_RR_i \tag{3.31}$$

Upon the introduction of Equation 3.25, into Equation 3.30, the energy equation became:

$$\rho \hat{C}_p \left(v_z \frac{\partial T}{\partial z} + v_r \frac{\partial T}{\partial r} \right) = \frac{1}{r} \frac{\partial}{\partial r} \left(r k_e \frac{\partial T}{\partial r} \right) - \Delta H_R A \exp\left(\frac{-E}{R_g T} \right) c_i \qquad (3.32)$$

3.4 The Momentum Equation

Unlike the species and energy equations, the flux in the momentum equation did not differ between a single or multi-component system. The stress tensor, τ, was expanded as it would be for a normal flow situation. Three components of the stress tensor appeared in Equations 3.8 and 3.9. These were τ_{rz}, τ_{zz}, and τ_{rr}. Using the assumption of a Newtonian fluid, they may be written as:

$$\tau_{rz} = -\mu \left(\frac{\partial v_z}{\partial r} + \frac{\partial v_r}{\partial z} \right) \qquad (3.33)$$

$$\tau_{rr} = -\mu \left[2 \frac{\partial v_r}{\partial r} - \frac{2}{3} (\nabla \cdot \mathbf{v}) \right] \qquad (3.34)$$

$$\tau_{zz} = -\mu \left[2 \frac{\partial v_z}{\partial z} - \frac{2}{3} (\nabla \cdot \mathbf{v}) \right] \qquad (3.35)$$

Assumption 6 was used to eliminate the term $\nabla \cdot \mathbf{v}$ from the normal stresses (i.e. $\nabla \cdot \mathbf{v} = 0$). The definitions of the stresses were incorporated into the momentum balance equations. Dimensionless groups were also introduced to yield the following dimensionless equations:

$$aRe\rho' \left(U \frac{\partial U}{\partial z^*} + V^* \frac{\partial u}{\partial r'} \right) = \frac{1}{r'} \frac{\partial}{\partial r'} \left(r' \mu' \frac{\partial U}{\partial r'} \right) + \frac{a^2}{r'} \frac{\partial}{\partial r'} \left(r' \mu' \frac{\partial V^*}{\partial z^*} \right) + 2a^2 \frac{\partial}{\partial z^*} \left(\mu' \frac{\partial U}{\partial z^*} \right) - \frac{\partial P'}{\partial z^*} \pm \beta_U \rho' \qquad (3.36)$$

$$a^3 Re\rho' \left(V^* \frac{\partial V^*}{\partial r'} + U \frac{\partial V^*}{\partial z^*} \right) = \frac{2a^2}{r'} \frac{\partial}{\partial r'} \left(r' \mu' \frac{\partial V^*}{\partial r'} \right) + a^4 \frac{\partial}{\partial z^*} \left(\mu' \frac{\partial V^*}{\partial z^*} \right) + a^2 \frac{\partial}{\partial z^*} \left(\mu' \frac{\partial U}{\partial r'} \right) - \frac{\partial P'}{\partial r'} \qquad (3.37)$$

where

$$r' = r/R \tag{3.38}$$

$$z^* = z/L \tag{3.39}$$

$$\rho' = \rho/\rho_o \tag{3.40}$$

$$\mu' = \mu/\mu_o \tag{3.41}$$

$$U = v_z/(2\langle v_z\rangle_o) \tag{3.42}$$

$$V^* = (v_r L)/(2\langle v_z\rangle_o R) \tag{3.43}$$

$$P' = (pR^2)/(2\langle v_z\rangle_o \mu_o L) \tag{3.44}$$

$$\beta_U = (\rho_o R^2 g_z)/(2\langle v_z\rangle_o \mu_o) \tag{3.45}$$

$$Re = (2R\langle v_z\rangle_o \rho_o)/\mu_o \tag{3.46}$$

$$a = R/L \tag{3.47}$$

In Equations 3.36 and 3.37 the dimensionless groups were chosen such that all of the gradients were of the same order of magnitude [30]. Because the reactor under study was a tubular reactor, it could be reasonably assumed that:

$$a = R/L \ll 1 \tag{3.48}$$

Application of the above assumption reduced the above equations to the following:

$$aRe\rho'\left(U\frac{\partial U}{\partial z^*} + V^*\frac{\partial u}{\partial r'}\right) = \frac{1}{r'}\frac{\partial}{\partial r'}\left(r'\mu'\frac{\partial U}{\partial r'}\right) - \frac{\partial P'}{\partial z^*} \pm \beta_U\rho' \tag{3.49}$$

$$0 = -\frac{\partial P'}{\partial r'} \tag{3.50}$$

The r-component of the momentum balance was therefore eliminated. It was further assumed that the Reynolds number, Re, was small with respect to β_U so that the product aRe was negligible. This removed the inertial terms from the z-component of the momentum equation to yield:

$$0 = \frac{1}{r'}\frac{\partial}{\partial r'}\left(r'\mu'\frac{\partial U}{\partial r'}\right) - \frac{\partial P'}{\partial z^*} \pm \beta_U\rho' \tag{3.51}$$

In the laboratory experiments that were performed as part of this study the values Reynolds numbers employed were between 80 and 100. The value of the aspect

ratio, a, for the reactor was .022. The maximum value of the product aRe was therefore approximately 2.2. The minimum value of β_U employed in any part of the investigation was 200. The removal of the inertial terms was therefore justified.

Previous investigations have also demonstrated that the inertial terms may be neglected. In particular, Kostin and Gray [14] in a study of free convection in a vertical reactor demonstrated that Equation 3.51 yielded results that were comparable to a streamline formulation in which the full momentum balance was considered. McLaughlin *et al* [29] examined the relative sizes of a number of the momentum balance terms in a polymerization reactor. They again found that even under circumstances of very large variations of the axial velocity that the inertial terms were not significant.

By removing the inertial terms the number of dimensionless groups developed later was reduced by one.

Further assumptions have been applied to the above equation depending on the context of a particular investigation. Most researchers studying polymerization reactions have assumed constant density. Using this assumption Equation 3.51 has been rearranged to yield an integral equation describing the velocity profile [23,27,29,30]:

$$\frac{v_z}{\langle v_z \rangle_o} = \frac{R^2 \int_r^R \frac{r}{\mu} dr}{\int_0^R \frac{r^3}{\mu} dr} \tag{3.52}$$

In studying free convection effects the normal practice has been to expand the density in Equation 3.51 using a Taylor series. This has proved to be successful when density was simply a function of temperature [12,13,14]. In the present study, system density was also a function of each of the component densities. If a Taylor series expansion was to be employed a Grashof term for each of the components would be required. This would increase the number of dimensionless groups associated with the problem unnecessarily. Potential ambiguities could also develop in terms of whether detected differences were the result of composition changes or the effect of flow direction. Instead of applying the Taylor series expansions the density was left as a single term in this study. In this way a negative sign associated with the buoyancy term implied upward flow and a positive sign implied downward flow.

3.5 Radial Velocities

Since the axial velocities were allowed to vary along the reactor, radial velocities were developed. The microscopic continuity equation was used to calculate radial velocities. Earlier studies did not include these velocities even when the axial velocities were changing. It has recently been shown by Vrentas and Huang [30] and McLaughlin *et al.* [29] that exclusion of the radial velocity from the reactor model resulted in as much as a 30% difference in calculated conversions compared to the case when the radial velocities were included.

The radial velocity at any point r was calculated by integrating the microscopic continuity equation (Equation 3.10) over the radius.

$$v_r = -\frac{1}{r}\int_R^r \left(\frac{\partial v_z}{\partial z}\right) r dr \tag{3.53}$$

3.6 Dimensionless Equations

Characteristic values of the variables appearing in the system equations were introduced to produce dimensionless equations. Most of these characteristic values were taken as the inlet value of the variable. The concentration c_i, temperature T, axial velocity v_z, and physical properties were treated in this manner. The characteristic radius was the radius at the wall. From these characteristic values the following dimensionless terms were defined:

$$r' = r/R \tag{3.54}$$

$$x_i = c_i/c_{i_o} \tag{3.55}$$

$$\theta = (T - T_o)/T_o \tag{3.56}$$

$$U = v_z/2\langle v_z\rangle_o \tag{3.57}$$

$$\rho' = \rho/\rho_o \tag{3.58}$$

$$\hat{C}'_p = \hat{C}_p/\hat{C}_{p_o} \tag{3.59}$$

$$k'_c = k_c/k_{c_o} \tag{3.60}$$

$$\mathcal{D}'_{im} = \mathcal{D}_{im}/\mathcal{D}_{im_o} \tag{3.61}$$

$$\mu' = \mu/\mu_o \tag{3.62}$$

The Arrhenius equation was rewritten in terms of the rate constant at T_o (k_{R_o}), the temperature at the inlet, such that:

$$k_R = k_{R_o} \exp\left(\frac{E\theta}{R_g T_o(\theta+1)}\right) \tag{3.63}$$

The above equation was used to define the following dimensionless group:

$$\gamma = \frac{E}{R_g T_o} \tag{3.64}$$

Incorporation of the above dimensionless variables into the species balance yielded:

$$\frac{2\langle v_z\rangle_o U}{k_{R_o}}\frac{\partial x_i}{\partial z} + \frac{v_r}{k_{R_o}R}\frac{\partial x_i}{\partial r'} = \frac{\mathcal{D}_{im_o}}{R^2 k_{R_o}}\frac{1}{r'}\frac{\partial}{\partial r'}\left(r'\rho'\mathcal{D}'_{im}\frac{\partial}{\partial r'}\left(\frac{x_i}{\rho'}\right)\right) - \exp\left(\frac{\gamma\theta}{(\theta+1)}\right)x_i \tag{3.65}$$

From the above equation the following dimensionless groups were defined:

$$z' = \frac{k_{R_o} z}{2\langle v_z\rangle_o} \tag{3.66}$$

$$V = \frac{v_r}{R k_{R_o}} \tag{3.67}$$

$$\alpha_x = \frac{\mathcal{D}_{im_o}}{R^2 k_{R_o}} \tag{3.68}$$

so that the species balance became:

$$U\frac{\partial x_i}{\partial z'} + V\frac{\partial x_i}{\partial r'} = \frac{\alpha_x}{r'}\frac{\partial}{\partial r'}\left(r'\rho'\mathcal{D}'_{im}\frac{\partial}{\partial r'}\left(\frac{x_i}{\rho'}\right)\right) - \exp\left(\frac{\gamma\theta}{(\theta+1)}\right)x_i \tag{3.69}$$

The other transport equations were treated similarly to yield:

$$\rho' C'_p\left(U\frac{\partial\theta}{\partial z'} + V\frac{\partial\theta}{\partial r'}\right) = \frac{\alpha_T}{r'}\frac{\partial}{\partial r'}\left(r' k'_c\frac{\partial\theta}{\partial r'}\right) + \beta_T \exp\left(\frac{\gamma\theta}{(\theta+1)}\right)x_i \tag{3.70}$$

$$0 = -\frac{dp'}{dz'} + \frac{1}{r'}\frac{\partial}{\partial r'}\left(r'\mu'\frac{\partial U}{\partial r'}\right) + \beta_U\rho' \tag{3.71}$$

$$V = -\frac{1}{r'}\int_1^{r'}\left(\frac{\partial U}{\partial z'}\right)r'dr' \tag{3.72}$$

$$\frac{1}{4} = \int_0^1 U r'\,dr' \tag{3.73}$$

In the above equations, the following additional dimensionless groups were also defined:

$$\alpha_T = \frac{k_{c_o}}{R^2 \rho_o C_{p_o} k_{R_o}} \tag{3.74}$$

$$\beta_T = \frac{-\Delta H_R C_{i_o}}{\rho_o C_{p_o} T_o} \tag{3.75}$$

$$p' = \frac{(p - p_o) k_{R_o} R^2}{4 \langle v_z \rangle_o^2 \mu_o} \tag{3.76}$$

$$\beta_U = \pm \frac{\rho_o g_z R^2}{2 \langle v_z \rangle_o \mu_o} \tag{3.77}$$

The axial momentum balance had previously been put into a dimensionless form as part of the exercise to eliminate the radial momentum balance. In that section a different dimensionless axial distance was employed. Upon using the axial dimensionless distance derived in this section, the dimensionless pressure was redefined as indicated above. The new balance contained a pressure that was consistent with the other terms defined above based on the dimensionless axial distance used.

The sign of the heat of reaction term was taken as positive for exothermic reactions and negative for endothermic reactions. Similarly, the buoyancy term, β_U, was positive for downward flow and negative for upward flow.

Using the definitions given above for the dimensionless terms, the boundary conditions were rewritten in dimensionless form to yield:
at $z' = 0$,

$$\theta = 0 \tag{3.78}$$

$$x_i = 1 \tag{3.79}$$

$$U = 1 - (r')^2 \tag{3.80}$$

$$V = 0 \tag{3.81}$$

$$p' = 0 \tag{3.82}$$

at $r' = 0$,

$$\frac{\partial x_i}{\partial r'} = \frac{\partial \theta}{\partial r'} = \frac{\partial U}{\partial r'} = V = 0 \tag{3.83}$$

at $r' = 1$,

$$\frac{\partial x_i}{\partial r'} = U = V = 0 \tag{3.84}$$

$$-k'_c \frac{\partial \theta}{\partial r'} = Bi(\theta_w - \theta_j) \tag{3.85}$$

where

$$Bi = \frac{h_c R}{k_{co}} \tag{3.86}$$

Of particular interest were the cup-mixed concentration and temperature. In terms of the dimensionless quantities, these could be expressed as:

$$\langle x_i \rangle = 4 \int_0^1 U x_i r' \, dr' \tag{3.87}$$

$$\langle \theta \rangle = 4 \int_0^1 U \theta r' \, dr' \tag{3.88}$$

In much of the ensuing work, the cup-mixed quantities were employed. Differences in these quantities under various conditions were examined to determine the effects of variable properties on reactor performance.

Several dimensionless systems have been used in studying laminar flow reactors. Different definitions of the dimensionless axial distance have created differences in the other dimensionless groups. Examination of the above equations showed that they were of the form:

$$\epsilon_y \left(U \frac{\partial y}{\partial z'} + V \frac{\partial y}{\partial r'} \right) = \frac{\alpha_y}{r'} \frac{\partial}{\partial r'} \left(r' k' \frac{\partial y}{\partial r'} \right) + \beta_y R_y \tag{3.89}$$

where, for this study:

$$y = x_i, \theta, U \tag{3.90}$$

$$\epsilon_y = 1, \rho' C'_p, 0 \tag{3.91}$$

$$\alpha_y = \alpha_x, \alpha_T, 1 \tag{3.92}$$

$$\beta_y = 1, \beta_T, \beta_U \tag{3.93}$$

$$k' = \mathcal{D}'_{im}, k'_c, \mu' \tag{3.94}$$

$$R_y = -\exp\left(\frac{\gamma\theta}{(1+\theta)}\right) x_i, \ \exp\left(\frac{\gamma\theta}{(1+\theta)}\right) x_i, \ -\frac{1}{\beta_U}\frac{dp'}{dz'} + \rho' \tag{3.95}$$

for the species, temperature, and momentum equations respectively.

The dimensionless groups employed in this study were related to more established groups in the following manner:

1. The Damköhler number has been defined as $Da = k_{R_o}R^2/\mathcal{D}_{im}$ by some investigators [7,12]. In this case $\alpha_x = 1/Da$. A heat Damköhler number may be similarly defined as $Da_H = k_{R_o}R^2\rho\hat{C}_p/k_e$ so that $\alpha_T = 1/Da_H$.

2. Other investigators have preferred to define $Da' = k_{R_o}R/\langle v_z \rangle$ [30]. With this definition the reciprocals of the heat and mass Peclet Numbers were the radial dispersion terms. The present radial dispersion terms were related to Da' by $\alpha_x = 1/(Da'Pe_M)$ and $\alpha_T = 1/(Da'Pe_H)$.

3. The Lewis number has also been employed [8,9,15,17]. It was related to the present groups by $Le = \alpha_T/\alpha_x$.

The present groups extended the formulation initially developed by Cleland and Wilhelm for an isothermal reactor [4]. They recognized that without a reaction occurring that there would not be any diffusion. Without diffusion there would not be a reason to include the Peclet numbers. The impact that the radial diffusion rate was therefore dependent upon the reaction itself. Incorporation of the two phenomena (i.e diffusion and reaction) into one group was therefore considered the best alternative.

As written, the dimensionless heat of reaction also became important in that it was precisely the dimensionless adiabatic temperature rise. Comparison of this value to cup-mixed temperature rises in the reactor was a good measure of heat removal efficiency.

The general balance equation, Equation 3.89, was expanded and rearranged to yield the following:

$$0 = \epsilon_y U \frac{\partial y}{\partial z'} - \frac{\alpha_y k'}{r'}\frac{\partial}{\partial r'}\left(r'\frac{\partial y}{\partial r'}\right) + (\epsilon_y V - \alpha_y f_y)\frac{\partial y}{\partial r'} - \alpha_y g_y y - \beta_y R_y \qquad (3.96)$$

In Equation 3.96, the first, second and fifth terms corresponded to the constant property model. The functions f_y and g_y were functions of the derivatives of the

transport properties appearing in Equation 3.89. In the energy and momentum equations the function g_y was 0. The species equation was unique because the density appeared in the radial Laplacian term in Equation 3.69. This resulted in the need for the term g_x defined below. To summarize, the functions defined above in Equation 3.96 were:

$$f_x = \frac{\partial \mathcal{D}'_{im}}{\partial r'} - \frac{\mathcal{D}'_{im}}{\rho'}\frac{\partial \rho'}{\partial r'} \tag{3.97}$$

$$f_T = \frac{\partial k'_c}{\partial r'} \tag{3.98}$$

$$f_U = \frac{\partial \mu'}{\partial r'} \tag{3.99}$$

$$g_x = \frac{\mathcal{D}'_{im}}{\rho'^2}\left(\frac{\partial \rho'}{\partial r'}\right)^2 - \frac{\mathcal{D}'_{im}}{\rho'}\frac{1}{r'}\frac{\partial}{\partial r'}(r'\rho') - \frac{1}{\rho'}\frac{\partial \mathcal{D}'_{im}}{\partial r'}\frac{\partial \rho'}{\partial r'} \tag{3.100}$$

If it was assumed that all physical and transport properties were constant then f_x, f_T, f_U, and g_x would disappear. The resultant equations would be those for a constant property reactor. Any one of the properties could be set to zero, thus, eliminating the respective radial derivative.

3.7 Numerical Solution

The Crank-Nicholson method has been the most widely used method for solving the system equations. The method has gradually been refined as more detailed descriptions of the reactor have been developed. Rothenberg and Smith developed the method to be used for the reactor under non-isothermal conditions [8,9].

The Crank-Nicholson method was originally developed as a method to solve a single linear PDE. To include the energy balance in the laminar flow reactor required some simplification in order to reduce the nonlinearity introduced by the temperature dependent rate constant. Solution schemes were developed that required very fine grids such that the numerical errors associated with the simplification were minimized. Basically, these solution schemes were developed to maintain the tridiagonal nature of the resultant matrix for the individual balance equations. Generally the equations were solved in the following manner [12,15,17]:

1. The solution space was discretized into a very fine grid in both the radial and axial directions such that it could be assumed that the differences in temperatures and compositions between grid points were very small.

2. Either the energy balance or the component balance was solved employing the data already available.

3. The remaining PDE was solved using the updated information determined from Step 2.

Because of the fine grid spacing used in the above solution, the results were generally adequate enough to not require iteration. With the inclusion of the momentum balance, the above solution became more complicated. It was recognized immediately that the momentum balance could not simply be introduced as a fourth step to the above solution. Coupled with the calculation of velocities was the calculation of a pressure. In this situation the number of unknowns was greater than the number of equations. The macroscopic continuity equation, which was not a PDE, needed to be used to balance the system's unknowns and equations. To solve this more complex system required iteration to be performed. This was accomplished by employing the above solution to solve for the composition and temperature. After this, the temperature and composition values were used to calculate the viscosities at the respective radial points. The axial velocities were consequently calculated using the momentum balance and corrected using the macroscopic continuity equation. This was continued until the values of the velocities stabilized. Once the velocities no longer changed, the new values could be replaced in the temperature and composition balances for further iteration or for proceeding to the next axial step [12].

Although effective, the above method could be slow due to the use of successive iterations and very small grid spacings. In this study alternatives were employed to reduce the excessive computation times required by the Crank-Nicholson method. The approach consisted of the simultaneous solution of all of the system equations in the following manner:

- Radial discretization to yield a system of ordinary differential equations.

- Axial integration of the system of ODE's by means of a suitable differential equation solver.

This approach has been termed 'the method of lines'. Two different radial discretization schemes were applied. Finlayson [43] has presented numerous methods including Finite Differences (FD), Finite Elements, and Orthogonal Collocation (OC) as viable for the solution of two dimensional plug flow reactor problems. In earlier work, Hopkins and Golding [44] determined that OC could be applied to an adiabatic laminar flow reactor. Although initially shown to be comparable to finite differences, the radial temperature profiles were found to oscillate considerably for other temperature boundary conditions.

These oscillations are shown for a 4-point collocation solution in Figure 3.1. The solutions for 10- and 40-point finite differences have also been plotted (10-point solution represented by symbols, 40-point solution represented by lines). In Figure 3.2 the corresponding radial concentration profiles are shown. It should be noted that again the two FD solutions yield quite comparable results. Orthogonal Collocation showed an appreciable difference from the FD solutions.

Another example is shown in Figures 3.3 and 3.4. In this particular example a 10-point FD solution has been compared with a 60-point solution. The wall heat transfer boundary condition to be used in this study has been employed. Except for small differences appearing between the two solutions at the wall in Figure 3.4, the radial profiles were similar. The axial cup-mixed concentrations and temperatures for this second example have been given in Table 3.1. Solutions for other finite difference grids have also been given in this table.

Since very little difference was observed between the solutions, a 10-point finite difference solution has been used throughout the study in order to conserve computer time. This was particularly useful when there were large changes in the velocity profile. The use of 10 radial points led to substantial savings. It was also observed in the course of this work that in many instances solutions using more than 10 points would not always converge. The observed convergence difficulties were linked to the momentum balance. Under some conditions the calaculated pressures would diverge creating numerical errors in the results. The program entered a loop

Table 3.1: Comparison of Axial Cup-mixed Concentrations and Temperatures for Different Radial Grid Sizes: Finite Difference Method

	$N = 10$		$N = 20$		$N = 40$		$N = 60$	
z'	$\langle x \rangle$	$\langle \theta \rangle$	$\langle x \rangle$	$\langle \theta \rangle$	$\langle x \rangle$	$\langle \theta \rangle$	$\langle x \rangle$	$\langle \theta \rangle$
.1	.8166	.0180	.8161	.0191	.8159	.0180	.8157	.0180
.2	.6456	.0342	.6449	.0343	.6446	.0342	.6538	.0334
.3	.4912	.0479	.4961	.0475	.4967	.0475	.4896	.0481
.4	.3590	.0585	.3571	.0587	.3574	.0586	.3574	.0586
.5	.2529	.0654	.2513	.0655	.2516	.0654	.2516	.0654
.6	.1706	.0686	.1688	.0686	.1695	.0685	.1701	.0685

to reduce these errors and would not exit this loop. The cause of this problem was not determined although similar problems have been encountered elsewhere [45].

In both of the examples given above, constant properties were assumed. The momentum balance was not required. In the second example, conditions were chosen to yield some of the larger radial gradients since it was under these conditions that the radial profiles especially should differ for different grid sizes. Upon the introduction of variable physical properties and velocity profile, little difference was observed between solutions using 10 grid points and those in which more grid points were employed.

3.7.1 Radial Discretization using Finite Differences

Central differencing was employed to perform the radial discretization. The radius of the reactor was divided into N intervals–not necessarily of the same size. Finite difference formulas were applied to estimate values of the radial partial derivatives. Simply put, the partial derivatives in the radial direction were written in terms of

finite difference equations such that at an interior radial point r'_j:

$$\left.\frac{\partial y}{\partial r'}\right|_{r'=r'_j} \approx \frac{1}{2}\left(\frac{y_{j+1}-y_j}{\Delta r'_j}+\frac{y_j-y_{j-1}}{\Delta r'_{j-1}}\right) \tag{3.101}$$

For the second derivative the corresponding finite difference equation was:

$$\left.\frac{\partial^2 y}{\partial r'^2}\right|_{r'=r'_j} \approx \frac{2}{(\Delta r'_j+\Delta r'_{j-1})}\left(\frac{y_{j+1}-y_j}{\Delta r'_j}-\frac{y_j-y_{j-1}}{\Delta r'_{j-1}}\right) \tag{3.102}$$

where

$$\Delta r'_j = r'_{j+1}-r'_j \tag{3.103}$$

If all values of $\Delta r'_j$ are equal (equal grid spacing) Equations 3.101 and 3.102 reduce to the usual central differencing formulas.

The above estimates of the radial derivatives were inserted into the species, energy, and momentum equations. The radial derivatives appearing in the functions given by Equations 3.97-3.100 were treated in a similar manner. For the general equation (Equation 3.96) the following finite difference equation was obtained:

$$\begin{aligned} 0 \;=\; & \epsilon_y U_j \left.\frac{dy}{dz'}\right|_j - \left[\frac{(V_j+\alpha_y f_y|_j)}{2\Delta r'_{i-1}} - \alpha_y k'_j f_{r,1}\right] y_{j-1} \\ & + \left[(V_j-\alpha_y f_y|_j) f_{r,3} + \alpha_y k'_j (f_{r,1}+f_{r,2}) + \alpha_y g_y|_j\right] y_j \\ & + \left[\frac{(V_j-\alpha_y f_y|_j)}{2\Delta r'_i} - \alpha_y k'_j f_{r,2}\right] y_{j+1} - \beta_y R_y \end{aligned} \tag{3.104}$$

where

$$f_{r,1} \;=\; -\frac{1}{2r'_j \Delta r'_{j-1}} + \frac{2}{\Delta r'_{j-1}(\Delta r'_j+\Delta r'_{j-1})} \tag{3.105}$$

$$f_{r,2} \;=\; \frac{1}{2r'_j \Delta r'_j} + \frac{2}{\Delta r'_j(\Delta r'_j+\Delta r'_{j-1})} \tag{3.106}$$

$$f_{r,3} \;=\; \frac{1}{2}\left(\frac{1}{\Delta r'_{j-1}} - \frac{1}{\Delta r'_j}\right) \tag{3.107}$$

The boundary conditions were also estimated by finite differences. By applying l'Hôpital's Rule, the indeterminate form at the centerline became:

$$\lim_{r'\to 0}\frac{1}{r'}\frac{\partial y}{\partial r'} = \lim_{r'\to 0}\frac{\partial^2 y}{\partial r'^2} \tag{3.108}$$

Making use of the boundary conditions at the centerline and noting the symmetry of the problem, the corresponding equation became:

$$0 = \epsilon_y U_1 \left.\frac{dy}{dz'}\right|_1 - \left(\frac{4\alpha_y k_1'}{\Delta r_1'^2} + 2\alpha_y k_1' g_y|_{r'=0}\right) y_1 - \frac{4\alpha_y k_1'}{\Delta r_1^2} y_2 - \beta_y R_y \tag{3.109}$$

At the reactor wall, $(j = N+1, r' = 1)$, a backward difference was applied such that;

$$\left.\frac{\partial y}{\partial r'}\right|_{r'=1} \approx \frac{3y_{N+1} - 4y_N + y_{N-1}}{2\Delta r_N} \tag{3.110}$$

Equation 3.110 was then rearranged to yield an expression for y_{N+1}. The particular expression for y_{N+1} depended on the boundary condition at the wall. The expression for y_{N+1} was then substituted into the N^{th} equation represented by Equation 3.104.

In total, N equations for species, N equations for temperature, and N equations for the axial velocity were formed. Each of the equations were put into vector notation to yield a system of equations:

$$\epsilon_y \mathbf{U} \frac{d\mathbf{y}}{dz'} = \mathbf{A}_y \cdot \mathbf{y} + \mathbf{R}_y \tag{3.111}$$

Properties described by integrals such as the cup-mixed concentration and temperature, radial velocity, and the macroscopic continuity equation were estimated using numerical integration techniques. In particular, Simpson's Rule was used to evaluate the cup-mixed properties and macroscopic continuity equation. Values of the radial velocity were calculated using the Trapezoidal Rule. The equations were similar to that given below for the macroscopic continuity equation:

$$\frac{1}{4} = \sum_{j=1}^{N+1} w_j U_j \tag{3.112}$$

3.7.2 Axial Integration using Gear's Method

The central differencing scheme employed caused the matrix $\mathbf{A}_y$ to be tridiagonal. In the Crank-Nicholson method this matrix was combined with the trapezoidal rule as the axial integration step [43,46]. Coupling of the sets of equations occurred

through the nonlinear terms represented by $\mathbf{R}_y$ and the vector $\mathbf{U}$. In earlier solution schemes [8,9,12,15,17] this nonlinearity was handled by using an excessively fine grid in both the radial and axial directions. In this way, each of the sets of equations was solved independently utilizing past values of the other variables in the $\mathbf{R}_y$ and $\mathbf{U}$ terms or updated values if they were available. These approximations were added to the diagonal terms of matrix $\mathbf{A}_y$ or simply as a constant value in the numerical equations.

With complex systems different procedures became necessary. Iteration was required to solve at least some of the equations, particularly the momentum balance. With this iteration, it became useful to examine alternative solution schemes. Gear's method was chosen as the axial integrator for this study. Some of the inherent characteristics made it useful in this respect. These included the Newton-Raphson solution procedure, the variable order, variable step size aspects of the method and its ability to solve stiff systems of equations. Although the routine was not originally intended to solve combined algebraic/differential equations, some modification of the original routine given by Gear [47] allowed for solution of this type of system.

The last point given above was important because the inclusion of the macroscopic continuity equation created a system of combined differential and algebraic equations since, numerically the integration was algebraic in form.

It has been shown by Petzold [45] that Gear's method could diverge under some circumstances due to improper error and step size control. This phenomenon was noted in some of the runs of this study when more than 20 radial points were employed. Under the majority of circumstances encountered in this study the method proved to be efficient and accurate.

3.8 The Computer Program

The computer program was written in double precision. Portions of the program were taken from Gear's DIFSUB program given in Gear [47]. This particular subroutine was adapted to allow for the simultaneous solution of the species, energy,

and momentum balances coupled with the macroscopic continuity equation. Details of the workings of this particular subroutine may be found in Chapter 11 of Gear. A LU decomposition program given in Finlayson was also employed for the solution of the resultant equations [43]. The program was run on the Amdahl 5860 mainframe computer at the University of Ottawa. Run times depended on the complexity of the problem. For simple cases in which the properties were assumed constant the most extreme conditions resulted in run times of approximately 6 cpu seconds. With increasing complexity the run times increased but never exceeded 60 cpu seconds. This compared very favorably with the results reported by Dussault [17] in which the run times were of the order of 150 cpu seconds for a constant property reactor. This was quite a large contrast considering the fact that the program written by Dussault used a single computation at every axial location. The present program required iteration at every axial location until the solution converged. The differences in the run times were the result of the smaller number of radial points used in the present program (10 compared to 100) and the ability of the DIFSUB subroutine to vary the axial spacing. In the method used by Dussault the axial spacing was held constant.

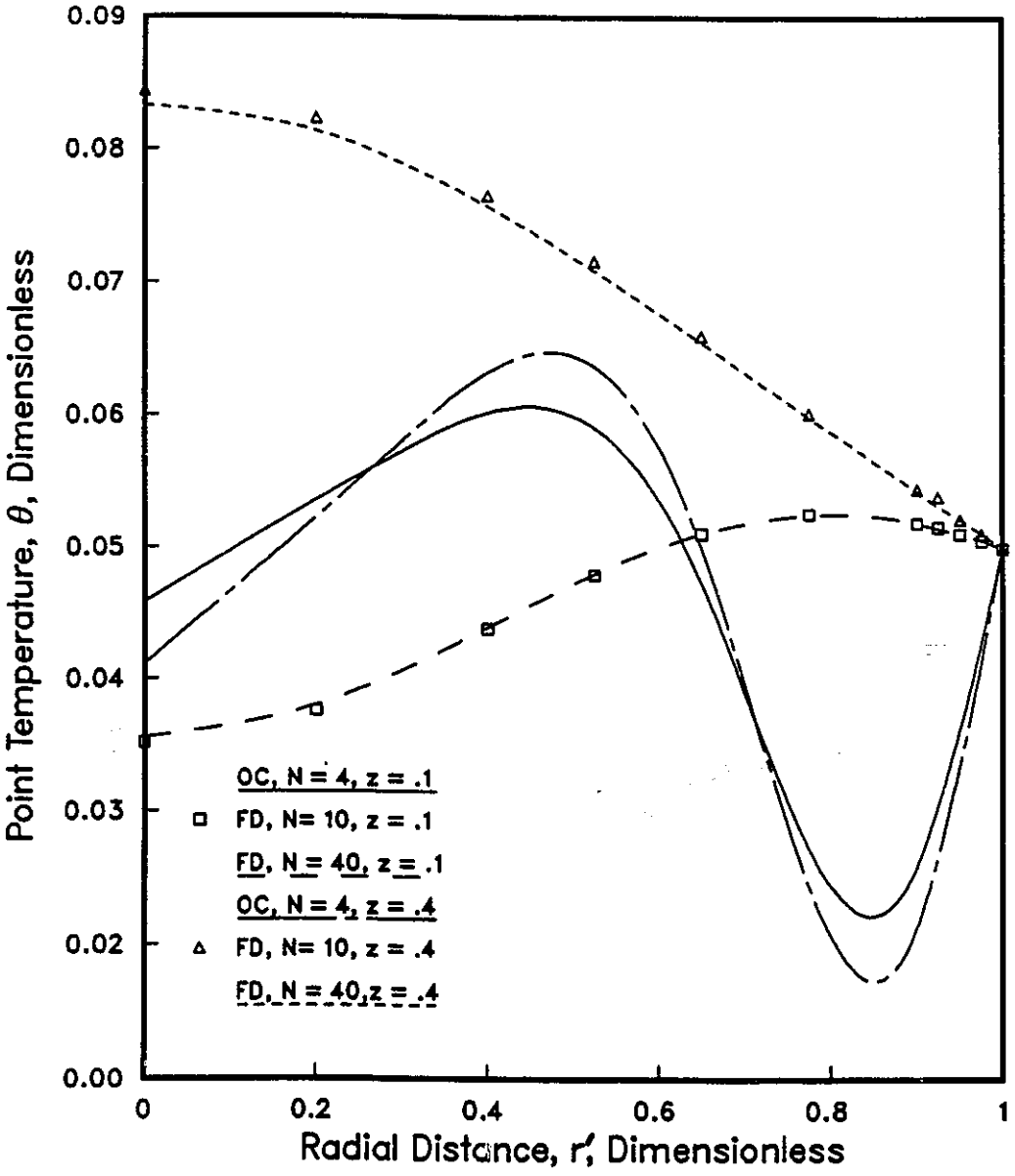

Figure 3.1: Comparison of Numerical Results for a Constant Wall Temperature Reactor: Radial Temperature Profiles

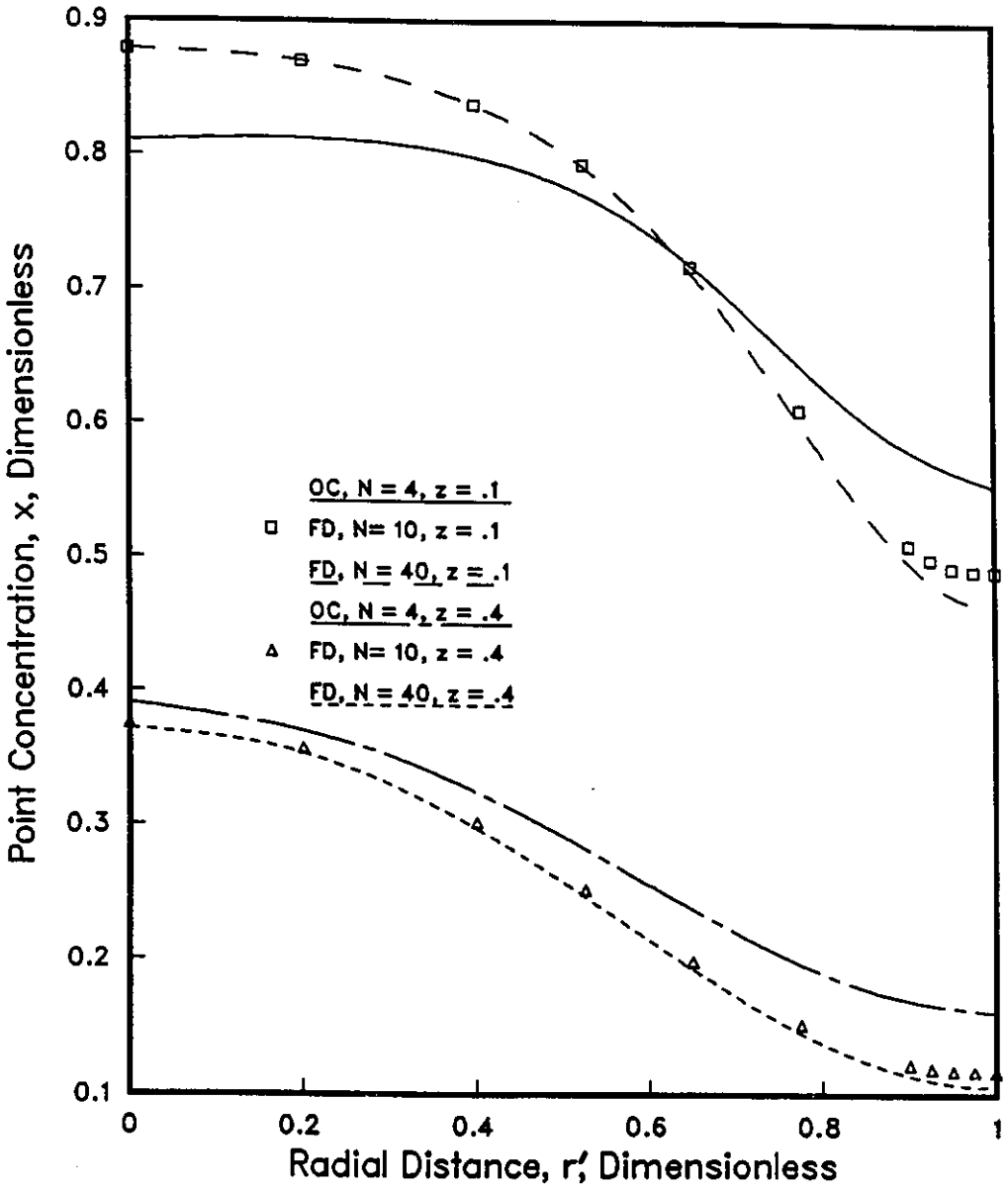

Figure 3.2: Comparison of Numerical Results for a Constant Wall Temperature Reactor: Radial Concentration Profiles

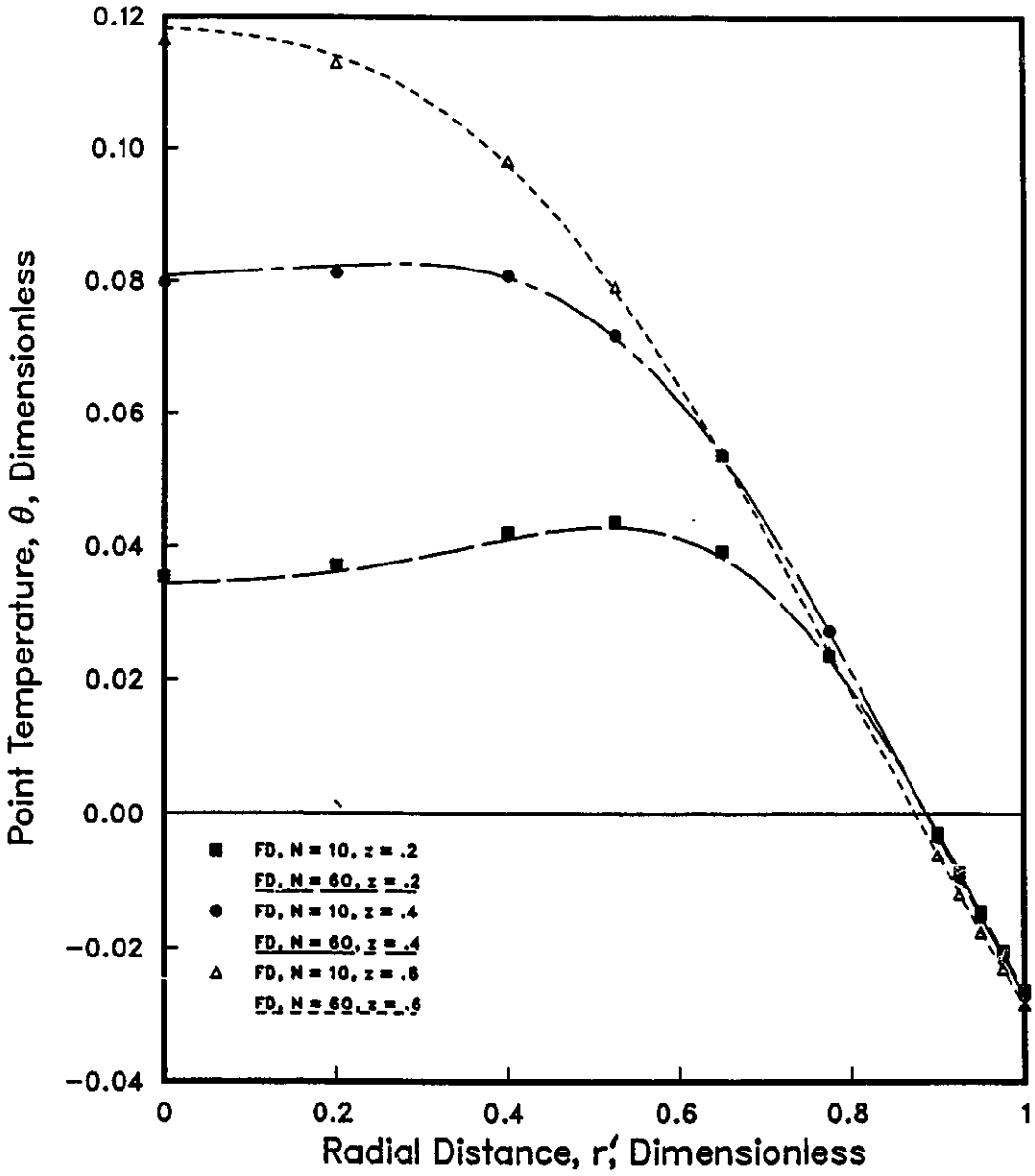

Figure 3.3: Comparison of Finite Difference Results, Wall Heat Transfer, Radial Temperature Profiles

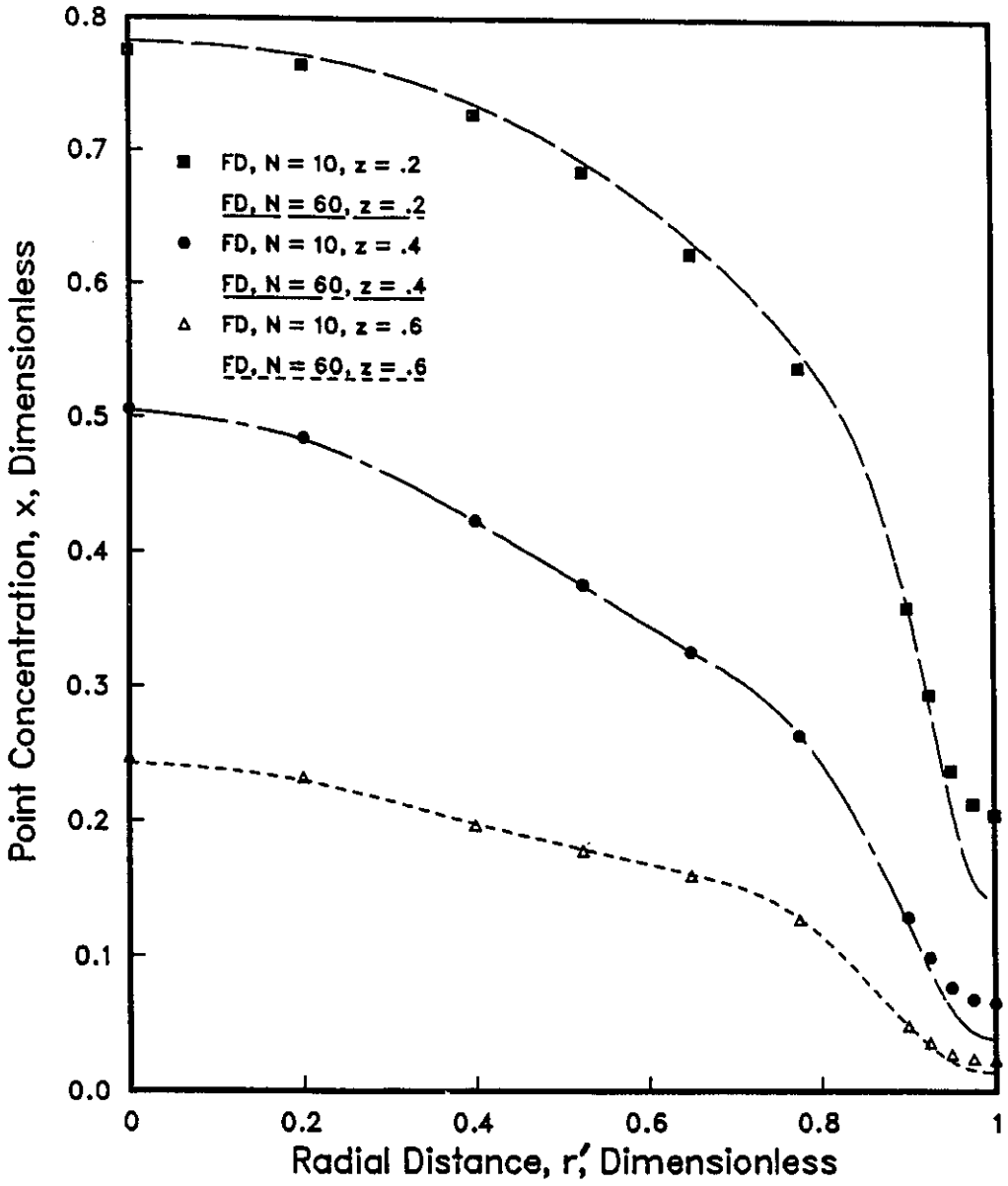

Figure 3.4: Comparison of Finite Difference Results, Wall Heat Transfer, Radial Concentration Profiles

Chapter 4

Numerical Simulation of Flow Reactor Performance

The developed computer model was employed to determine under what conditions physical properties could affect reactor performance. This was accomplished by performing a comprehensive series of computations over a wide range of physical situations.

A simple reaction system was employed in the numerical study. This system consisted of reactant R converting into product P in the presence of an inert medium or solvent I. In all instances it was assumed that one mole of R converted into one mole of P i.e.

$$R + I \rightarrow P + I \tag{4.1}$$

Through increasing the reactant concentrations and decreasing the concentration of inerts in the simulations the behaviour of the reactor for a number of variable physical property situations was examined.

4.1 Factors Determining the Effect of Variable Physical Properties

A number of factors could be expected to affect reactor performance. Initially they were separated into two groups.

Dimensionless Groups The process of reducing the equations to dimensionless form created a number of dimensionless constants. The values of these constants for a particular run were expected to influence the performance of the reactor. Examination of the reactor equations and boundary conditions yielded the following seven dimensionless groups: α_x, α_T, β_T, γ, β_U, Bi, and, θ_c.

Physical Property Changes Changes in concentration and temperature through the reactor could be expected to change the values of the physical properties. The following possibilities were examined:

1. Dilute solutions in which the properties were those of the solvent. In this instance, the physical properties changed with temperature only.
2. Concentrated solutions where compositional effects could also be expected to be significant.

The dimensionless parameters appearing in the balance equations of the laminar flow tubular reactor were important in determining radial and axial temperature and concentration profiles. Because of these differences of temperature and composition the resultant changes in physical properties could also affect the profiles. These differences in physical properties in the reactor could contribute greatly to reactor performance. Because of the large number of parameters involved in the model, factorial design methods were chosen to analyze reactor performance. A large amount of information could be collected using this approach with a relatively small number of runs. The various values of the dimensionless constants used in the study have been given in Table 4.1. Values for the dimensionless parameters were

Table 4.1: The Ranges of the Dimensionless Parameters used in the Theoretical Study

Parameter	Designation	Low Value (-1)	High Value (+1)	Midpoint (0)
α_T	x_1	0.1	10	1
α_x	x_2	0.001	0.1	0.01
Bi	x_3	0.1	10	1
θ_j	x_4	-0.05	0.05	0.0
γ	x_5	13.75	21.25	17.50
β_T	x_6	0.10	0.15	.125
β_U	x_7	0.0	-200	-100

chosen to reflect a wide spectrum of reactor states. These included conditions approaching adiabatic performance and other situations approaching a constant wall temperature. Conditions between these extremes were also generated.

The values given in Table 4.1 were representative of values encountered in the literature for previous theoretical and experimental studies. They were also chosen to minimize the computational time required as much as possible. The values given for β_U were lower than what could be expected in practice but higher values resulted in convergence difficulties or large run times. The sign associated with β_U implied a vertical reactor in upward flow. When any results indicated that free convection was important, the runs were repeated with a positive value of β_U to determine whether flow direction had a significant effect.

For the temperature dependent property study the reactor performance was examined for three different reaction media. These were water, ethanol, and benzene. Models for the physical properties of these substances were found in Reference [48]. These models were included in the computer program. The chosen models were of

the form given below:

1. Density

$$\rho = AB^{-(1-\frac{T}{C})^{2/7}} \tag{4.2}$$

2. Heat Capacity

$$C_p = A + BT + CT^2 + DT^3 \tag{4.3}$$

3. Viscosity

$$\log \mu = A + \frac{B}{T} + CT + DT^2 \tag{4.4}$$

4. Thermal Conductivity

$$k_c = A + BT + CT^2 \tag{4.5}$$

The temperature dependence of diffusivity was represented by:

$$\frac{D_{ij}\mu}{T} = c \tag{4.6}$$

where c was a constant. Once the diffusivity was reduced to dimensionless form this constant disappeared.

The values of the parameters used are given in Table 4.2.

An inlet temperature (T_o) of 300K was used throughout the study.

Compositional dependence of the physical properties was modelled through the use of simple mixing rules. For density, Amagat's Law was employed. Heat capacity was converted to a molar basis. The mixture heat capacity was then calculated as the mole fraction average value. The viscosity and thermal conductivity of the mixtures were directly evaluated on a mole fraction weighted basis. The diffusivity of the mixtures was assumed to be a function of the viscosity as given above. Although more complex mixing rules could have been employed, the simpler mixing rules allowed for changing compositions without creating computational difficulties.

The effects associated with composition dependent properties were examined using a factorial design. This was accomplished by having the properties vary in different directions as the reaction proceeded. The procedure was as follows:

Table 4.2: Values of the Parameters appearing in the Temperature Dependent Physical Property Equations

	Water			
Property	A	B	C	D
ρ	.3471	.2700	647.4	
C_p	.6741	2.825×10^{-3}	-8.371×10^{-6}	8.601×10^{-9}
μ	-10.73	1828	1.966×10^{-2}	-1.466×10^{-5}
k_c	-9.166×10^{-4}	1.255×10^{-5}	-1.521×10^{-8}	
	Ethanol			
ρ	.2903	.2765	516.3	
C_p	-.3499	9.559×10^{-3}	-3.786×10^{-5}	5.459×10^{-8}
μ	-2.697	700.9	2.682×10^{-3}	-4.917×10^{-6}
k_c	6.28×10^{-4}	-9.188×10^{-7}	5.28×10^{-10}	
	Benzene			
ρ	.3051	.2714	562.1	
C_p	-1.481	1.546×10^{-2}	-4.37×10^{-5}	4.409×10^{-8}
μ	2.003	64.66	-1.105×10^{-2}	9.648×10^{-6}
k_c	4.243×10^{-4}	1.14×10^{-8}	-9.03×10^{-10}	

1. A solution containing 25% reactant and 75% solvent was allowed to react to form a product. At completion, the solution would contain 25% product and 75% solvent.

2. As the reaction proceeded, the physical properties were evaluated from both the temperature and compositional data at a given point. The compositional effects were determined based upon the system properties given in Table 4.3.

From the data given in Table 4.3, the amounts of change in the properties with respect to compositional effects were evaluated and given in Table 4.4. Within the scope of the experimental program, the values given in Table 4.4 represented the amount that the properties would change at 100% conversion. They were either initial or final values depending upon whether a property was increasing or decreasing with conversion in the simulations.

4.2 Factorial Designs for Theoretical Studies

Numerous effects that could occur in the reactor have been discussed in the previous section. These effects were a result of the values of different dimensionless groups and of potential changes in the physical properties. Two different types of reactor were examined in this study. In the first case, heat transfer at the wall was assumed to be occurring. In the second case, an adiabatic reactor was examined. In the adiabatic reactor, the number of dimensionless parameters was decreased since Bi and θ_j were not required. In this way, the effects of the other dimensionless groups could be examined in greater detail.

The values of some of the dimensionless constants were changed in the adiabatic portion of the study. Specifically, the maximum heat of reaction was increased from .15 to .30. Under these conditions it was possible to carry out a more comprehensive investigation of free convection with upward and downward flow being examined. The magnitude of β_U was increased to 400. Simulations assuming that free convection was negligible were also performed.

For the heat transfer study, the number of possible significant variables included

Table 4.3: Hypothetical Properties of the Components for Composition Dependent Reactions

Situation	Solvent (I)	Reactant (R)	Product (P)
Increasing density	Benzene	Ethanol	Water
Decreasing density	Benzene	Water	Ethanol
Increasing heat capacity	Benzene	Ethanol	Water
Decreasing heat capacity	Benzene	Water	Ethanol
Increasing viscosity	Water	Benzene	Ethanol
Decreasing viscosity	Water	Ethanol	Benzene
Increasing conductivity	Benzene	Ethanol	Water
Decreasing viscosity	Water	Ethanol	Benzene
Decreasing viscosity	Water	Ethanol	Benzene
Decreasing conductivity	Benzene	Water	Ethanol

Table 4.4: Amount of Hypothetical Changes in Physical Properties resulting from Changes in Composition

Property	Low Value	High Value
$\rho(g/cm^3)$	.849	.899
$C_p(cal/g\ K)$	.453	.558
$\mu(cp)$	.828	.935
$k_c(\mu cal/s\ cm\ K)$	364	626

seven dimensionless groups and five physical properties. In order to study all 12 of these variables in as comprehensive a manner as possible, a 2^{7-2} fractional factorial design was devised with respect to the dimensionless groups. Additionally, a three level fractional factorial design was employed to alleviate any potential problems resulting from ambiguities that might occur in the regression analysis of the results. The three level design also allowed for the determination of any curvature or quadratic effects in the data. The total number of runs including a center point was 89 with respect to the dimensionless groups.

The two level portion of the design (with variables given in coded form) has been presented in Table 4.5. The three level portion has been given in Table 4.7. With respect to the two level design, the defining relation was:

$$I = x_1x_2x_3x_4x_6 = x_1x_3x_4x_5x_7 = x_2x_5x_6x_7 \tag{4.7}$$

The confounding effects that could have resulted from this defining relationship have been given in Table 4.6. Of particular concern were those second order effects confounded with each other. By including the three level design, it was possible to examine which of these second order interactions was probably the significant one by analyzing the data from this part of the design alone.

The use of factorial designs was based upon the fitting of experimental data to the linear equation:

$$\begin{aligned} y &= \beta_0 + \beta_1x_1 + \beta_2x_2 + \cdots + \beta_px_p \\ &\quad + \beta_{12}x_1x_2 + \beta_{13}x_1x_3 + \cdots + \beta_{p-1,p}x_{p-1}x_p + \cdots + \beta_{1\cdots p}x_1\cdots x_p \end{aligned} \tag{4.8}$$

For p different independent variables, a total of 2^p different pieces of information could conceivably be obtained if a full factorial design was implemented.

The values of the variables were in coded form when evaluating the regression coefficients (β_i). This meant that they were normalized such that the values of the variables were equal to 1 at their maximum and -1 at their minimum. For example, referring to Table 4.1, the maximum value of the heat of reaction term was .15. In terms of the coded variables, the value was 1. For β_T = .1, the coded value was

Table 4.5: Two Level Fractional Factorial Design Points in Coded Form

Run	x_1 ($\log \alpha_T$)	x_2 ($\log \alpha_x$)	x_3 ($\log Bi$)	x_4 (θ_j)	x_5 (γ)	x_6 (β_T)	x_7 (β_U)
1	-1	-1	-1	-1	-1	1	1
2	1	-1	-1	-1	-1	-1	-1
3	-1	1	-1	-1	-1	-1	1
4	1	1	-1	-1	-1	1	-1
5	-1	-1	1	-1	-1	-1	-1
6	1	-1	1	-1	-1	1	1
7	-1	1	1	-1	-1	1	-1
8	1	1	1	-1	-1	-1	1
9	-1	-1	-1	1	-1	-1	-1
10	1	-1	-1	1	-1	1	1
11	-1	1	-1	1	-1	1	-1
12	1	1	-1	1	-1	-1	1
13	-1	-1	1	1	-1	1	1
14	1	-1	1	1	-1	-1	-1
15	-1	1	1	1	-1	-1	1
16	1	1	1	1	-1	1	-1
17	-1	-1	-1	-1	1	1	-1
18	1	-1	-1	-1	1	-1	1
19	-1	1	-1	-1	1	-1	-1
20	1	1	-1	-1	1	1	1
21	-1	-1	1	-1	1	-1	1
22	1	-1	1	-1	1	1	-1
23	-1	1	1	-1	1	1	1
24	1	1	1	-1	1	-1	-1
25	-1	-1	-1	1	1	-1	1
26	1	-1	-1	1	1	1	-1
27	-1	1	-1	1	1	1	1
28	1	1	-1	1	1	-1	-1
29	-1	-1	1	1	1	1	-1
30	1	-1	1	1	1	-1	1
31	-1	1	1	1	1	-1	-1
32	1	1	1	1	1	1	1
33	0	0	0	0	0	0	0

-1. The midpoint was .125 and had the coded value of 0. The coded values for the variables given in Tables 4.5 and 4.7 were evaluated using the logarithms for α_x, α_T, and Bi. The true values were used for the other dimensionless constants.

The formula for the generation of the coded values for an actual variable, X_i, was

$$x_i = \frac{X_i - \overline{X_i}}{1/2 \text{ Range of } X_i} \tag{4.9}$$

The full design discussed above was used to generate data for the following cases:

1. The reactor simulations were run under the assumption of constant physical properties under the conditions given for each run.

2. The runs were repeated for each of the solvent cases discussed above to yield data on temperature dependent physical properties.

The above experimental design was also the basis for the study of the effect of composition dependent physical properties upon reactor performance. This allowed for the direct comparison of all components of the study. To generate data, each of the runs given above was run at 8 different conditions representing the physical properties changing in different ways. In effect, a further fractional factorial design was imposed on each of the different run conditions. This was accomplished by generating the runs such that:

$$I = x_\rho x_{C_p} x_\mu x_{k_c} \tag{4.10}$$

Table 4.6: The Confounding Relationships of the Primary and Second Order Interaction Terms

Variable	Confounded Terms
x_2	$x_5x_6x_7$
x_5	$x_2x_6x_7$
x_7	$x_2x_5x_6$
x_1x_2	$x_3x_4x_6$
x_1x_3	$x_2x_4x_6$, $x_4x_5x_7$
x_1x_4	$x_2x_3x_6$, $x_3x_5x_7$
x_1x_5	$x_3x_4x_7$
x_1x_6	$x_2x_3x_4$
x_1x_7	$x_3x_4x_5$
x_2x_3	$x_1x_4x_6$
x_2x_4	$x_1x_3x_6$
x_2x_5	x_6x_7
x_2x_6	x_5x_7
x_2x_7	x_5x_6
x_3x_4	$x_1x_2x_6$, $x_1x_5x_7$
x_3x_5	$x_1x_4x_7$
x_3x_6	$x_1x_2x_4$
x_3x_7	$x_1x_4x_5$
x_4x_5	$x_1x_3x_7$
x_4x_6	$x_1x_2x_3$
x_4x_7	$x_1x_3x_5$

The respective physical property increased with conversion for a value of 1 and decreased with a value of -1 as shown in Table 4.8. The diffusivity was assumed to be a function of viscosity so its composition dependence was dependent upon the composition dependence of the viscosity.

For the heat transfer reactor, these runs were performed for a first order reaction and a Newtonian fluid. It was felt that although other fluid models and reaction types could have been tested, the major trends that would be established in this study would be applicable to other situations.

4.3 Adiabatic Reactor

The same concepts of the previous section were applied to an adiabatic reactor. When an adiabatic reactor was considered, the number of factors decreased since the conditions of wall heat transfer were predetermined. Because of this, a greater degree of certainty in the effects of the remaining variables was achieved with a minimum of computational effort. In the experimental design for the adiabatic reactor the following approach was taken:

1. A full factorial design in the variables α_T, α_x, γ, and β_T was employed.

2. The characteristics of the adiabatic reactor under the assumption of constant physical properties for both first and second order reactions were determined.

3. First and second order reactions were examined under the conditions of composition dependent properties.

4. Free convection was investigated more fully. The full design was performed under the conditions of upward and downward flow and the assumption of no free convection. The same cases as described earlier for the wall heat transfer reactor were employed for the composition dependencies (Tables 4.2, 4.3, 4.4, and 4.8).

Table 4.7: Three Level Fractional Factorial Design Points in Coded Form

Run	x_1 ($\log \alpha_T$)	x_2 ($\log \alpha_x$)	x_3 ($\log Bi$)	x_4 (θ_j)	x_5 (γ)	x_6 (β_T)	x_7 (β_U)
124.1	-1	-1	0	-1	0	0	0
124.2	1	-1	0	-1	0	0	0
124.3	-1	1	0	-1	0	0	0
124.4	1	1	0	-1	0	0	0
124.5	-1	-1	0	1	0	0	0
124.6	1	-1	0	1	0	0	0
124.7	-1	1	0	1	0	0	0
124.8	1	1	0	1	0	0	0
135.1	-1	0	-1	0	-1	0	0
135.2	1	0	-1	0	-1	0	0
135.3	-1	0	1	0	-1	0	0
135.4	1	0	1	0	-1	0	0
135.5	-1	0	-1	0	1	0	0
135.6	1	0	-1	0	1	0	0
135.7	-1	0	1	0	1	0	0
135.8	1	0	1	0	1	0	0
167.1	-1	0	0	0	0	-1	-1
167.2	1	0	0	0	0	-1	-1
167.3	-1	0	0	0	0	1	-1
167.4	1	0	0	0	0	1	-1
167.5	-1	0	0	0	0	-1	1
167.6	1	0	0	0	0	-1	1
167.7	-1	0	0	0	0	1	1
167.8	1	0	0	0	0	1	1
236.1	0	-1	-1	0	0	-1	0
236.2	0	1	-1	0	0	-1	0
236.3	0	-1	1	0	0	-1	0
236.4	0	1	1	0	0	-1	0
236.5	0	-1	-1	0	0	1	0
236.6	0	1	-1	0	0	1	0
236.7	0	-1	1	0	0	1	0
236.8	0	1	1	0	0	1	0

Table 4.7 Continued

Run	x_1 ($\log \alpha_T$)	x_2 ($\log \alpha_x$)	x_3 ($\log Bi$)	x_4 (θ_j)	x_5 (γ)	x_6 (β_T)	x_7 (β_H)
257.1	0	-1	0	0	-1	0	-1
257.2	0	1	0	0	-1	0	-1
257.3	0	-1	0	0	1	0	-1
257.4	0	1	0	0	1	0	-1
257.5	0	-1	0	0	-1	0	1
257.6	0	1	0	0	-1	0	1
257.7	0	-1	0	0	1	0	1
257.8	0	1	0	0	1	0	1
347.1	0	0	-1	-1	0	0	-1
347.2	0	0	1	-1	0	0	-1
347.3	0	0	-1	1	0	0	-1
347.4	0	0	1	1	0	0	-1
347.5	0	0	-1	-1	0	0	1
347.6	0	0	1	-1	0	0	1
347.7	0	0	-1	1	0	0	1
347.8	0	0	1	1	0	0	1
456.1	0	0	0	-1	-1	-1	0
456.2	0	0	0	1	-1	-1	0
456.3	0	0	0	-1	1	-1	0
456.4	0	0	0	1	1	-1	0
456.5	0	0	0	-1	-1	1	0
456.6	0	0	0	1	-1	1	0
456.7	0	0	0	-1	1	1	0
456.8	0	0	0	1	1	1	0

Table 4.8: The Factorial Design Points for the Composition Dependent Cases

Case	x_ρ	x_{C_p}	x_μ	x_{k_c}
1	-1	-1	-1	-1
2	1	-1	-1	1
3	-1	1	-1	1
4	1	1	-1	-1
5	-1	-1	1	1
6	1	-1	1	-1
7	-1	1	1	-1
8	1	1	1	1

4.4 The Dependent Variables

A large amount of data was obtained in the process of running the simulations. In order to elicit useful information from the data, the following dependent variables were analyzed from the factorial design:

1. For the constant property experiments, the length required to obtain 90% conversion was evaluated. This result was then applied as a reference point for the variable property reactor simulations.

2. The length obtained above was designated as the outlet of the variable property reactor. The conversion obtained at this point was compared with 90% conversion such that:

$$y = \frac{< x >_{nc,90}}{0.1} \tag{4.11}$$

The analysis was also extended to include some characterization of the reactor based upon the type of heat transfer occurring. A clearer understanding of the various mechanisms occurring in the reactor with respect to variable property effects was attained through this analysis.

Chapter 5

Results and Discussion of the Numerical Simulations

5.1 Overview of Experimental Cases and Analyses

The experimental design outlined in the previous chapter was used to investigate the behaviour of the reactor under a number of different conditions. In the first instance, the length of reactor required to achieve 90% conversion assuming constant properties was evaluated. Initially, the analysis was based solely upon the conversion characteristics. Upon examination of the cup-mixed average temperature profiles of the reactor, the analysis was refined to take into consideration the three distinct heat transfer regimes that were subsequently identified.

In the second analysis, temperature dependent physical properties were considered. In carrying out these calculations, the reaction medium was assumed to have the properties of either water, ethanol, or benzene. Each of these systems was analyzed to obtain overall models of the ratio of the conversion assuming physical properties were temperature dependent to that for constant properties.

Multi-component systems were handled in a similar manner. Extensions to the multi-component results were also made. Some of the more interesting results

encountered in these experiments were repeated under the condition of downward rather than upward flow. These results clearly illustrated that the flow direction was important in determining the deviations in conversions, for the cases considered. Comparison of the regression coefficient values and of the parameters for the density term for the two directions showed very clearly the great impact that free convection had in a vertical flow reactor.

Many of the above calculations indicated that an adiabatic reactor or a reactor in which the heat loss was very small had the greatest deviations in conversion. This reactor also had fewer uncertainties associated with its analysis since two terms (Bi and θ_j) were eliminated. Because of this, an adiabatic reactor was investigated under the conditions of upward or downward flow, or without free convection occurring. The results of this aspect of the study were compared in a qualitative manner with the performance of an actual experimental reactor. Additionally, the influence of reaction order was investigated in this part of the study.

In order to compare the effects that the various dimensionless groups and physical properties had upon the reactor performance, the data collected through the factorial designs were evaluated through linear regression. The results of this process included an intercept ($\hat{\beta}_0$), and the parameters that represented the slopes or sensitivity of the dependent variables to the various terms (the $\hat{\beta}$'s given in Equation 4.8 in the preceeding chapter).

By examining the magnitudes of the various slopes or coefficients calculated in this manner the more significant effects could be determined. Through this method those variables that were truly important in affecting the reactor behaviour were discovered. This was particularly useful in determining which variable physical properties should be considered in the modelling of the reactor and the reasons they were significant. The regression analysis was performed on the independent variables in coded form (i.e. -1, 0 and +1). The values of the regression coefficients given in the ensuing tables were those that were calculated for these coded values. The actual parameters represented by these coefficients may be determined by referring to Table 4.1.

In the following discussion reference has been made to a number of different

runs. The conditions corresponding to these runs may be found in Tables 4.5 and 4.7.

The use of factorial design implied that the regression coefficients of a simple linear model were to be determined. From these coefficients, those factors that governed the values of the dependent variable could be discerned. In this study the regression was carried out using the regression functions of the Quattro Pro spreadsheet. It was simple to manipulate these regression results to formulate residuals and prepare residual plots. These plots were valuable instruments in determining the adequacy of the regression models in fitting the data.

Since the data to be analyzed in this study were derived from a deterministic computer simulation, random error could not be calculated using center point data as is frequently done. Consequently, a pure error was estimated as:

$$\hat{\sigma} = \frac{SSR}{n-p} \tag{5.1}$$

The problem with this definition occurred when attempting to employ some quantitative methods of determining lack of fit in the regression models. This was overcome by a method based on the R^2 statistic [49].

R^2 was used by calculating:

$$Q = \frac{R^2/(p)}{(1-R^2)/(n-p-1)} \tag{5.2}$$

The above ratio was compared with the statistic F_{ν_1,ν_2}, where

$$\nu_1 = p \tag{5.3}$$

$$\nu_2 = n-p-1 \tag{5.4}$$

If $Q > F_{\nu_1,\nu_2}$, then the regression was significant. This test was calculated for each of the regression models. The results have been given in Table A.3 in Appendix A. Relevant residual plots for the models have also been included in this appendix.

In the following discussion only those regression coefficients that were determined to be significant have been presented. They have been referred to as either coefficients or parameters in the case of those associated with the initial 7 dimensionless groups. Those coefficients associated with the concentration dependent

physical properties have been referred to as sensitivities when they were examined on an individual run-by-run basis.

5.2 Reactor Performance under the Constant Property Assumption

In this portion of the study, the variables that affected the length required to achieve 90% conversion were determined. Results of the 89 simulations involved in the study, coupled with the calculated values and residuals for plausible models, have been given in Appendix A. It was found that the best model of the overall data included a quadratic term for θ_j.

Before discussing the model, a number of results around the center point of the model will be discussed. In Figure 5.1, the reactor length for 90 % conversion has been given as a function of the coded values of the parameters. The curves for α_T, α_x, and Bi displayed a characteristic 's'-shape suggesting an asymptotic approach to maximum and minimum limiting values. To some degree, this behaviour was examined previously. For example, Bosworth [1] and Cleland and Wilhelm [4] studied the influence of α_x in an isothermal reactor. Similar to the result discussed by Cleland and Wilhelm, the shape of the curve demonstrated the behaviour between the case of no radial mass diffusion and that of infinite mass diffusion. At infinite diffusion, the reactor approached the performance of a plug flow reactor.

The two heat transfer parameters, α_T and Bi, displayed similar qualities. In both cases, identical limits were approached. The high limit for each corresponded to the case of an isothermal reactor. In this case, the reactor approached the inlet temperature, $\theta_j = 0$, since the jacket temperature was the same as the inlet temperature. At the lower values of α_T and Bi, the results approached those of an adiabatic reactor.

It was observed from these two curves that both wall heat transfer and internal heat transfer contributed to a condition approaching the adiabatic reactor. It was also noted that these two variables had a larger influence than that observed for

the mass diffusion term (α_x). In setting up the experimental design, the high and low values for α_T and Bi were chosen such that the steepest part of the curves given in Figure 5.1 were represented. Ideally, the same should have been done for α_x. However, this would have led to some runs in which $\alpha_x > \alpha_T$ which for liquid systems, was not considered physically realistic.

The curves around the center point for γ and β_T were approximately straight and horizontal. This occurred because the center point represented a reactor operating very close to isothermal conditions at the inlet temperature. Under the heat transfer conditions at this point, the heat of reaction was lost through the wall as it was created. Since there was no large temperature change in the reactor at these conditions, the dimensionless activation energy did not play a role. The heat transfer conditions at this point caused the jacket temperature (θ_j) to have a major influence in determining reactor length. This curve displayed an exponential trend. In the design region itself, it was the only parameter to display significant curvature, manifesting itself in a quadratic term from the regression analysis. Under specific conditions the heat of reaction and activation energy could be expected to be significant contributors to reactor behaviour.

The parameter β_{θ} did not affect the length of reactor when the physical properties were assumed constant. It was only a significant variable when a density change occurred.

The parameters that were calculated to be most significant in determining the length of the reactor have been given in Table 5.1. As was suggested by Figure 5.1, the jacket temperature influenced the reactor length to the greatest degree. The significant curvature displayed in the jacket temperature plot was determined in the regression analysis through the presence of the quadratic term in Table 5.1. It was quite clear that the use of the empirical model was limited to the data within the experimental design. Any extrapolation beyond the coded value of +1 could be highly erroneous. Also, the residual plots demonstrated a minor trend for higher values of the reactor length. This was attributed to the true nonlinear behaviour of the system. For the overall design mass transfer was not a significant variable. Previous research has concluded that mass transfer was important in the laminar

Table 5.1: Significant Variables Affecting the 90% Conversion Length assuming Constant Properties

Coefficient (Coded Form)	Coefficient Value	Confidence Interval (2σ)
$\hat{\beta}_0$	0.894	.128
$\hat{\beta}_1$	.580	.098
$\hat{\beta}_3$	.267	.098
$\hat{\beta}_4$	-.689	.098
$\hat{\beta}_{14}$	-.621	.116
$\hat{\beta}_{34}$	-.241	.116
$\hat{\beta}_{45}$	-.158	.116
$\hat{\beta}_{44}$	.351	.161

flow reactor. This was determined explicitly through a term such as α_x (usually under isothermal conditions) or implicitly through the Lewis number (α_T/α_x). The present results clearly indicated that the heat transfer characteristics of the system were the most important factor in determining the reactor's performance.

5.2.1 Heat Transfer Regimes

The heat transfer parameters were found to be significant factors in the performance of the reactor. Because of this it was felt that the degree of heat transfer occurring in the simulations might be significant in establishing the behaviour of the reactor. In the first analysis it was determined that the jacket temperature on the average had more influence in establishing the temperature of the reactor than the heat of reaction. The above observations were made over the full range of data.

It was suspected that the range of data was too large to adequately describe the processes occurring in the reactor in detail. Intuition and theory suggested that the heat of reaction should play a significant role under some circumstances. This also applied to the case of the dimensionless activation energy which had only a minor role when the full data set was examined. A qualitative analysis of the cup-mixed concentration and temperature profiles indicated that a number of different heat transfer situations existed (Figures 5.2 and 5.3).

Runs 456.8 and 25 were both rapid reactions. Up to a high level of conversion, the two temperature profiles were similar. In the case of Run 456.8, the reactor cooled to the jacket temperature, θ_j. On the other hand, Run 25 demonstrated behaviour that was very close to adiabatic, as evidenced by the nearly horizontal component of the temperature profile upon completion of the reaction. In both of these examples, the fact that the cup-mixed temperature profiles went beyond the jacket temperature suggested that the dimensionless heat of reaction, (β_T), should be a significant parameter. This was not reflected in the results given in Table 5.1.

By contrast, Run 22 was an example in which the heat transfer was so rapid that the reactor was operating under effectively isothermal conditions. In this particular case, the reactor operated at a jacket temperature, $\theta_j = -.05$. At this lower temperature, it has been shown in Figure 5.2 that the reaction proceeded comparatively

slowly.

The other examples given in Figures 5.2 and 5.3 reflected average or general behaviour determined from the boundary condition of the energy equation (Equation 3.85). In these instances, the temperature gradually approached the jacket temperature.

An examination of the temperature profiles led to the identification of three types of heat transfer behaviour.

1. High Heat Transfer or Isothermal Regime - Regime 1

2. Medium Heat Transfer Regime - Regime 2

3. Low Heat Transfer or 'Pseudo'-Adiabatic Regime - Regime 3

The third regime has been dubbed 'pseudo'-adiabatic because the runs in this regime yielded results similar to an adiabatic reactor but were not truly adiabatic. To be truly adiabatic, the Biot number should be 0. In the case of the 'pseudo'-adiabatic cases presented here, heat was retained because α_T was low. In essence, the reactor retained heat generated by the reaction due to the fluid being a poor heat transfer medium. The reaction occurred more rapidly than the heat transfer with the surroundings. As a result, the reaction was complete before most of the heat was transferred. Effectively, this resulted in near adiabatic behavior. The dimensionless heat of reaction (β_T), by definition, corresponded to the dimensionless adiabatic temperature rise. In Figure 5.3 the maximum bulk temperature for Run 25 was approximately .125. The conditions for run 25 given in Table 4.5 indicated that the maximum temperature for the run should be .1. However, θ_j for this run was .05, suggesting that initially some heat was gained through the wall.

Upon identification of the three heat transfer regimes, it was possible to determine which factors influenced the heat transfer and the degree to which they influenced the thermal properties of the reactor. Subsequently, the effect that the thermal conditions had upon the conversion characteristics of the reactor were determined. This again was accomplished through the linear regression procedures outlined above. The regression calculations yielded the model given in Table 5.2.

Table 5.2: Variables That Determine the Heat Transfer Properties in the Reactor

Coefficient (Coded Form)	Coefficient Value	Confidence Interval (2σ)
$\hat{\beta}_0$	2.06	.05
$\hat{\beta}_1$	-.77	.06
$\hat{\beta}_3$	-.23	.06
$\hat{\beta}_4$	.21	.06
$\hat{\beta}_{134}$	-.25	.08

The data have been given in Appendix A.

The experimental values were determined by assigning an appropriate value corresponding to the heat transfer regimes given above. The calculated values were determined from the regression model given in Table 5.2. Overall the model adequately estimated the heat transfer regime for each of the runs. The model has determined quite accurately runs that were best described as lying in areas between the regimes such as Runs 124.6 and 124.3. These two runs had characteristics in between Regimes 1 and 2 and between Regimes 2 and 3 respectively.

Upon the segregation of the runs into different heat transfer regimes, the variables that characterized the reactor in each regime were examined. In this way, a more detailed picture of the reactor performance was developed.

It should be noted that the average condition over the whole range of data was in the medium heat transfer regime. It was also noted that the greatest contributor towards defining the type of heat transfer was the internal heat transfer rate α_T. Because of the great influence exerted by α_T, the vast majority of simulation runs in the high heat transfer area were those in which $\alpha_T = 10$. Conversely, the value of α_T in the low heat transfer regime was almost exclusively 10^{-1}. Because the values of α_T effectively did not change in these regimes, the effect of this particular dimensionless group could not be determined. However it was shown in Figure 5.1 that beyond

the values of the factorial design, α_T had only a minor effect. The present results suggested that rough limits establishing the heat transfer behaviour in the laminar flow reactor could be defined. Basically, for $\alpha_T \geq 10$, isothermal operation could be expected. For $\alpha_T \leq 10^{-1}$ the reactor approached adiabatic behaviour. The internal heat transfer had little influence in determining the reactor length for α_T beyond either of these limits.

5.2.2 Factors Influencing Reactor Performance in the High Heat Transfer Regime

The reactor operated under approximately isothermal conditions at high heat transfer rates. The temperature of the reactor was the jacket temperature under these conditions. The cup-mixed temperature profiles of this regime were typically flat (Figure 5.4). Similarly, the radial temperature profiles of the isothermal regime were effectively flat and at the jacket temperature. In other words, the temperature in the reactor could be considered uniform over most of its length.

Under these conditions, the range of reactor lengths required to attain 90% conversion was large. They varied from .513 for Run 32 to 4.76 for Run 22. The large range in lengths has been illustrated in Figure 5.5. In this figure, a large difference was noted in the conversion levels between Runs 22 and 32. This was the largest range exhibited by any of the heat transfer regimes. A total of 26 simulations were determined to belong to this regime or to have nearly isothermal behaviour (i.e. behaviour lying between Regimes 1 and 2). With the exception of 2 runs, both lying in the transition region between Regimes 1 (high heat transfer) and 2 (medium heat transfer), the value of α_T was 10.

The radial concentration profiles were well defined. The residence time distribution was a major factor in establishing the shape of the profile. In other words, the conversion was greatest at the wall where the velocity was 0, decreasing towards the middle where the velocity was at a maximum. The rate of mass transfer measured by α_x was also important. As may be seen in Figure 5.6 the profiles tended to flatten with an increase in α_x. Each of the profiles were those calculated at a length of

Table 5.3: Significant Variables in the Isothermal Reactor Regime

Coefficient (Coded Form)	Coefficient Value	Confidence Interval (2σ)
$\hat{\beta}_0$	1.362	.246
$\hat{\beta}_2$	-.297	.174
$\hat{\beta}_3$	-.23	.06
$\hat{\beta}_4$	-1.353	.180
$\hat{\beta}_{45}$	-.384	.202
$\hat{\beta}_{44}$	.407	.312

50% of the length required for 90% conversion for each of the respective simulations given. Each of the runs appeared to have reached comparable levels of conversion at this proportionately similar length. The results of the regression analysis indicated that mass transfer had a minor influence in this heat transfer regime (Table 5.3).

Data were collected around a new center point for this regime. For this new center point the value of α_T was set at 10. The effects of the other operating variables were then examined. As may be seen in Figure 5.7, the jacket temperature displayed a similar exponential behaviour to that observed in Figure 5.1. Similarly a quadratic term was calculated in the regression analysis of this regime. This quadratic term has been included in Table 5.3. In a finding similar to that of other researchers [1,4], the mass diffusion term (α_x) was deemed to have an effect on reactor length. As may be seen in Figure 5.7 this effect was minor. It was also evident that the heat of reaction and activation energy were of little importance individually, although the activation energy was important in conjunction with the jacket temperature. (Table 5.3).

The regression analysis was adequate with respect to R^2. Plots of the residuals against the values z_u and $\hat{z}_u$ indicated that the model was also adequate in this respect. In terms of the residuals plotted against the actual simulated lengths, z_u,

Table 5.4: Actual (z_u) and Calculated ($\hat{z}_u$) Reactor Lengths around the Isothermal Regime Center Point ($\alpha_T = 10^1$)

Variable	Value	z_u	$\hat{z}_u$	Confidence Interval (2σ)
$\log \alpha_x$	10^{-3}	1.52	1.65	0.10
$\log \alpha_x$	10^{-1}	1.29	1.06	0.10
$\log Bi$	10^{-1}	0.98	1.01	0.10
$\log Bi$	10^{1}	1.52	1.72	0.10
θ_j	$-.05$	3.67	3.12	0.10
θ_j	.05	0.67	0.42	0.10
center point	–	1.47	1.36	0.09

a slight downward trend was evident with increasing length. This was deemed to be caused by modelling the exponential trend of θ_j by a quadratic.

The response around the center point was estimated using the parameters in Table 5.3. These results have been compared with values obtained from the computer simulation (see Table 5.4). It was suspected that any of the differences were a result of the non-linearities discussed earlier (i.e. 's'-shaped curves).

5.2.3 Factors Influencing Reactor Performance in the Medium Heat Transfer Regime

The influence of internal heat transfer could be determined in this regime since all three values of α_T were present. In all, 48 runs were identified as belonging to this regime or the pertinent transition areas.

The range of lengths required to achieve 90% conversion in this regime was almost as large as that in the isothermal regime (Figure 5.8). The lengths varied from .332 for Run 456.8 to 3.20 for Runs 347.2 and 347.6. Some of the different cup

- mixed temperature profiles encountered in the medium heat transfer regime have been shown in Figure 5.9. A feature common to all of these runs was the gradual approach of the cup-mixed temperature to the jacket temperature. This was either a monotonic approach, such as that displayed by Run 347.2, or with a maximum occurring in the curve, such as displayed by Runs 456.8 and 257.2. This latter behaviour was typical of an exothermic reaction. Each of these simulations had different jacket temperatures so that they were each approaching different values. Run 347.2 had a jacket temperature less than the inlet temperature, Run 456.8 had a jacket temperature greater than the inlet whereas, the jacket temperature for Run 257.2 was equal to the inlet temperature. These differences resulted in the different cup-mixed profiles given in Figure 5.9 In all cases, the curves were not as abrupt as those exhibited by the isothermal results given earlier. The speed at which this approach occurred was a significant factor in determining the reactor performance. To some degree it was also the determining factor in assigning a given simulation to this regime.

Since heat transfer played a tangible role in this regime, radial temperature profiles became well defined. Some of the different types of behaviour of the radial temperature profiles have been given in Figures 5.10, 5.11, and 5.12.

The radial temperature profiles for Run 347.2 have been given in Figure 5.10. Over the length of the reactor, the wall temperature was nearly constant with the maximum temperature always occurring at the center line. In this example Bi was high.

The behaviour of Run 456.8 given in Figure 5.11 was different. Initially , the maximum temperature occurred near the wall. As the reaction proceeded the temperature increased and the maximum temperature moved towards the center line of the reactor. The dimensionless heat of reaction, β_T, was higher for this run than it was for the other 2 runs presented in this section. This was likely the cause for the different behaviour of the temperature profiles in this case.

As shown in Figure 5.12, the maximum temperature was always at the center line for Run 257.2. Unlike the results for Run 347.2 the wall temperature was not constant. Also the cup-mixed temperature in the reactor went through a maximum

value in this example. This run differed from Run 347.2 in that Bi had a lower value. Therefore, heat did not leave the reactor as rapidly in this simulation.

The radial concentration profiles had varying degrees of steepness similar to those for the isothermal regime (Figure 5.13). Unlike the isothermal regime however the cause of these different profiles was not completely due to mass transfer or residence time. Each of the profiles given in Figure 5.13 was calculated at the same proportionate length. As may be seen from the figure the degree of conversion was significantly less for Run 456.8, and the profile for this simulation was much more pronounced. Although the other two simulations had different values of α_x, they had similar profiles and extents of conversion.

The significant parameters calculated by the regression analysis have been given in Table 5.5. In this regime, α_T was found to be a significant variable. Similar to the behavior in the isothermal regime, the jacket temperature was found to be significant. Unlike the behavior in the isothermal regime, the heat of reaction was also important. The last two observations were important in that the purpose of cooling the reactor would be for the removal of excess heat created by the reaction. Up to this point, the heat of reaction had not been determined to be a significant factor.

Mass transfer was not significant in this regime. This was also found to be true when the full data set was analyzed. This observation suggested that heat transfer factors were of much greater importance than the mass transfer factors.

All of the statistical quantities indicated that the model adequately fitted the data. The coefficient of determination, R^2, had a value of .901, indicating a high degree of correlation between the reactor length and the dimensionless parameters. Also, the intercept $\hat{\beta}_0$ was close to the data center point (.828 and .826 respectively).

Comparison of the values obtained for $\hat{\beta}_4$ and $\hat{\beta}_{44}$ in this regime with those in the high heat transfer regime demonstrated that the reactor was less sensitive to the jacket temperature. The interaction terms $\hat{\beta}_{14}$ and $\hat{\beta}_{34}$ illustrated that the influence of the jacket temperature was highly dependent upon the internal and wall heat transfer rates.

Calculated results around the center point were in good agreement with those

Table 5.5: Significant Variables in the Medium Heat Transfer Reactor Regime

Coefficient (Coded Form)	Coefficient Value	Confidence Interval (2σ)
$\hat{\beta}_0$	.828	.114
$\hat{\beta}_1$	.870	.174
$\hat{\beta}_3$	.467	.108
$\hat{\beta}_4$	-.693	.118
$\hat{\beta}_6$	-.129	.096
$\hat{\beta}_{11}$	.525	.448
$\hat{\beta}_{44}$	.440	.164
$\hat{\beta}_{13}$	.588	.334
$\hat{\beta}_{14}$	-1.203	.400
$\hat{\beta}_{34}$	- .641	.083

Table 5.6: Actual (z_u) and Calculated ($\hat{z}_u$) Reactor Lengths around the Medium Heat Transfer Regime Center Point

Variable	Value	z_u	$\hat{z}_u$	Confidence Interval (2σ)
α_T	10^{-1}	0.54	0.49	0.45
α_T	10^{1}	1.46	2.22	0.45
Bi	10^{-1}	0.52	0.36	0.16
Bi	10^{1}	1.22	1.30	0.16
θ_j	$-.05$	2.13	1.96	0.16
θ_j	.05	0.50	0.58	0.16
β_T	.10	0.97	0.96	0.15
β_T	.15	0.67	0.70	0.15
center point	-	0.83	0.83	0.11

determined from the computer simulation (Table 5.6). Typical 's'-shaped curves should be expected for those pertinent variables if runs outside of the design region were to be explored.

5.2.4 Factors Influencing Reactor Performance in the Low Heat Transfer Regime

The runs of this regime gave results that approached adiabatic behaviour due to poor heat transfer within the reactor. This contrasted with the usual adiabatic condition resulting from $Bi = 0$. Examination of the runs that comprised this regime indicated that the majority of them had α_T equal to 10^{-1}. The two exceptions had $\alpha_T = 1$ and $Bi = 0.1$, which approached the true adiabatic state mentioned above. These two runs were actually calculated to belong to the transition area between

the low and medium heat transfer regimes and were included in the analyses of both regimes.

Comparisons between the state represented by the runs of this regime and true adiabatic runs have been illustrated in Figures 5.14 and 5.15. As can be seen from these two figures, the correspondence between the two cases was evident. This correspondence extended to the radial profiles as well.

Radial temperature profiles for some representative runs of this regime have been given in Figure 5.16. Little difference between the radial profiles for these runs and the corresponding adiabatic runs was evident. The radial temperature profiles also displayed a certain amount of diversity in their shape. Some of the profiles were similar to those encountered in the medium heat transfer regime. For example, at smaller reactor lengths the shapes of the curves shown for Runs 9 and 25 were not much different from those of Figure 5.11. On the other hand, the radial temperature profile for Run 27 was quite pronounced, with the maximum appearing close to the wall. The maximum temperature remained close to the wall over the entire reactor length in this example. In most other instances, the maximum temperature eventually moved towards the center line.

The concentration profiles were similar to those encountered previously. Again, the residence time was a primary factor in establishing this profile. Temperature also played a large role. As may be seen in Figure 5.17, although Run 27 had the higher rate of mass transfer, the concentration gradient was greatest for this simulation. The only discernible differences in the conditions of Run 27 and the other two runs illustrated in Figures 5.16 and 5.17 were that Run 27 was operating at a higher heat of reaction and higher mass transfer. It was already determined that mass transfer should not have a significant effect in liquid systems. The differences observed in the concentration profiles were therefore concluded to be a function of the heat of reaction and residence time.

As may be seen in Table 5.7, the two major variables affecting length were the activation energy (γ) and the heat of reaction (β_T). The fact that some heat transfer through the wall was taking place appeared through the presence of the Bi term. The small range of lengths in this regime (.342 for Run 27 to .764 for Run 9) was

Table 5.7: Significant Variables in the Low Heat Transfer Reactor Regime

Coefficient (Coded Form)	Coefficient Value	Confidence Interval (2σ)
$\hat{\beta}_0$	.545	.012
$\hat{\beta}_3$	.019	.015
$\hat{\beta}_5$	-.106	.015
$\hat{\beta}_6$	-.086	.015

reflected in the small values for the coefficients in Table 5.7. The appearance of the heat of reaction and activation energy in this regime as important variables was not surprising. Without an appreciable amount of heat transfer taking place the heat generated by the reaction accelerated the rate of reaction. The magnitude of this acceleration was determined by the activation energy.

The results around the center point, presented in Table 5.8, showed excellent agreement between the results calculated from the model and the computer simulation. The excellent fit was further reflected in R^2 which had a value of .935. The pertinent residual plots also did not exhibit any trends.

In Figure 5.18 the influences of the activation energy and the heat of reaction were evident, as was the exponential nature of their curves. As may be seen, the influence of the jacket temperature was minimal. An interesting phenomenon was observed in the curve of α_x. Beyond the factorial design region with increasing α_x there was a sudden drop in the required reactor length. For decreasing values of α_x the curve flattened. It was mentioned earlier that the value of α_x should be much lower than that of α_T for liquid systems. Keeping this fact in mind it was therefore concluded that in a real system there would not be the large drop off such as that found in the numerical simulations. For this study at this particular point the value of α_T was 10^{-1}. Those runs at the high end of the values for α_x were either equal to or greater than 10^{-1}.

The results for a true adiabatic reactor have been given in Table 5.9 to compare

Table 5.8: Actual (z_u) and Calculated ($\hat{z}_u$) Reactor Lengths around the Low Heat Transfer Regime Center Point

Variable	Value	z_u	$\hat{z}_u$	Confidence Interval (2σ)
Bi	10^{-1}	0.52	0.53	0.052
Bi	10^{1}	0.60	0.57	0.052
γ	13.75	0.67	0.65	0.047
γ	21.25	0.44	0.44	0.047
β_T	.10	0.65	0.63	0.047
β_T	.15	0.45	0.49	0.047
center point	–	0.54	0.55	0.030

with those for the low heat transfer regime. The coefficient for the activation energy was almost identical in both cases. The range in both cases was the same – extending from $\gamma = 13.75$ to $\gamma = 21.25$. On the other hand, the value of the coefficient associated with the heat of reaction in the adiabatic reactor was greater than that for the low heat transfer regime. This was in part due to the differences in the ranges employed in each instance. For the adiabatic reactor the heat of reaction ranged from .1 to .3 instead of .1 to .15 as was the case for the bulk of the work. Since the range of the heat of reaction term was larger, it followed that the coefficient should be greater, as was observed in the results. The larger range for the heat of reaction also contributed to a smaller value of $\hat{\beta}_0$ since the lengths were smaller at the higher heat of reaction value.

The effect of internal heat transfer, α_T, could be determined for the adiabatic reactor since it could vary in this case. It was found to be an insignificant variable indicating that the internal structure of the reactor temperature was not important in determining the length of the reactor. Coupling this information with that given earlier suggested that lower values of α_T (i.e. $\alpha_T < .1$) would not affect reactor

Table 5.9: Significant Variables in the Adiabatic Reactor

Coefficient (Coded Form)	Coefficient Value	Confidence Interval (2σ)
$\hat{\beta}_0$	.411	.013
$\hat{\beta}_5$	-.084	.013
$\hat{\beta}_6$	-.203	.013
$\hat{\beta}_{56}$	.022	.013

length while higher values of α_T would move the reactor into the medium heat transfer regime (Table 5.2).

5.3 Reactor Performance: Temperature Dependent Properties

To measure the differences between the reactor under the assumption of constant properties and temperature dependent properties, the ratio of the concentration assuming variable physical properties at the reactor length for 90% conversion assuming constant properties to the 90% conversion level was employed (Equation 4.11). The same factorial design points were applied assuming that the system had the properties of either water, ethanol, or benzene. It was found that overall, the type of medium did not greatly affect the results. Differences lay in some of the magnitudes of the regression coefficients from one to the other but many of the same terms appeared for each case examined.

5.3.1 Analysis for the Entire Factorial Design

Similar to some of the observations made earlier for the constant property reactor, the analysis for all 89 simulations tended to dampen any major conclusions regarding reactor behaviour. This was initially reflected in the values of R^2 for the ethanol

and benzene results. Additionally, a qualitative examination of the data suggested some very clear trends regarding the effect of physical properties which were not reflected in the results of the regression analysis.

In Figure 5.19 the deviations from the constant property reactor have been plotted as a function of the dimensionless groups with water as the medium. It was immediately evident that the jacket temperature had the greatest influence around the center point. It was also worth noting that α_x displayed considerable influence at coded values greater than 1. At values less than -1, α_x no longer had an effect. Based on the notion that the Lewis number for a liquid system was approximately 10 or greater and that at the center point the value of α_T was 10, the Lewis number for coded values of α_x less than 1 represented values of the Lewis number that were not applicable to a liquid system. The more realistic areas for a liquid were those values in which α_x displayed little or no effect.

Another aspect of importance illustrated in Figure 5.19 was the fact that a number of the curves displayed an 's'-shape similar to the characteristics of the curves of length as a function of the dimensionless groups. In particular the effects of α_T and Bi were indicative of this behaviour. These two curves tended towards a deviation of $y = 1$ as they increased. Intuitively this would be expected due to the fact that as they increased the rate of heat loss through the wall increased and therefore no change in temperature was experienced in the reactor. Without a change in temperature there was no change in the values of the physical properties. The influence of β_u appeared to be linear in the region of the design, but one would expect that this curve would tend towards upper and lower limits over a wider range, for example, the flow within the reactor would not entirely cease due to free convection. In a plot to be shown later it will be seen that the deviations in one direction tended to yield results similar to a plug flow reactor.

With respect to the individual media, the regression results have been presented in Tables 5.11, 5.12, and 5.13. In terms of some of the statistical tests, only the water system yielded highly acceptable results with respect to R^2. All of the systems were deficient in the residual plots. Definite downward trends were observed in the plot of the residuals against the experimental values. Although some lack of fit

was observed, many of the same parameters were calculated as being significant. In particular the values of a number of the parameters were similar. This was especially evident in those interaction terms involving α_T (x_4). In each of the media these interaction terms yielded similar values in both magnitude and sign. The other significant parameters common to all of the systems behaved in a similar manner. A difference was observed in the value of $\hat{\beta}_0$. For water the variable properties tended to accelerate the reaction, whereas for ethanol and benzene the reaction proceeded more slowly than it did when the properties were assumed constant.

Overall, the water data yielded the greatest range in results. The greatest deviations between the runs using constant properties and those using temperature dependent properties were observed for Run 11 for all of the media. The ratio y was less than 1 for this simulation, which indicated that the reaction proceeded more rapidly when the physical properties changed. The values ranged from .517 for water to .628 for benzene. The largest ratios were observed for Run 23 for water, Run 13 for benzene (1.148 and 1.193 respectively) and Run 135.7 for ethanol (1.222). The ranges of data for each of the media may be seen in Table 5.10

The parameter values derived from the regression analysis were all comparable in size. This suggested that no one dimensionless group was particularly influential in determining reactor performance. The presence of the interaction terms associated with α_T suggested that the rate of internal heat transfer was important in determining whether physical property changes were necessary in evaluating reactor performance. It was previously found that this dimensionless group was very important in establishing the temperature and heat transfer characteristics in the reactor. Its presence in all of the medium models - especially in the interaction terms - suggested that the internal heat transfer was a very important factor. The value of $\hat{\beta}_{13}$ was among the largest in magnitude for all of the systems. This interaction term consisted of the two groups that were most important in establishing the heat transfer characteristics of the reactor (i.e. α_T and Bi). Along with the jacket temperature they were also important in determining the temperature of the reactor. In all of the systems the significance of free convection was governed by the internal heat transfer rate. Examination of the data indicated that free convection

Table 5.10: Minimum and Maximum Deviations for Each Heat Transfer Regime

Solvent	Minimum (Run)	Maximum (Run)
High Heat Transfer Regime		
Water	.932 (347.6)	1.002 (8)
Ethanol	.948 (32)	1.043 (8)
Benzene	.942 (347.6)	1.035 (8)
Medium Heat Transfer Regime		
Water	.843 (124.3)	1.148 (23)
Ethanol	.898 (23)	1.222 (135.7)
Benzene	.892 (23)	1.139 (135.7)
Low Heat Transfer Regime		
Water	.517 (11)	1.132 (135.7)
Ethanol	.559 (11)	1.222 (135.7)
Benzene	.628 (11)	1.193 (13)

had its greatest effect when $\alpha_T = 10^{-1}$. It was also observed that free convection and the subsequent velocity changes were the most significant factor governing the deviations caused by physical property changes. Only one example was observed (Run 27) in which free convection did not contribute greatly to the deviations.

In summary, when examined in an overall context it was difficult to determine which properties and to what degree these changing properties affected reactor performance. Upon qualitative examination of the data it was clear that the most significant contribution was due to free convection. Free convection was observed to be significant only when $\alpha_T = 10^{-1}$. All of the observations were consistent when it was considered that heat retention was important in creating the temperature differences required to change the values of the physical properties.

Table 5.11: Significant Parameters when Water was the Medium

Coefficient (Coded Form)	Coefficient Value	Confidence Interval (2σ)
$\hat{\beta}_0$	.972	.024
$\hat{\beta}_1$	.040	.016
$\hat{\beta}_2$	-.035	.016
$\hat{\beta}_3$	-.052	.016
$\hat{\beta}_4$	-.030	.016
$\hat{\beta}_7$	.022	.016
$\hat{\beta}_{12}$	.032	.018
$\hat{\beta}_{13}$	-.057	.018
$\hat{\beta}_{17}$	-.027	.018
$\hat{\beta}_{24}$	-.028	.018
$\hat{\beta}_{67}$	.023	.018
$\hat{\beta}_{11}$	-.047	.026
$\hat{\beta}_{55}$	.030	.026

Table 5.12: Significant Parameters when Ethanol was the Medium

Coefficient (Coded Form)	Coefficient Value	Confidence Interval (2σ)
$\hat{\beta}_0$	1.017	.024
$\hat{\beta}_2$	-.045	.018
$\hat{\beta}_3$	.028	.018
$\hat{\beta}_{12}$	.043	.022
$\hat{\beta}_{13}$	-.044	.022
$\hat{\beta}_{17}$	-.024	.022
$\hat{\beta}_{24}$	-.023	.022
$\hat{\beta}_{22}$	-.041	.030

Table 5.13: Significant Parameters when Benzene was the Medium

Coefficient (Coded Form)	Coefficient Value	Confidence Interval (2σ)
$\hat{\beta}_0$	1.013	.022
$\hat{\beta}_1$	.018	.018
$\hat{\beta}_2$	-.033	.018
$\hat{\beta}_7$	.021	.018
$\hat{\beta}_{12}$	.029	.018
$\hat{\beta}_{13}$	-.032	.020
$\hat{\beta}_{17}$	-.030	.020
$\hat{\beta}_{67}$	.022	.020
$\hat{\beta}_{22}$	-.037	.028

5.3.2 High Heat Transfer and Temperature Dependent Properties

It was immediately observed that the range of data in the high heat transfer regime was small for all of the media (Table 5.10). The small range manifested itself in the resultant regression analyses (Tables 5.14, 5.15, and 5.16). None of the significant parameters were large in magnitude. Of importance was the fact that each medium yielded similar results. The same parameters appeared in all models. The values of R^2 were all low suggesting that there was only a small degree of correlation between the dependent and independent variables.

Not surprisingly, the terms that contributed to deviations between non-constant properties and constant properties were those associated with establishing the temperature within the reactor. Of particular importance was the interaction term of θ_j and Bi. As was previously discussed, the heat transfer rate was sufficiently high for these runs that the reactor operated at the jacket temperature. If the jacket temperature was different from the inlet temperature, then the properties would change in the reactor. The presence of the terms that included the wall heat transfer and the heat of reaction were indicative of these terms contributing to the speed at which the reactor achieved the jacket temperature. These were perhaps indicative of the sensitivity of the reactor to minute differences in local concentration and temperature. These differences were not large enough to greatly affect the overall behaviour of the reactor.

The various profiles in this regime showed only small differences in the curves between the constant and variable property cases. None of the examples showed any large deviation in the velocity profiles, which indicated that neither free convection nor viscosity changes were factors. It was suspected that a variable viscosity would only become important in instances in which a steep radial temperature profile was encountered.

Table 5.14: Significant Parameters for the High Heat Transfer Regime: Water

Coefficient (Coded Form)	Coefficient Value	Confidence Interval (2σ)
$\hat{\beta}_0$	.991	.009
$\hat{\beta}_4$	-.020	.010
$\hat{\beta}_{26}$	-.076	.032
$\hat{\beta}_{34}$	.074	.030
$\hat{\beta}_{36}$	-.021	.012

Table 5.15: Significant Parameters for the High Heat Transfer Regime: Ethanol

Coefficient (Coded Form)	Coefficient Value	Confidence Interval (2σ)
$\hat{\beta}_0$	.990	.009
$\hat{\beta}_4$	-.016	.011
$\hat{\beta}_{26}$	-.047	.033
$\hat{\beta}_{34}$	.050	.031
$\hat{\beta}_{36}$	-.021	.012

Table 5.16: Significant Parameters for the High Heat Transfer Regime: Benzene

Coefficient (Coded Form)	Coefficient Value	Confidence Interval (2σ)
$\hat{\beta}_0$	.997	.009
$\hat{\beta}_{26}$	-.053	.033
$\hat{\beta}_{34}$	.050	.030
$\hat{\beta}_{36}$	-.017	.012

5.3.3 Medium Heat Transfer and Temperature Dependent Properties

In this heat transfer regime, many factors were found to be significant in determining the deviations in reactor performance. There were also differences in the significant interaction terms of some of the dimensionless groups. In all instances free convection had some importance, although its importance was coupled with other terms through interactions. For water, free convection was coupled with the heat of reaction. In the cases of ethanol and benzene the coupling occurred with the internal heat transfer term. In all of the cases, the importance of radial heat transfer was evident. For water, this importance was in terms of interactions with the wall heat transfer and the jacket temperature. For benzene and ethanol the importance of radial heat transfer manifested itself as a first order term and in its interaction with the buoyancy term (Tables 5.17, 5.18, and 5.19).

The range of deviations in the medium heat transfer regime was only slightly greater than that for the isothermal regime. The magnitudes of the regression coefficients in this regime were not significantly larger than those in the isothermal regime. The few that were the cause of the larger overall range were due to operating points intermediate to the medium and low heat transfer regimes.

The importance of free convection in determining reactor performance became clearer in the results of this regime. For free convection to be significant it was found that the internal heat transfer rate needed to be small ($\alpha_T \leq 10^{-1}$). What was not immediately clear was whether the free convection was important due to a more pronounced radial temperature profile or due to the retention of heat in the reactor. Previous studies concluded that free convection was the result of a steep radial temperature gradient [12,13,14]. Results of this study indicated that it was more likely due to overall retention of heat and the resultant axial temperature gradients.

Table 5.17: Significant Parameters for the Medium Heat Transfer Regime: Water

Coefficient (Coded Form)	Coefficient Value	Confidence Interval (2σ)
$\hat{\beta}_0$	1.016	.020
$\hat{\beta}_2$	-.033	.017
$\hat{\beta}_3$	.045	.017
$\hat{\beta}_{13}$	-.109	.041
$\hat{\beta}_{14}$	-.051	.036
$\hat{\beta}_{67}$	.032	.031
$\hat{\beta}_{33}$	-.064	.030

Table 5.18: Significant Parameters for the Medium Heat Transfer Regime: Ethanol

Coefficient (Coded Form)	Coefficient Value	Confidence Interval (2σ)
$\hat{\beta}_0$	0.992	.020
$\hat{\beta}_1$	-.050	.017
$\hat{\beta}_2$	-.040	.017
$\hat{\beta}_{17}$	.039	.032
$\hat{\beta}_{45}$	.025	.023
$\hat{\beta}_{55}$	.044	.026

Table 5.19: Significant Parameters for the Medium Heat Transfer Regime: Benzene

Coefficient (Coded Form)	Coefficient Value	Confidence Interval (2σ)
$\hat{\beta}_0$	0.991	.016
$\hat{\beta}_1$	-.029	.018
$\hat{\beta}_2$	-.036	.014
$\hat{\beta}_{12}$	.028	.021
$\hat{\beta}_{17}$	.027	.026
$\hat{\beta}_{55}$	.040	.021

5.3.4 Low Heat Transfer and Temperature Dependent Properties

Although some significant effects were determined in the other regimes the magnitude of these effects were small. Very little deviation occurred between the results for a constant and non-constant property reactor. This was due to the fact that very little heat was retained in the reactor. Because of this the temperature dependent properties did not experience an appreciable change.

Most of the coefficients calculated for the previous models were not of the type that would indicate that variations in the physical properties would have a significant effect in reactor performance. One of the most significant factors in determining the length of the reactor in the high and medium heat transfer regimes was the jacket temperature. Although this was the temperature eventually attained by the reactor, it was not affected by the physical properties since it was an external influence on reactor performance. Many of the other dimensionless constants that were significant in determining reactor performance were evaluated over at least two orders of magnitude. A local value of some of the dimensionless parameters

such as $k'_r \alpha_T$, could be considered. This particular term was the product of the dimensionless thermal conductivity that varied in the reactor and the dimensionless radial heat dispersion term that was a function of initial conditions. The term made up of the product of the two should affect reactor behaviour much as the constant dimensionless group did. In other words, if the dimensionless thermal conductivity or mass diffusivity were varying over the length of the reactor then one could expect some changes in reactor performance. However, reactor length was found to be a function of the pertinent dimensionless groups only when these groups (α_x and α_T) were examined over several orders of magnitude. In terms of temperature dependence of the physical properties, the dimensionless properties did not change over that great a range. This indicated that the mechanisms involved relating reactor performance to physical property changes were primarily due to viscosity and density changes and their effect on velocity profile distortions.

One possible exception to the above argument involved the significance of the term α_x. It was found to be significant in several of the previous statistical models. This significance was the result of the observed sensitivity of the reactor to a low Lewis Number. It was shown in Figures 5.1, 5.7, 5.18, and 5.19 that α_x had considerable influence in a range more reflective of a gaseous medium. This effect was also observed in the low heat transfer regime (Figure 5.20). The probable mechanism of this effect was the fact that as temperature increased in the reactor the local values of the Lewis number decreased due to the manner in which the physical properties behaved. Because of this, any simulations that were run at the lower value of Lewis Number were driven into this area of high sensitivity. This was the reason for α_x having such a large influence in the design region. It would seem that from the aforementioned figures that for a liquid system this significance could in large part be ignored, based on the fact that the curves tended to flatten at lower values of α_x.

The velocity profile distortions were most predominant in the low heat transfer regime. Some examples also occurred in the medium heat transfer regime but the magnitude of the effects was not as large. This was previously shown in the results given in Table 5.10. Small effects that might have been the result of some of the

other physical properties were also evident in the low heat transfer regime. This was demonstrated by the different behaviour exhibited by each of the different reaction media given in Tables 5.20, 5.21, and 5.22. The natural tendency for the water results was towards a greater conversion than when the properties were assumed constant ($\hat{\beta}_0 < 1$). On the other hand, the natural tendency for the organic substances was towards a slower rate of conversion ($\hat{\beta}_0 > 1$).

The results of Run 11 showed the greatest amount of deviation. As may be seen in Figures 5.21, 5.22, 5.23, 5.24, and 5.25 many of the characteristics of the reactor were dramatically changed. Of note was the flattening of the velocity profile particularly demonstrated by the water simulation. What was equally important was the resultant flattening of the radial temperature and concentration profiles. The overall effect was that the reactor had characteristics that were very close to those of a plug flow reactor.

Not all of the runs in this regime yielded higher conversions. The exceptions had some differences that were a result of thermal conditions at the wall. In those instances in which $y > 1$, the primary reason was a wall whose temperature was significantly lower than the rest of the reactor. In these instances the radial temperature gradient had the same characteristics that it had when constant porperties were assumed and the reactor velocity profile was elongated rather than compressed. In this manner, the residence time towards the center of the reactor was greater, which consequently decreased conversion.

The significance of free convection was evident in the regression coefficients calculated for this regime (Tables 5.20, 5.21, and 5.22). All of the media tested displayed similar results. The fact that the same parameters were significant for all cases suggested that the same types of mechanisms applied to each of the media. A main cause of differences between the behaviour of the media might be due to the fact that for water $\hat{\beta}_6$ and $\hat{\beta}_7$ were identical, whereas for the two organic media the value of $\hat{\beta}_6$ was somewhat smaller than $\hat{\beta}_7$. Any of the differences in behaviour could be traced back to the small differences in the behaviour of the physical properties for the given substances.

All of the substances were affected by the heat of reaction in a similar manner.

Table 5.20: Significant Parameters for the Low Heat Transfer Regime: Water

Coefficient (Coded Form)	Coefficient Value	Confidence Interval (2σ)
$\hat{\beta}_0$	0.959	.046
$\hat{\beta}_2$	-.095	.038
$\hat{\beta}_3$	.087	.035
$\hat{\beta}_6$	-.061	.037
$\hat{\beta}_7$	.060	.034
$\hat{\beta}_{22}$	-.098	.058

The results for water appeared to indicate that the heat of reaction was as important as the buoyancy term. Presumably, there was a larger density decrease with the greater heat of reaction, such that the velocity profile experienced a greater deviation. The sensitivity of the system to the wall heat transfer coefficient was most likely due to small differences in the amount of heat retained in the reactor. These differences would create small differences in the temperature of the reactor such that the effects of viscosity and density would be slightly altered.

The results of this heat transfer regime indicated that the retention of heat was the primary driving force towards the creation of deviations between the constant and non-constant physical property conditions. Although the mechanisms differed slightly from substance to substance, all of the runs in this regime displayed a sensitivity towards the same parameters. Specifically, the presence of free convection was noted as being instrumental in generating the deviations through the formation of velocity profile distortions. This could not be considered a surprising result, since the physical properties were a function of temperature, and hence were changing due to the influence of the heat retention in what was virtually an adiabatic reactor.

Table 5.21: Significant Parameters for the Low Heat Transfer Regime: Ethanol

Coefficient (Coded Form)	Coefficient Value	Confidence Interval (2σ)
$\hat{\beta}_0$	1.044	.044
$\hat{\beta}_2$	-.111	.034
$\hat{\beta}_3$	.078	.034
$\hat{\beta}_6$	-.034	.034
$\hat{\beta}_7$	.073	.032
$\hat{\beta}_{22}$	-.116	.054

Table 5.22: Significant Parameters for the Low Heat Transfer Regime: Benzene

Coefficient (Coded Form)	Coefficient Value	Confidence Interval (2σ)
$\hat{\beta}_0$	1.023	.052
$\hat{\beta}_2$	-.073	.042
$\hat{\beta}_3$	.044	.040
$\hat{\beta}_6$	-.039	.042
$\hat{\beta}_7$	.081	.038
$\hat{\beta}_{22}$	-.100	.064

5.4 Reactor Performance under the Combined Influence of Temperature and Concentration Dependent Physical Properties

In the earlier analyses the reactor performance was evaluated as a function of the dimensionless groups. Basically the performance was a function of the initial conditions occurring in the reactor. Although one might be able to infer that a variable density, for example, should be included in the reactor model due to the important role played by β_U, the role of the other properties was not clear. In this part of the study, the roles of the various properties in each of the heat transfer regimes were determined. Similar to the previous calculations, little was learned from analyzing the full range of data. In other words, a large number of terms were found to be significant such as was noted in Tables 5.1, 5.11, 5.12, and 5.13.

In Table 5.23 the more significant effects for the full data set have been presented. What was immediately noted was that the terms that were previously identified as being important in defining the degree of heat transfer in the reactor were prominent in the results of this particular regression. The internal heat transfer played a prominent role in that it was coupled with a number of terms. It was particularly important in defining the degree of significance played by both density and heat capacity. Its role was most likely attached to its role in defining the various heat transfer regimes. Thermal conductivity was especially significant in its interaction with the wall heat transfer coefficient and with the jacket temperature. This result was interesting in that it suggested that a varying thermal conductivity was most significant in governing the heat transfer with the surroundings. Its role in establishing the temperature profiles in the reactor was less significant. All of the above observations suggested that the roles of varying physical properties were in fact closely tied to the degree of heat transfer occurring in the reactor. It appeared that it would be useful to examine the effects of varying physical properties in each of the regimes.

The factorial design approach employed for examining the concentration dependent properties was useful in that a clearer understanding of the role that variable physical properties had on reactor performance emerged. As a result of using the 'factorial design within a factorial design' implied by the fractional factorial design for the physical properties, the effect of variable physical properties for each of the simulation conditions was determined. This was accomplished by calculating the sensitivity of each of the simulations to variable physical properties individually using the standard linear regression techniques. The values of the regression coefficients (i.e. the $\hat{\beta}_i$'s) calculated through linear regression were indicative of the sensitivity of the reactor to physical properties variations.

In many respects the importance of including a variable physical property in the modelling of the reactor depended very much on the thermal characteristics determined earlier. In hindsight the variations in properties that were determined in this phase of the study could be intuitively included in any reactor modelling situation. For example, a varying heat capacity would not be necessary in an isothermal reactor since the temperature of the reactor would already have been established through some other mechanism. The results of this study confirmed that type of intuitive notion. The question would then become under what circumstances the changes occurring in heat capacity indeed became important.

5.4.1 Reactor Performance with Concentration Dependence in the High Heat Transfer Regime

The sensitivity of the reactor performance continued to be comparatively low in this regime. The deviations ranged from .81 for Run 347.2, Cases 1 and 7 to 1.323 for Run 14, Case 2. (For the conditions defining the Cases given above refer to Table 4.8).

More important than the overall values of the deviations were the deviations that occurred for a given set of simulation conditions (i.e Run 14) for different physical property changes. A difference in conversion of 10% or more could be observed depending on how the physical properties varied for the simulation. The

Table 5.23: Significant Parameters for Composition Dependent Physical Properties

Coefficient (Coded Form)	Coefficient Value	Confidence Interval (2σ)
$\hat{\beta}_0$	1.036	.016
$\hat{\beta}_2$	-.048	.020
$\hat{\beta}_3$	.048	.020
$\hat{\beta}_{12}$	.042	.022
$\hat{\beta}_{13}$	-.095	.022
$\hat{\beta}_{14}$	.064	.022
$\hat{\beta}_\rho$	.131	.016
$\hat{\beta}_{C_p}$	.087	.016
$\hat{\beta}_{k_c}$	.092	.016
$\hat{\beta}_{1\rho}$	-.074	.020
$\hat{\beta}_{7\rho}$	-.108	.020
$\hat{\beta}_{1C_p}$	-.079	.020
$\hat{\beta}_{3C_p}$	-.045	.020
$\hat{\beta}_{3k_c}$	.086	.020
$\hat{\beta}_{4k_c}$	-.045	.020

concentration profiles for constant properties, Case 1, and Case 2 for Run 14 have been given in Figure 5.26.

The manner in which the properties affected the reactor performance in the simulation was not clear from this figure alone. In Figure A.1 given in Appendix A the corresponding cup-mixed temperature profiles have been plotted. As may be seen from this figure, the temperatures did not vary to a large degree for any of the cases. This suggested that the distortion of the velocity profile was most likely involved in the creation of these differences. This was confirmed through the results given in Figure 5.27, in which the centerline velocity has been plotted against axial position. As may be seen, the centerline velocity was greater than 1 for Case 2 and less than 1 for Case 1. As a result conversion for Case 2 was not as large as it was for Case 1. Each of the cases also occurred on different sides of the constant property line given in Figure 5.26. All of the even numbered cases had a behaviour similar to Case 2 (Refer to Table 4.8). Conversely, all of the odd numbered cases were similar to Case 1. The property that was varying consistently in this pattern was the density. In each of the odd numbered cases the density was decreasing with conversion. On the other hand, the density increased with conversion with the even numbered cases.

The concentration profiles for Run 347.2 have been plotted in Figure 5.28. The cup-mixed temperature and center line velocity profiles, Figures A.2 and A.3, have been given in Appendix A. Examination of the cup-mixed temperature profiles and the centerline velocities indicated that the deviations in the concentration profiles were caused by both velocity profile distortions and distortion in the temperature profile. Case 7 had a small deviation in the velocity. The simulation lost heat to the surroundings at a much slower rate than was the case for constant properties. Because of this, the conversion was more rapid than it was for constant properties. For case 8, the velocity profile and heat transfer both contributed to slowing the conversion in the reactor. These results suggested that the thermal conductivity could also be of importance in the high heat transfer regime.

The results given in Table 5.24 illustrated that both varying density and thermal conductivity were of possible significance in the high heat transfer regime. When

the results were examined it was evident that density was important in the presence of the buoyancy term (β_U). Also, thermal conductivity gained significance primarily for those simulations that were calculated as being between the high and medium heat transfer regimes. There were not any instances in which either heat capacity or viscosity were detected as being significant.

Data around the center point for the high heat transfer regime have been plotted in Figure 5.29. These data suggested that, similar to previous discussions, the effects of changing physical properties might tend towards limiting values.

A comparison between the general characteristics of the cup-mixed temperature profiles of the two examples illustrated why thermal conductivity was important for Run 347.2. For Run 14 the reactor reached the isothermal condition almost immediately. For Run 347.2 the approach to the jacket temperature was more gradual. This implied that internal heat transfer was important in the process both when the properties were constant and also when they were varying.

The other results presented in Table 5.24 followed trends similar to the examples. In other words runs such as 124.6 and 124.8 had characteristics similar to 347.2. Most of the other runs behaved in a fashion similar to Run 14. Density was significant only when the buoyancy term β_U was present. This was further illustrated in Table 5.25. The values associated with the density and the interaction between density and β_U were such that if $\beta_U = 0$ then the density effect was effectively nullified.

5.4.2 Reactor Performance with Concentration Dependence in the Medium Heat Transfer Regime

In this regime the influences were more varied. From the results given in Table 5.26 the larger number of influences was evident. Both thermal conductivity and density changes were determined to be important in this regime much as they were in the high heat transfer regime. Variable heat capacity was also determined to be significant. The magnitude of the sensitivity of the reactor to changes in density and thermal conductivity increased compared with the results in the high heat transfer

Table 5.24: Sensitivity of Runs in the High Heat Transfer Regime to Physical Property Changes

Run	$\hat{\beta}_0$	$\hat{\beta}_\rho$	$\hat{\beta}_{C_p}$	$\hat{\beta}_\mu$	$\hat{\beta}_{k_c}$	Calculated Heat Transfer Regime
2	1.034	.121	-.016	.010	.020	1.1
4	1.025	.032	-.031	.014	.016	1.1
6	1.002	.000	-.000	.013	.014	1.1
8	1.049	-.004	.000	.013	.007	1.1
14	1.067	.212	.001	.000	.025	1.0
16	.967	.082	.002	.012	.028	1.0
18	1.001	-.006	-.018	.015	.028	1.1
20	1.014	-.015	-.040	.014	.024	1.1
22	1.002	.076	.003	.038	.012	1.1
24	1.043	.011	.000	.010	.007	1.1
30	0.967	.003	-.004	.023	.063	1.0
32	0.929	.005	.007	.007	.074	1.0
124.2	1.013	.052	-.001	.012	.014	1.1
124.4	1.049	.009	.002	.014	.012	1.1
124.6	0.999	.097	.013	-.003	.042	1.5
124.8	0.950	.052	.004	.011	.049	1.5
135.2	1.051	.088	-.006	.014	.016	1.5
135.4	1.015	.066	.000	.014	.019	1.1
135.6	1.029	.108	.011	.015	.033	1.5
135.8	0.998	.063	-.003	.014	.029	1.1
167.2	1.033	.138	-.002	.011	.022	1.3
167.4	1.042	.141	-.001	.010	.032	1.3
167.6	.993	-.001	-.001	.014	.020	1.3
167.8	0.997	-.002	-.001	.014	.031	1.3
347.2	1.026	.067	-.008	.012	.165	1.6
347.6	1.003	-.003	-.007	.012	.165	1.6

Table 5.25: Significant Effects in the High Heat Transfer Regime for Combined Temperature and Composition Dependent Physical Properties

Coefficient (Coded Form)	Coefficient Value	Confidence Interval (2σ)
$\hat{\beta}_0$	1.007	.008
$\hat{\beta}_4$	-.020	.010
$\hat{\beta}_{24}$	-.019	.010
$\hat{\beta}_\rho$	.053	.008
$\hat{\beta}_{k_c}$	.035	.008
$\hat{\beta}_{2\rho}$	-.024	.010
$\hat{\beta}_{3k_c}$	.014	.010
$\hat{\beta}_{\tau\rho}$	-.051	.010

regime. This was illustrated in the range of the deviations in this regime. The deviations ranged from .464 for Run 456.7, Case 7 to 2.196 for Run 23 Case 8.

The diversity of effects attributable to variable physical properties was evident in the figures to be presented. In the case of Run 21 the differences were clearly a result of changes to the thermal conductivity. As may be seen in Figure 5.30 there was a spread of approximately 15% in the conversions achieved between Cases 1 and 8. The cup-mixed temperature profile (Figure 5.31) illustrated the large differences that occurred in the heat transfer for the different cases. For Case 1, in which the thermal conductivity was decreasing with conversion, the peak cup-mixed temperature was much larger than it was for both constant physical properties and Case 8. The peak temperature for Case 8 was much smaller and occurred earlier in the reactor. The centerline velocity (Figure 5.32 in Appendix A) varied in a similar manner for both cases. Neither case had a large velocity profile distortion and in both instances the nature of the distortion would lead to less conversion than for the constant property case. Run 23 had results similar to Run 21. As may be seen from Table 5.27, the heat capacity was also important in Run 23.

For Run 26 two varying properties contributed to the deviations in the results (Figures 5.33, A.4, and A.5). Examination of the cup-mixed temperature profile (Figure A.4) showed that the differences in heat transfer were important. As may be seen in Figure A.5 the differences in the velocity profile distributions were also appreciable.

Run 456.7 was another example in which the thermal conductivity was very important (Figures 5.34, A.6, and A.7). This simulation differed from Runs 21 and 23 because the thermal conductivity had a profound effect on the performance of the reactor. This importance was not through a particularly large range of deviations at the outlet. The main effect was that the shape of the concentration profiles were such that the reactor length to achieve a specified conversion could be large. In Figure 5.34 it was noted that the range between the different cases was not that wide. The conversion curves displayed a distinct flattening at approximately the same axial distance. Since the curves were tending towards the horizontal a large range of axial lengths were required to reach a given conversion in some

circumstances. Other runs in which the thermal conductivity was significant also displayed this type of behaviour.

The range of deviations in this regime was considerably larger than it was for the analogous temperature dependent case. Many different factors were contributing to differences in reactor performance. Of these factors free convection was clearly important. The heat transfer and temperature characteristics in the reactor were also important. This was illustrated by the presence of heat capacity and thermal conductivity as important factors. The influences of these properties around the center point have been given in Figure 5.35.

Table 5.26: Significant Effects in the Medium Heat Transfer Regime for Combined Temperature and Composition Dependent Physical Properties

Coefficient (Coded Form)	Coefficient Value	Confidence Interval (2σ)
$\hat{\beta}_0$	1.033	.020
$\hat{\beta}_1$	-.141	.032
$\hat{\beta}_7$	-.055	.026
$\hat{\beta}_{13}$	-.198	.042
$\hat{\beta}_\rho$	.124	.018
$\hat{\beta}_{C_p}$	.083	.018
$\hat{\beta}_{k_c}$	.165	.018
$\hat{\beta}_{7\rho}$	-.103	.026
$\hat{\beta}_{3k_c}$	.141	.024
$\hat{\beta}_{4k_c}$	-.048	.024
$\hat{\beta}_{5k_c}$	.048	.024
$\hat{\beta}_{3C_p}$	-.047	.024

Table 5.27: Sensitivity of Runs in the Medium Heat Transfer Regime to Physical Property Changes

Run	$\hat{\beta}_0$	$\hat{\beta}_\rho$	$\hat{\beta}_{C_p}$	$\hat{\beta}_\mu$	$\hat{\beta}_{k_c}$	Calculated Heat Transfer Regime
5	1.456	.195	.025	-.009	.420	2.1
7	1.416	.131	.068	-.004	.378	2.1
10	1.023	.016	.057	.014	.008	2.0
12	0.930	.003	.041	.015	.006	2.0
21	1.379	.024	.081	.013	.689	2.1
23	1.465	.061	.214	-.002	.510	2.1
26	1.156	.422	.174	.001	-.027	2.0
28	1.005	.201	.102	.019	.001	2.0
33	1.040	.107	.033	.011	.234	2.1
124.1	1.190	.260	.210	.019	.009	2.6
124.3	0.962	.147	.196	.023	.006	2.6
124.6	0.999	.097	.013	-.003	.042	1.5
124.8	0.950	.052	.004	.011	.049	1.5
135.2	1.051	.088	-.006	.014	.016	1.5
135.3	1.251	.160	.084	.009	.212	2.6
135.6	1.029	.108	.011	.015	.033	1.5
135.7	1.368	.263	.194	-.006	.273	2.6
236.1	1.054	.185	.144	.019	.005	2.3
236.2	0.977	.115	.158	.021	.004	2.3
236.3	0.971	.060	-.001	.006	.258	1.8
236.4	0.985	.017	-.001	.011	.192	1.8
236.5	1.087	.273	.238	.012	-.011	2.3
236.6	1.002	.198	.250	.032	.003	2.3
236.7	0.943	.055	.002	.000	.437	1.8
236.8	0.956	.021	-.002	.012	.328	1.8

Table 5.27 Continued

Run	$\hat{\beta}_0$	$\hat{\beta}_\rho$	$\hat{\beta}_{C_p}$	$\hat{\beta}_\mu$	$\hat{\beta}_{k_c}$	Calculated Heat Transfer Regime
257.1	1.084	.206	.016	.000	.173	2.1
257.2	1.020	.091	.015	.015	.111	2.1
257.3	1.180	.273	.075	-.015	.311	2.1
257.4	1.085	.146	.073	.004	.178	2.1
257.5	0.976	.004	.014	.006	.199	2.1
257.6	0.969	.004	.019	.021	.125	2.1
257.7	1.020	.019	.070	.033	.338	2.1
257.8	1.014	.015	.075	.005	.205	2.1
347.1	1.146	.388	.187	.000	-.002	2.1
347.2	1.026	.067	-.008	.012	.165	1.6
347.3	1.145	.418	.190	.007	-.025	2.5
347.4	1.166	.263	.047	-.022	.257	2.0
347.5	0.980	.051	.183	.017	.021	2.1
347.6	1.003	-.003	-.007	.012	.165	1.6
347.7	1.003	.067	.216	.032	-.007	2.5
347.8	1.020	.009	.047	.026	.295	2.0
456.1	1.011	.039	-.028	.012	.173	1.8
456.2	1.039	.140	.060	.011	.041	2.3
456.3	0.998	.029	-.040	.013	.241	1.8
456.4	1.090	.211	.125	.011	.032	2.3
456.5	0.996	.043	-.031	.011	.271	1.8
456.6	1.073	.169	.092	.010	.082	2.3
456.7	0.982	.035	-.044	.010	.478	1.8
456.8	1.083	.248	.232	.004	.068	2.3

5.4.3 Reactor Performance with Concentration Dependence in the Low Heat Transfer Regime

Similar to the results obtained for the temperature dependent situation, the largest deviations occurred in this regime. The deviations ranged from .191 for Run 17, Case 1 to 2.219 for Run 29, Case 8. The data were also similar to the temperature dependent runs in that the same runs showed the greatest degree of change. In terms of sensitivity to changes in the physical properties, density was again very important. Heat capacity also had a significant effect. Since there was very little heat transfer with the environment in this regime, thermal conductivity was of less significance.

The few runs that were significantly influenced by thermal conductivity tended to be those in the transition area between the medium heat transfer regime and the low heat transfer regime (Table 5.29). Comparison of the results between Tables 5.26 and 5.28 indicated that the heat capacity doubled in significance. The density displayed a similar trend. This was due to retention of energy in the system under the low heat transfer conditions. Through the heat capacity this retention in energy manifested itself in either larger or smaller temperature rises in the reactor for a given set of conditions. These large differences in the temperature of the reactor from different variations in the heat capacity have been illustrated in Figures A.8 and A.10. According to the conditions outlined in Table 4.5 the maximum temperature to be expected in the reactor was .15 (i.e. the adiabatic temperature rise for constant properties). The maximum temperature attained for Case 1 for the two examples was in fact larger than .15. In both instances the temperature rises were approaching .16. The lowering of heat capacities with conversion in these cases created larger temperature rises. Since reaction rate was a function of of temperature through the Arrhenius Law, reactions occurred at a more rapid rate at these higher temperatures. The opposite effect was experienced by Case 8. The overall range of differences in conversion was quite large (Figures 5.36 and 5.37). As may be seen from Figures A.9 and A.11 velocity profile distortions were also considerable and contributed to the deviations.

Table 5.28: Significant Effects in the Low Heat Transfer Regime for Combined Temperature and Composition Dependent Physical Properties

Coefficient (Coded Form)	Coefficient Value	Confidence Interval (2σ)
$\hat{\beta}_0$	1.007	.010
$\hat{\beta}_2$	-.132	.016
$\hat{\beta}_3$	-.102	.018
$\hat{\beta}_{26}$	-.175	.053
$\hat{\beta}_{34}$	-.169	.050
$\hat{\beta}_\rho$	.227	.013
$\hat{\beta}_{C_p}$	.186	.013
$\hat{\beta}_{2\rho}$	-.085	.016
$\hat{\beta}_{7\rho}$	-.174	.015

The effects of variable density and heat capacity in this regime have been illustrated in Figure 5.38. As may be seen from this figure the specific trends were similar to those that were encountered in the other regimes. The main difference lay in the larger slopes associated with the curves in this regime. It should be noted that the curves from the simulation data for both properties displayed a flattening near the lower end of the curves. In other words, the curves were beginning to approach a lower limit. This was particularly evident in the heat capacity curve.

The parallels between this heat transfer regime and the adiabatic reactor were established earlier for the constant property reactor. As may be seen in Table 5.30 many of the same factors were important in a true adiabatic reactor. Many of the differences in the results of the two systems could be attributed to the expanded ranges employed for β_T and β_U. Since a higher heat of reaction was used, the

Table 5.29: Sensitivity of Runs in the Low Heat Transfer Regime to Physical Property Changes

Run	$\hat{\beta}_0$	$\hat{\beta}_\rho$	$\hat{\beta}_{C_p}$	$\hat{\beta}_\mu$	$\hat{\beta}_{k_c}$	Calculated Heat Transfer Regime
1	0.996	.060	208	.022	-.053	3.1
3	0.891	.035	.133	.012	.008	3.1
9	1.061	.351	.123	.004	-.008	3.0
11	0.626	.161	.185	.025	.098	3.0
13	0.992	.060	.199	.021	-.051	3.1
15	0.901	.018	.076	.017	-.007	3.1
17	1.154	.703	.186	.098	-.129	3.1
19	0.776	.241	.203	.036	.042	3.1
25	0.960	.061	.219	.028	-.061	3.0
27	0.704	.064	.257	.041	-.131	3.0
29	1.259	.683	.219	.007	.070	3.1
31	0.883	.249	.132	.027	.006	3.1
124.1	1.190	.260	.210	.019	.009	2.6
124.3	0.962	.147	.196	.023	.006	2.6
124.5	1.013	.276	.206	.019	-.040	3.0
124.7	0.757	.169	.181	.036	-.019	3.0
135.1	0.935	.207	.159	.004	-.006	3.1
135.3	1.251	.160	.084	.009	.212	2.6
135.5	0.951	.324	.265	.022	-.035	3.1
135.7	1.368	.263	.194	-.006	.273	2.6
167.1	1.104	.378	.133	-.004	-.010	2.8
167.3	1.096	.510	.220	-.005	-.015	2.8
167.5	1.011	.042	.148	.031	-.015	2.8
167.7	0.978	.078	.236	.036	-.052	2.8
347.3	1.145	.418	.190	.007	-.025	2.5
347.7	1.003	.067	.216	.032	-.007	2.5

heat capacity had a larger role than it did for the low heat transfer case. Density and its interaction with the buoyancy term also increased due to the larger range of values used for β_U. The effects of the internal heat transfer term (α_T) could be evaluated for the adiabatic reactor. It was found that the value of this term contributed to the effects of density and heat capacity. This was most likely through its role in establishing the radial concentration and temperature profiles initially. The interaction between heat capacity and activation energy (γ) was attributed to similar conditions.

The simulations for the adiabatic reactor were repeated for a second order reaction. In general the reaction proceeded at a slower rate for a given set of run conditions. Also the magnitude of the deviations under varying physical property situations were not as large. However, the same types of deviations occurred. The heat capacity and density were both significant. A comparison of the regression coefficients for the first order adiabatic reaction with those of the second order reaction (Table 5.31) indicated that, although the magnitudes of the coefficients changed, the directions of the deviations were similar.

5.5 Effect of Flow Direction

Most of the work performed in the study was done assuming a vertical reactor operating in upward flow. In order to get some idea of the effect that flow direction had upon the reactor performance, some of the simulations were performed under the assumption of downward flow. This condition in particular was expected to be important with respect to free convection. In order to make the comparisons, sensitivities similar to those given in Tables 5.24, 5.27, and 5.29 were determined. In this manner one could determine whether the flow direction affected the significance of variable properties other than density.

As may be seen from the results given in Tables 5.32, 5.33, and 5.34 , the most obvious effect of flow direction was that the sign of the sensitivity of the reactor to density changes was reversed. This behaviour was expected since the flow direction and thus free convection was operating in the opposite direction. Heat

Table 5.30: Significant Effects in an Adiabatic Reactor for Combined Temperature and Composition Dependent Physical Properties

Coefficient (Coded Form)	Coefficient Value	Confidence Interval (2σ)
$\hat{\beta}_0$	.971	.046
$\hat{\beta}_1$	.117	.042
$\hat{\beta}_7$	.155	.062
$\hat{\beta}_{16}$	.064	.046
$\hat{\beta}_{17}$	-.125	.056
$\hat{\beta}_{67}$	.121	.056
$\hat{\beta}_\rho$	.058	.046
$\hat{\beta}_{C_p}$	.308	.040
$\hat{\beta}_{7\rho}$	-.277	.062
$\hat{\beta}_{1C_p}$	.095	.040
$\hat{\beta}_{5C_p}$	.059	.040
$\hat{\beta}_{6C_p}$	.133	.040

Table 5.31: Significant Effects in an Adiabatic Reactor for Combined Temperature and Composition Dependent Physical Properties: Second Order Reaction

Coefficient (Coded Form)	Coefficient Value	Confidence Interval (2σ)
$\hat{\beta}_0$	1.007	.026
$\hat{\beta}_7$	.037	.034
$\hat{\beta}_{12}$	.068	.024
$\hat{\beta}_{17}$	-.041	.032
$\hat{\beta}_{25}$	.034	.024
$\hat{\beta}_{26}$	.039	.024
$\hat{\beta}_\rho$	.050	.026
$\hat{\beta}_{C_p}$	.164	.024
$\hat{\beta}_{7\rho}$	-.105	.036
$\hat{\beta}_{6\rho}$	.031	.024
$\hat{\beta}_{6C_p}$	.070	.024

Table 5.32: Comparison of the Reactor Performance based on Sensitivities to Physical Property Changes and Flow Direction: Run 5

Coefficient (Coded Form)	Coefficient Value (Upward)	Parameter Value (Downward)
$\hat{\beta}_0$	1.456	1.218
$\hat{\beta}_\rho$	.195	-.090
$\hat{\beta}_{C_p}$	.025	.035
$\hat{\beta}_\mu$	-.010	.017
$\hat{\beta}_{k_c}$	.420	.463

capacity effects were not affected by the flow direction whereas the effect of thermal conductivity was affected in areas in which it was of less significance (Table 5.34).

5.6 Summary of the Major Results of the Numerical Study

Through the numerical study a number of different characteristics of the laminar flow reactor were determined. These characteristics were determined under a number of different situations with respect to the heat transfer conditions of the reactor and also the different types of physical property changes that could occur with reaction. In a constant property reactor the following observations were made.

- The type of heat transfer could be categorized into three regimes. These regimes were a function of the values of three of the operating variables under study. These variables were:
  - Radial dispersion of heat in the reactor (α_T)
  - Wall heat transfer coefficient (Bi)
  - Jacket or ambient temperature (θ_j).

Table 5.33: Comparison of the Reactor Performance based on Sensitivities to Physical Property Changes and Flow Direction: Run 17

Coefficient (Coded Form)	Coefficient Value (Upward)	Parameter Value (Downward)
$\hat{\beta}_0$	1.154	1.648
$\hat{\beta}_\rho$	.703	-.942
$\hat{\beta}_{C_p}$	.186	.321
$\hat{\beta}_\mu$	.098	.021
$\hat{\beta}_{k_c}$	-.129	-.126

Table 5.34: Comparison of the Reactor Performance based on Sensitivities to Physical Property Changes and Flow Direction: Run 29

Coefficient (Coded Form)	Coefficient Value (Upward)	Parameter Value (Downward)
$\hat{\beta}_0$	1.259	1.543
$\hat{\beta}_\rho$	.683	-.840
$\hat{\beta}_{C_p}$	.219	.241
$\hat{\beta}_\mu$	.007	-.040
$\hat{\beta}_{k_c}$	.070	-.130

Of the three factors listed above the most important in determining the type of heat transfer was the radial dispersion, α_T. At low values of this dimensionless group the reactor assumed many of the characteristics typical of an adiabatic reactor. As this group increased the type of heat transfer ranged from medium heat transfer to high heat transfer, at which point the reactor was effectively isothermal.

- The reactor performance in each of the described heat transfer regimes was affected by the dimensionless groups in different ways. These effects were determined by examining the way the groups affected the length of reactor required to achieve 90% conversion. For each of the heat transfer regimes the following effects were observed.

  High Heat Transfer Regime: In the high or isothermal heat transfer regime the reactor very quickly reached the jacket temperature. This temperature had the largest effect upon the reactor length. As this temperature increased the reactor length decreased. Of minor significance were the mass dispersion group α_x and the wall heat transfer group. According to the results of the regression analysis both of the parameters decreased the reactor length when they were increased. In particular, the reactor length was affected by mass dispersion, consistent with the findings of previous studies. Activation energy was found to be coupled with the jacket temperature through an interactive term. Since the activation energy was combined with temperature through the Arrhenius equation and the jacket temperature was the reactor temperature, this result was reasonable.

  Medium Heat Transfer Regime: The number of parameters affecting reactor length in this regime was much larger than that of the high heat transfer regime. In this regime the influence of the jacket temperature was not as great as it was in the high heat transfer regime. Conversely, wall heat transfer became more important. In this regime a more typical heat transfer situation occurred. All of the factors that were involved in

heat transfer with the surroundings were significant. Increasing the radial heat transfer term increased the reactor length. The wall heat transfer term had the same effect. The jacket temperature had less influence and depended upon the values of the other two parameters through interaction terms. The strongest of these interactions was that between radial dispersion and jacket temperature. The heat of reaction also played a significant role, with a larger heat of reaction resulting in a shorter reactor. A surprising result was the fact that the dimensionless activation energy was insignificant. This was perhaps due to the fact that the ways in which the temperature changed in the reactor were too diverse in this regime. The type of interaction could not be evaluated by the regression analysis. The mass dispersion term was also insignificant in this regime.

Low Heat Transfer Regime: In this particular regime the reactor had characteristics that were typical of the adiabatic reactor. Comparisons between these results and those of a true adiabatic reactor confirmed this. In this regime the two most significant parameters were the heat of reaction and the activation energy. Increases in both of these quantities led to decreases in the reactor length. Except for a small effect associated with the wall heat transfer regime none of the other parameters were important. Similar results were obtained in a true adiabatic reactor.

- The heat transfer regimes discussed above were also useful in characterizing the reactor with respect to varying physical properties. Temperature dependent physical properties were most important in the low heat transfer range. This was to be expected since this range was the one in which the temperature non-uniformities in the reactor were greatest. Of particular importance was the effect that free convection had upon the reactor. In situations in which free convection acted to compress the velocity profile it was discovered that the reactor concentration and temperature profiles were flattened. The behaviour of the reactor under these circumstances was essentially that of a plug flow reactor. The buoyancy term did not need to be very large to instigate

this effect.

- When combined temperature and composition dependent physical properties were examined the effect of the individual properties upon reactor performance was determined. These effects were again a function of the heat transfer regime.

  High Heat Transfer Regime: The physical properties that were most influential in this regime were the density and thermal conductivity. Density was important in establishing free convection. Thermal conductivity was important in varying the speed at which the system reached the isothermal state characteristic of this regime. In particular a decrease in the thermal conductivity with conversion was important when the jacket temperature was low. Under this condition the reactor length was shortened considerably.

  Medium Heat Transfer Regime: Density and thermal conductivity continued to be significant in this regime, and heat capacity was significant as well. The effects of density and thermal conductivity were similar to their influence in the high heat transfer regime. The difference lay in the magnitude of their influence. For example, the interaction term between thermal conductivity and wall heat transfer increased from .014 in the high heat transfer regime to .14 in the medium heat transfer regime. The first order term for thermal conductivity increased almost fivefold. The effect of density approximately doubled.

  Low Heat Transfer Regime: In this regime transfer of energy with the surroundings was minimal. Because of this, the thermal conductivity ceased to be significant. The effects of density and heat capacity were double their respective values in the medium heat transfer regime.

The simulations that were performed to screen the effects of the individual properties were a combination of temperature and composition dependent properties. The contribution of the temperature dependency could be discerned through the values

of $\hat{\beta}_0$ that appeared in the tables of sensitivities presented earlier (Tables 5.24, 5.27, and 5.29). These average physical property effects have been given in Table 5.35 and compared to the values of the ratio y obtained for each of the media. In most instances the values of all of the quantities were similar. In this sense the effect of temperature dependent physical properties could be deduced.

In investigating the performance of the laminar flow reactor through the several simulations the one factor that was immediately apparent was that the system was very complex. Numerous considerations were required in order to fully understand the nature of the reactor. Although the dimensionless groups were determined to govern reactor behaviour under the assumption that physical properties were constant, it should be apparent that many of the factors determined in this aspect of the study would also be important in situations in which the physical properties varied. For example, the length of the reactor in the low heat transfer regime was very sensitive to the heat of reaction. This fact should be considered in any examination of a reactor when the properties were expected to be varying. Both of the influences (i.e. initial value of the dimensionless groups, and variable properties) should be included in the analysis.

The above point was verified in the following analysis of a pilot plant scale reactor.

Table 5.35: Comparison of the Temperature Dependent Deviations y and the Intercepts β_o of the Multi-component Analysis

Run	Multi-Component Intercepts ($\hat{\beta}_o$)	Water Deviations, y	Ethanol Deviations, y	Benzene Deviations, y
1	0.996	0.929	1.026	1.035
2	1.034	1.005	1.008	1.007
3	0.891	0.828	0.878	0.903
4	1.025	1.027	1.022	1.018
5	1.456	1.124	1.174	1.129
6	1.002	1.001	1.001	1.001
7	1.416	0.992	1.071	1.021
8	1.048	1.052	1.043	1.035
9	1.061	0.907	0.984	0.949
10	1.023	1.006	1.036	1.033
11	0.626	0.517	0.559	0.628
12	0.930	0.926	0.951	0.962
13	0.992	1.120	1.212	1.193
14	1.067	0.995	1.020	1.007
15	0.901	0.908	0.948	0.960
16	0.967	0.956	0.956	0.965
17	1.154	0.658	0.785	0.810
18	1.001	1.005	1.007	1.007
19	0.776	0.742	0.726	0.787
20	1.014	1.022	1.022	1.019
21	1.379	1.093	1.059	1.081
22	1.002	0.962	0.964	0.962
23	1.465	1.148	0.898	0.892
24	1.043	1.040	1.033	1.025
25	0.960	0.941	1.023	1.023
26	1.156	0.917	1.009	0.993
27	0.704	0.706	0.842	0.900
28	1.005	0.906	0.954	0.961
29	1.259	0.852	0.960	0.705
30	0.967	0.978	0.993	0.995
31	0.883	0.815	0.842	0.878
32	0.929	0.938	0.948	0.954
33	1.040	1.020	1.020	1.020

Table 5.35 Continued

Run	Multi-Component Intercepts	Water	Ethanol	Benzene
124.1	1.190	1.038	1.118	1.095
124.2	1.013	1.001	1.002	1.003
124.3	0.962	0.843	0.904	0.926
124.4	1.049	0.977	0.969	0.958
124.5	1.013	0.907	0.980	0.988
124.6	0.999	0.989	0.989	1.000
124.7	0.757	0.716	0.752	0.807
124.8	0.950	0.955	0.958	0.967
135.1	0.935	0.808	0.953	0.976
135.2	1.051	0.941	0.950	1.011
135.3	1.251	1.123	1.149	1.110
135.4	1.015	0.999	0.998	0.998
135.5	0.951	0.866	0.958	0.932
135.6	1.029	1.013	0.950	1.010
135.7	1.368	1.132	1.222	1.139
135.8	0.998	0.992	0.991	0.953
167.1	1.104	0.966	1.018	1.017
167.2	1.033	1.001	0.999	1.000
167.3	1.096	0.778	0.878	0.882
167.4	1.042	0.997	1.000	0.999
167.5	1.011	0.971	1.030	1.033
167.6	0.993	1.005	1.005	1.005
167.7	0.978	0.924	1.079	1.069
167.8	0.997	1.003	1.003	1.008
236.1	1.054	0.957	1.001	1.001
236.2	0.977	0.921	0.965	0.980
236.3	0.971	1.033	1.020	1.021
236.4	0.985	0.923	0.921	0.920
236.5	1.087	0.971	1.074	1.057
236.6	1.002	0.849	0.985	1.009
236.7	0.943	0.967	0.958	0.952
236.8	0.956	0.920	0.911	0.910

Table 5.35 Continued

Run	Multi-Component Intercepts	Water	Ethanol	Benzene
257.1	1.084	1.035	1.048	1.036
257.2	1.020	0.976	0.994	0.993
257.3	1.180	1.095	1.111	1.097
257.4	1.085	1.020	1.044	1.038
257.5	0.976	1.013	1.002	1.014
257.6	0.969	0.967	0.967	0.970
257.7	1.020	1.057	1.050	1.044
257.8	1.014	1.016	1.007	1.010
347.1	1.146	0.952	1.023	1.028
347.2	1.026	0.940	0.962	0.952
347.3	1.145	0.935	0.986	0.988
347.4	1.166	1.053	1.060	1.042
347.5	0.980	0.938	1.001	0.999
347.6	1.003	0.932	0.95	0.942
347.7	1.003	0.915	1.016	0.993
347.8	1.020	1.029	1.008	1.007
456.1	1.017	1.083	1.091	1.089
456.2	1.039	0.977	1.001	0.988
456.3	0.998	1.030	1.048	1.035
456.4	1.090	0.961	1.013	1.013
456.5	0.996	1.049	1.053	1.033
456.6	1.073	0.992	1.007	1.040
456.7	0.982	1.046	1.053	1.044
456.8	1.083	0.975	1.087	1.071

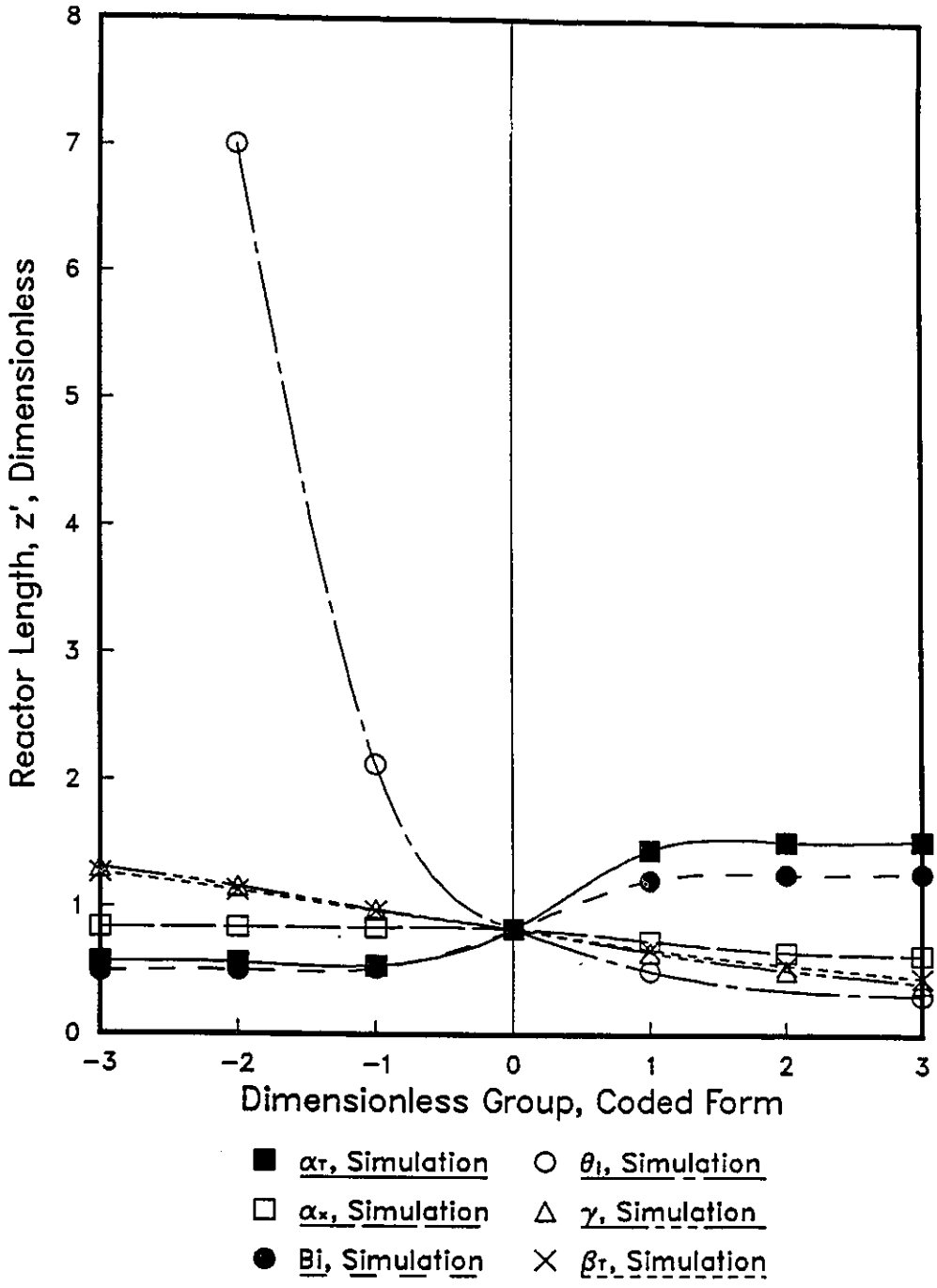

Figure 5.1: The Reactor Length for Constant Physical Properties as a Function of the Dimensionless Parameters in Coded Form

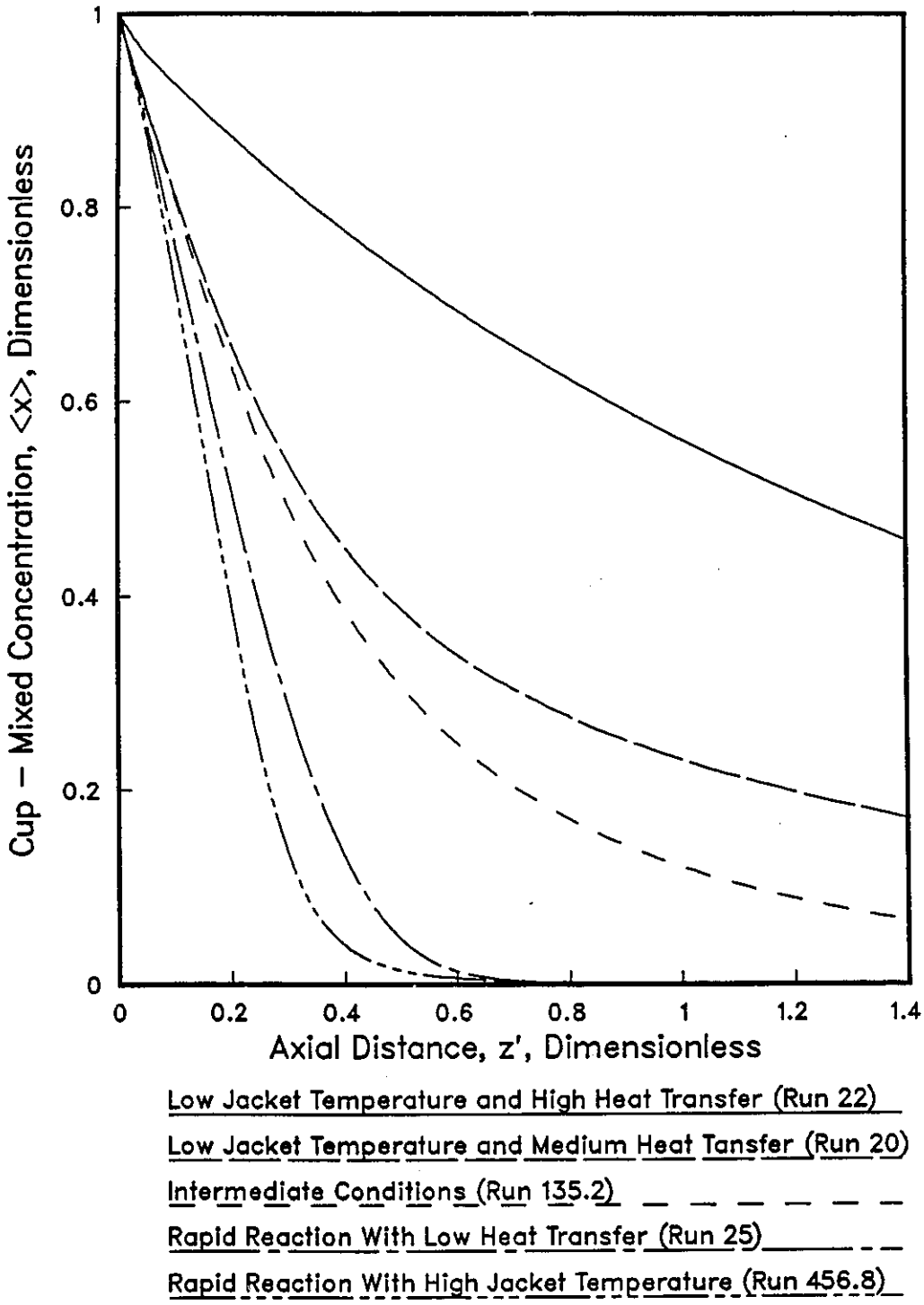

Figure 5.2: Typical Axial Cup - Mixed Concentration Profiles in the Reactor

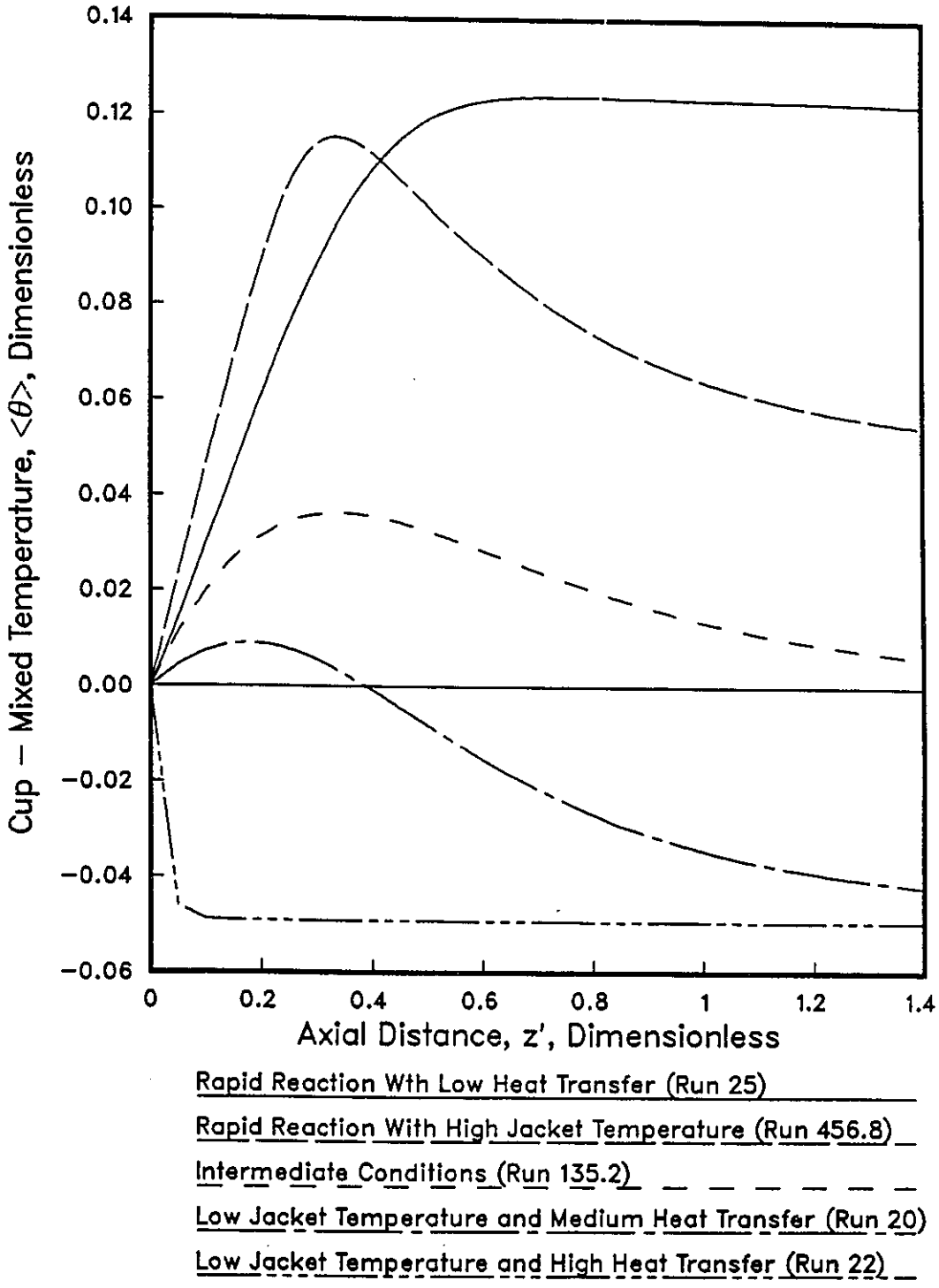

Figure 5.3: Typical Axial Cup - Mixed Temperature Profiles in the Reactor

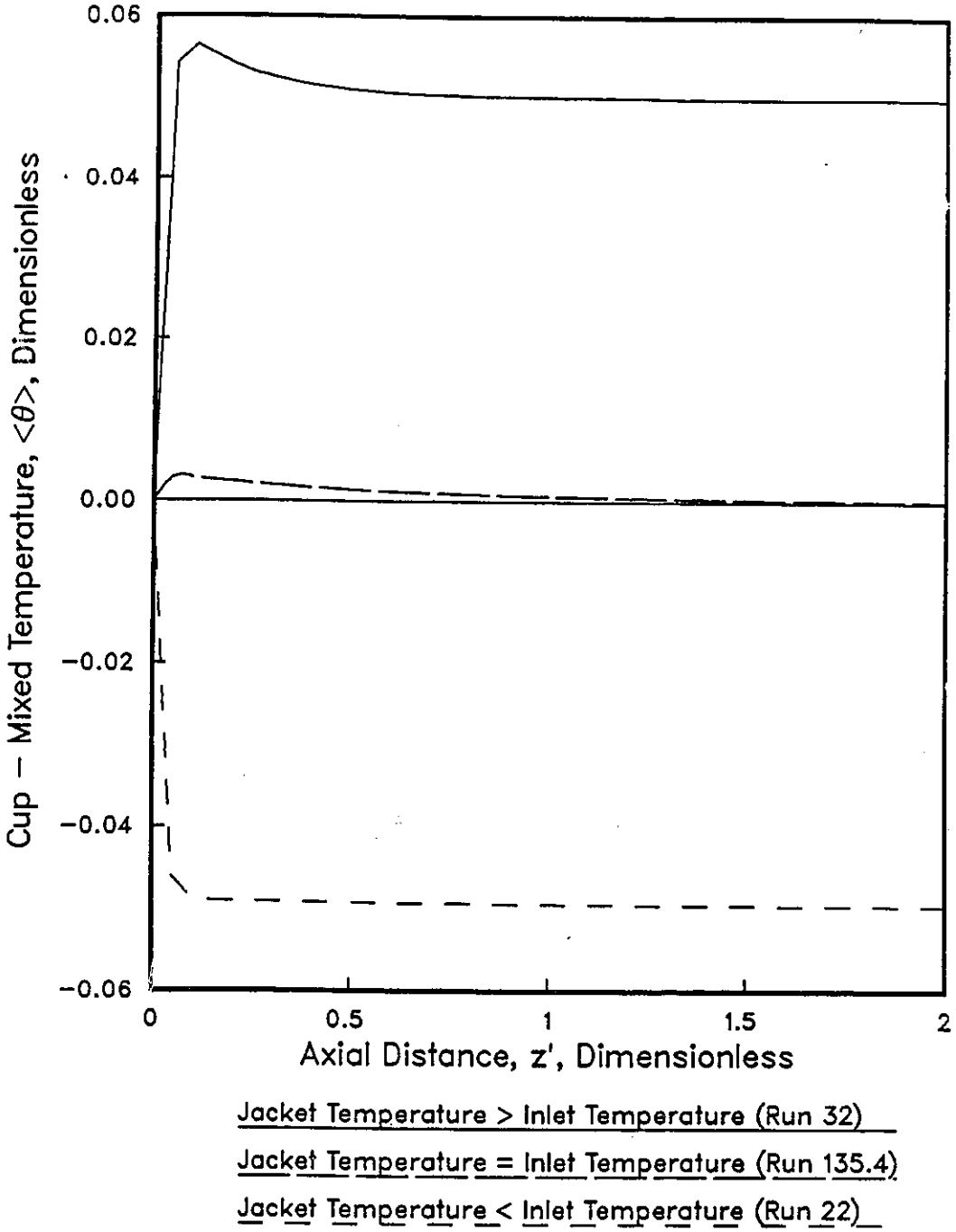

Figure 5.4: Axial Cup - Mixed Temperature Profiles in the Isothermal Regime

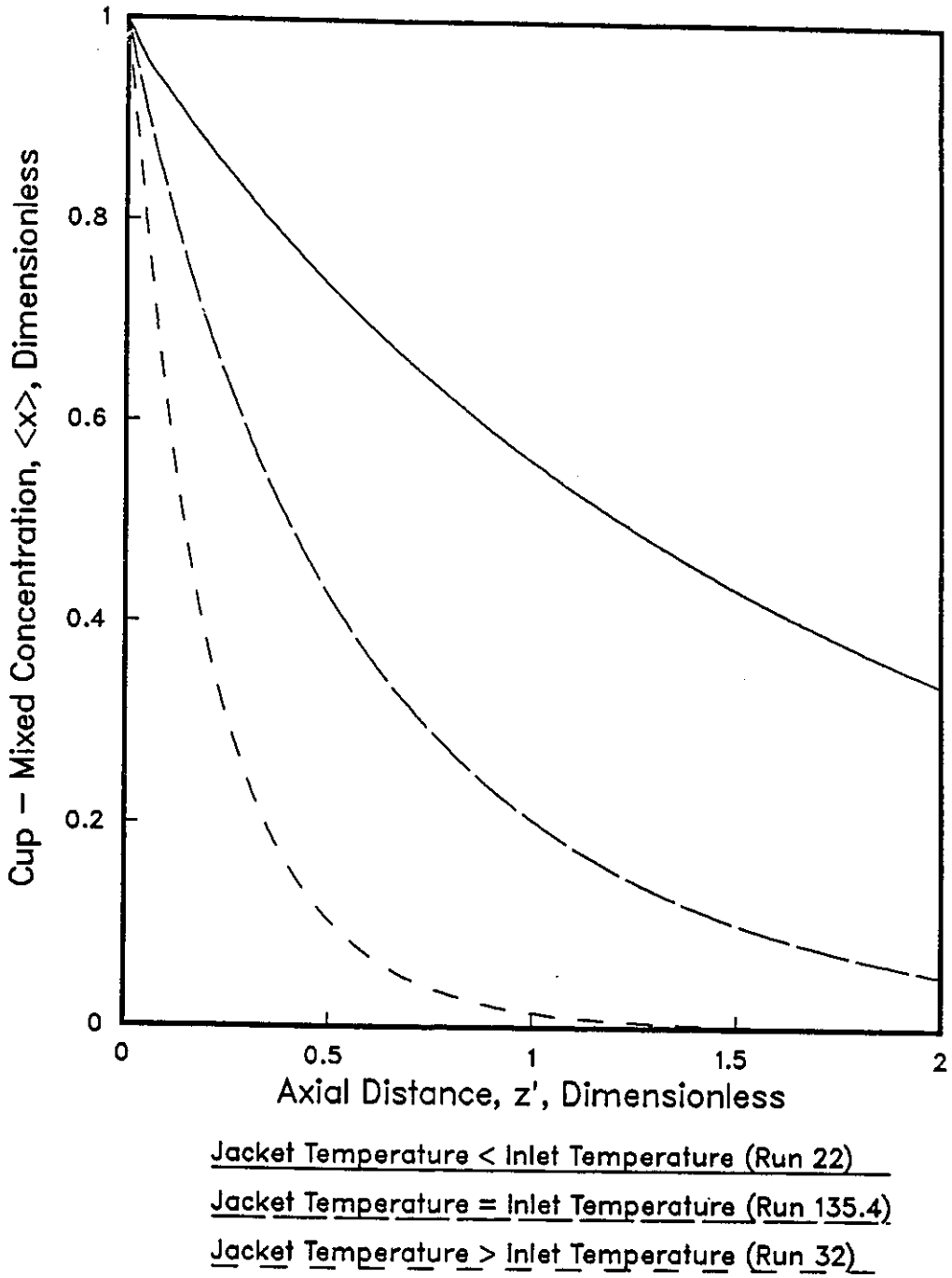

Figure 5.5: Axial Cup - Mixed Concentration Profiles in the Isothermal Regime

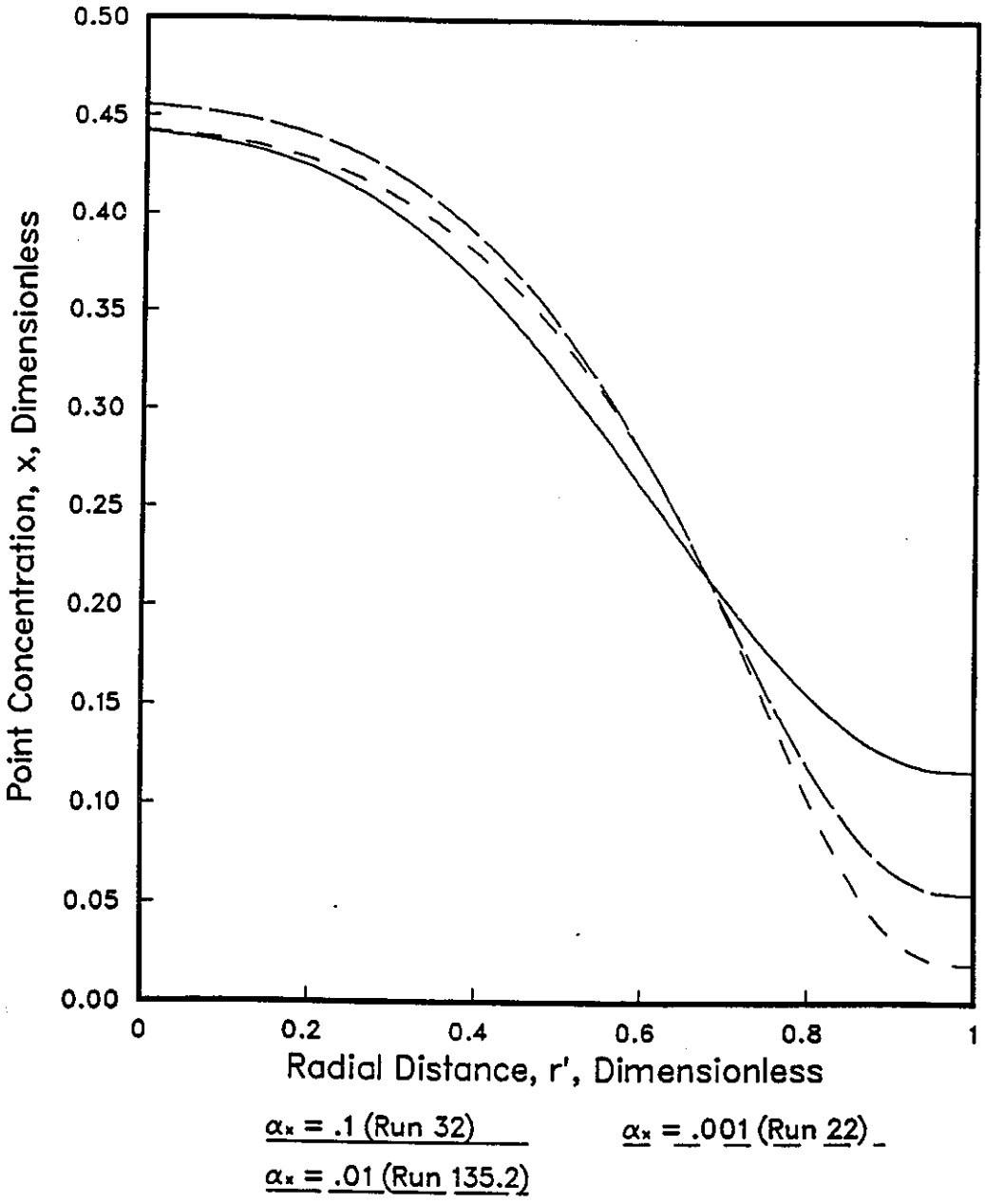

Figure 5.6: Comparison of Radial Concentration Profiles in the High Heat Transfer Regime at .5 of the 90% Conversion Length

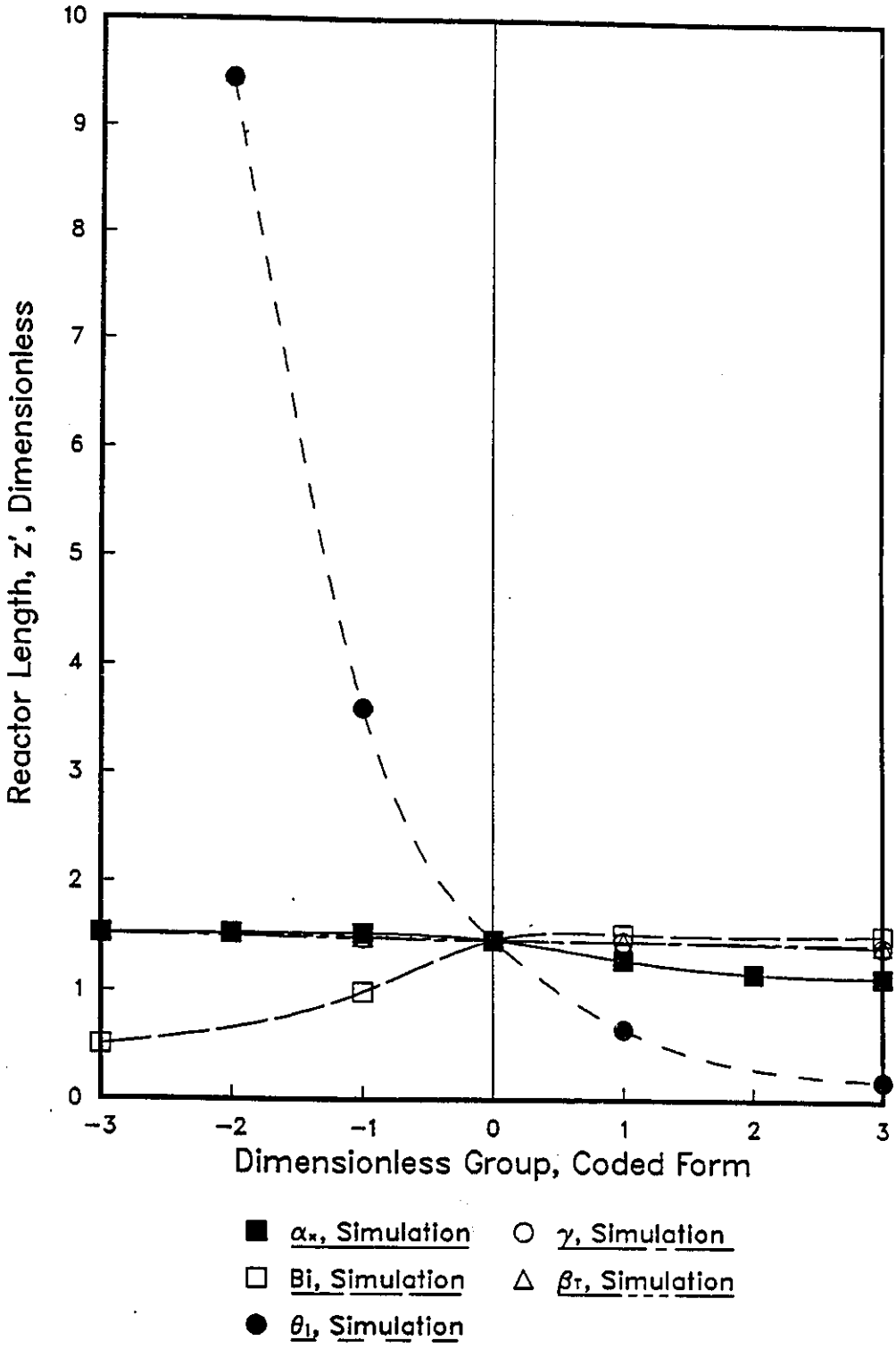

Figure 5.7: Influence of the Dimensionless Groups Around the Isothermal Regime Center Point ($\alpha_T = 10$)

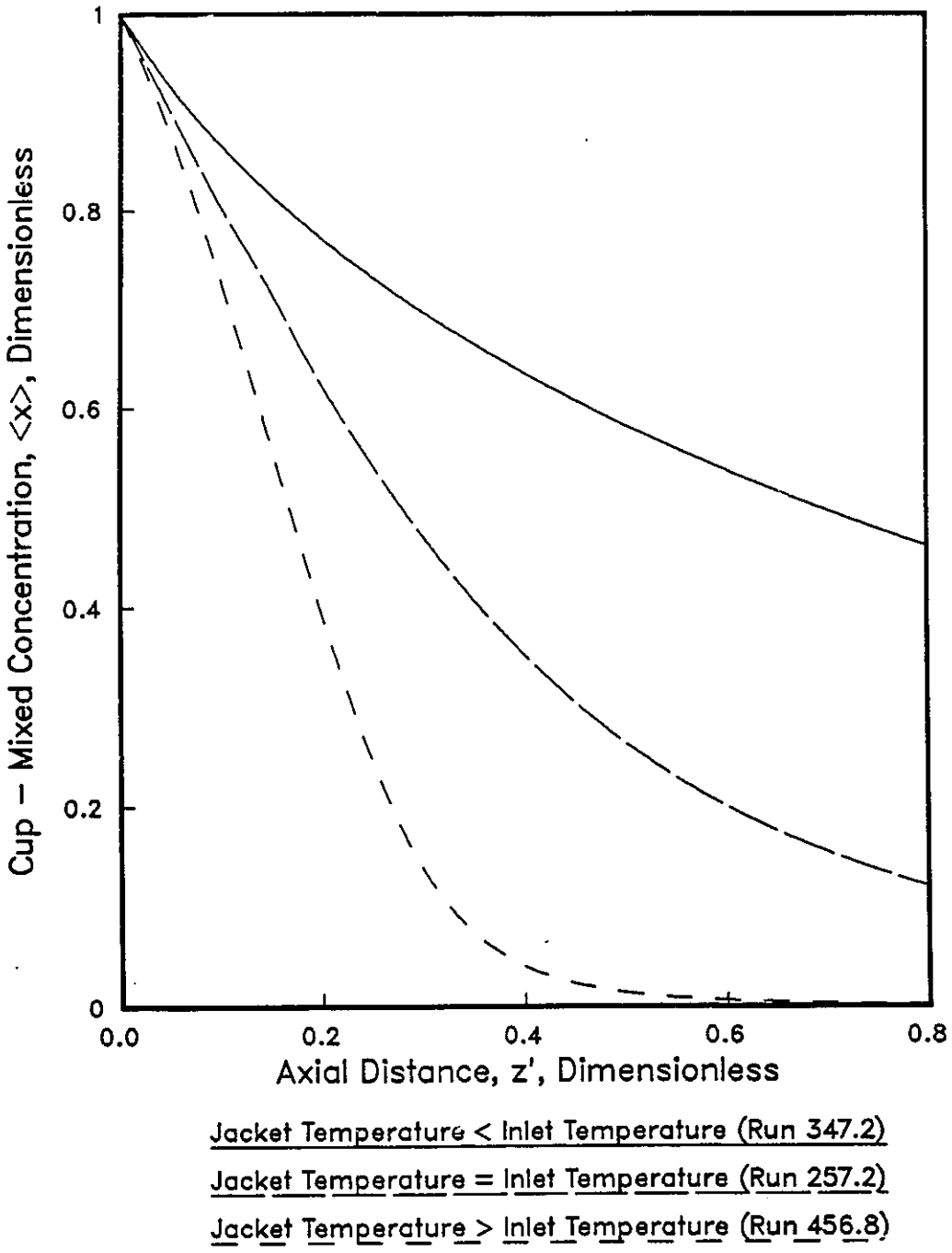

Figure 5.8: Axial Cup - Mixed Concentration Profiles in the Medium Heat Transfer Regime

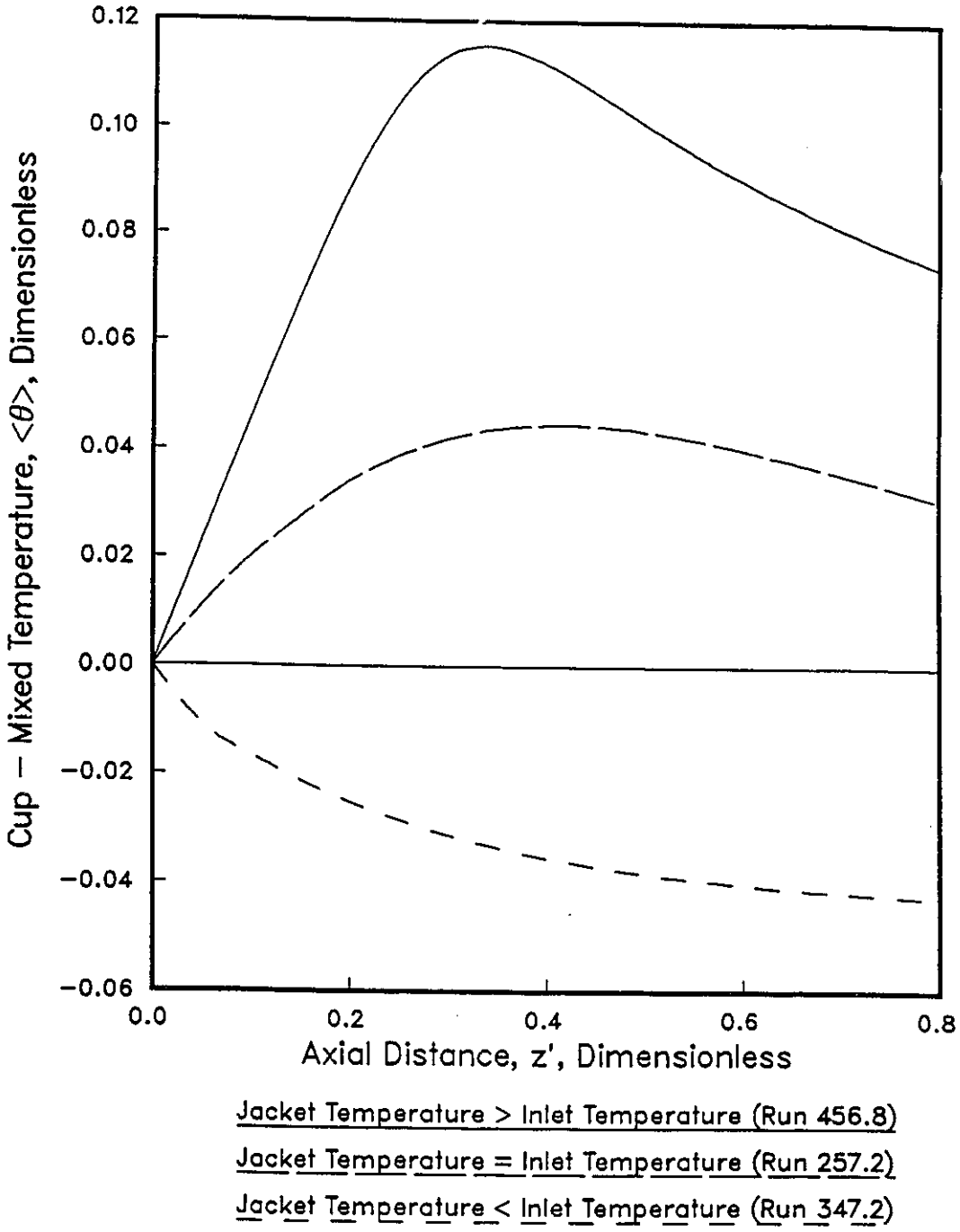

Figure 5.9: Axial Cup - Mixed Temperature Profiles in the Medium Heat Transfer Regime

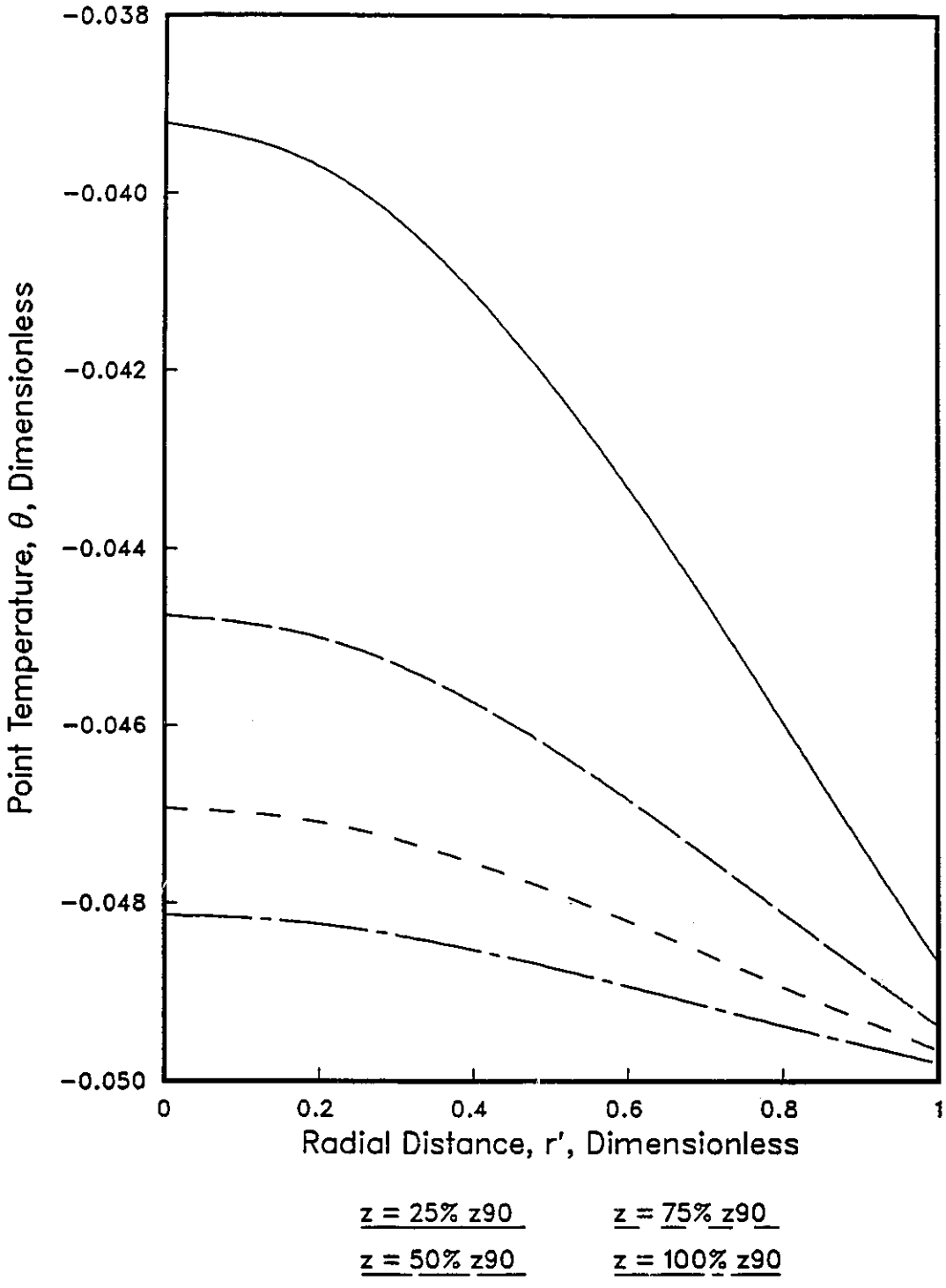

Figure 5.10: Radial Temperature Profiles for Run 347.2

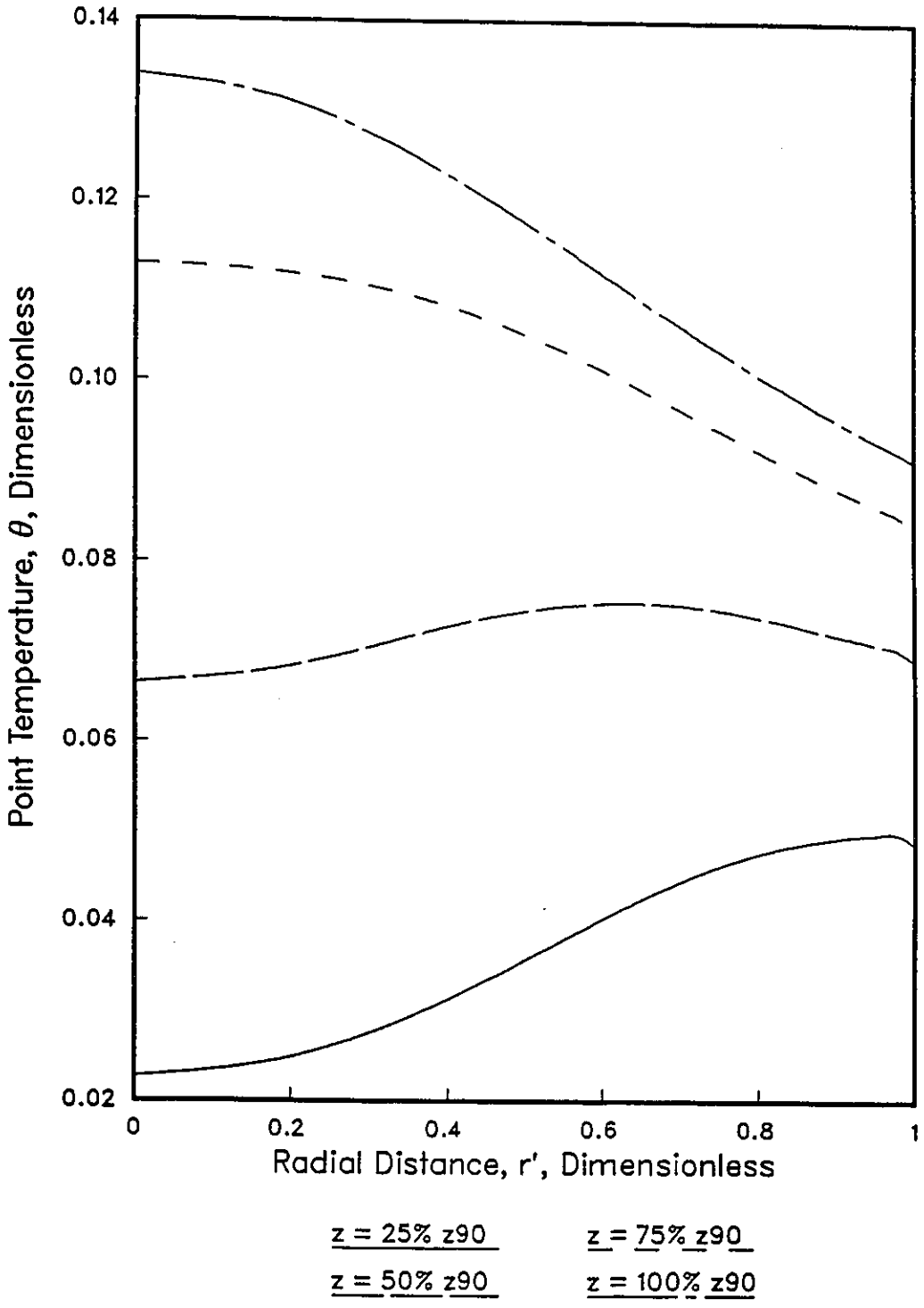

Figure 5.11: Radial Temperature Profiles for Run 456.8

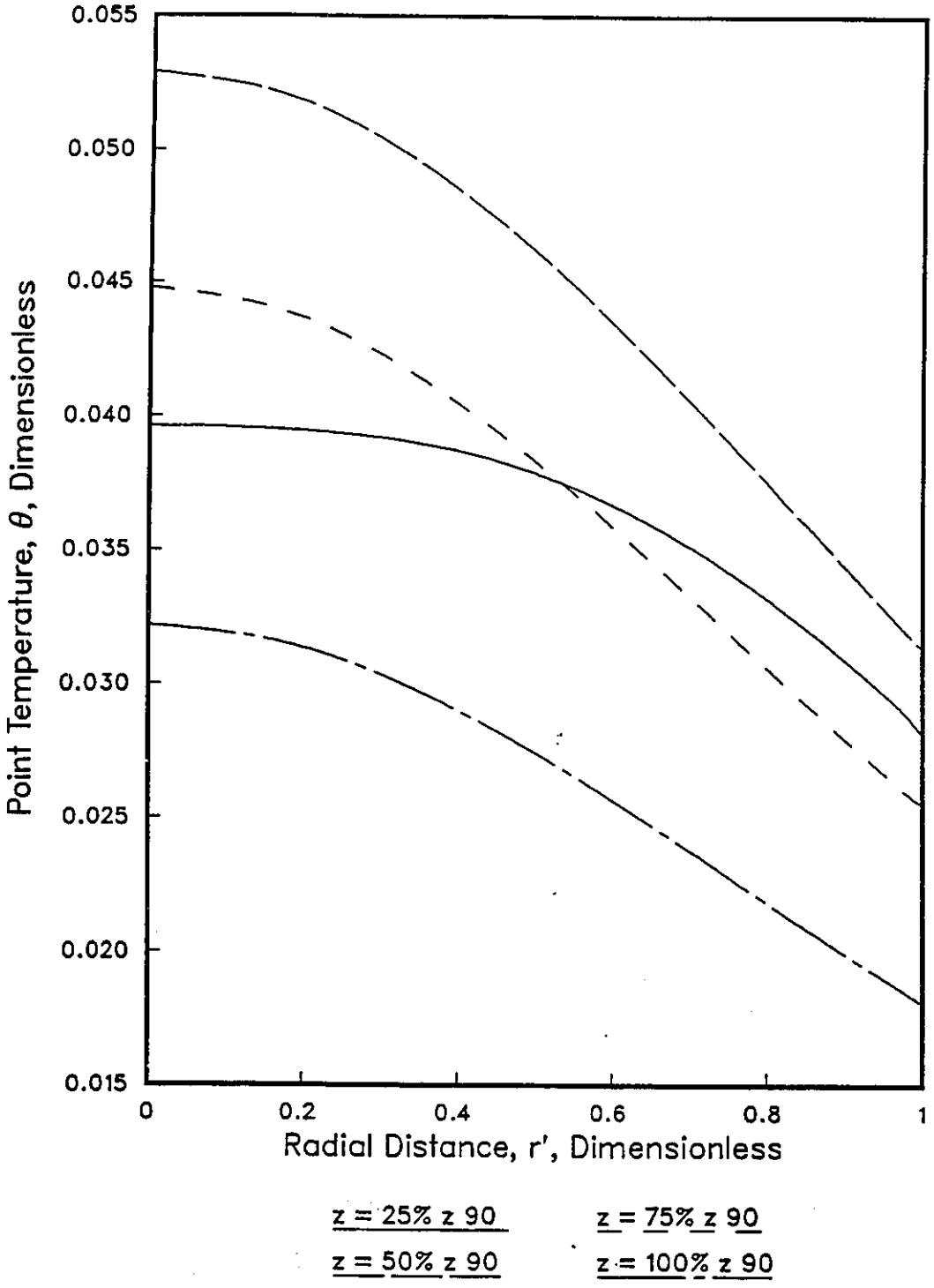

Figure 5.12: Radial Temperature Profiles for Run 257.2

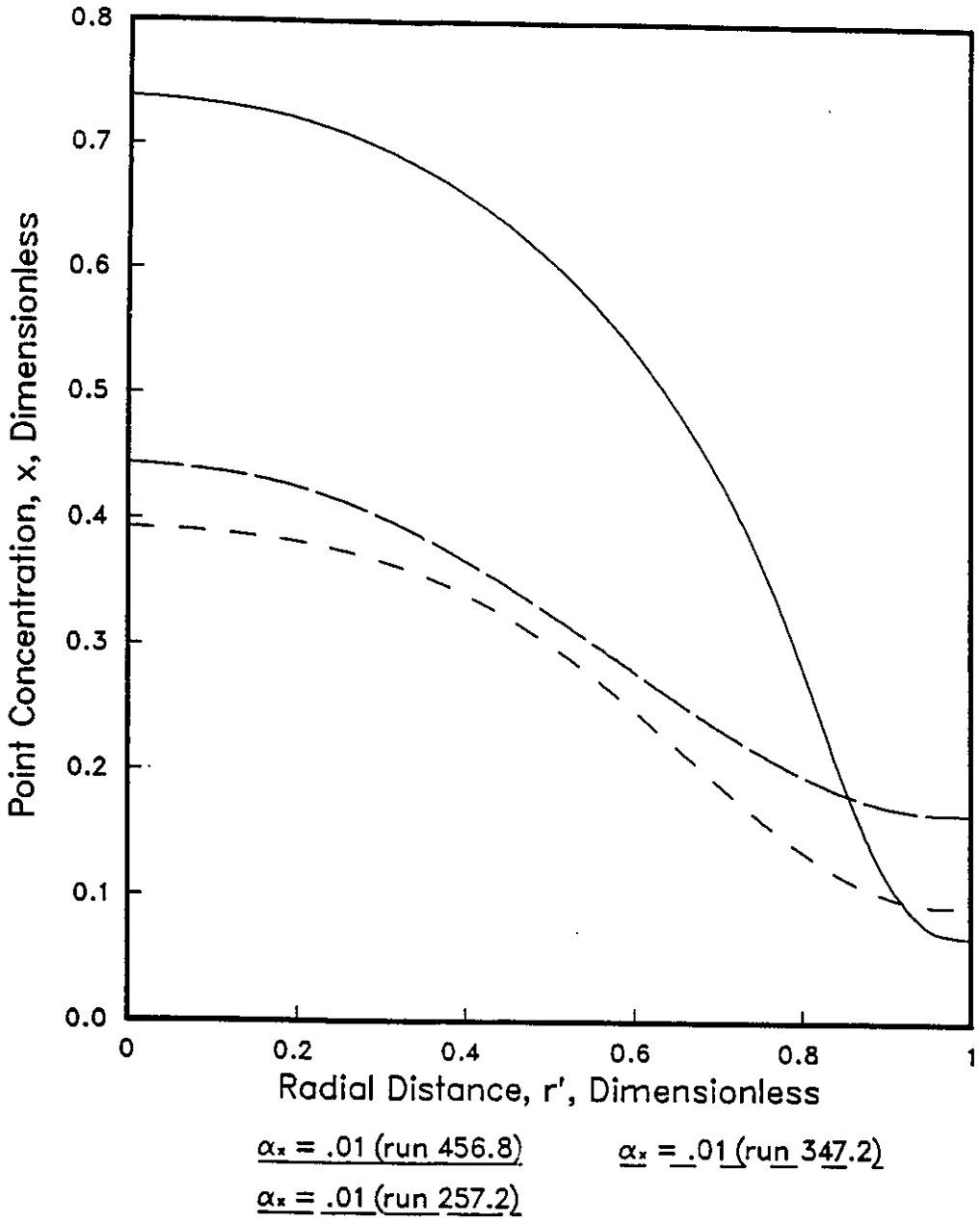

Figure 5.13: Comparison of Radial Concentration Profiles in the Medium Heat Transfer Regime at .5 of the 90% Conversion Length

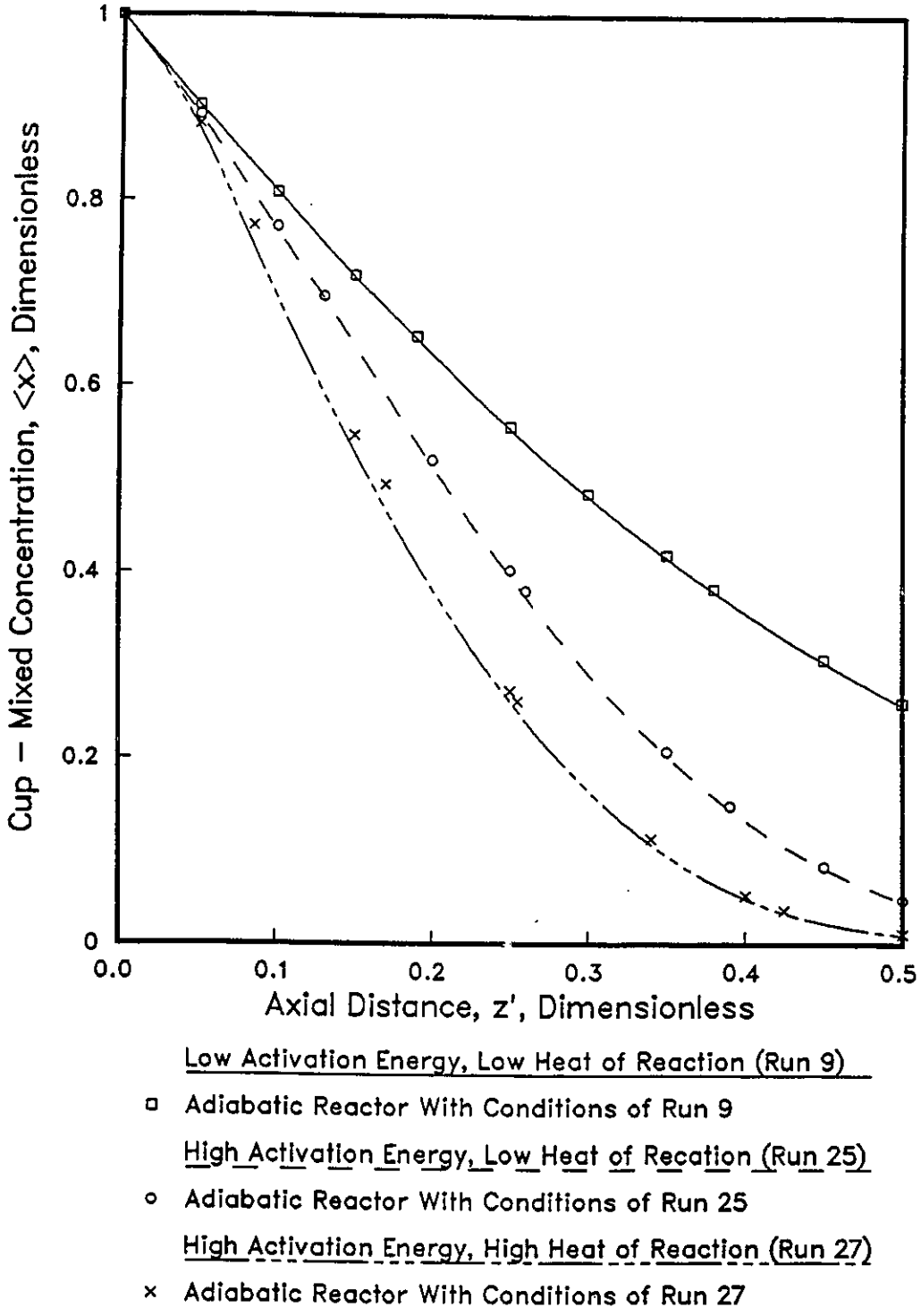

Figure 5.14: Axial Cup - Mixed Concentration Profiles in the Pseudo - Adiabatic Regime

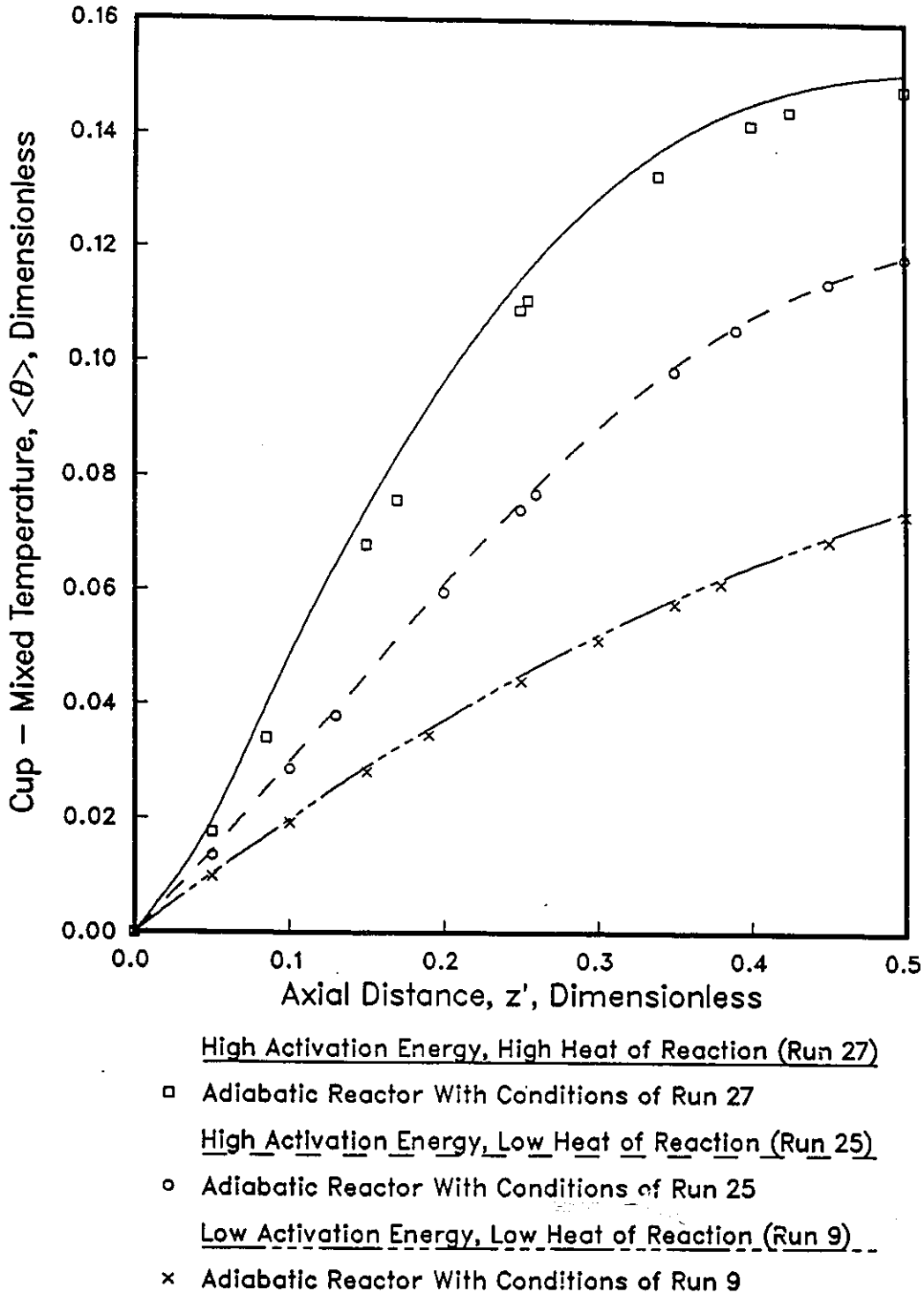

Figure 5.15: Axial Cup - Mixed Temperature Profiles in the Pseudo - Adiabatic Regime

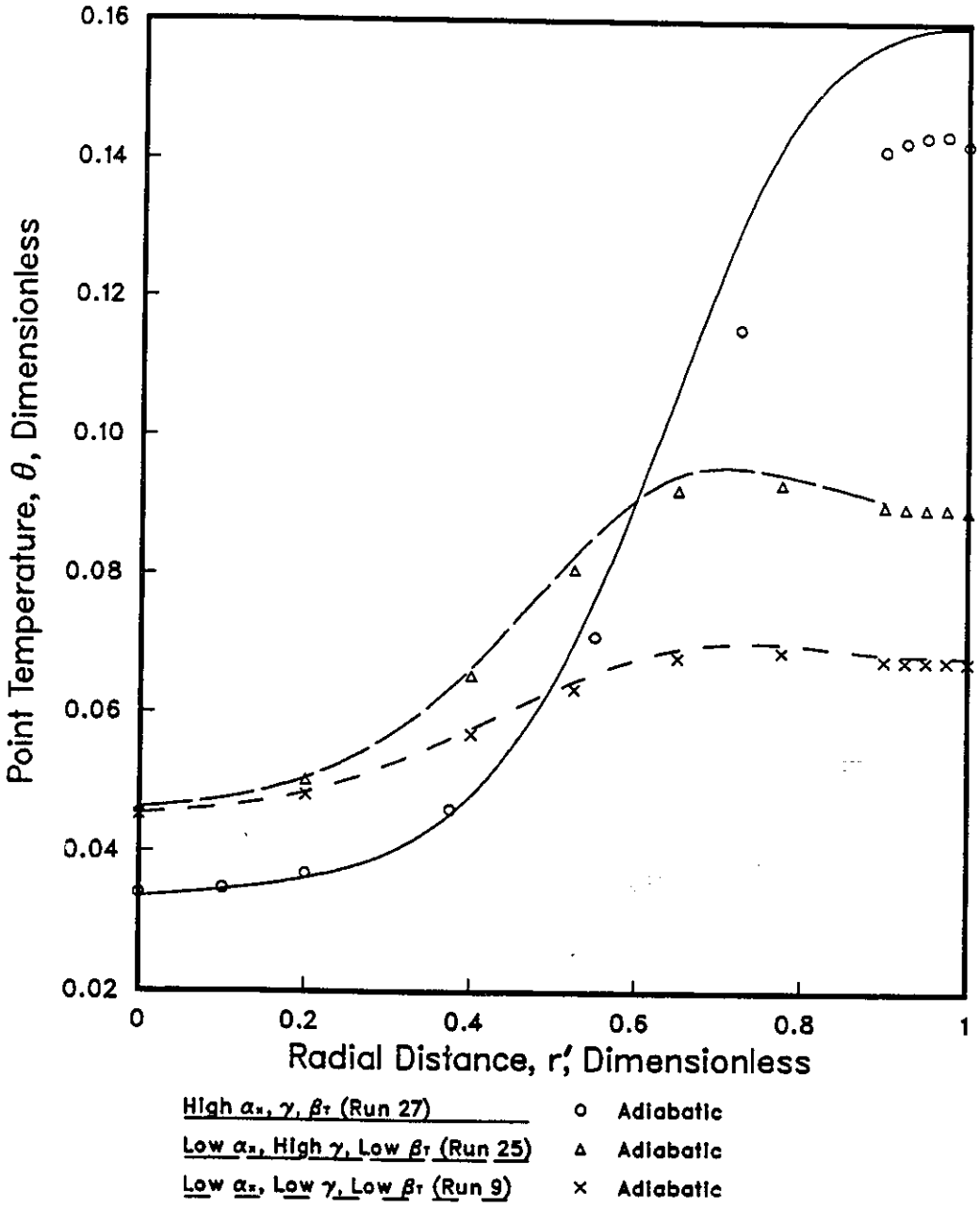

Figure 5.16: Comparison of Radial Temperature Profiles in the Low Heat Transfer Regime at .5 of the 90% Conversion Length

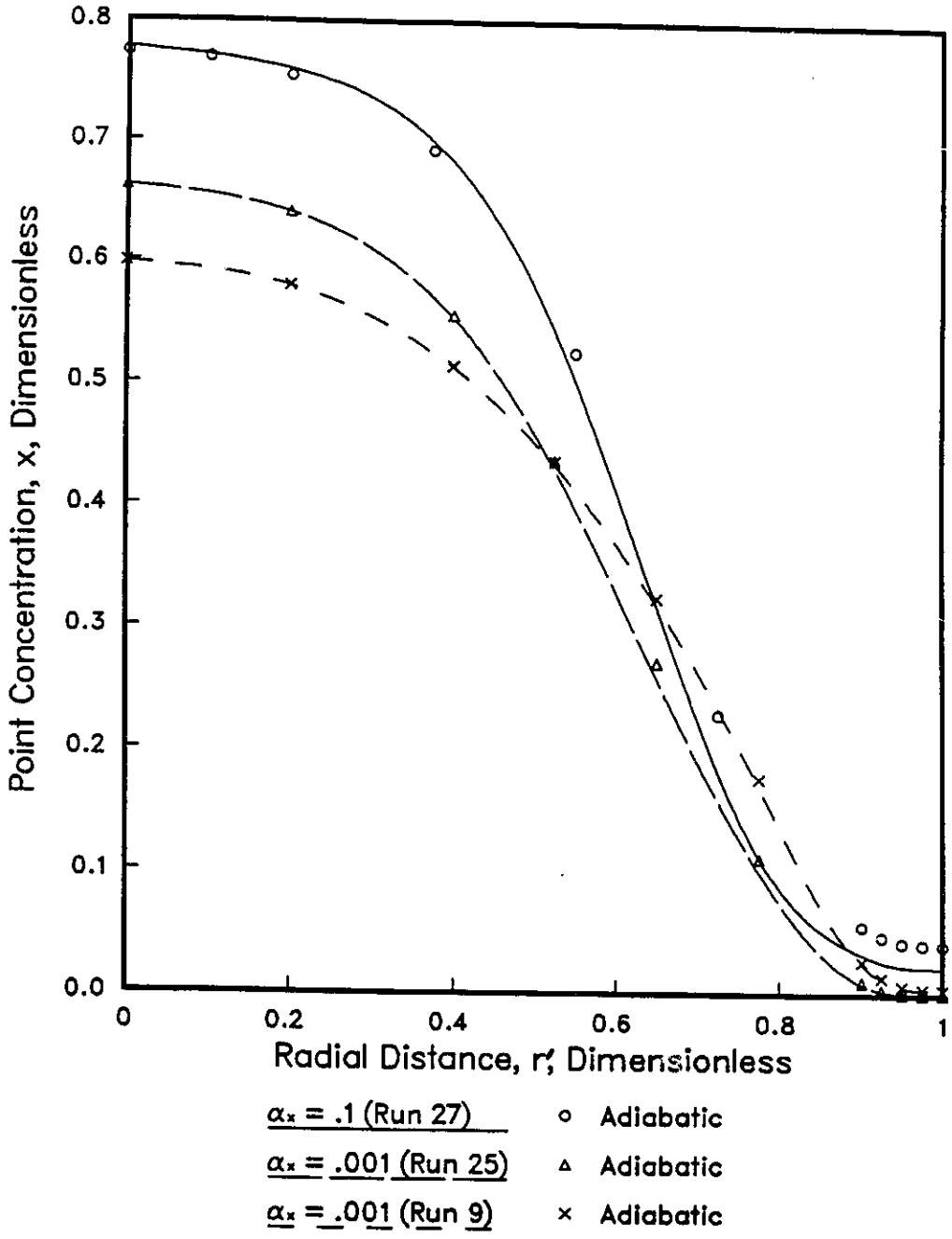

Figure 5.17: Comparison of the Radial Concentration Profiles in the Low Heat Transfer Regime at .5 of the 90% Conversion Length

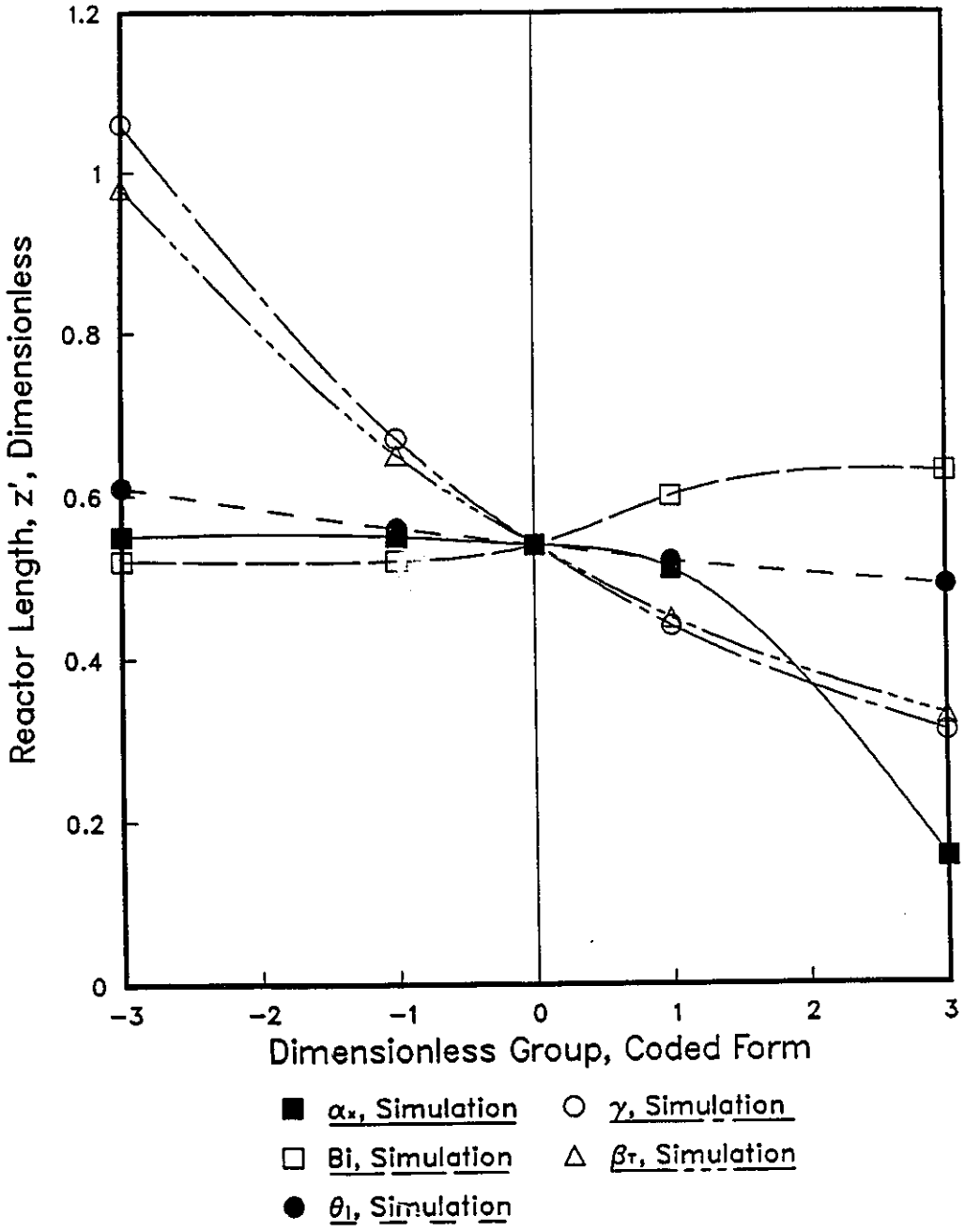

Figure 5.18: Influence of the Dimensionless Groups Around the Adiabatic Regime Center Point ($\alpha_T = 10^{-1}$)

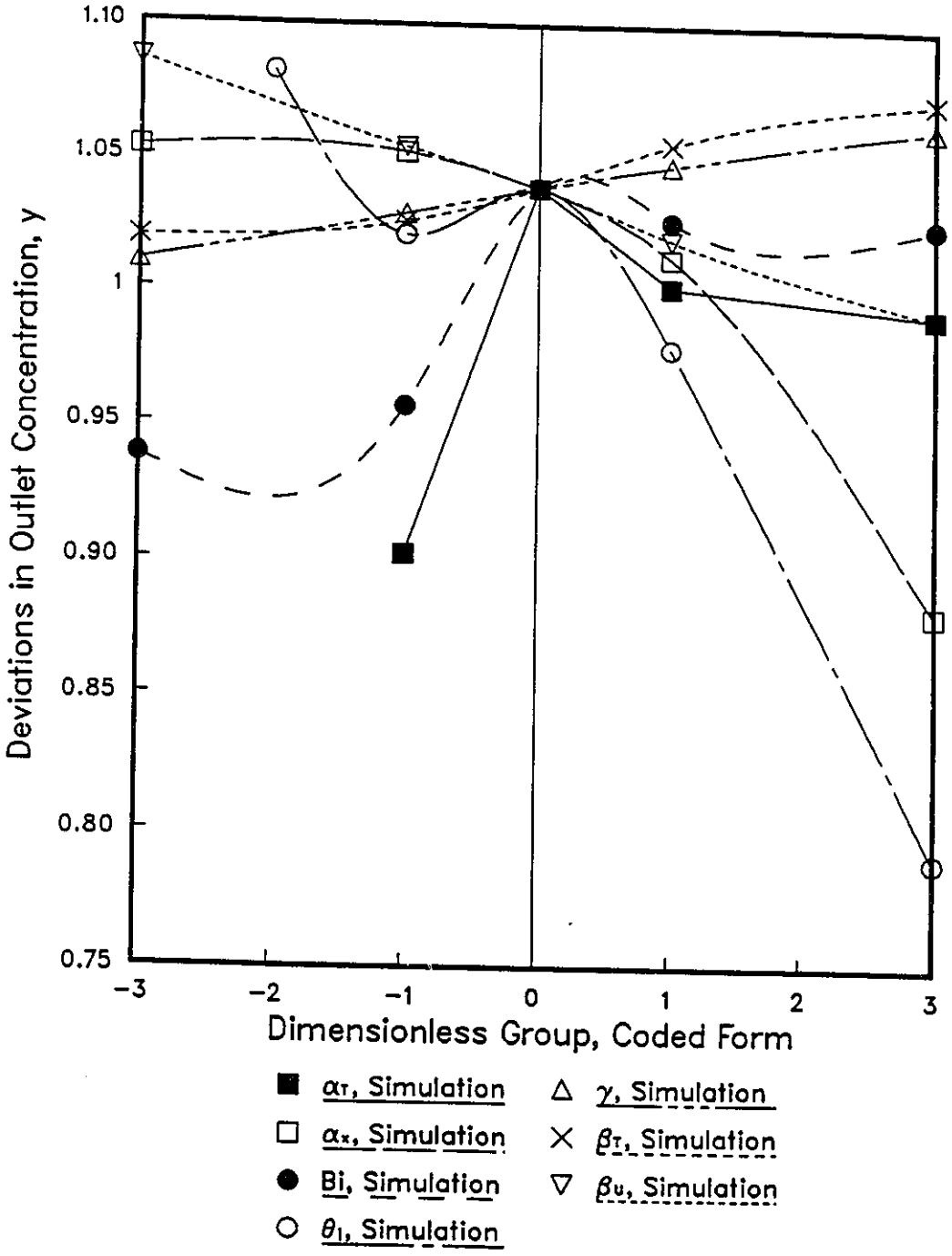

Figure 5.19: Deviations From the Constant Property Assumption as a Function of the Dimensionless Groups in Coded Form

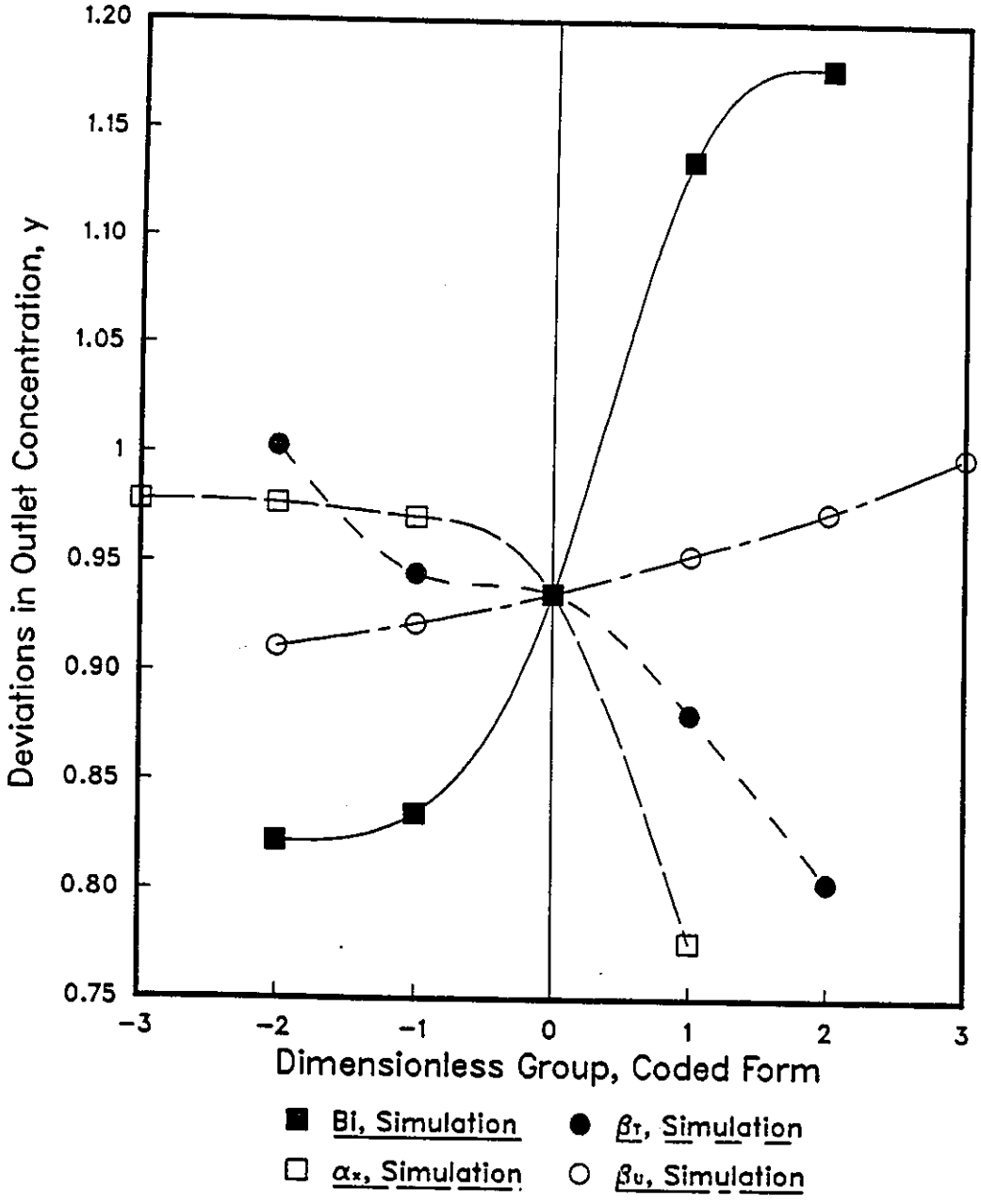

Figure 5.20: Deviations From the Constant Property Assumption as a Function of the Dimensionless Groups in Coded Form in the Low Heat Transfer Regime

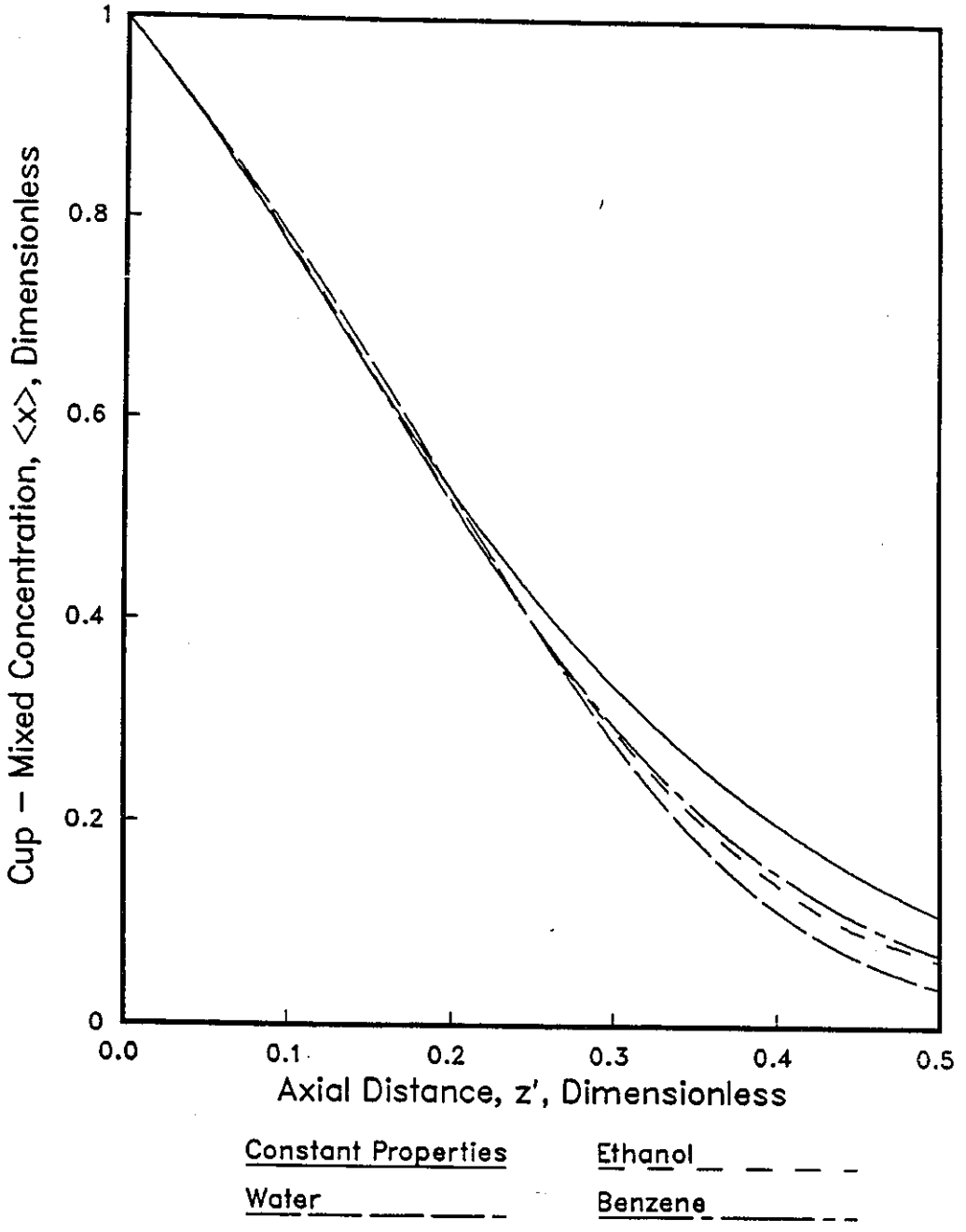

Figure 5.21: Comparison of Cup-Mixed Conversions for Run 11: Constant and Non-Constant Physical Properties

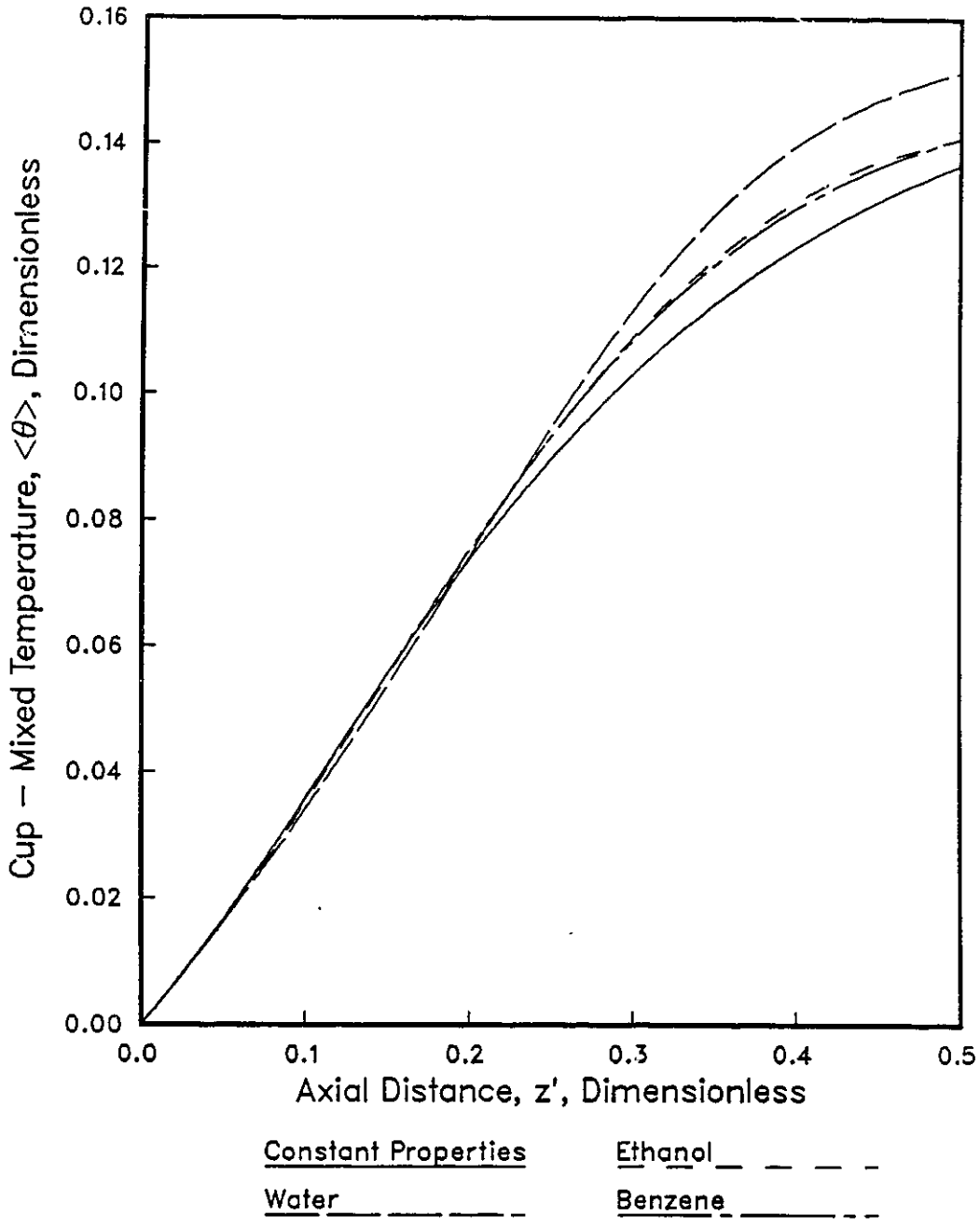

Figure 5.22: Comparison of Cup-Mixed Temperatures For Run 11: Constant and Non-Constant Physical Properties

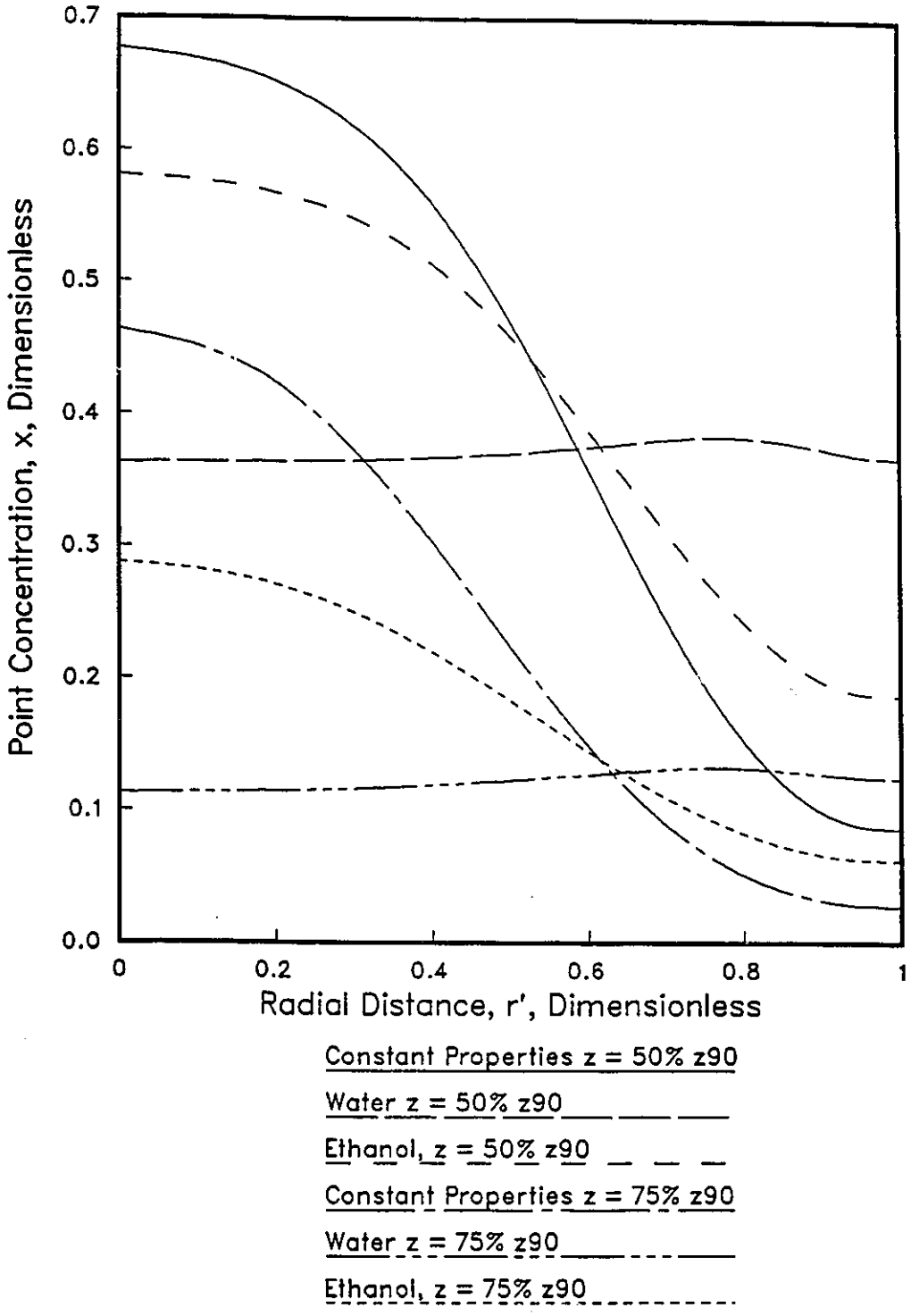

Figure 5.23: Comparison of Radial Concentrations For Run 11: Constant and Non-Constant Physical Properties

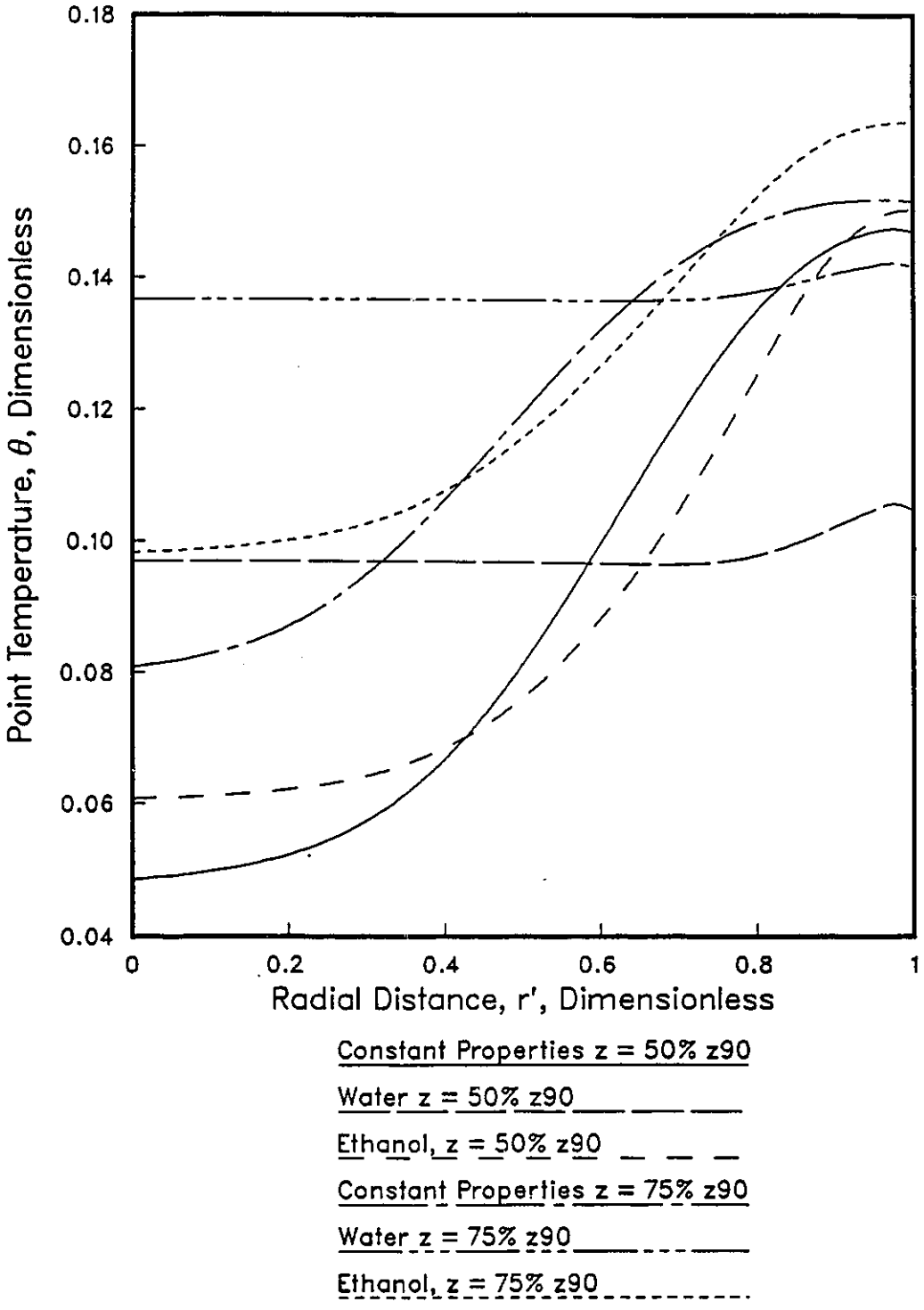

Figure 5.24: Comparison of Radial Temperatures For Run 11: Constant and Non-Constant Physical Properties

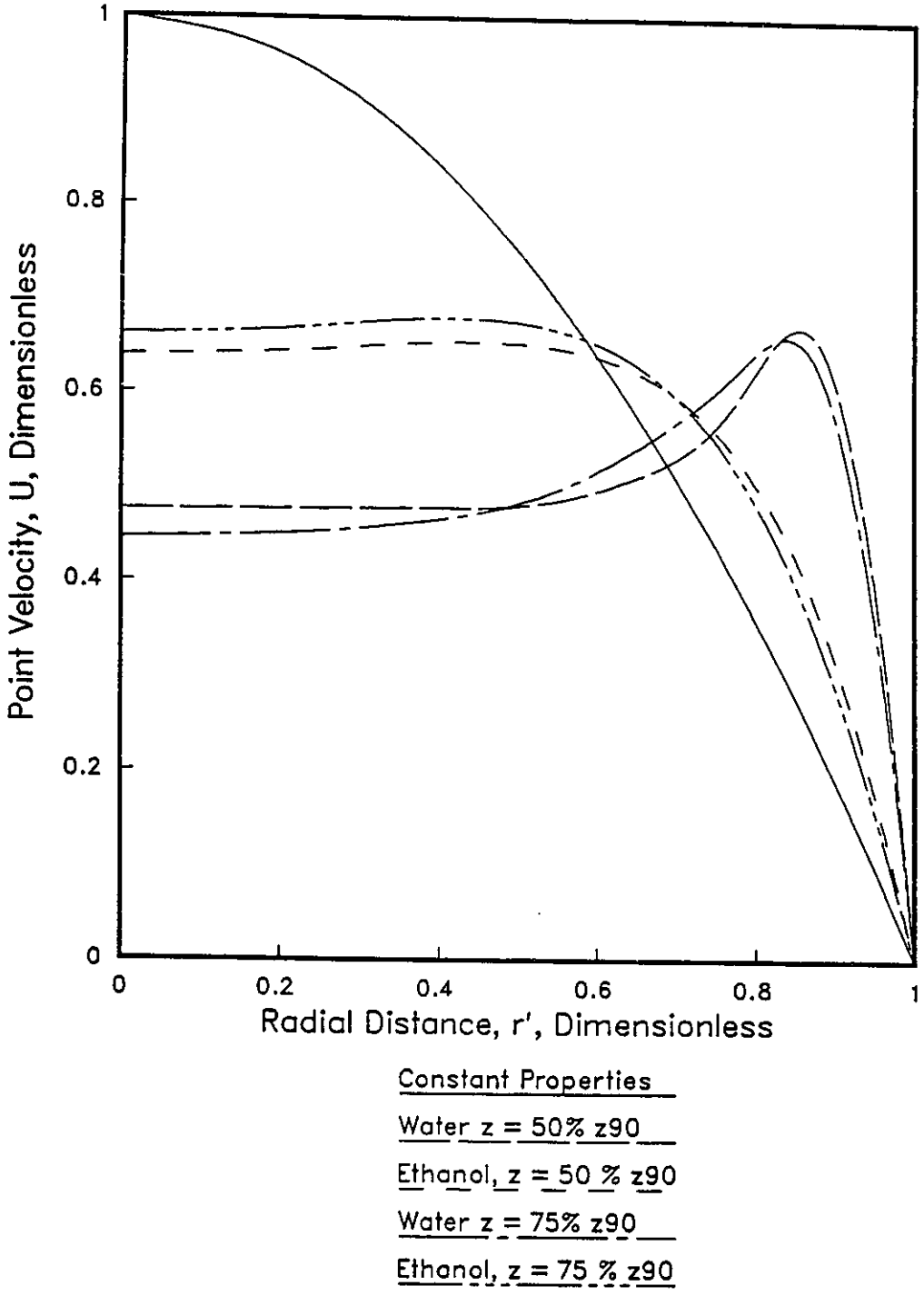

Figure 5.25: Comparison of the Axial Velocity Profiles For Run 11: Constant and Non-Constant Physical Properties

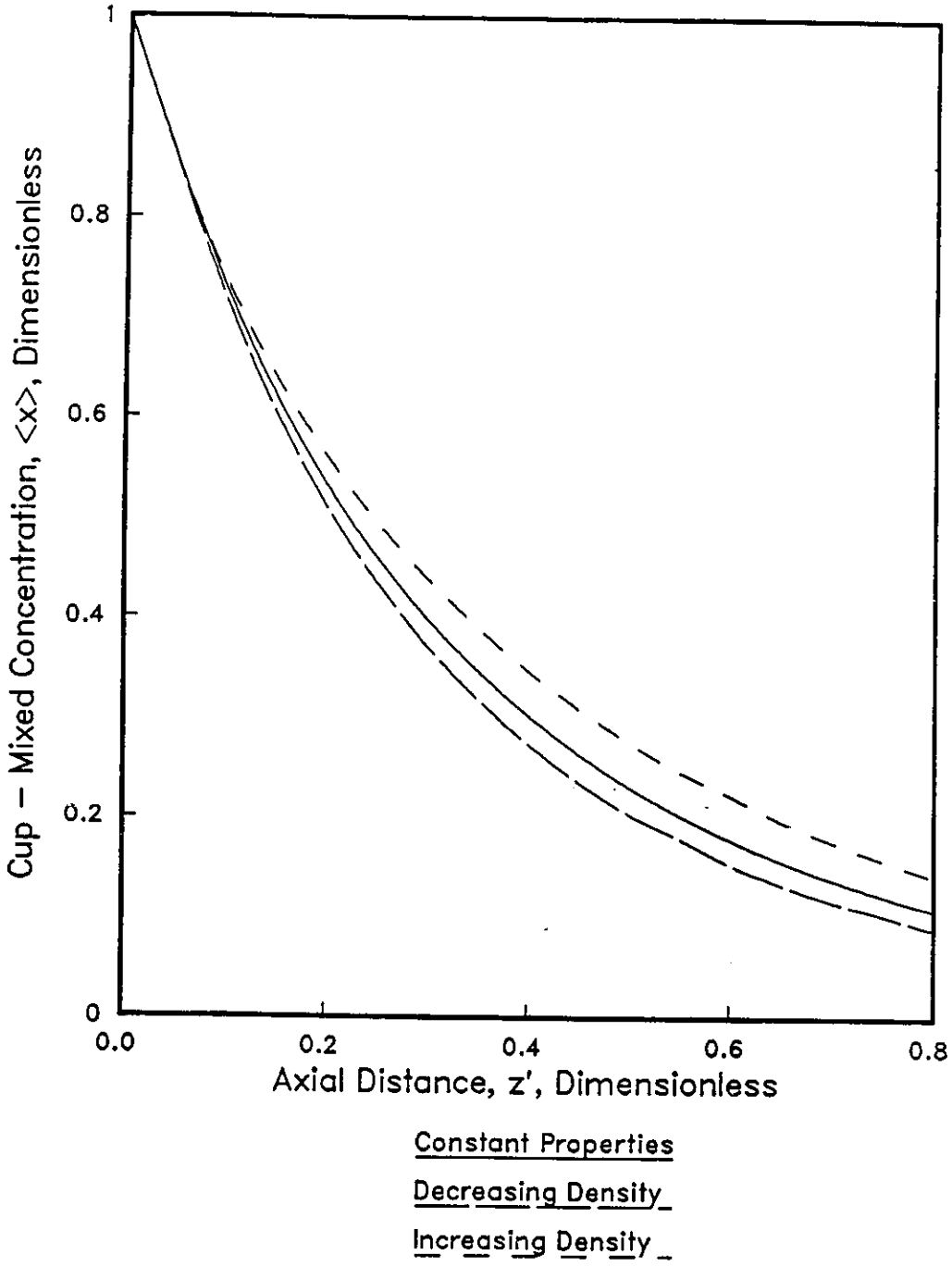

Figure 5.26: Cup-mixed Concentration Profiles for Run 14

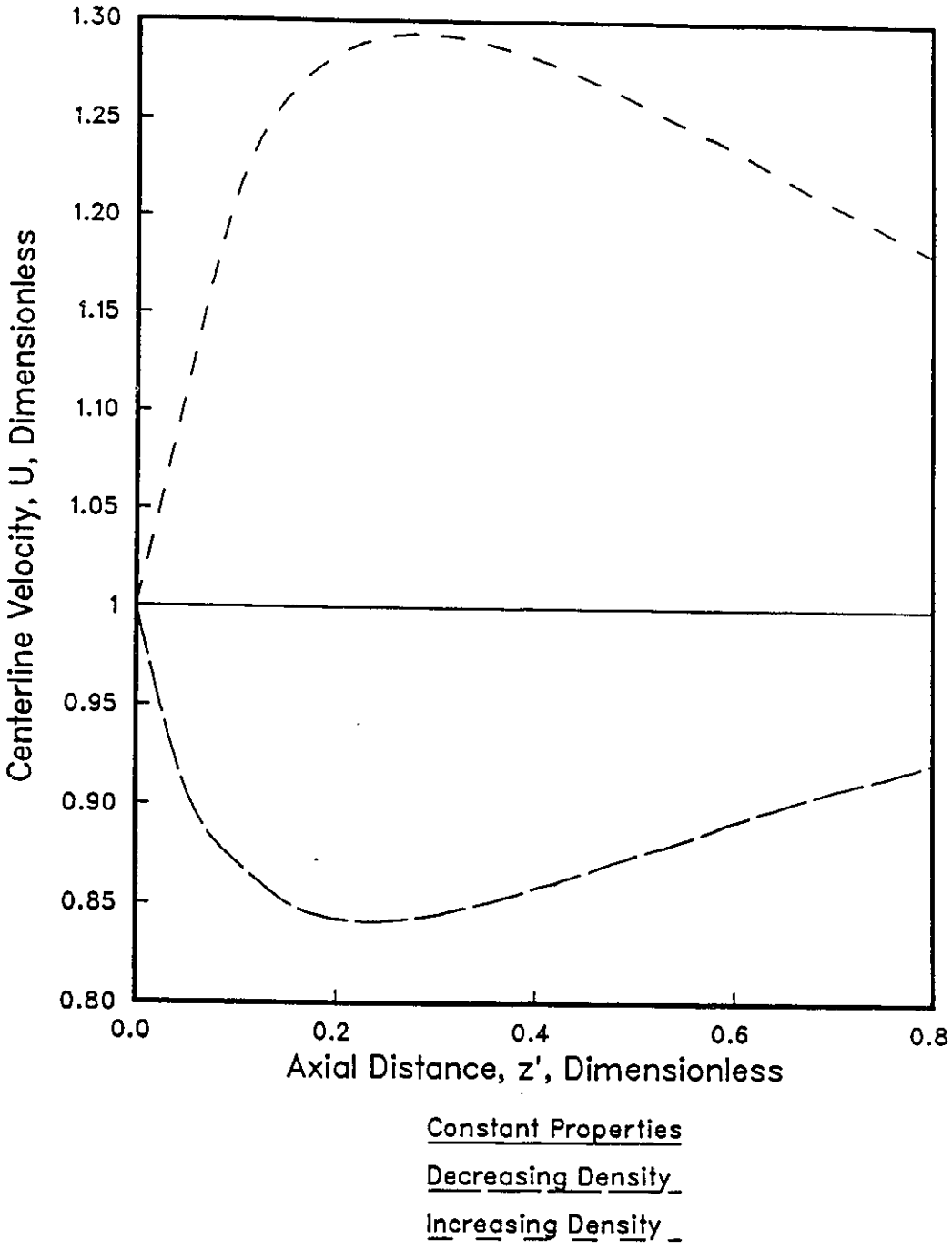

Figure 5.27: Centerline Velocities for Run 14

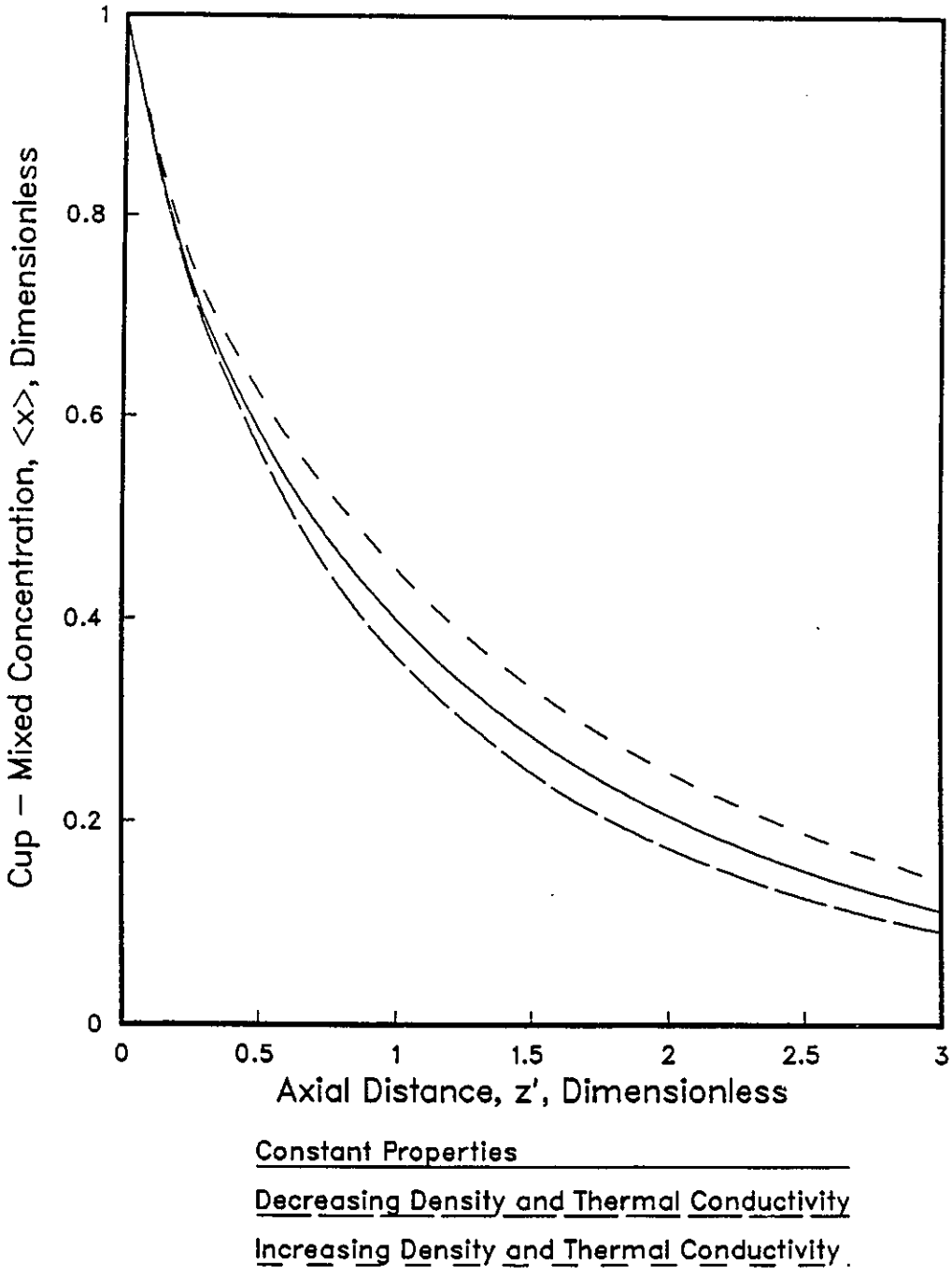

Figure 5.28: Cup-mixed Concentration Profiles for Run 347.2

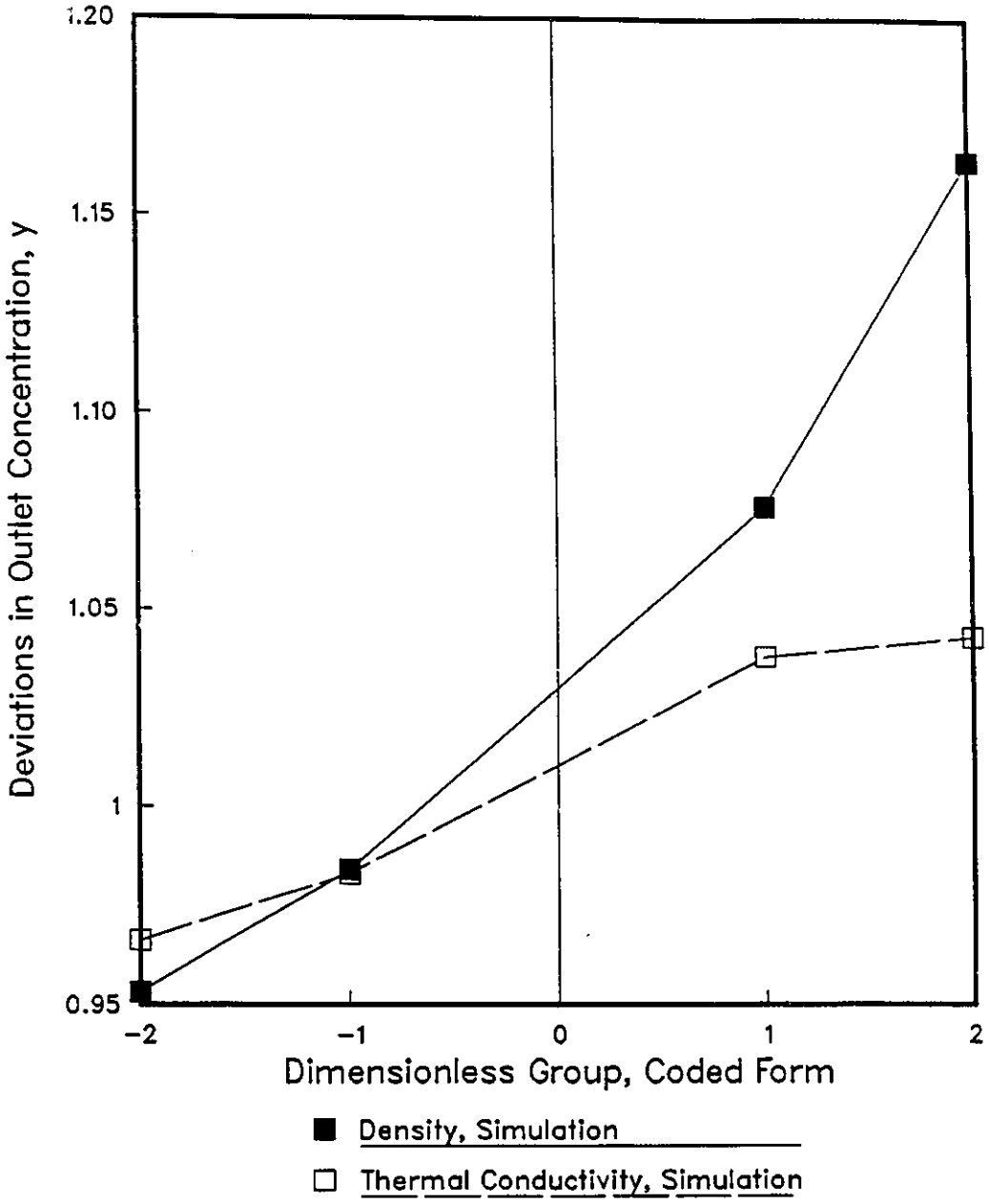

Figure 5.29: Influence of Variable Density and Thermal Conductivity around the High Heat Transfer Regime Center Point

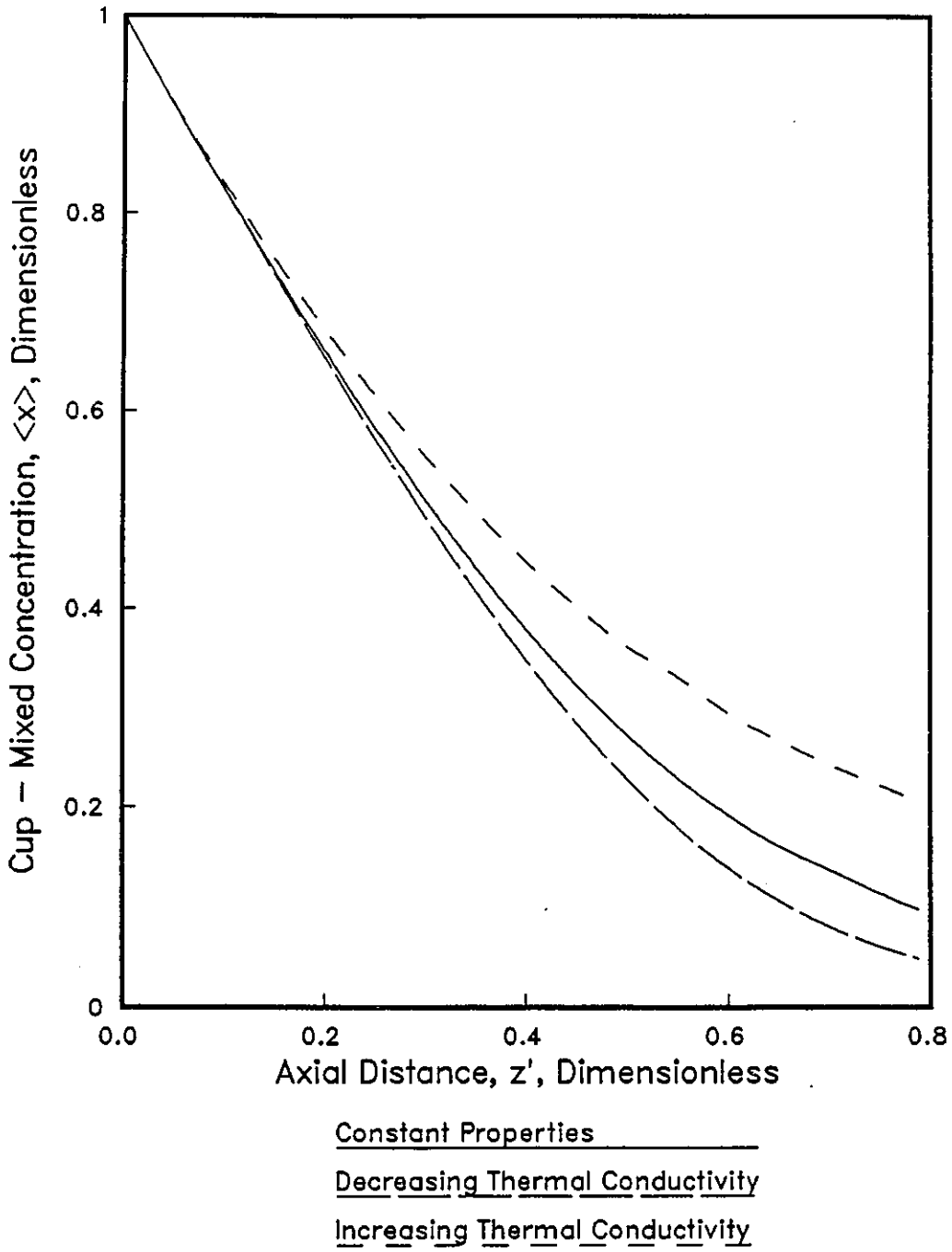

Figure 5.30: Cup-mixed Concentration Profiles for Run 21

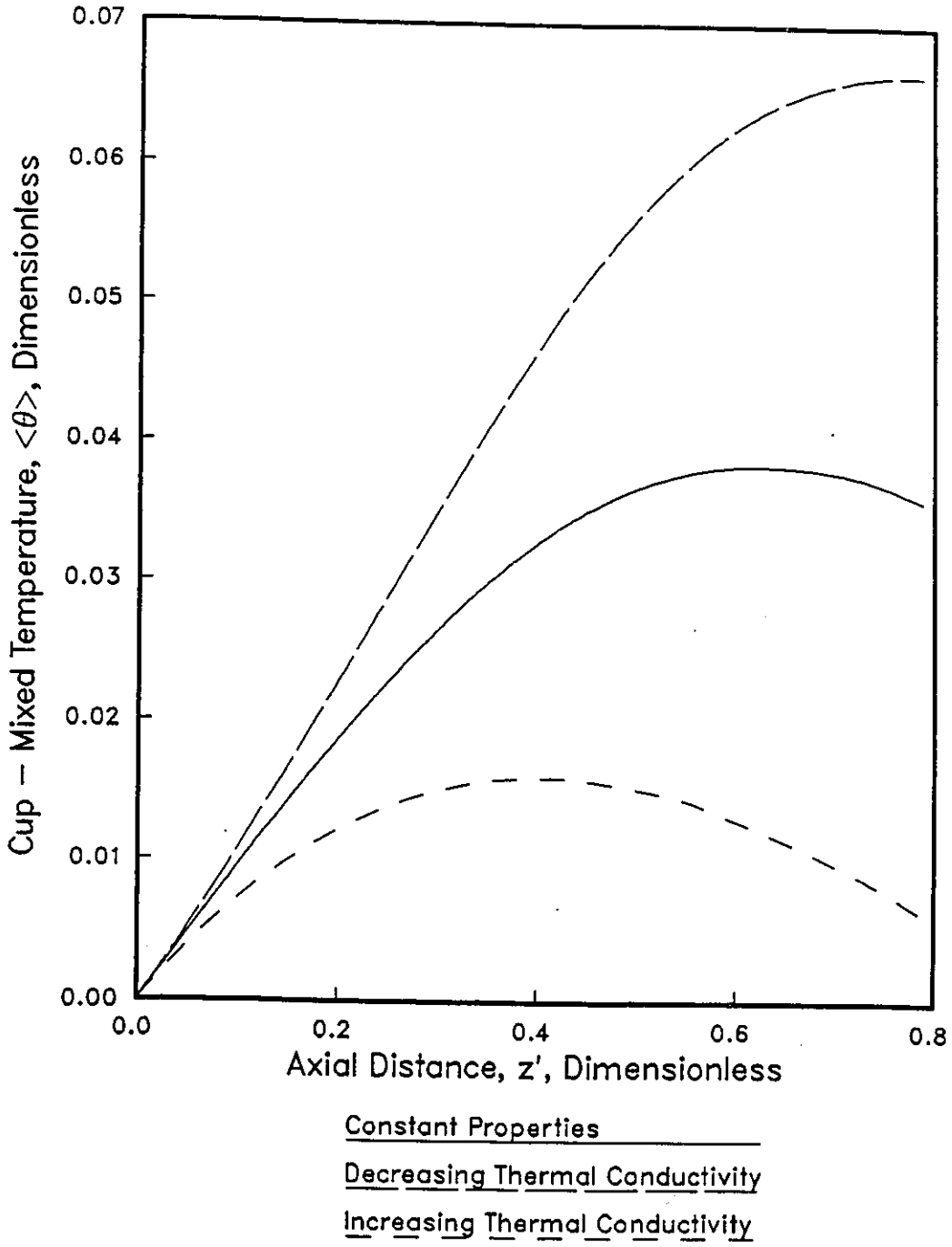

Figure 5.31: Cup-mixed Temperature Profiles for Run 21

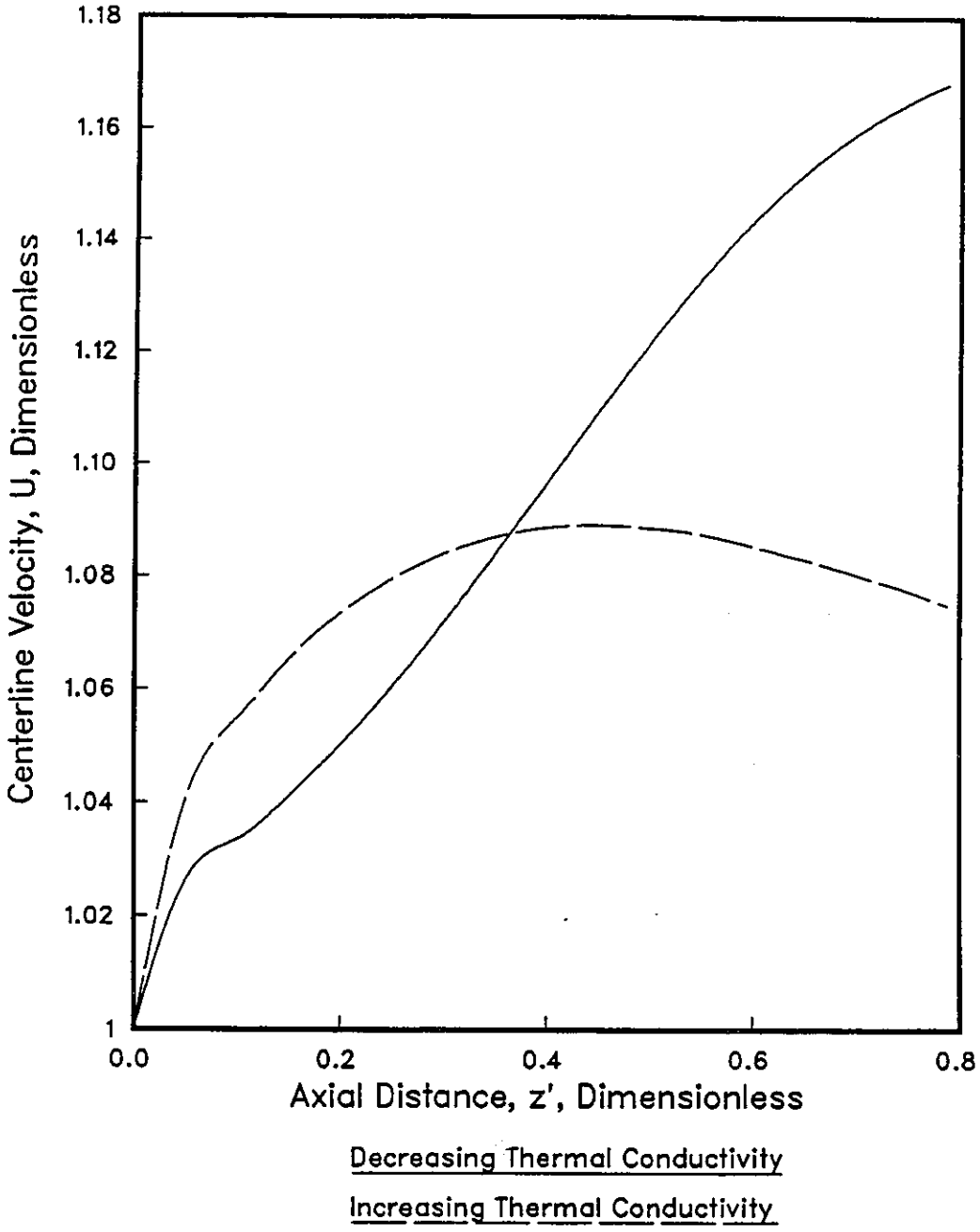

Figure 5.32: Centerline Velocities for Run 21

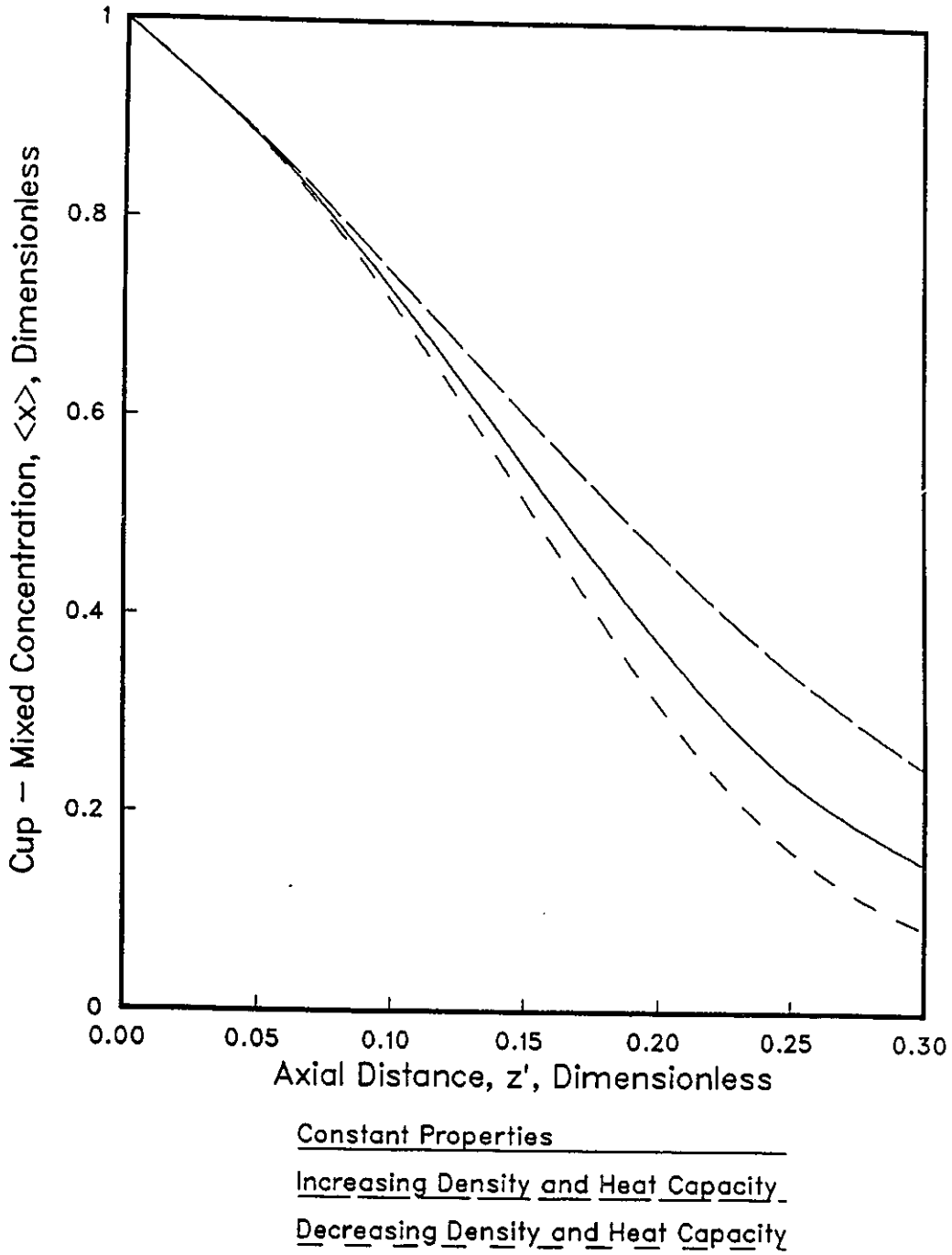

Figure 5.33: Cup-mixed Concentration Profiles for Run 26

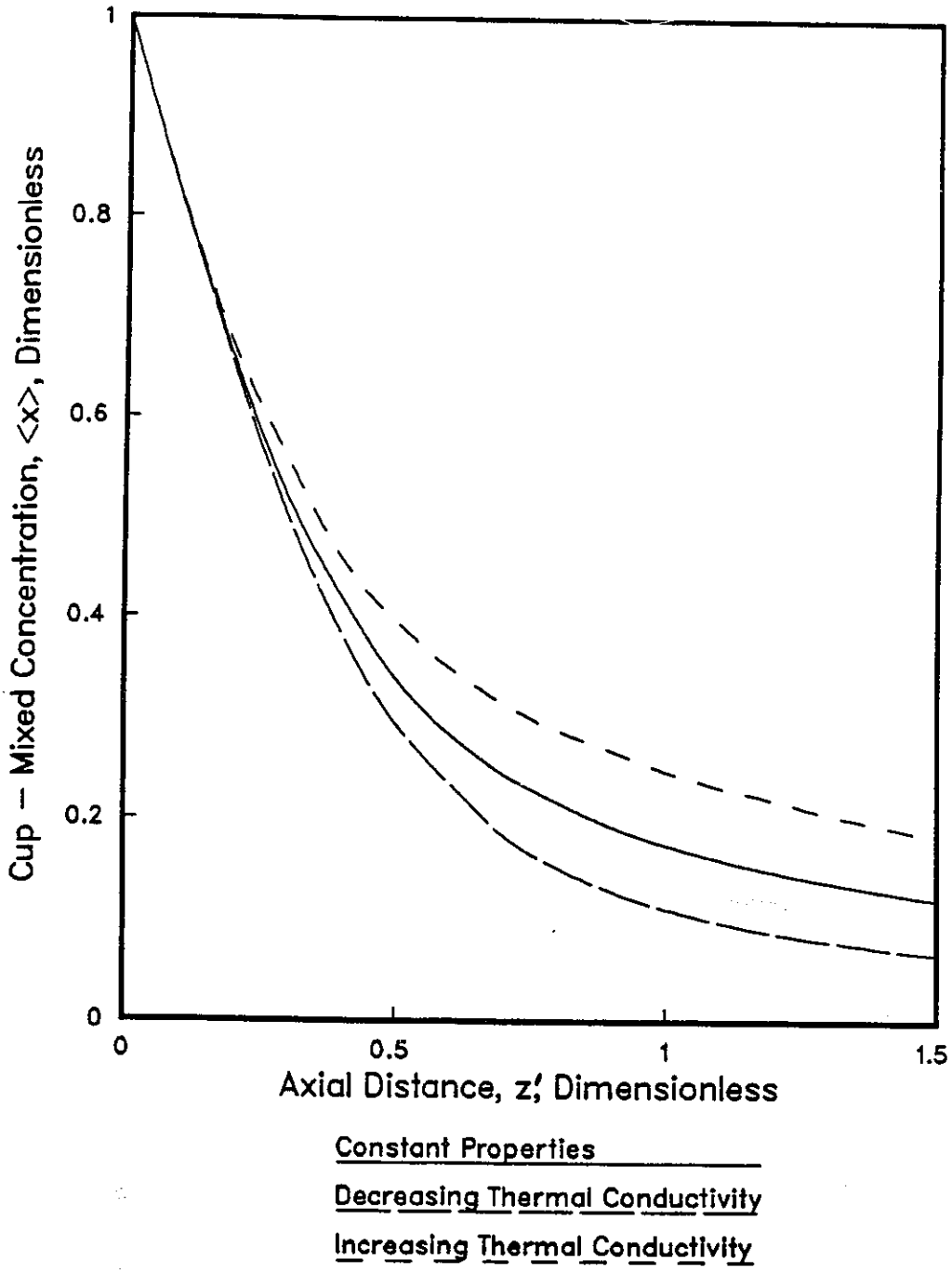

Figure 5.34: Cup-mixed Concentration Profiles for Run 456.7

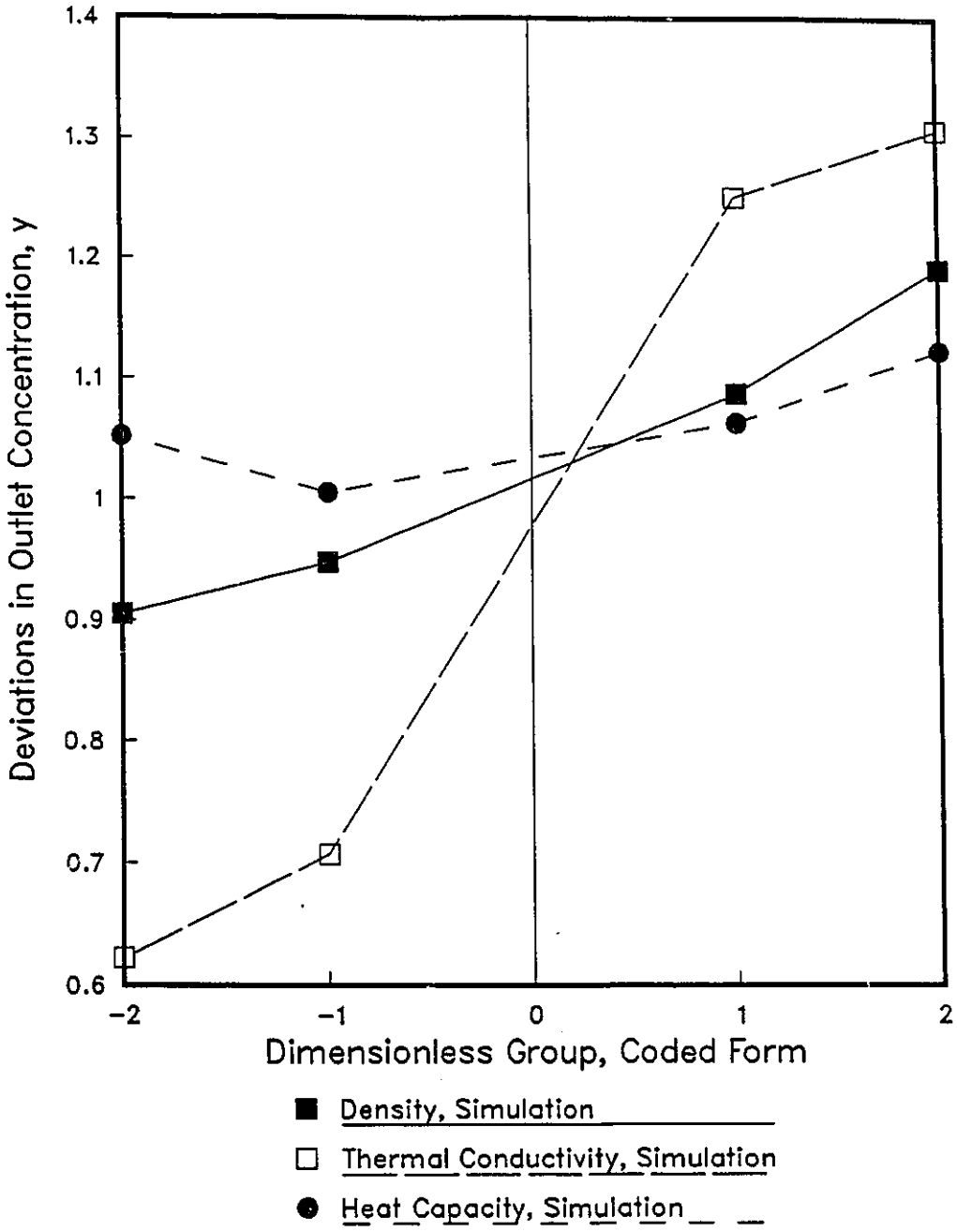

Figure 5.35: Influence of Changing Physical Properties around the Medium Heat Transfer Regime Center Point

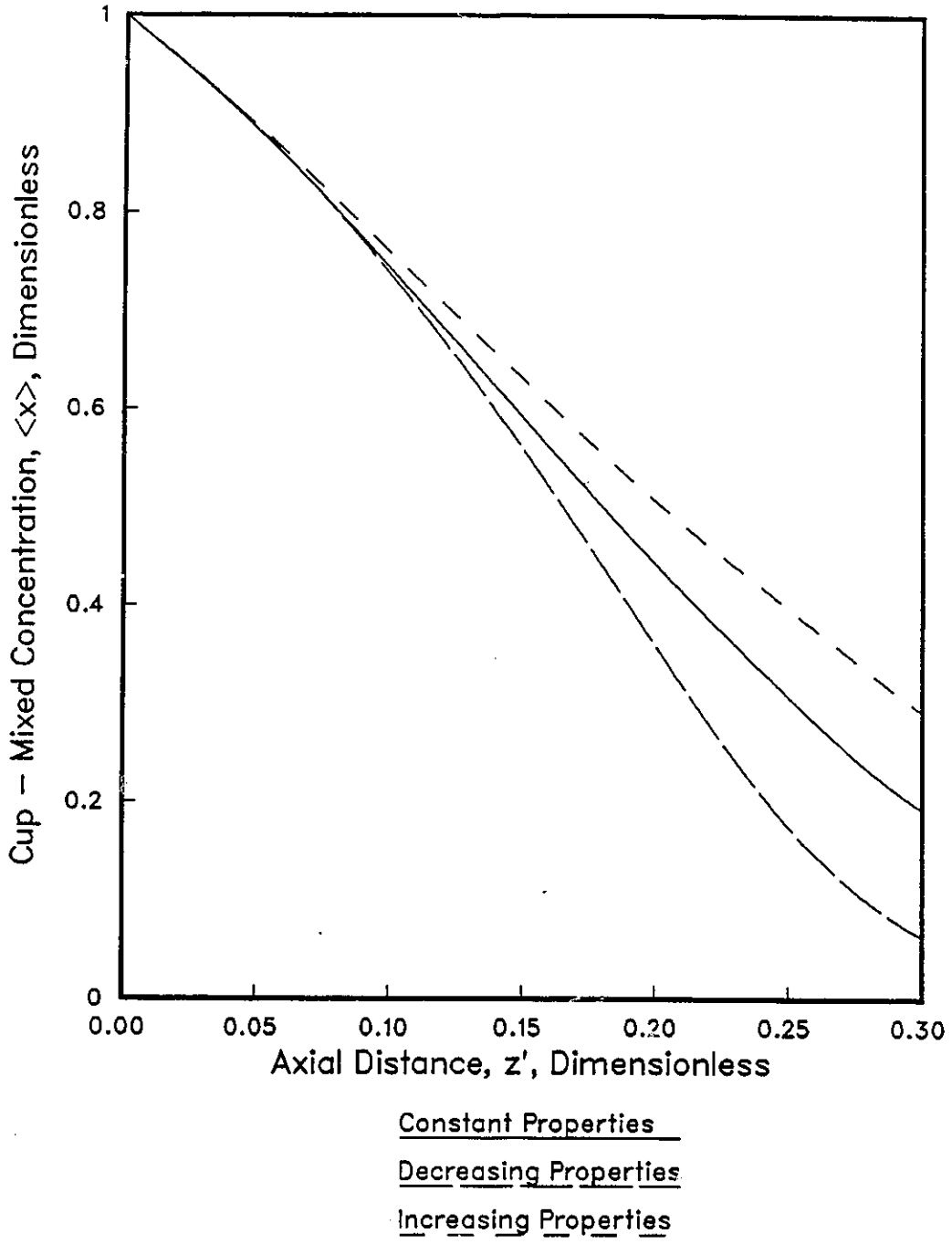

Figure 5.36: Cup-mixed Concentration Profiles for Run 17

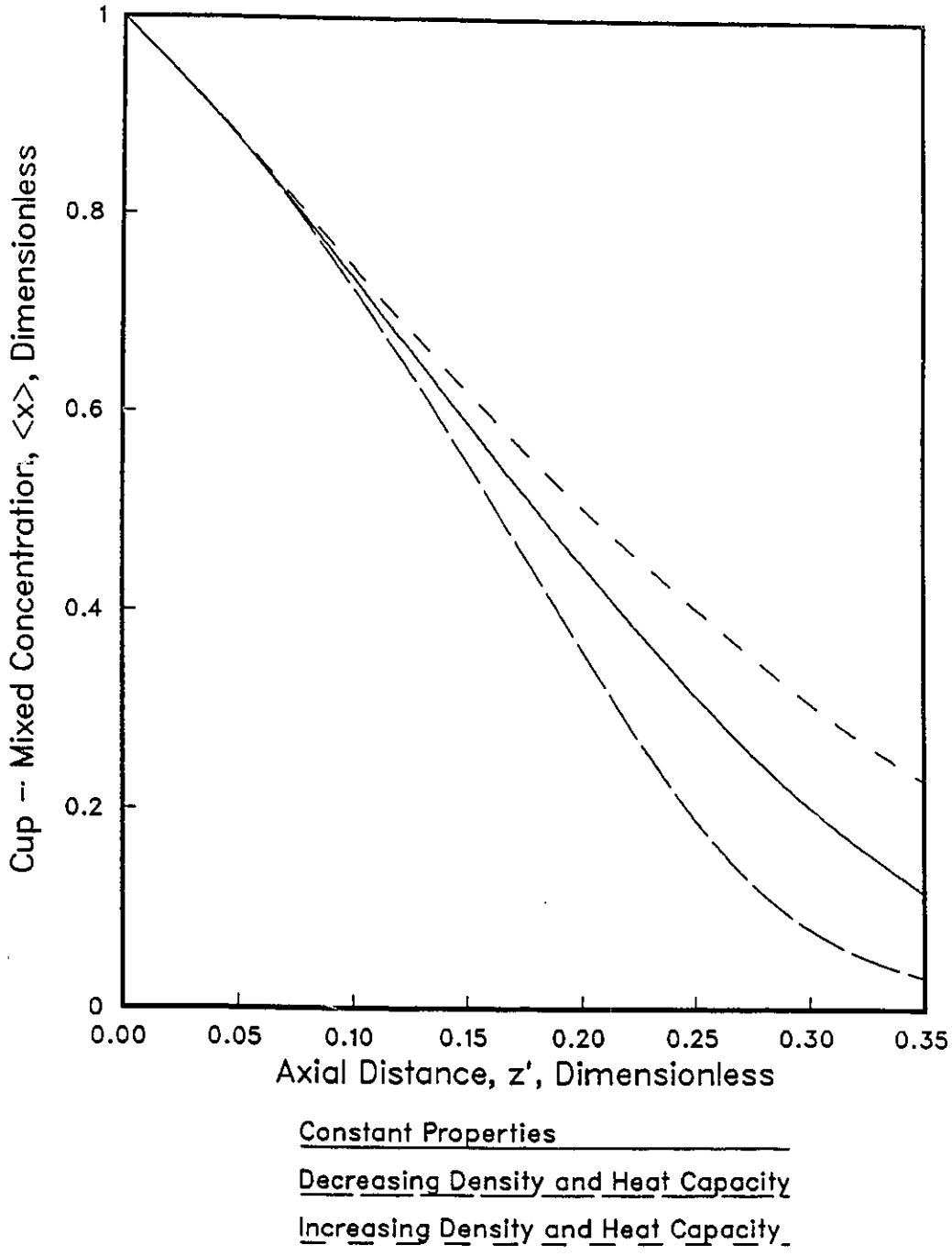

Figure 5.37: Cup-mixed Concentration Profiles for Run 29

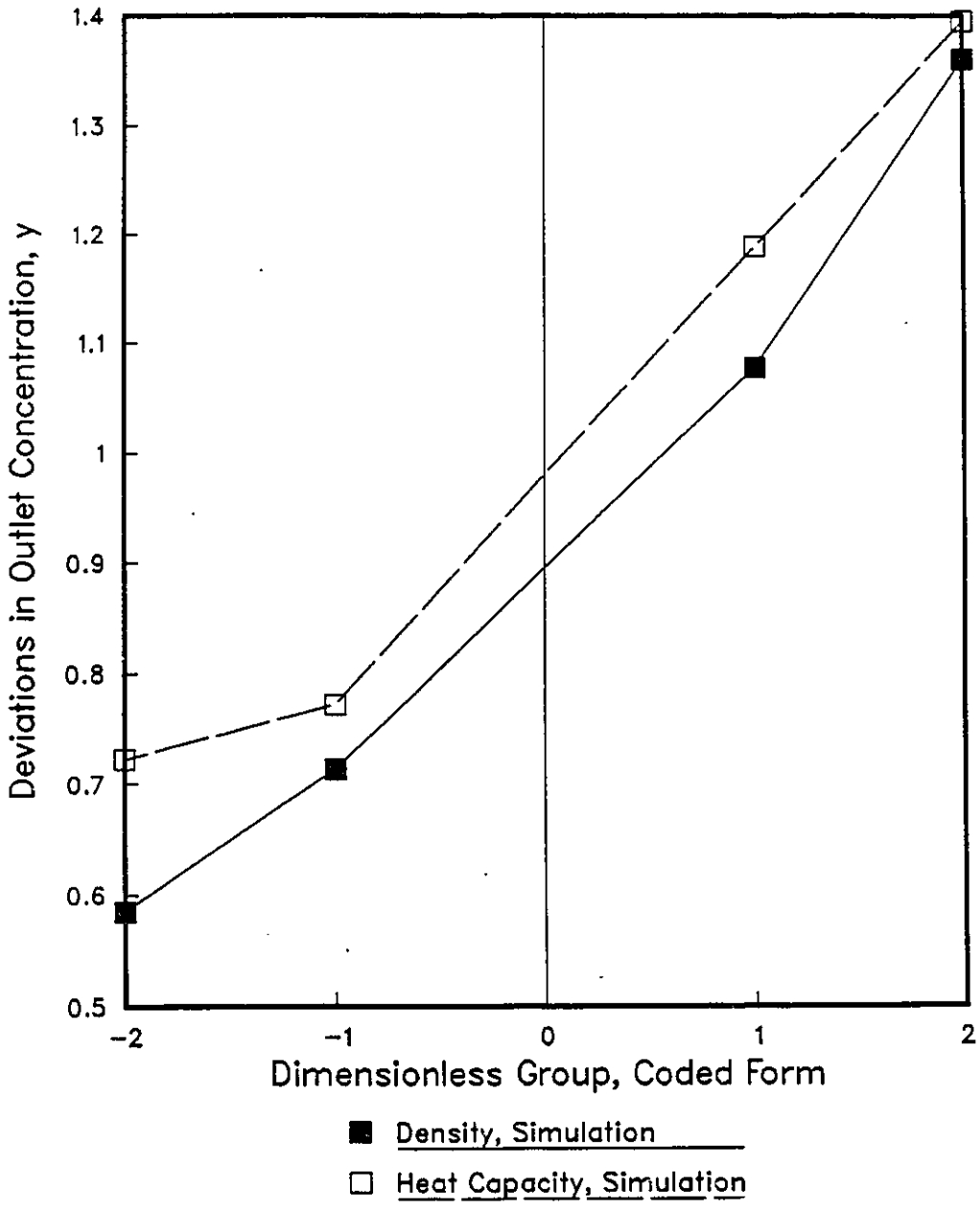

Figure 5.38: Effects of Variable Density and Heat Capacity around the Low Heat Transfer Regime Center Point

Chapter 6

Comparisons Between Theory and Experiment

In the study of the laminar flow reactor the number of theoretical investigations has outnumbered the number of experimental investigations. This may be attributed the fact that it has been difficult to find a system in which all of the pertinent data are available. These data should include well-established kinetics including the mechanism, Arrhenius parameters, and the heat of reaction, as well as the behaviour of the physical and transport properties as functions of both temperature and composition. In previous experimental investigations the tendency has been to work with dilute systems in an aqueous medium [4,5,12,15,17]. In this way it could be assumed that the properties were approximately those of water and had the temperature dependency of water. The assumption of temperature dependent properties could be employed [12]. The problem that has arisen in the use of dilute solutions with respect to examining the effect of variable properties has been that under these conditions temperature rises were small since the heat generated was small.

Temperature changes in the reactor may be achieved in two basic ways. In the first instance the reactor can be exposed to an ambient temperature that is different from the inlet temperature [12]. In this way heat transfer with the surroundings may occur. Much of the data of the high and medium heat transfer ranges in the

present study considered this case. As was seen in the simulation data collected in this study, changes due to temperature dependent properties obtained in this manner were not great. This was partially due to the small differences between the jacket and inlet temperatures used. In his study, Shinohara [12] did not detect large deviations in his data when they were examined with respect to constant or varying physical properties. In his experimental work he employed temperature differences of approximately $10K$. The numerical simulations of this study employed temperature rises due to heat transfer of approximately $15K$. This temperature rise was not large enough to create significant deviations even when accompanied by a much larger heat of reaction than that employed by Shinohara ($\beta_T \approx 2 \times 10^{-5}$ for Shinohara compared to .125 for the present study).

The second way to create the temperature differences would be to use the heat of reaction in an adiabatic reactor [15,17]. Temperature changes generated in this manner are a function of the amounts of reactants added to the system. In this second approach the number of unknown factors is reduced since there is not a concern for the wall heat transfer, the jacket temperature, and the possibility that these quantities might in fact be changing along the length of the reactor. In this manner the system may be simplified. The problem lies in the fact that greater concentrations of reactants are required to achieve appreciable temperature differences. Higher concentrations of reactants would increase the heat of reaction. If the concentrations were large enough properties would vary due to both temperature and composition changes.

A potentially suitable reaction that has often been used in the study of laminar flow reactors in the past has been the hydrolysis of acetic anhydride [4,15,17]. It has been assumed in these previous investigations that the reaction was first order with respect to the anhydride. If the solution was sufficiently dilute then this condition would in fact hold, since the other reactant, water, would be in excess. However, at low concentrations the amount of heat generated was low. Two of the studies cited above employed the acetic anhydride hydrolysis in an adiabatic reactor [15,17].

The numerical simulations presented earlier in this study showed that in an adiabatic reactor or one that was approximately adiabatic the effect of varying physical

Table 6.1: Comparison of Results of the Present Study with Those of Vena

Run	Outlet Concentrations ($\langle x \rangle$)			Outlet Temperatures ($\langle \theta \rangle$)	
	Exp	Vena	Present	Exp	Present
1A	.220	.250	.226	.021	.024
2A	.252	.271	.247	.015	.017
3A	.295	.280	.255	.011	.015
1B	.115	.104	.086	.024	.028
2B	.130	.116	.097	.020	.023
3B	.249	.125	.105	.015	.020

properties was greatest. These large variations encountered in the simulations were contingent on a number of factors. Among these was the requirement that the heat of reaction be large enough to generate an appreciable amount of heat. In the previously cited studies the concentrations were low such that the dimensionless heat of reaction was small. The results given by Vena [15] and Dussault [17] were examined in this study. Comparisons between the experimental (Exp) and predicted values of the above investigators (Vena or P.-D.) and the predicted values of this present study have been given in Tables 6.1 and 6.2. In all of the cases the properties have been assumed to be constant. As may be seen, the predicted and experimental results of Vena were reasonably close. On the other hand the conversions were overestimated by the numerical models for the data presented by Dussault.

Because of the low temperature rises encountered in the above investigations, there was no reason to consider examining the data in the context of varying properties. In order to examine results in an experimental reactor it was necessary to attempt to perform runs at concentrations greater than those employed by previous investigators.

Table 6.2: Comparsion of Results of the Present Study with Those of Pilon-Dussault

Run	Outlet Concentrations ($\langle x \rangle$)			Outlet Temperatures ($\langle \theta \rangle$)
	Exp.	P.-D.	Present	Present
2P	.703	.591	.602	.024
2PC	.760	.615	.625	.022
3P	.599	.502	.512	.027
3PC	.609	.519	.531	.025
31PC	.625	.401	.404	.032
32PC	.485	.295	.301	.035
33PC	.396	.221	.227	.032
4P	.514	.383	.392	.024
4PC	.523	.401	.410	.024
7PC	.526	.509	.513	.016
34PC	.244	.150	.153	.024
37PC	.356	.252	.257	.018

6.1 The Reaction Rate of the Hydrolysis of Acetic Anhydride

The hydrolysis of acetic anhydride may be written as follows:

$$(CH_3CO)_2O + H_2O \rightarrow 2CH_3COOH \tag{6.1}$$

Several studies have been performed on this reaction although the majority of them have been performed at low reactant concentrations [50,51,52,53,54,55,56,57]. Most of the above studies were performed at low concentrations of the anhydride due to its low solubility in water (12 g anhydride/100 g water [58]). As a consequence the system has been modelled as a first order reaction with respect to anhydride concentration. By observing the reaction in concentrated acetic acid solution Greathouse *et al* were able to obtain second order rate constants [55,56]. Several of the results of these investigations have been compiled and reported elsewhere [17,18].

Monguló and Garcia [57] employed data compiled by Dussault [17] to develop the following empirical rate equation:

$$R_A = (k_1 + k_2 c_A) c_C^{k_5} \exp(-(k_3 + k_4 c_A)/T) c_A \tag{6.2}$$

where

$$\begin{aligned} k_1 &= 1.254 \times 10^9 \\ k_2 &= -1.094 \times 10^9 \\ k_3 &= 5574.3 \\ k_4 &= -104.4 \\ k_5 &= -.47 \end{aligned}$$

Because the concentration of water was not included in the definition of the reaction rate, the equation was limited to lower concentrations of anhydride. It was interesting to note that their model was both dependent upon the concentration of the anhydride, c_A, and also was hindered by the presence of acid, c_C. The values of the activation energy and the frequency factor both decreased with increasing amounts of anhydride. They employed this model to examine the behaviour of a stirred

tank reactor. Initial concentrations of the acid and anhydride of approximately .80-1.06 and .20-.76 mol/l respectively were employed. A mathematical model yielded results in good agreement with experimental results in the investigation [57].

Higher concentrations of anhydride and acid were examined by Rao and Parey [59]. In their study of the kinetics they derived the following rate equation:

$$R_A = -k_m c_A c_B c_C^{0.7} \tag{6.3}$$

where

$$k_m = 2.1462 \times 10^{11} \exp(-6877.6/T) \frac{(cm^3)^{1.7}}{(mol)^{1.7}(min)} \tag{6.4}$$

This equation was developed at much higher concentrations of both anhydride and acid and less water. It was interesting to note that the behaviour of this equation contradicted the results of the previous investigation since an increase in acetic acid enhanced the reaction rate. Equation 6.2 indicated that the reaction rate should decrease with an increase of acetic acid concentration. A thermometric method was employed to determine the constants in Equations 6.3 and 6.4. This suggested that the use of these equations should be particularly useful in predicting the temperature profiles of the reactor. Temperature rises of up to 100K were reported. This was due to the fact that the concentrations of all reactants were much higher. The concentrations of the reactants were in the range 3.8 mol/l for anhydride , 17.9 mol/l for water, and 4.8 mol/l for acetic acid. In light of the significant temperature rises developed at these concentrations it seemed reasonable to employ similar concentrations in the present investigation and use this model for comparisons between the numerical study and experimental data.

6.2 Experimental Procedure

A stainless steel reactor 1.15 meters in length with an inner diameter of 5.1 cm was used (Refer to Figure 6.1). The reactor was wrapped in fiberglass insulation to make it adiabatic.

Thermocouples of 1/16" diameter were employed to measure the radial temperature profiles along the length of the reactor. They were capable of sliding into the

reactor and were placed every 23 cm along its length. These sliding thermocouples were bent in the direction of flow to ensure that the point temperatures measured were representative of the true conditions. It was felt that this arrangement would minimize any conduction effects along the length of the thermocouples. Two additional thermocouples were placed at these locations recessed in the wall to measure the wall temperature. Thermocouples were also placed at the inlet and outlet of the reactor. The sliding thermocouples were placed next to the wall until steady state was reached in order to minimize flow disturbances. At steady state, the radial temperature profiles were measured beginning from the location closest to the outlet. This was done to ensure that the effect of flow disturbances were again minimized.

The reactants were fed into the reactor by means of a duplex metering pump with one side pumping an aqueous solution of acetic acid and the other pumping acetic anhydride. Two surge tanks were placed between the reactor and pumps to dampen flow pulsations. A system of valves and nylon tubing were arranged so that the reactor could be operated in either downward or upward flow (Figure 6.1). The product leaving the reactor either entered a recycle tank for replenishing the acetic acid feed or was disposed of down the drain.

Chemical and equipment details may be found in Appendix B.

The system was allowed to run until steady state was achieved. Steady state was assumed to be reached when the exit temperature was constant for at least 5 minutes. Typically at least 45 minutes to one hour was required for this to occur.

When steady state was reached the radial temperature profiles in the reactor were measured using the sliding thermocouples. The wall, entrance, and exit temperatures were also recorded.

After the temperatures were recorded a total of 8 samples were withdrawn from the reactor and analyzed for acetic anhydride and acetic acid using the aniline-water method (Appendix B).

6.3 Comparison of Experimental Data with the Numerical Model

In order to use the computer program to predict the reactor behaviour at the experimental points modifications were required in the definitions of the dimensionless groups to account for the fact that the reaction did not follow first order kinetics. In the modification procedure the rate constant, k_R, appearing in any of the dimensionless groups was replaced by a term that reflected the kinetics given by Equation 6.3.

The procedure that was employed was as follows:

1. Rao and Parey stated in their work that the rate constant could be written in terms of the initial concentration of acetic acid, c_C. Therefore a revised rate constant was defined as:

$$k'_R = k_m c_{C_o} \tag{6.5}$$

2. The reactant that was traced through the reactor was the acetic anhydride. The concentration of water was rewritten in terms of the initial concentration of anhydride in the rate equation such that the result was:

$$R'_A = -k'_R c_A^2 x\left(\frac{c_{B_o}}{c_{A_o}} - (1 - x)\right) \tag{6.6}$$

As a consequence of the above modification of the rate equation, the dimensionless groups that contained the reaction rate were evaluated such that the reaction rate k_R was replaced with the term $k'_R c_{A_o}$. Use of the above term ensured that the groups were dimensionless.

The properties of the mixture were calculated by employing mole fraction averaged values. In the case of density this involved use of Amagat's Law using specific volumes. The temperature dependence of the various properties of each component were not readily available in all cases. Since water had been used as a medium in the numerical study, all of the temperature dependent equations were available in Yaws [48]. The temperature dependency of acetic acid and anhydride were estimated from the Rackett or modified Rackett equation [60]. The parameters required for

using this equation were available in Reid *et. al.* [61] and Spencer and Adler [60]. Coefficients were also available to employ the Andrade Equation to evaluate the temperature dependence of the viscosity of the acid and anhydride [61]. Values for the thermal conductivity and heat capacity for the acid and anhydride at $300K$ were taken from those given by Vena [15]. The temperature dependency of these properties was not found. Therefore temperature dependencies of the mixture properties for thermal conductivity and heat capacity were assumed to follow those of water.

From the values of the mixture properties estimated in this manner the dimensionless groups for the experimental runs were determined (Appendix B).

6.4 Results and Discussion

Comparisons between the experimental results and the numerical model were accomplished by using the dimensionless groups that were estimated to apply to the experimental runs.

The experimental results have been given in Table 6.3. Preliminary values of the compositions and temperature rises predicted by the model assuming constant physical properties have also been included. Theoretically, since the reaction occurred in an adiabatic reactor, the experimental adiabatic temperature rise (β_T) could be determined by the equation given below:

$$\beta_T = \frac{\langle\theta\rangle_{exp}}{1 - \langle x\rangle_{exp}} \tag{6.7}$$

As may be seen, the values of the apparent heats of reaction for the first three runs seemed to be very much out of range. This was possibly due to the fact that these values were obtained from the reactor before a design modification. Initially the tubing connecting the reactor to the pumps fed directly into the reactor. Under this condition there was a sudden expansion or contraction for the inlet and outlet streams respectively. It was felt that this design might have resulted in poor mixing of the liquid at the outlet, such that the outlet concentration was not the cup-mixed concentration. Instead, it was possible that the concentrations measured at

the outlet were more representative of the concentrations near the centerline. It should be noted that the values of the radial dispersion term α_T were high enough that the radial temperature profiles were uniform (Appendix B). Therefore, the temperature at the centerline was close to the cup-mixed temperature. Flat radial temperature profiles were in fact observed for all of the experimental runs. The results of the numerical study indicated that the conversion achieved towards the center of the reactor was less than that for the overall reactor. If this was the case for the experimental system then the apparent dimensionless heat of reaction calculated in Equation 6.7 would in fact be larger than the true value. This type of trend was evident in the data for the first three points.

In order to overcome this, distributors were added to the inlet and outlet so that the outlet compositions would be more representative of the cup-mixed values.

The first 8 runs given in Table 6.3 were operated in the upward flow mode. The last three runs were performed in downward flow. It was immediately evident that the values of the outlet concentrations for the downward flow runs were less than those for the upward flow cases. These differences could be attributed to the presence of free convection.

The theoretical results were recalculated employing variable physical properties. The use of variable properties at this stage did not greatly improve the correspondence between the experimental and theoretical values.

In the preceding chapters a number of topics were discussed. In the initial stage the effect that the dimensionless groups had upon the reactor length was examined. In the case of an adiabatic reactor these lengths were determined to be a strong function of the dimensionless heat of reaction or adiabatic temperature rise, β_T. Conversely, the degree of conversion for a given reactor length would be expected to be a strong function of β_T also. Examination of this term showed that it was a function of the initial temperature, heat of reaction, density, and heat capacity of the system. The system under study consisted of three components forming a non-ideal mixture. It was therefore reasonable to assume that the mixture properties calculated for the system could be in error. An error of as much as 15% was not considered unreasonable.

Table 6.3: Comparison of Experimental Results with Preliminary Results Calculated using the Numerical Model assuming Constant Physical Properties

	Experimental Values			Calculated Values		
Run	$\langle x \rangle$	$\langle \theta \rangle$	β_T (From Eq. 6.7)	$\langle x \rangle$	$\langle \theta \rangle$	β_T
1	.780	.097	.441	.118	.156	.177
2	.622	.124	.328	.488	.073	.143
3	.682	.134	.421	.002	.247	.247
4	.320	.185	.272	.018	.353	.360
5	.605	.080	.203	.165	.220	.265
6	.136	.236	.273	.017	.212	.216
7	.294	.170	.241	.038	.234	.243
8	.456	.128	.235	.049	.187	.197
9	.000	.229	.229	.168	.198	.239
10	.028	.222	.228	.004	.239	.240
11	.243	.092	.121	.125	.169	.194

The experimental and predicted results of Run 9 were examined in more detail. Since the run went to 100% conversion, the heat of reaction should have been reflected in the outlet temperature. With the inclusion of variable physical properties and various values of β_U the conversion approached 100%. However, the predicted outlet temperature was much higher. This suggested that the value of β_T employed in the theoretical model was too high. According to the theoretical study, an adiabatic reactor was sensitive to the dimensionless heat of reaction (Table 5.9). This could result in values of conversion being overestimated by the model.

The value of β_T was reduced to .208 and β_U was varied again. As may be seen in the results given in Table 6.5, a small reduction in the heat of reaction had a profound affect on the performance of the reactor. The effect of the buoyancy term was also evident.

Upon comparing the data in Tables 6.4 and 6.5 it was evident that the heat of reaction and the buoyancy term were both important in governing reactor performance. The conversion at the outlet was no longer 100%; however, examination of the trend given in Table 6.5 showed that with increasing β_U the outlet composition was decreasing. Presumably, if the value of β_U was sufficiently large, 100% conversion would be observed. Based on the experimental conditions, the value of β_U was actually of the order of 10^7. Although the computer program did not converge at this high a value, it should be noted that the calculated outlet conversion was approaching the experimental conversion with much lower values of β_U.

By investigating the reactor performance beyond the value of the reactor length (calculated from inlet conditions), it was discovered that the value of $\beta_T = .208$ yielded an adiabatic temperature rise of .233 upon complete conversion. This agreed well with the experimental rise of .229. Presumably the approach to the ultimate conversion would be asymptotic in nature such as was demonstrated by the results in Table 6.5. In other words, it would not be necessary to use an exact value of β_U to calculate the outlet properties with the computer model.

Table 6.4: Evaluation of Effect of Variable Properties on Run 9 with $\beta_T = .239$

β_U	$\langle x \rangle$	$\langle \theta \rangle$
200	.035	.263
400	.024	.267
600	.018	.268
800	.014	.270
1000	.012	.270

Table 6.5: Numerical Results for Experimental Run 9 with $\beta_T = .208$

β_U	$\langle x \rangle$	$\langle \theta \rangle$
Constant Properties	.402	.121
200	.318	.102
1000	.252	.167
1500	.193	.186
2000	.183	.189
5000	.183	.189
10000	.131	.199

Table 6.6: Comparison of Experimental and Predicted Data with Adjusted Values of β_T and $|\beta_U| = 600$

Run	Experimental $\langle x \rangle$	Experimental $\langle \theta \rangle$	Initial β_T	Revised β_T	β_U	Predicted $\langle x \rangle$	Predicted $\langle \theta \rangle$
5	.605	.080	.265	.212	Const. Prop.	.510	.103
5					-600	.604	.090
6	.136	.236	.216	.210	Const. Prop.	.030	.204
6					-600	.046	.223
7	.294	.170	.243	.225	Const. Prop.	.135	.194
7					-600	.304	.172
10	.028	.222	.240	.200	Const. Prop.	.129	.174
10					600	.030	.214

Examination of the experimental results indicated that many of the runs could benefit from slight adjustments in the value of β_T. This was in fact done for most of the experimental results of Table 6.3. As a result, the inclusion of variable physical properties in the numerical model yielded good agreement with the experimental results. This agreement has been shown in Table 6.6. It should be noted that not all of the runs could be simulated at higher values of β_U. However, in light of the previous discussion it was felt that a value of 600 in magnitude would be sufficient to approximate the effect of free convection to an adequate degree.

The runs that were not included in Table 6.6 were those in which the conversions were apparently low. This was attributed to poor measurement of outlet concentrations of the hot acid solutions. Also, the first three runs were already assumed to be in error due to poor mixing. The runs that have been presented in Table 6.6 displayed good agreement between theoretical and experimental values. It should be noted that although numerically the theoretical and experimental data were not in agreement in the other runs, the specific trend of the data with respect to variable physical properties was similar with that presented.

The fact that the temperature profiles could be measured through the probes placed in the reactor allowed for the acquisition of the cup-mixed temperature profile for any of the runs. As may be seen from the profiles, when the reactor was in downward flow, the adiabatic nature of the reactor was evident (Figures 6.2 and 6.3). What was also evident was that increasing the value of β_U tended to improve the rather poor fit in the reactor between the inlet and outlet. In both of these examples the experimental outlet concentration was in agreement with the theoretical values (Figures 6.4 and 6.5). However, given that the theoretical temperature profile was not as good, it was likely that the theoretical concentration profile was only an approximation to the actual profile.

In upward flow the situation was quite different. Both the experimental and theoretical temperature profiles were in good agreement for the 2 runs presented in Figures 6.6 and 6.7. In light of the correspondence between theoretical and experimental conversions, it was concluded that the numerical model successfully reflected the experimental data in these instances (Figures 6.8 and 6.9).

The acetic anhydride reaction was an extremely difficult system with which to work, and large amounts of reactant were required for any run, leading to a high cost. It would have been desirable to continue with the experimental program to further verify the promising results outlined above. The results as given, however, demonstrated the plausibility of the results obtained in the theoretical study. In particular, the experimental runs highlighted the fact that all portions of the study were of equal significance. It was shown that very small changes in the value of the dimensionless heat of reaction would affect the numerical values of conversion. Variable heat capacity and density were also significant in this regard. Both of these variables underwent changes with reaction in the theoretical model. Qualitatively, the different temperature profiles observed between upward and downward flow demonstrated the presence of free convection.

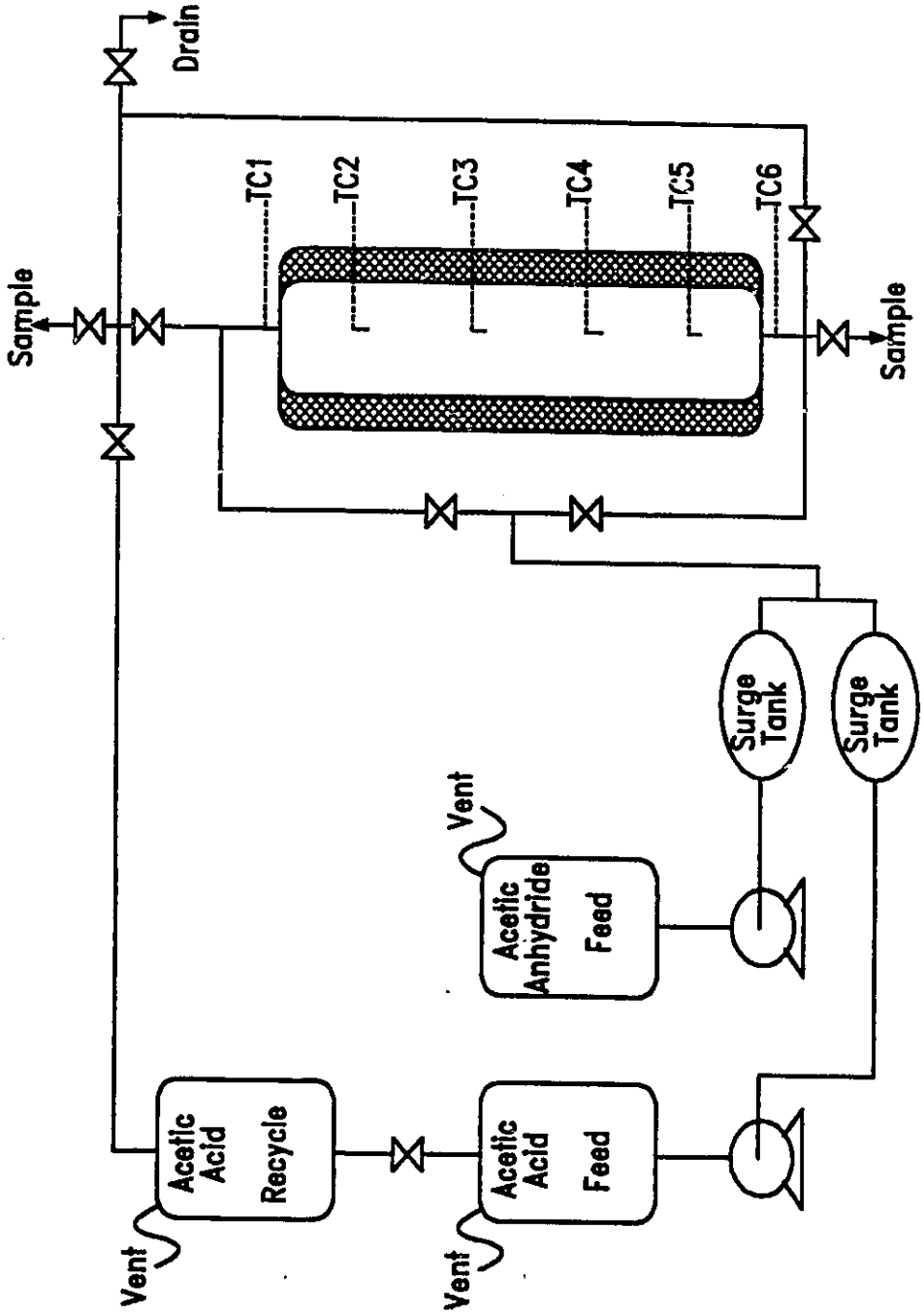

Figure 6.1: Flow Sheet for Experimental Equipment

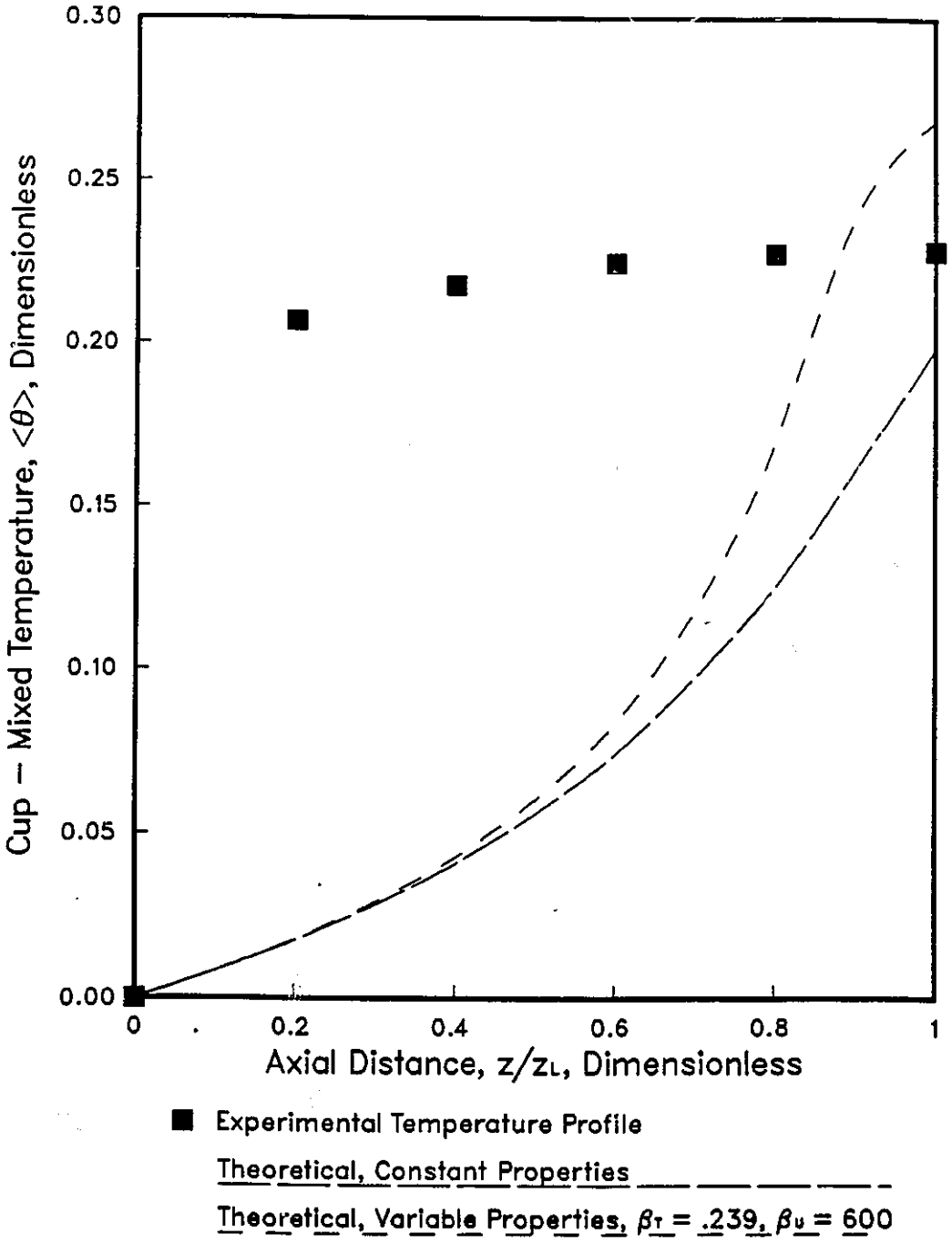

Figure 6.2: Cup-Mixed Temperature Profile for Experimental Run 9: Experimental and Theoretical Curves

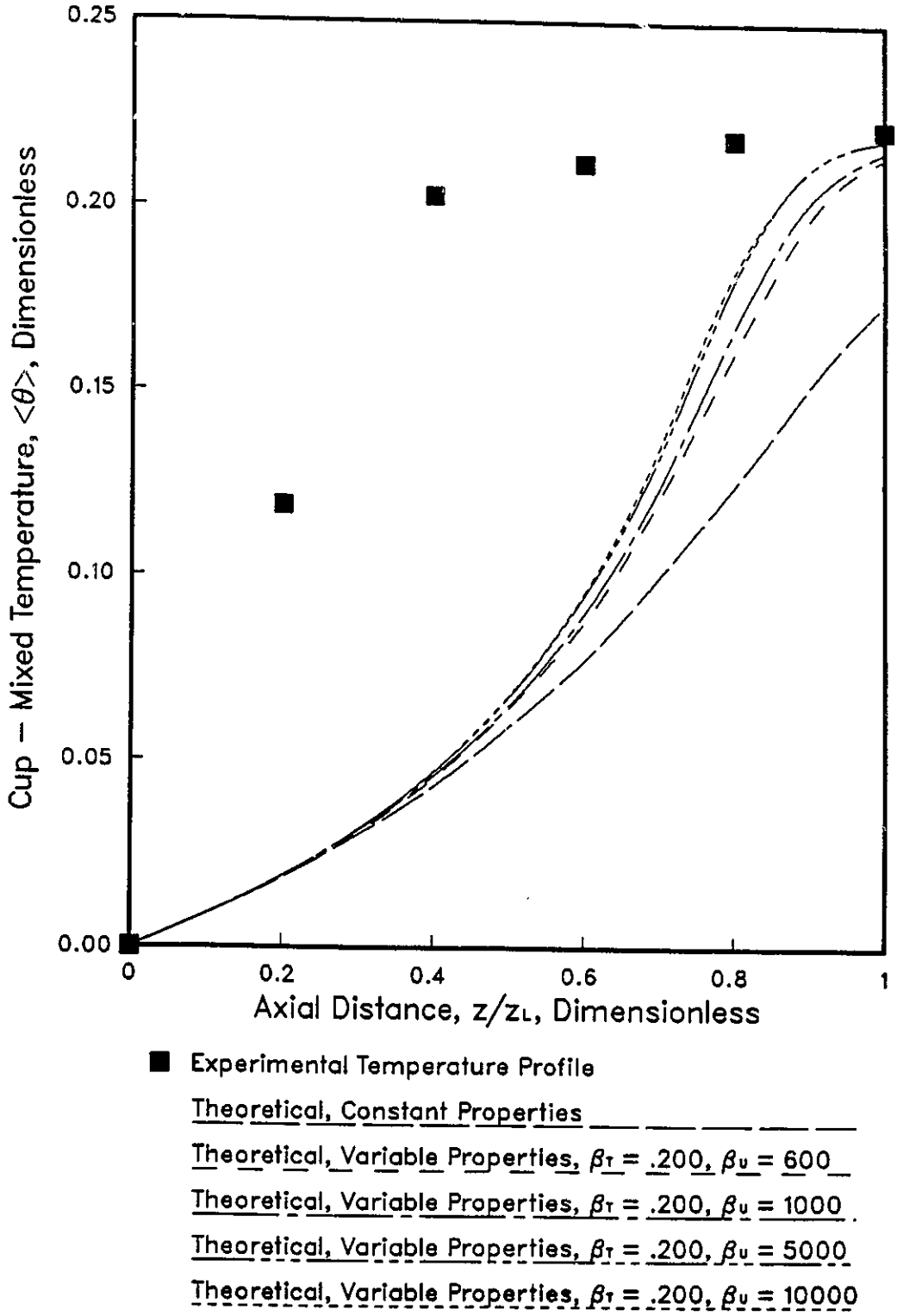

Figure 6.3: Cup-Mixed Temperature Profile for Experimental Run 10: Experimental and Theoretical Curves

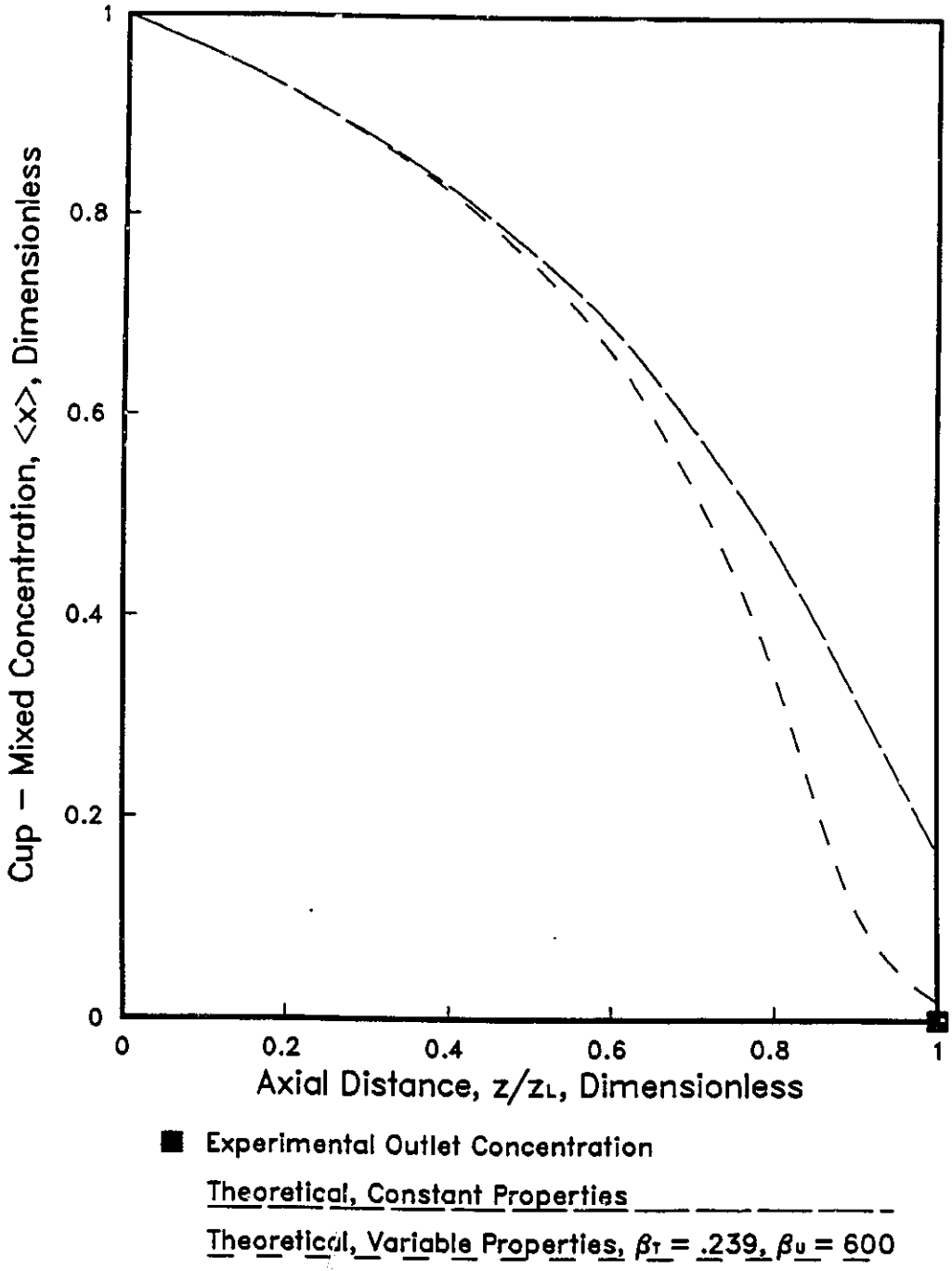

Figure 6.4: Theoretical Cup-Mixed Concentration Profiles and Experimental Outlet Concentration for Experimental Run 9

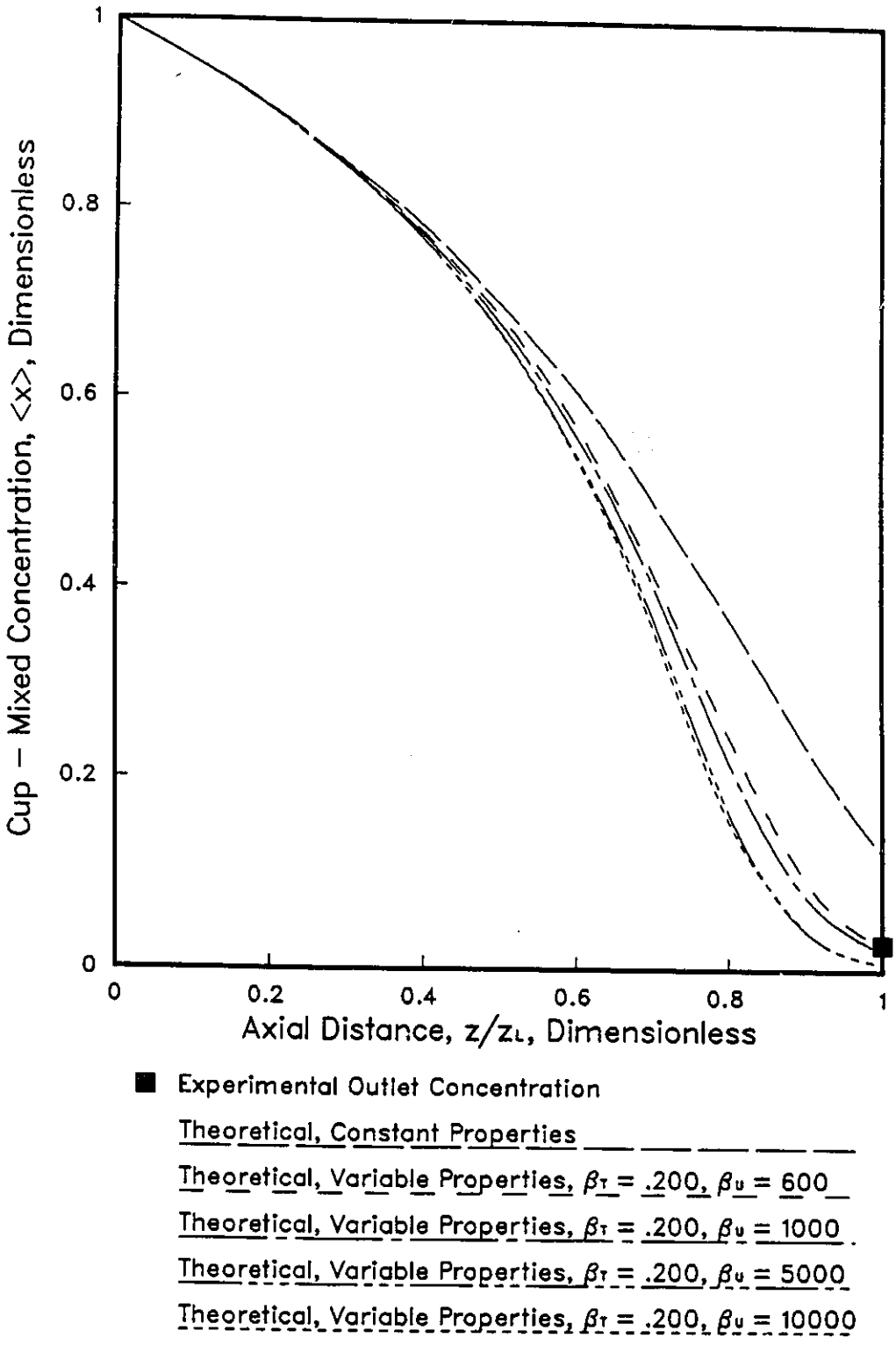

Figure 6.5: Theoretical Cup-Mixed Concentration Profiles and Experimental Outlet Concentration for Experimental Run 10

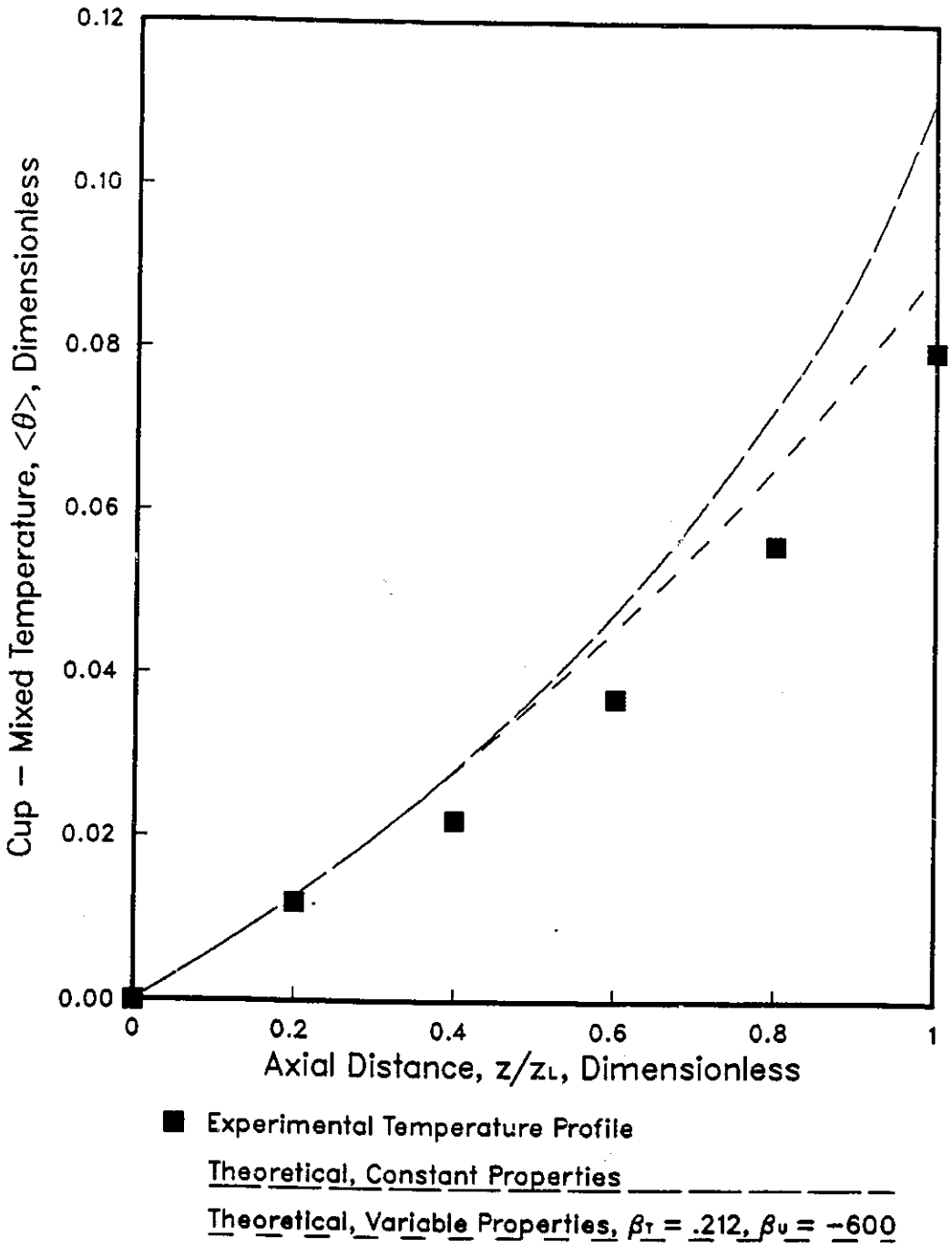

Figure 6.6: Cup-Mixed Temperature Profile for Experimental Run 5: Experimental and Theoretical Curves

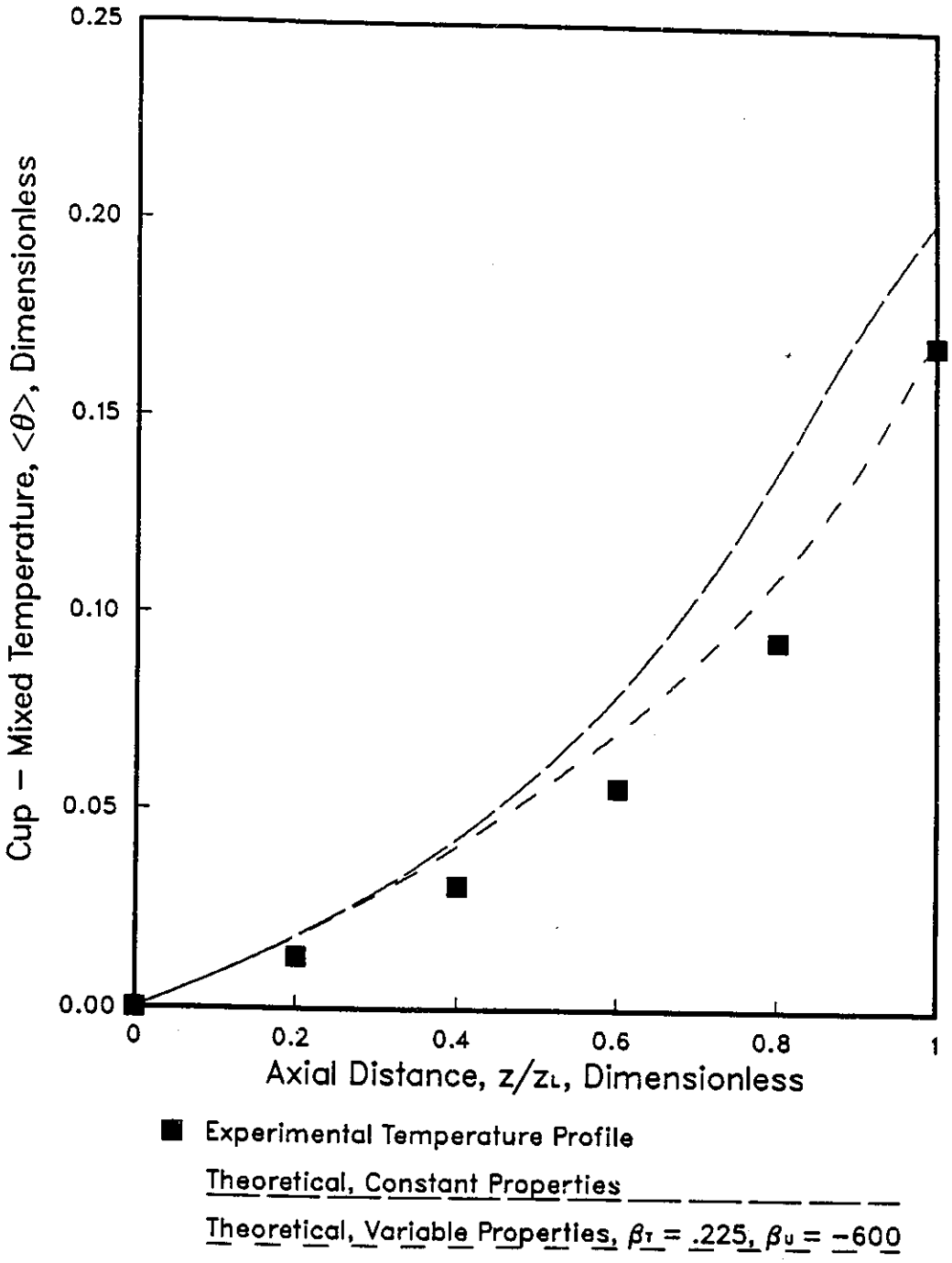

Figure 6.7: Cup-Mixed Temperature Profile for Experimental Run 7: Experimental and Theoretical Curves

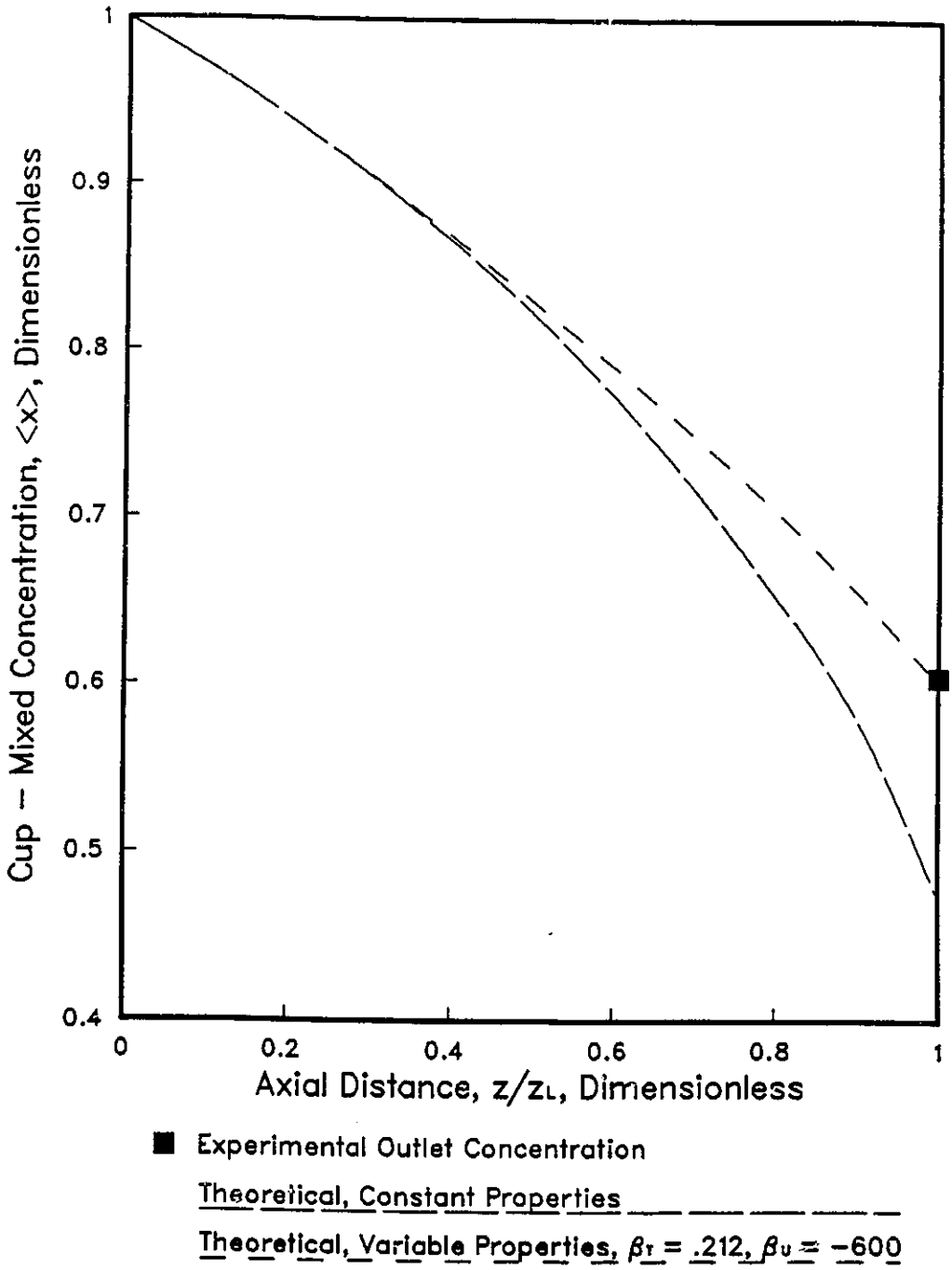

Figure 6.8: Theoretical Cup-Mixed Concentration Profiles and Experimental Outlet Concentration For Experimental Run 5

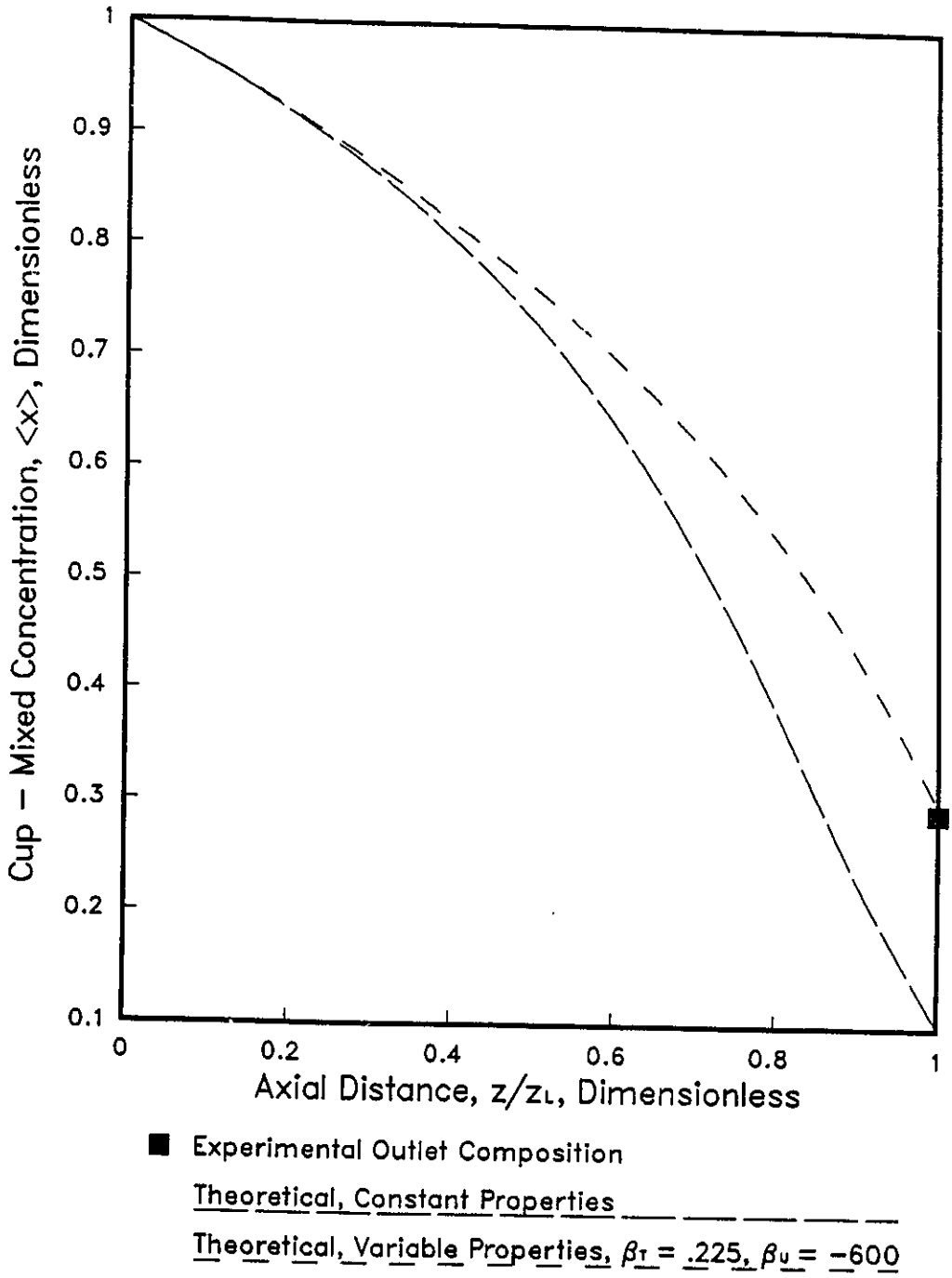

Figure 6.9: Theoretical Cup-Mixed Concentration Profiles and Experimental Outlet Concentration For Experimental Run 7

Chapter 7

Conclusions and Recommendations

Factorial designs and linear regression were employed to determine the characteristics of a mathematical model describing a laminar flow tubular reactor undergoing heat transfer. The study consisted of examining the effect that heat transfer and variable physical properties had upon the reactor based on this numerical model. Based upon the data collected from the factorial design the following conclusions were reached:

1. Heat transfer in the reactor was of major importance. Three heat transfer regimes were identified: the high, medium, and low regimes. These 3 regimes characterized the level of heat transfer occurring both within the reactor in the radial direction and subsequent transfer of heat to the environment through the wall. The most significant factor in determining in which regime a particular simulation belonged was the internal heat transfer parameter, α_7. Of secondary influence were the wall heat transfer coefficient, Bi, and the ambient or jacket temperature, θ_j.

2. In the high heat transfer regime, the reactor operated under isothermal conditions. Under these conditions, the reactor length required to achieve 90% conversion was most greatly affected by the jacket or ambient temperature.

3. In the medium heat transfer regime the reactor underwent heat transfer with the surroundings typical of nonisothermal reactor behaviour reported in the literature.

4. In the low heat transfer regime the reactor behaviour was similar to adiabatic operation. Under these circumstances the dimensionless heat of reaction and activation energy were the most significant terms in determining reactor behaviour. Increases in either of these terms decreased the reactor length required for 90% conversion. The similarity between this type of heat transfer and an adiabatic reactor was verified with simulations performed under adiabatic conditions.

5. The heat transfer regimes that were identified above also determined whether the reactor was affected by temperature dependent properties. It was observed that temperature dependent properties were only significant in the low heat transfer regime. This was a result of the fact that the temperature rises in this regime were the greatest. A large difference in temperature was the prerequisite for the inclusion of temperature dependent properties.

6. Combined composition and temperature dependent properties were found to be important in all 3 heat transfer regimes. It was interesting to note that these regimes were also important in determining regions in which given property changes were significant.

   (a) In the high heat transfer regime the significant properties were density and thermal conductivity. Density changes were significant due to the action of free convection and its role in velocity profile distortion. Thermal conductivity was significant in retarding the rate of heat transfer. When the simulation conditions were close to those of the medium heat transfer regime, a decrease in the thermal conductivity was sufficient to increase the reaction rate. Slight increases in the reaction rate could greatly affect the outlet conversions.

(b) In the medium heat transfer regime, density, thermal conductivity, and heat capacity were significant. Density and thermal conductivity had the same effect that they had in the high heat transfer regime. Because of generally higher temperatures in the medium heat transfer regime, the heat capacity became significant. As heat capacity underwent changes with the reaction, these were reflected by higher or lower temperature rises. Through the Arrhenius Law, these temperature differences led to either faster or slower reactions. These differences were again reflected in outlet conversions.

(c) In the low heat transfer regime, energy exchange with the environment was slow with respect to the rate of reaction. As a result of this thermal conductivity ceased to be a factor. The roles of density and heat capacity increased in the previously discussed manner. Since a temperature dependent density was observed to have a significant role, it was concluded that it was also significant in this portion of the study. In fact it was probable that the heat capacity had a dual effect in that it either increased or decreased the temperature rises in the reactor. These increases or decreases in temperature had a role in determining the degree of distortion in the velocity profile.

7. The flow direction in a vertical reactor was found to be significant through the effects of free convection.

8. Simulations performed under adiabatic conditions yielded results similar to those for the low heat transfer regime. A second order reaction was also investigated for the adiabatic reactor. It was found that the effects were not as great for the second order reaction. This was due to the slower kinetics of this system. Since the reaction rates were not as great, they were not as sensitive to minor changes in the local conditions.

9. The numerical simulations suggested that experimental verification of the results could be established by investigating a system with a high concentration

of reactants. Previous investigations were performed at rather low concentrations. The hydrolysis of acetic anhydride was selected as the experimental system. Experiments were run in the reactor in both upward and downward flow directions. Differences in the shapes of the temperature profiles generated in these two directions verified the large influence that free convection had upon the reactor performance. In attempting to use the numerical model to represent the experimental data the following observations were made:

(a) All aspects of the numerical study were important. Initial values of the properties needed to be determined. This was reflected in the fact that a minor adjustment in the dimensionless heat of reaction was sufficient to render good or poor agreement between experimental and theoretical values.

(b) Decreasing the value of the dimensionless heat of reaction by as little as 10% was often sufficient to improve the agreement. These decreases were accompanied by variable density and heat capacity.

(c) The magnitude of the buoyancy term was set at 600. In reality the magnitude of this term was approximately 10^7. In the upward flow runs this small value was adequate to model the system with respect to the axial temperature profile. In the downward flow examples it was shown that the outlet temperature was adequately modelled but that the axial temperature profile was not. Convergence difficulties in the program made the use of higher values of β_U impossible. It was shown, however, that as the value increased the theoretical temperature profile began to achieve the shape of the experimental profile.

The numerical model developed for this study was more than adequate in achieving the objectives but improvements could be made.

1. Initial testing of the program indicated that efficiency and convergence were greatly affected by the number of radial points. Although 10 points were sufficient to reflect the general qualities of the numerous profiles, greater accuracy could be achieved through a finer grid. The cause of these convergence

problems should be investigated.

2. Even with 10 radial points there were problems with convergence when severe changes in the velocity profile occurred. This was particularly evident in the adiabatic simulations. Some of these problems might be alleviated with modifications to the velocity loop. In the program no provision was made for the possibility of stagnant regions or backward flow. If these conditions were occurring during the numerical iteration procedure, the program failed.

Considering the large amount of literature that has appeared regarding the influence of a variable viscosity in these systems it was surprising to note that it had little effect in this investigation. It might be useful to examine its role coupled with density by increasing the amount it changes with composition. Although much of the data collected indicated that mass transfer in general played a very minor role, the influence of a variable diffusivity could be more extensively investigated. This would be of interest, for example, in a system with a catalytic wall.

Only a limited number of experimental runs could be carried out. It was difficult to work with the acetic anhydride system. Although precautions were taken to limit exposure to the reagents, withdrawal of samples (among other exposures) were inevitable. A reaction involving less irritating reagents should be studied in the future. All pertinent information required to investigate a system should be well known. This experimental investigation pointed out the fact that under the conditions that the reactor was operated, a better knowledge of the density, heat capacity and initial concentrations of the mixture should be known. Also the kinetics and heat of reaction should be well established. The literature on the hydrolysis of acetic anhydride contained some contradictory information. Determination of reaction kinetics and physical properties of reacting mixtures were beyond the scope of this study.

A more precise and accurate analytical technique to determine concentration other than titration would be useful. Since the best that could be accomplished was estimation of the physical properties of the mixture using simple mixing rules, the more accurate the compositions used the more reliable these estimations might

be. Again these estimates would appear to be most important in establishing the dimensionless groups. The simple mixing rules were adequate in terms of reflecting reactor behaviour in the context of changing properties with the extent of reaction.

Bibliography

[1] R. C. L. Bosworth. Distribution of reaction times for laminar flow in cylindrical reactors. *Phil. Mag.*, **39**:847–862, 1948.

[2] K. G. Denbigh. Kinetics of continuous reaction processes: Application to polymerization. *J. Appl. Chem. (London)*, **1**:227–236, 1951.

[3] H. S. Lauwerier. A diffusion problem with chemical reaction. *Appl. Sci. Res.*, **A8**:366–376, 1959.

[4] F. A. Cleland and R. H. Wilhelm. Diffusion and reaction in viscous-flow tubular reactor. *AIChE J.*, **2**:489–497, 1956.

[5] J. P. Vignes and P. J. Trambouze. Diffusion et réaction chimique dans un réacteur tubulaire en regime laminaire. *Chem. Engng. Sci.*, **17**:73–86, 1962.

[6] P. L. Chambré. On chemical reactions in internal flow systems. *Appl. Sci. Res.*, **A9**:157–168, 1960.

[7] M. Trombetta and J. Happel. Analysis and design of gas flow reactors with applications to hydrocarbon pyrolysis. *AIChE J.*, **11**:1041–1050, 1965.

[8] R. I. Rothenberg and J. M. Smith. Heat transfer and reaction in laminar tube flow. *AIChE J.*, **12**:213–220, 1966.

[9] R. I. Rothenberg and J. M. Smith. Dissociation and heat transfer in laminar flow. *Can. J. Chem. Engng.*, **44**:67–73, 1966.

[10] T. S. Andersen and J. Coull. Evaluation of models for tubular, laminar flow reactors. *AIChE J.*, **16**:542–553, 1970.

[11] L. S. Merrill, Jr and C. E. Hamrin, Jr. Conversion and temperature profiles for complex reactions in laminar and plug flow. *AIChE J.*, **16**:194–198, 1970.

[12] T. Shinohara. *An Experimental and Theoretical Study of a Laminar-Flow Reactor.* PhD thesis, University of Utah, 1971.

[13] F. Santarelli and E. P. Foraboschi. Free convection in mixed laminar convection in a reacting fluid. *Chem. Eng. (Lausanne)*, **6**:59–68, 1973.

[14] W. G. Gray and M. D. Kostin. Velocity, temperature, and concentration profiles in a vertical flow reactor. *Chem. Engng. Sci.*, **30**:931–936, 1975.

[15] F. Vena. *An Experimental and Theoretical Study of Conversions and Temperature Rises in an Adiabatic Liquid-Flow Reactor.* Master's thesis, University of Ottawa, 1975.

[16] J. A. Golding and R. Dussault. Prediction of concentration and temperature distributions in a flow reactor: Homogeneous liquid phase reaction. *Int. J. Heat Mass Transfer*, **19**:493–501, 1976.

[17] R. Dussault. *Experimental and Theoretical Study of a Tubular Flow Reactor: Homogeneous Liquid-Phase Reaction.* PhD thesis, University of Ottawa, 1977.

[18] J. A. Golding and R. Dussault. Conversions and temperature rises in a laminar flow reactor for the hydration of acetic anhydride. *Can. J. Chem. Engng.*, **56**:564–569, 1978.

[19] J. A. Golding, F. Vena, and D. Gorowski. Conversions and temperature rises in a tubular flow reactor with uncontrolled wall heat transfer. *Can. J. Chem. Engng.*, **59**:705–709, 1981.

[20] S. H. Lin. Nonisothermal non-Newtonian chemical reactions in a tubular reactor under conditions of variable viscosity. *Appl. Sci. Res.*, **32**:195–206, 1976.

[21] J.-L. Houzelot and J. Villermaux. Mass transfer in annular cylindrical reactors in laminar flow. *Chem. Engng. Sci.*, **32**:1465–1470, 1977.

[22] C.-Y. Chang and Y.-T. Chern. Laminar flow diffusion of power-law fluids in a tube with arbitrary order heterogeneous and homogeneous reactions. *Can. J. Chem. Engng.*, **63**:772–777, 1985.

[23] S. Lynn and J. E. Huff. Polymerization in tubular reactor. *AIChE J.*, **17**:475–485. 1971.

[24] R. Sala. F. Valz-Gris, and L. Zanderighi. A fluid-dynamic study of a continuous polymerisation reactor. *Chem. Engng. Sci.*, **29**:2205–2212, 1974.

[25] A. Ya. Malkin. Rheology in polymerization processes. *Polymer Engng Sci.*, **20**:1035–1044. 1980.

[26] A. Ya. Malkin, L. I. Sherysheva, S. G. Kulichikhin, and P. V. Zhirkov. The flow of a polymerizing liquid in a cylindrical pipe. *Polymer Engng Sci.*, **23**:804–809, 1983.

[27] P. E. Baillagou and D. S. Soong. Free-radical polymerization of methyl methacrylate in tubular reactors. *Polymer Engng Sci.*, **25**:212–231, 1985.

[28] P. E. Baillagou and D. S. Soong. Free-radical polymerization of methyl methacrylate at high temperatures. *Polymer Engng Sci.*, **25**:232–224, 1985.

[29] H. S. McLaughlin, R. Mallikarjun, and E. B. Nauman. Effect of radial velocities on laminar flow. tubular reactor models. *AIChE J.*, **32**:419–425, 1986.

[30] J. S. Vrentas and W. J. Huang. Radial transport in tubular polymerization reactors. *Chem. Engng. Sci.*, **41**:2041–2051, 1986.

[31] R. Cintron-Cordero, R. A. Mostello. and J. A. Biesenberger. Reactor dynamics and molecular weight distributions: Some aspects of continuous polymerization in tubular reactors. *Can. J. Chem. Engng.*, **46**:434–443, 1968.

[32] J. P. A. Wallis, R. A. Ritter, and H. Andre. Continuous production of polystyrene in a tubular reactor: Part 1. *AIChE J.*, **21**:686–690, 1975.

[33] J. P. A. Wallis, R. A. Ritter, and H. Andre. Continuous production of polystyrene in a tubular reactor: Part 2. *AIChE J.*, **21**:691–698, 1975.

[34] G. I. Taylor. Dispersion of soluble matter flowing slowly through a tube. *Proc. Roy. Soc.*, **A219**:186–203, 1953.

[35] R Aris. On the dispersion of a solute in a fluid flowing through a tube. *Proc. Roy. Soc. (London.)*, **A235**:67–77, 1956.

[36] Wan C.-G. and E. N. Ziegler. On the axial dispersion approximation for laminar flow reactors. *Chem. Engng. Sci.*, **25**:723–727, 1970.

[37] K. D. P. Nigam and K. Vasudeva. Diffusion and reaction in tubular reactor with with non-Newtonian laminar flow. *Chem. Engng. Sci.*, **32**:673–677, 1977.

[38] K. D. P. Nigam and K. Vasudeva. Consecutive reactions in a non-ideal tubular reactor. *Chem. Engng. Sci.*, **32**:1119–1121, 1977.

[39] A. Varma and R. Aris. Stirred pots and empty tubes. In L. Lapidus and N. Amundson, editors, *Chemical Reactor Theory A Review*, pages 79–155, Prentice-Hall, 1977.

[40] K. M. Sundaram and G. F. Froment. Comparison of simulation models for empty tubular reactors. *Chem. Engng. Sci.*, **34**:117–124, 1979.

[41] R. B. Bird, W. E. Stewart, and E. N. Lightfoot. *Transport Phenomena.* John Wiley and Sons, Inc., 1960.

[42] T. E. Tezduyar, Y. J. Park, and H. A. Deans. Finite element procedures for time-dependent convection-diffusion-reaction systems. *Int. J. for Num. Meth. in Fluids*, **7**:1013–1033, 1987.

[43] B. A. Finlayson. *Nonlinear Analysis in Chemical Engineering.* McGraw-Hill, 1980.

[44] J. S. Hopkins and J. A. Golding. The prediction of conversions and temperature rises along a tubular reactor under complex reaction conditions. In *Proceedings of the 37th Canadian Chemical Engineering Conference*, pages 394–396, May 1987.

[45] L. Petzold. Differential/Algebraic equations are not ODE's. *SIAM J. Sci. Stat. Comput.*, **3**:367–384, 1982.

[46] B. Carnahan, H. A. Luther, and J. O. Wilkes. *Applied Numerical Methods*. John Wiley and Sons, 1969.

[47] C. W. Gear. *Numerical Initial Value Problems in Ordinary Differential Equations*. Prentice-Hall, 1971.

[48] C. L. Yaws. *Physical Properties: A Guide to the Thermodynamic, and Transport Property Data of Industrially Important Chemical Compounds*. McGraw-Hill, 1977.

[49] S. Makridakis, S. C. Wheelwright, and V. E. Mcgee. *Forecasting: Methods and Application*. John Wiley and Sons, 1983.

[50] K. J. P. Orton and M. Jones. Hydrolysis of acetic anhydride. *J. Chem. Soc. (London)*, **101**:1708–1720, 1912.

[51] J. F. M. Caudri. Velocity of hydrolysis and alcoholysis of acetic anhydride in mixtures of water and ethyl and methyl alcohol. *Rec. Trav. Chim.*, **44**:1–16, 1930.

[52] S. E. Vles. The determination of the velocity of hydrolysis of acid anhydrides by the aniline-water method 1. *Rec. Trav. Chim.*, **52**:809–826, 1933.

[53] E. K. Plyler and E. S. Barr. The reaction rate of acetic anhydride and water. *J. Chem. Phys.*, **3**:679–682, 1935.

[54] J. B. Conn, G. B. Kistaikowsky, R. M. Roberts, and E. A. Smith. Heats of organic reactions XIII. Heats of hydrolysis of some acid anhydrides. *J. Am. Chem. Soc*, **64**:1747–1752, 1942.

[55] L. H. Greathouse, H. J. Janssen, and C. H. Haydel. Thermometric determinations of water and acetic anhydride in acetic acid. *Analytical Chem.*, **28**:357–361, 1956.

[56] H. J. Janssen, C. H. Haydel, and L. H. Greathouse. Hydrolysis of acetic anhydride in concentrated acetic acid without catalysis. *Ind. and Engng. Chem.*, **49**:197–201, 1957.

[57] M. del Claustra Prat Monguló and F. Cunill Garcia. Comportamiento dinámico de un reactor contínuo tanque agitado: Hidrólisis del anhídrido acético. *Afinidad*, **40**:150–155, 1983.

[58] R. H. Perry and C. H. Chilton, editors. *Chemical Engineers' Handbook*. Mcgraw-Hill, 5 edition, 1973.

[59] D. Phaneswara Rao and S. K. B. Parey. Modelling and simulation of an exothermic reaction in a batch reactor. *Indian Chem. Eng.*, **30**:33–41, 1988.

[60] C. F. Spencer and S. B. Adler. A critical review of equations for predicting saturated liquid density. *J. Chem. and Engng. Data*, **23**:82–89, 1978.

[61] R. C. Reid, J. M. Prausnitz, and T. K. Sherwood. *The Properties of Gases and Liquids*. McGraw-Hill, 3 edition, 1977.

Appendix A

Results, Supplementary Figures, and Residual Plots of the Numerical Study

A.1 Data Calculated from Numerical Simulations

Table A.1: Results of the Study

Run	Constant Property (z)	Deviations Water (y)	Deviations Ethanol (y)	Deviations Benzene (y)	Apparent Heat Transfer Regime
1	0.573	0.929	1.026	1.035	3
2	2.614	1.005	1.008	1.007	1
3	0.687	0.828	0.878	0.903	3
4	1.797	1.027	1.022	1.018	1
5	1.061	1.124	1.174	1.129	2
6	3.232	1.001	1.001	1.001	1
7	0.751	0.992	1.071	1.021	2
8	2.645	1.052	1.043	1.035	1
9	0.764	0.907	0.984	0.949	3
10	0.624	1.006	1.036	1.033	2
11	0.521	0.517	0.559	0.628	3
12	0.664	0.926	0.951	0.962	2
13	0.581	1.12	1.212	1.193	3
14	0.834	0.995	1.020	1.007	1
15	0.714	0.908	0.948	0.960	3
16	0.735	0.956	0.956	0.965	1
17	0.356	0.658	0.785	0.810	3
18	3.687	1.005	1.007	1.007	1
19	0.498	0.742	0.726	0.787	3
20	2.238	1.022	1.022	1.019	1
21	0.788	1.093	1.059	1.081	2
22	4.768	0.962	0.964	0.962	1
23	0.477	1.148	0.898	0.892	2
24	3.843	1.040	1.033	1.025	1
25	0.532	0.941	1.023	1.023	3
26	0.339	0.917	1.009	0.993	2
27	0.342	0.706	0.842	0.900	3
28	0.443	0.906	0.954	0.961	2
29	0.363	0.852	0.96	0.705	3
30	0.575	0.978	0.993	0.995	1
31	0.516	0.815	0.842	0.878	3
32	0.513	0.938	0.948	0.954	1
33	0.826	1.020	1.020	1.020	2

Table A.1 Continued

Run	Constant Property (z)	Deviations Water (y)	Deviations Ethanol (y)	Deviations Benzene (y)	Apparent Heat Transfer Regime
124.1	0.566	1.038	1.118	1.095	3
124.2	3.853	1.001	1.002	1.003	1
124.3	0.535	0.843	0.904	0.926	3
124.4	3.105	0.977	0.969	0.958	1
124.5	0.529	0.907	0.98	0.988	3
124.6	0.663	0.989	0.989	1.000	2
124.7	0.494	0.716	0.752	0.807	3
124.8	0.597	0.955	0.958	0.967	2
135.1	0.644	0.808	0.953	0.976	3
135.2	1.128	0.941	0.950	1.011	2
135.3	0.743	1.123	1.149	1.110	2
135.4	1.528	0.999	0.998	0.998	1
135.5	0.429	0.866	0.958	0.932	3
135.6	0.829	1.013	0.950	1.010	2
135.7	0.487	1.132	1.222	1.139	3
135.8	1.515	0.992	0.991	0.953	1
167.1	0.651	0.966	1.018	1.017	3
167.2	1.491	1.001	0.999	1.000	1
167.3	0.453	0.778	0.878	0.882	3
167.4	1.459	0.997	1.000	0.999	1
167.5	0.651	0.971	1.030	1.033	3
167.6	1.491	1.005	1.005	1.005	1
167.7	0.453	0.924	1.079	1.069	3
167.8	1.459	1.003	1.003	1.008	1
236.1	0.659	0.957	1.001	1.001	2
236.2	0.596	0.921	0.965	0.980	2
236.3	1.340	1.033	1.020	1.021	2
236.4	1.171	0.923	0.921	0.920	2
236.5	0.445	0.971	1.074	1.057	2
236.6	0.409	0.849	0.985	1.009	2
236.7	1.185	0.967	0.958	0.952	2
236.8	1.054	0.920	0.911	0.910	2

Table A.1 Continued

Run	Constant Property (z)	Deviations Water (y)	Deviations Ethanol (y)	Deviations Benzene (y)	Apparent Heat Transfer Regime
257.1	1.023	1.035	1.048	1.036	2
257.2	0.889	0.976	0.994	0.993	2
257.3	0.679	1.095	1.111	1.097	2
257.4	0.605	1.020	1.044	1.038	2
257.5	1.023	1.013	1.002	1.014	2
257.6	0.889	0.967	0.967	0.970	2
257.7	0.679	1.057	1.050	1.044	2
257.8	0.605	1.016	1.007	1.010	2
347.1	0.574	0.952	1.023	1.028	2
347.2	3.200	0.940	0.962	0.952	2
347.3	0.494	0.935	0.986	0.988	3
347.4	0.556	1.053	1.060	1.042	2
347.5	0.574	0.938	1.001	0.999	2
347.6	3.200	0.932	0.95	0.942	2
347.7	0.494	0.915	1.016	0.993	3
347.8	0.556	1.029	1.008	1.007	2
456.1	2.151	1.083	1.091	1.089	2
456.2	0.729	0.977	1.001	0.988	2
456.3	2.794	1.030	1.048	1.035	2
456.4	0.478	0.961	1.013	1.013	2
456.5	1.758	1.049	1.053	1.033	2
456.6	0.584	0.992	1.007	1.040	2
456.7	1.823	1.046	1.053	1.044	2
456.8	0.332	0.975	1.087	1.071	2

Table A.2: Results of the Composition Dependent Simulations

Run	Case 1	Case 2	Case 3	Case 4
1	0.761	0.792	1.071	1.271
2	0.891	1.184	0.903	1.117
3	0.698	0.794	0.993	1.028
4	0.993	1.091	0.967	0.995
5	0.759	2.08	1.676	1.345
6	0.976	1.003	1.003	0.975
7	0.807	1.884	1.701	1.701
8	1.033	1.04	1.047	1.026
9	0.564	1.03	0.795	1.563
10	0.925	0.978	1.053	1.079
11	0.232	0.664	0.694	0.815
12	0.865	0.888	0.941	0.964
13	0.759	0.781	1.075	1.269
14	0.821	1.323	0.862	1.264
15	0.786	0.834	0.913	1.000
16	0.849	1.067	0.887	1.015
17	0.191	1.304	0.692	2.038
18	0.984	1.024	1.005	0.932
19	0.278	0.809	0.739	1.135
20	1.032	1.050	1.050	0.915
21	0.499	2.036	2.064	0.867
22	0.896	1.020	0.922	1.017
23	0.630	1.863	2.092	1.280
24	1.015	1.051	1.029	1.037
25	0.708	0.722	1.025	1.270
26	0.566	1.384	1.828	1.828
27	0.506	0.328	0.744	1.075
28	0.675	1.096	1.292	1.292
29	0.258	1.799	0.841	2.107
30	0.887	1.000	1.002	0.886
31	0.453	0.779	0.74	1.255
32	0.838	0.991	0.996	0.865
33	0.640	1.367	1.144	0.964

Table A.2 Continued

Run	Case 1	Case 2	Case 3	Case 4
167.1	0.597	1.344	0.839	1.650
167.2	0.863	1.195	0.895	1.137
167.3	0.363	1.359	0.772	1.911
167.4	0.859	1.217	0.909	1.142
167.5	0.787	0.871	1.076	1.186
167.6	0.961	0.998	0.999	0.957
167.7	0.670	0.744	1.041	1.317
167.8	0.957	1.012	1.015	0.950
124.1	0.693	1.186	1.145	1.660
124.2	0.934	1.071	0.959	1.041
124.3	0.581	0.891	1.015	1.268
124.4	1.011	1.053	1.040	1.033
124.5	0.542	1.01	0.886	1.537
124.6	0.828	1.13	0.939	1.019
124.7	0.400	0.690	0.715	1.079
124.8	0.838	1.038	0.929	0.952
135.1	0.558	0.972	0.879	1.314
135.2	0.938	1.153	0.951	1.107
135.3	0.746	1.548	1.352	1.322
135.4	0.916	1.091	0.950	1.049
135.5	0.334	0.946	0.855	1.581
135.6	0.860	1.152	0.938	1.108
135.7	0.591	1.753	1.589	1.632
135.8	0.896	1.082	0.942	1.017
236.1	0.695	1.092	0.997	1.355
236.2	0.680	0.918	1.002	1.226
236.3	0.664	1.301	1.135	0.759
236.4	0.771	1.185	1.140	0.801
236.5	0.578	1.087	1.043	1.594
236.6	0.535	0.926	0.995	1.421
236.7	0.470	1.460	1.288	0.556
236.8	0.604	1.299	1.223	0.649

Table A.2 Continued

Run	Case 1	Case 2	Case 3	Case 4
257.1	0.692	1.470	1.019	1.154
257.2	0.780	1.199	1.018	1.021
257.3	0.515	1.772	1.215	1.276
257.4	0.677	1.349	1.147	1.151
257.5	0.738	1.166	1.165	0.81
257.6	0.788	1.066	1.077	0.864
257.7	0.531	1.287	1.341	0.791
257.8	0.682	1.161	1.244	0.947
347.1	0.567	1.344	0.919	1.752
347.2	0.810	1.266	1.088	0.894
347.3	0.537	1.349	0.855	1.812
347.4	0.593	1.692	1.160	1.306
347.5	0.714	0.854	1.110	1.173
347.6	0.845	1.153	1.153	0.813
347.7	0.696	0.814	1.105	1.268
347.8	0.596	1.279	1.293	0.809
456.1	0.830	1.245	1.094	0.827
456.2	0.767	1.150	0.970	1.227
456.3	0.780	1.298	1.147	0.713
456.4	0.662	1.217	1.005	1.432
456.5	0.716	1.342	1.159	0.723
456.6	0.701	1.254	1.036	1.263
456.7	0.519	1.559	1.327	0.483
456.8	0.503	1.189	1.078	1.545

Table A.2 Continued

Run	Case 5	Case 6	Case 7	Case 8
1	0.673	0.924	1.238	1.234
2	0.965	1.156	0.892	1.16
3	0.734	0.806	0.998	1.074
4	1.053	1.088	0.961	1.054
5	1.727	1.157	0.881	2.02
6	1.029	1.001	1.001	1.029
7	1.639	1.063	0.996	1.951
8	1.074	1.051	1.058	1.061
9	0.608	1.276	0.87	1.505
10	0.977	0.985	1.072	1.114
11	0.371	0.500	0.566	1.168
12	0.921	0.883	0.982	0.994
13	0.691	0.940	1.202	1.219
14	0.886	1.234	0.852	1.296
15	0.835	0.845	0.997	0.994
16	0.930	1.014	0.875	1.096
17	0.197	2.179	0.724	1.906
18	1.066	1.001	0.973	1.021
19	0.403	0.802	0.72	1.320
20	1.110	1.031	0.980	0.998
21	2.061	0.597	0.799	2.112
22	0.958	1.121	0.927	1.153
23	1.746	0.764	1.145	2.196
24	1.049	1.058	1.035	1.073
25	0.644	0.889	1.217	1.202
26	0.585	1.394	0.943	1.708
27	0.254	0.702	1.056	0.968
28	0.727	1.116	0.933	1.322
29	0.457	1.643	0.745	2.219
30	1.060	0.936	0.906	1.060
31	0.559	1.015	0.787	1.278
32	1.001	0.858	0.862	1.024
33	1.172	0.846	0.774	1.409

Table A.2 Continued

Run	Case 5	Case 6	Case 7	Case 8
167.1	0.681	1.344	0.866	1.591
167.2	0.931	1.154	0.895	1.200
167.3	0.411	1.372	0.800	1.781
167.4	0.946	1.149	0.889	1.221
167.5	0.841	0.956	1.174	1.199
167.6	1.029	0.986	0.987	1.026
167.7	0.655	0.900	1.235	1.267
167.8	1.045	0.979	0.979	1.041
124.1	0.775	1.265	1.106	1.686
124.2	0.99	1.058	0.962	1.087
124.3	0.642	0.952	1.023	1.324
124.4	1.065	1.057	1.044	1.086
124.5	0.532	1.143	0.987	1.464
124.6	0.967	1.018	0.871	1.126
124.7	0.413	0.801	0.823	1.134
124.8	0.958	0.950	0.865	1.068
135.1	0.579	0.996	0.897	1.285
135.2	1.001	1.135	0.96	1.161
135.3	1.275	1.096	0.991	1.674
135.4	0.984	1.070	0.948	1.112
135.5	0.379	1.088	0.94	1.487
135.6	0.966	1.096	0.922	1.190
135.7	1.252	1.171	1.059	2.039
135.8	0.984	1.044	0.919	1.102
236.1	0.746	1.107	1.036	1.401
236.2	0.729	0.951	1.037	1.274
236.3	1.170	0.754	0.675	1.311
236.4	1.174	0.815	0.787	1.209
236.5	0.574	1.160	1.062	1.600
236.6	0.597	0.949	1.089	1.500
236.7	1.315	0.519	0.478	1.457
236.8	1.292	0.636	0.622	1.321

Table A.2 Continued

Run	Case 5	Case 6	Case 7	Case 8
257.1	1.059	1.053	0.744	1.482
257.2	1.061	0.978	0.856	1.243
257.3	1.173	0.960	0.726	1.802
257.4	1.076	0.946	0.854	1.477
257.5	1.185	0.760	0.800	1.184
257.6	1.109	0.838	0.887	1.126
257.7	1.354	0.629	0.778	1.452
257.8	1.187	0.723	0.882	1.283
347.1	0.598	1.327	0.945	1.712
347.2	1.128	0.932	0.810	1.283
347.3	0.560	1.372	0.956	1.717
347.4	1.156	1.034	0.701	1.683
347.5	0.780	0.839	1.109	1.258
347.6	1.188	0.856	0.840	1.178
347.7	0.754	0.884	1.190	1.312
347.8	1.338	0.679	0.817	1.35
456.1	1.175	0.907	0.789	1.222
456.2	0.931	1.069	0.929	1.269
456.3	1.244	0.830	0.705	1.265
456.4	0.846	1.135	1.000	1.419
456.5	1.263	0.786	0.675	1.302
456.6	0.924	1.048	0.955	1.405
456.7	1.476	0.550	0.464	1.477
456.8	0.730	0.983	1.030	1.604

A.2 Supplementary Figures for Simulation Results

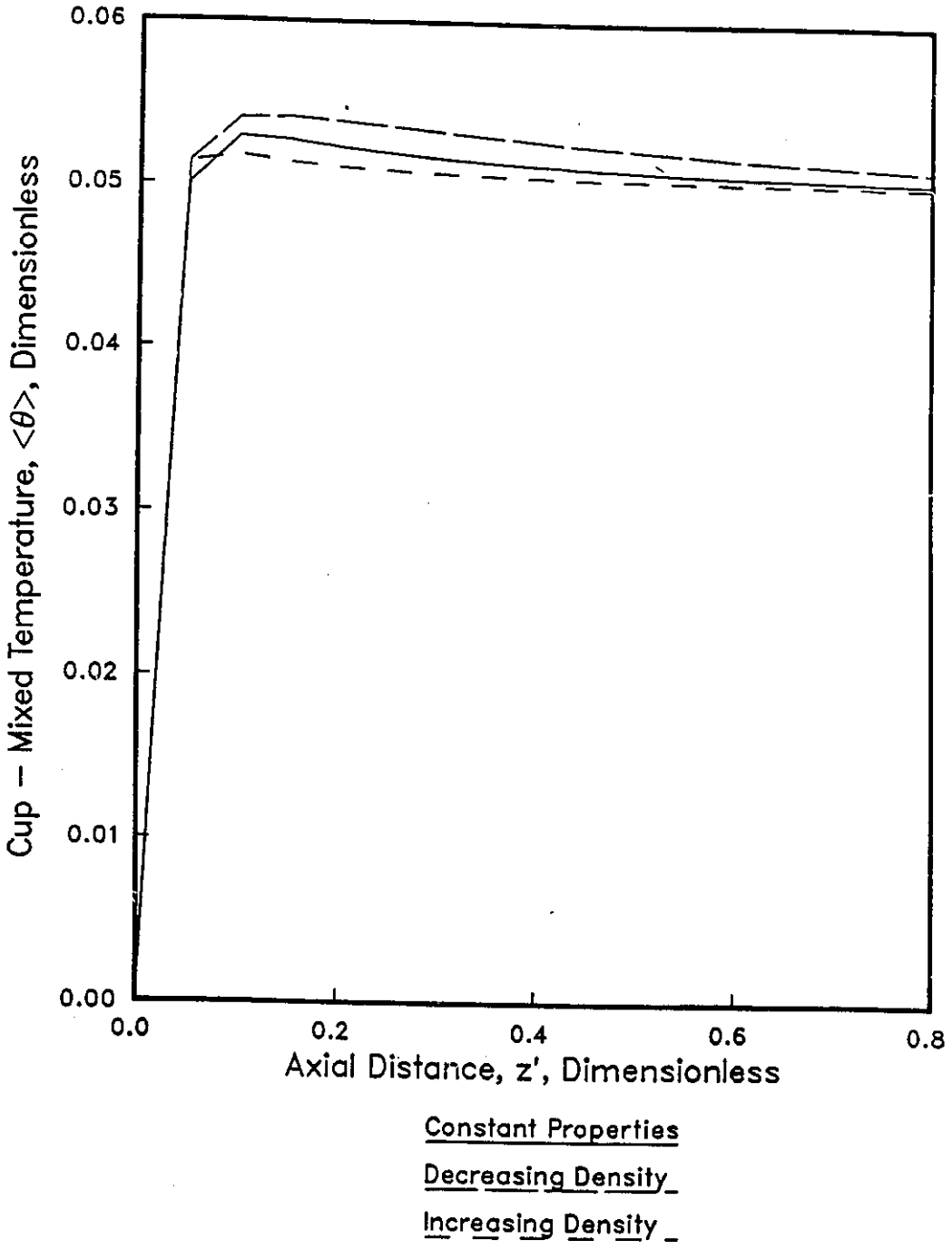

Figure A.1: Cup-mixed Temperature Profiles for Run 14

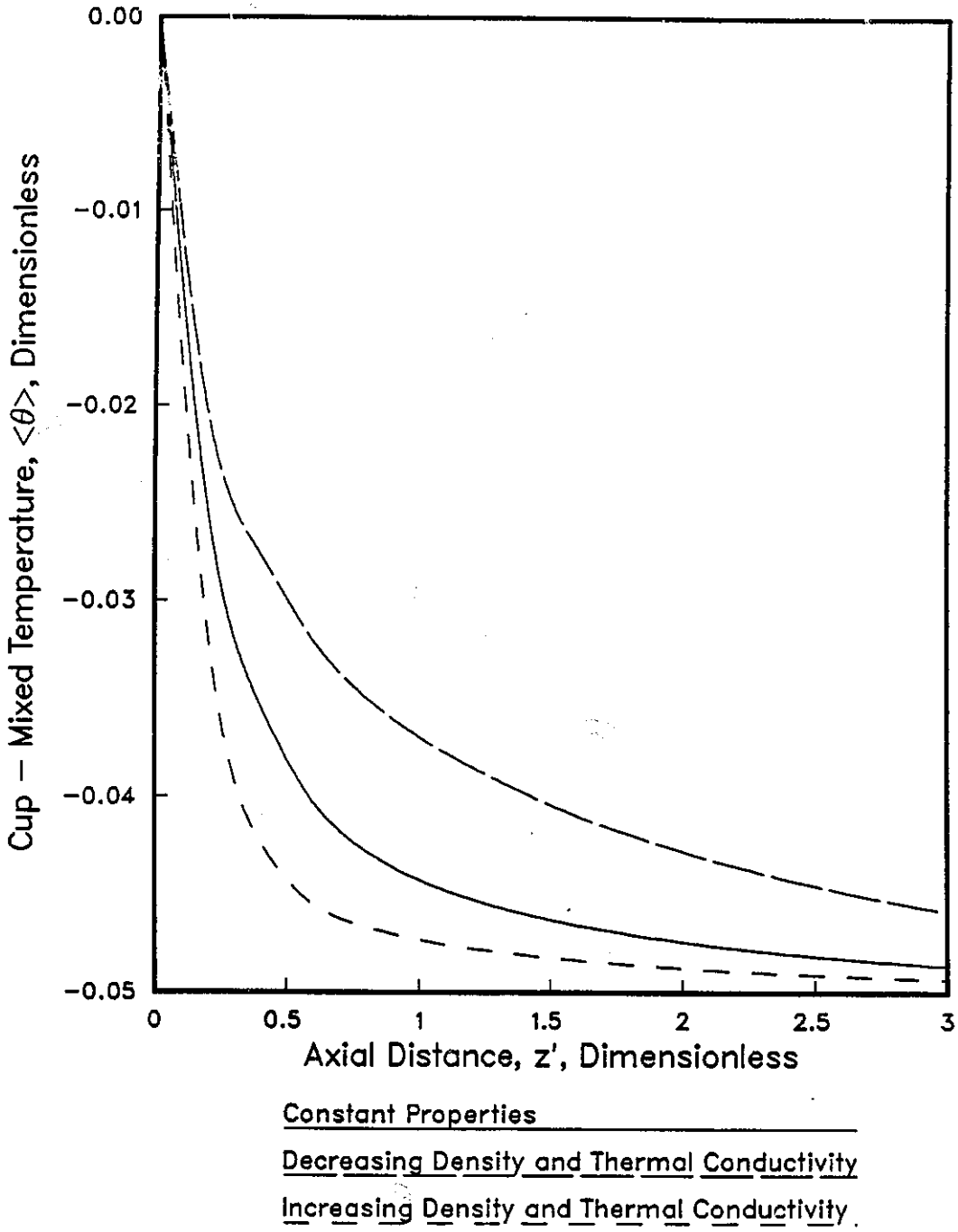

Figure A.2: Cup-mixed Temperature Profiles for Run 347.2

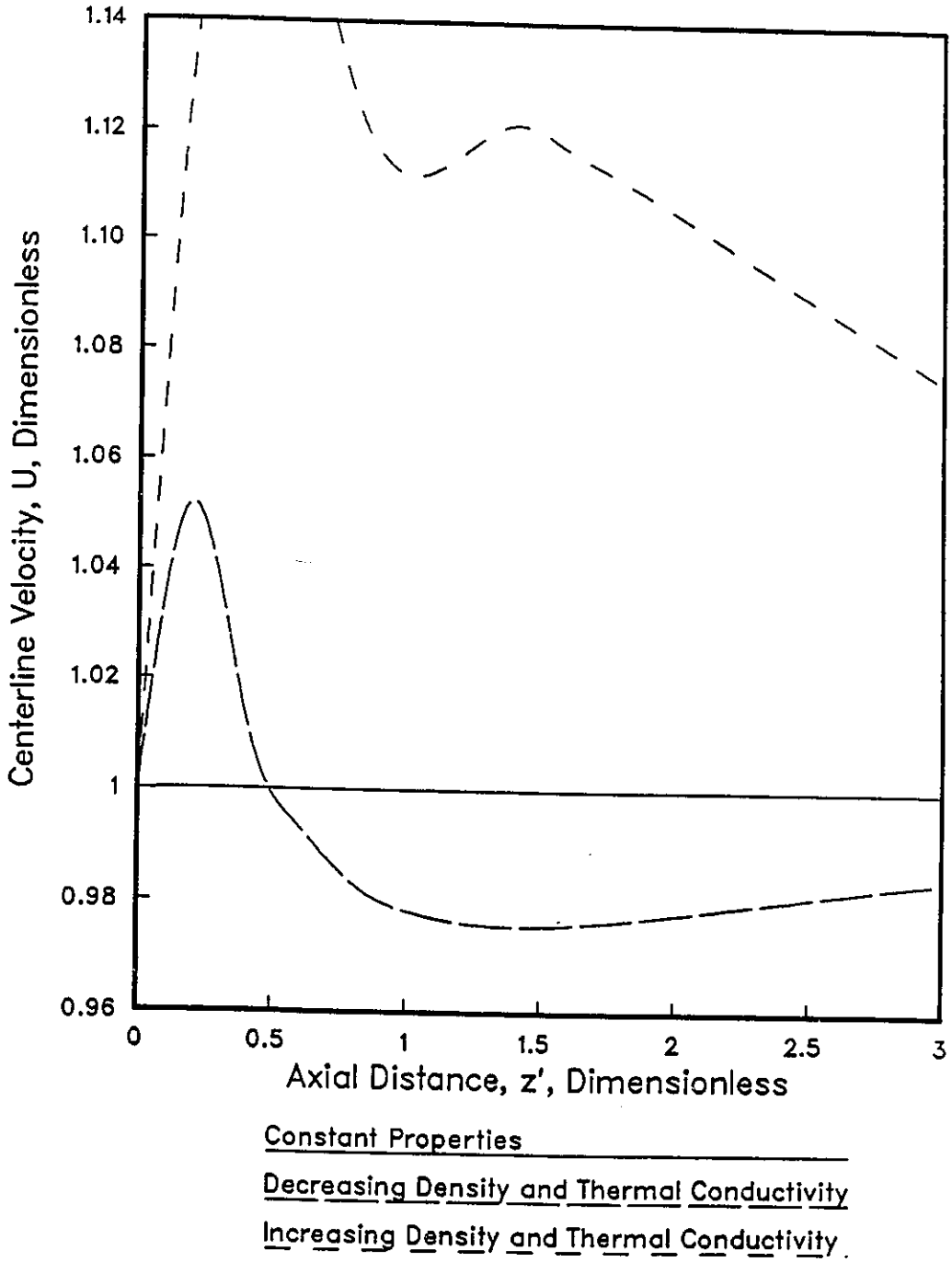

Figure A.3: Centerline Velocities for Run 347.2

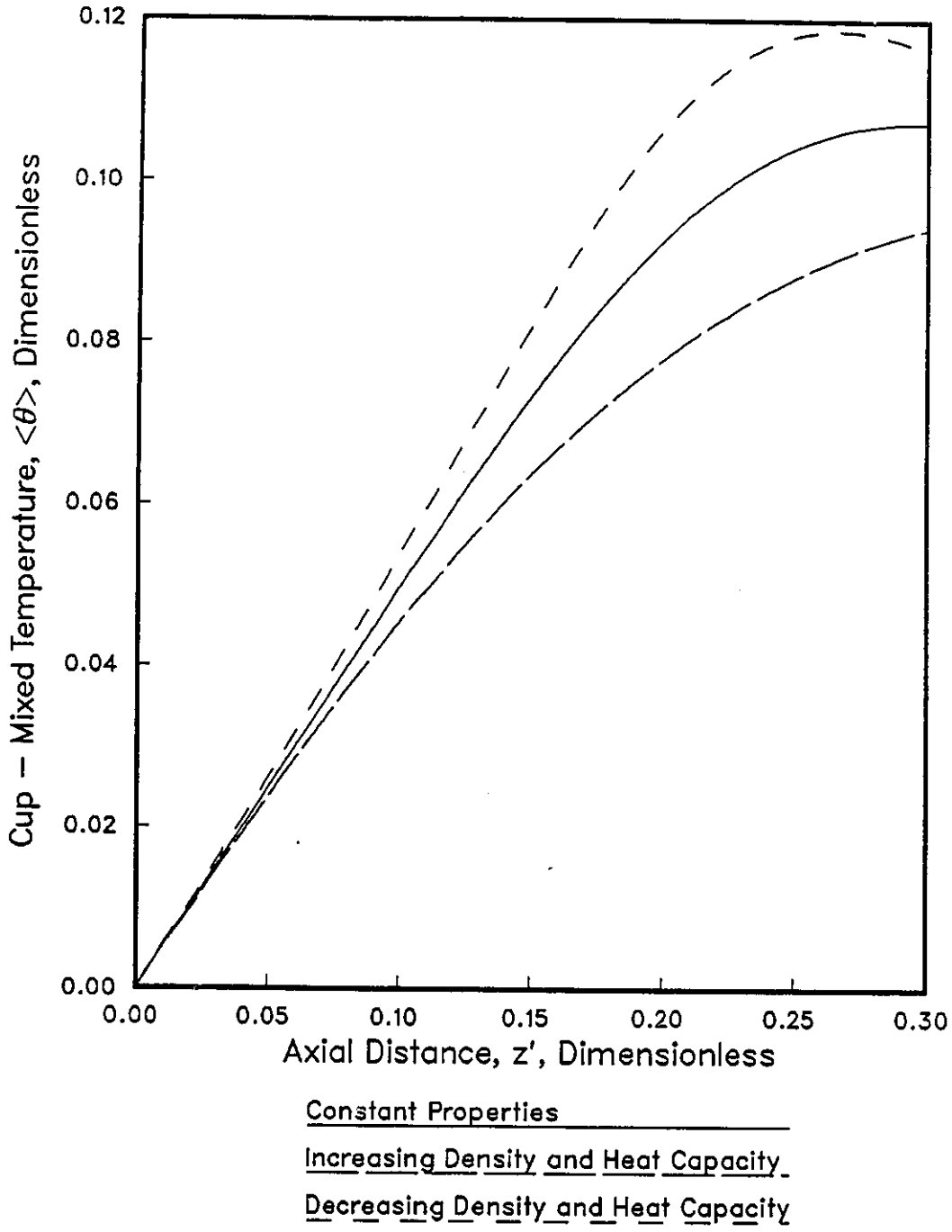

Figure A.4: Cup-mixed Temperature Profiles for Run 26

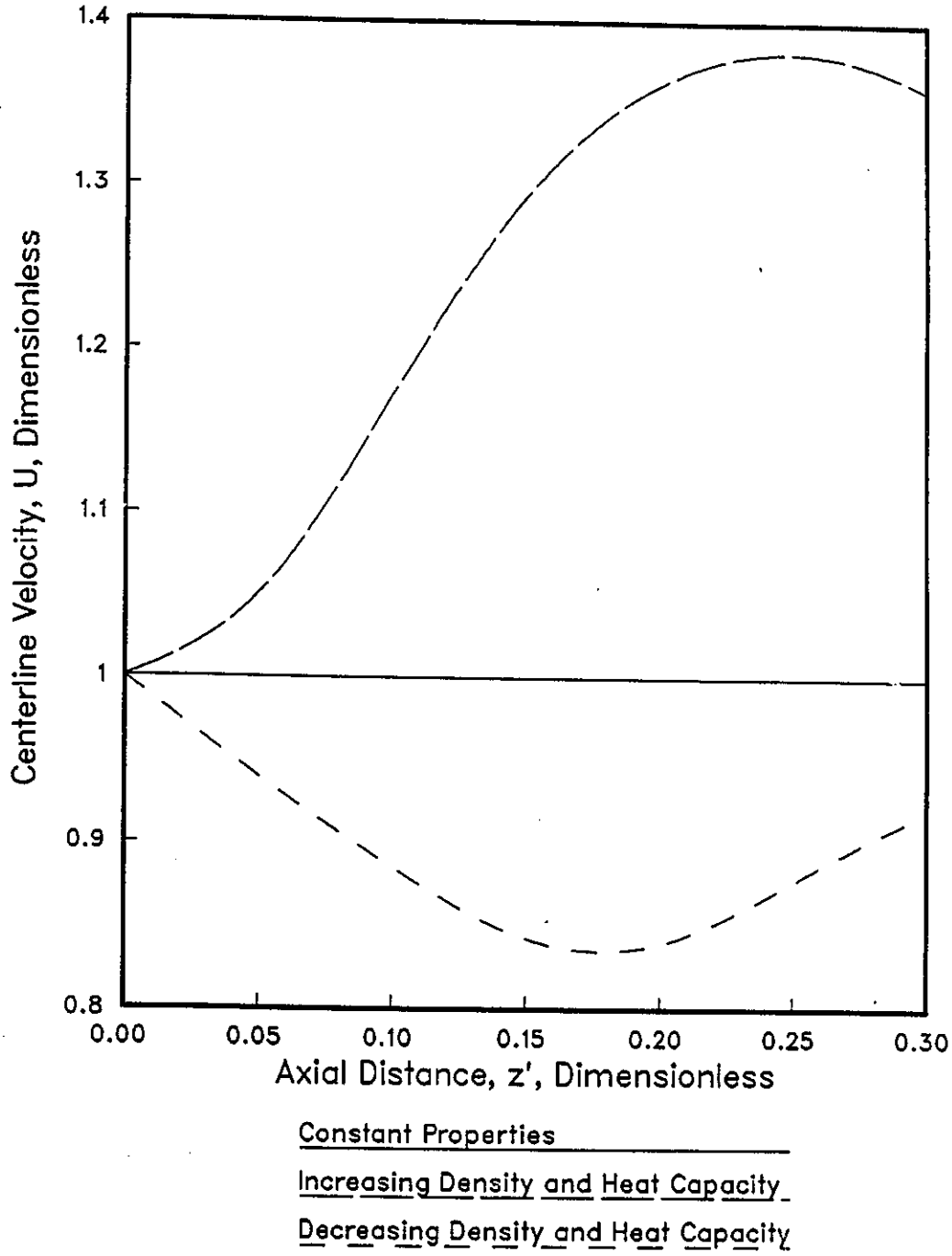

Figure A.5: Centerline Velocities for Run 26

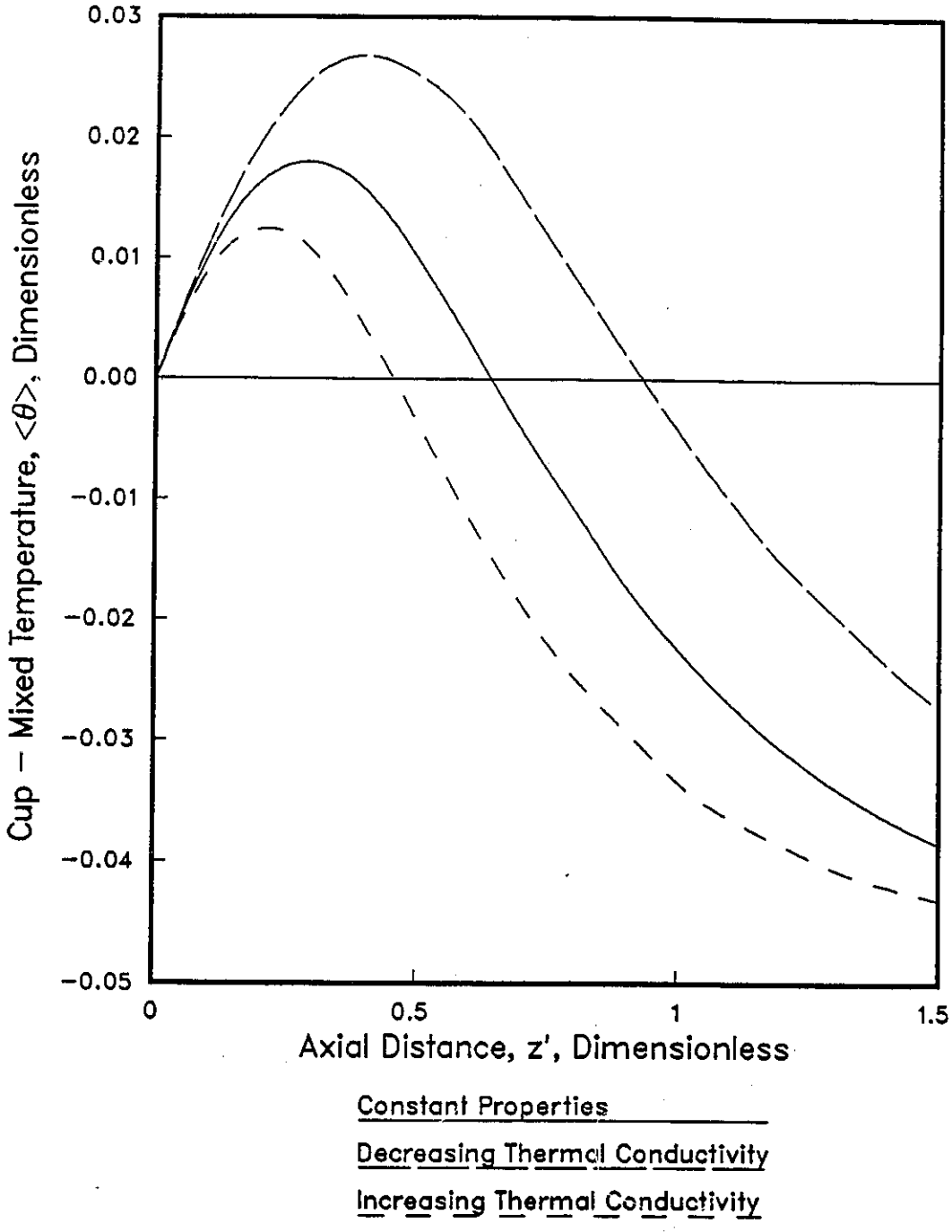

Figure A.6: Cup-mixed Temperature Profiles for Run 456.7

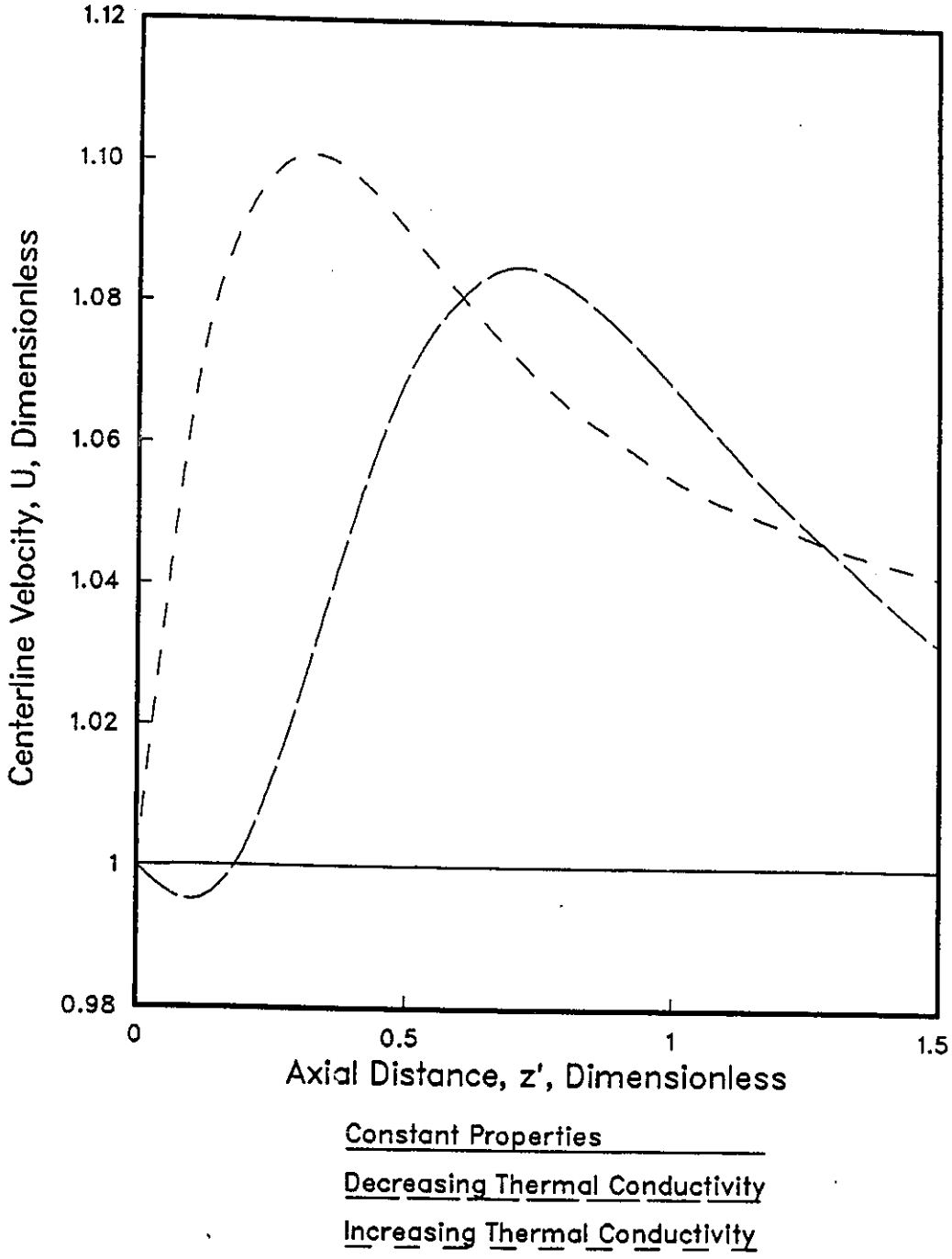

Figure A.7: Centerline Velocities for Run 456.7

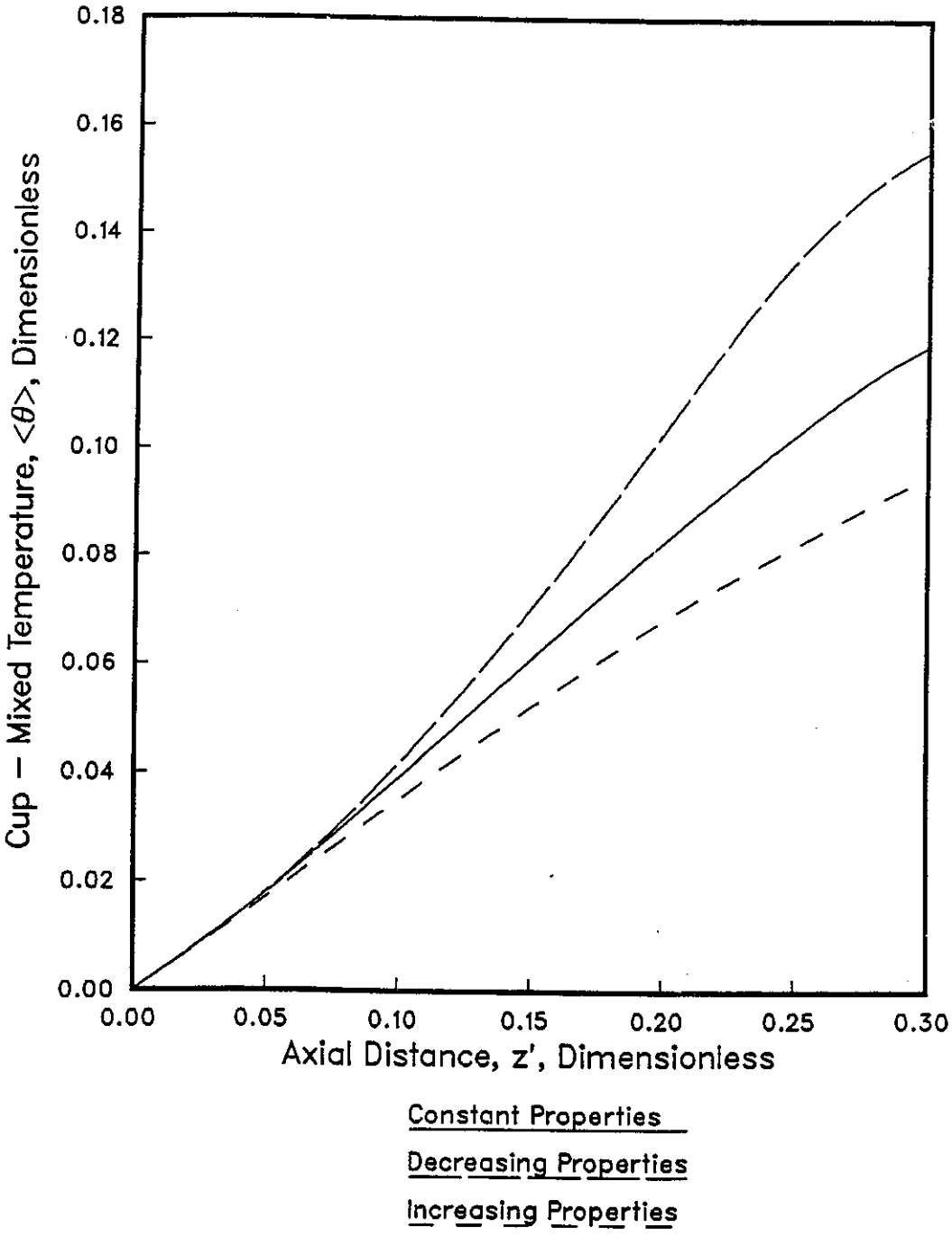

Figure A.8: Cup-mixed Temperature Profiles for Run 17

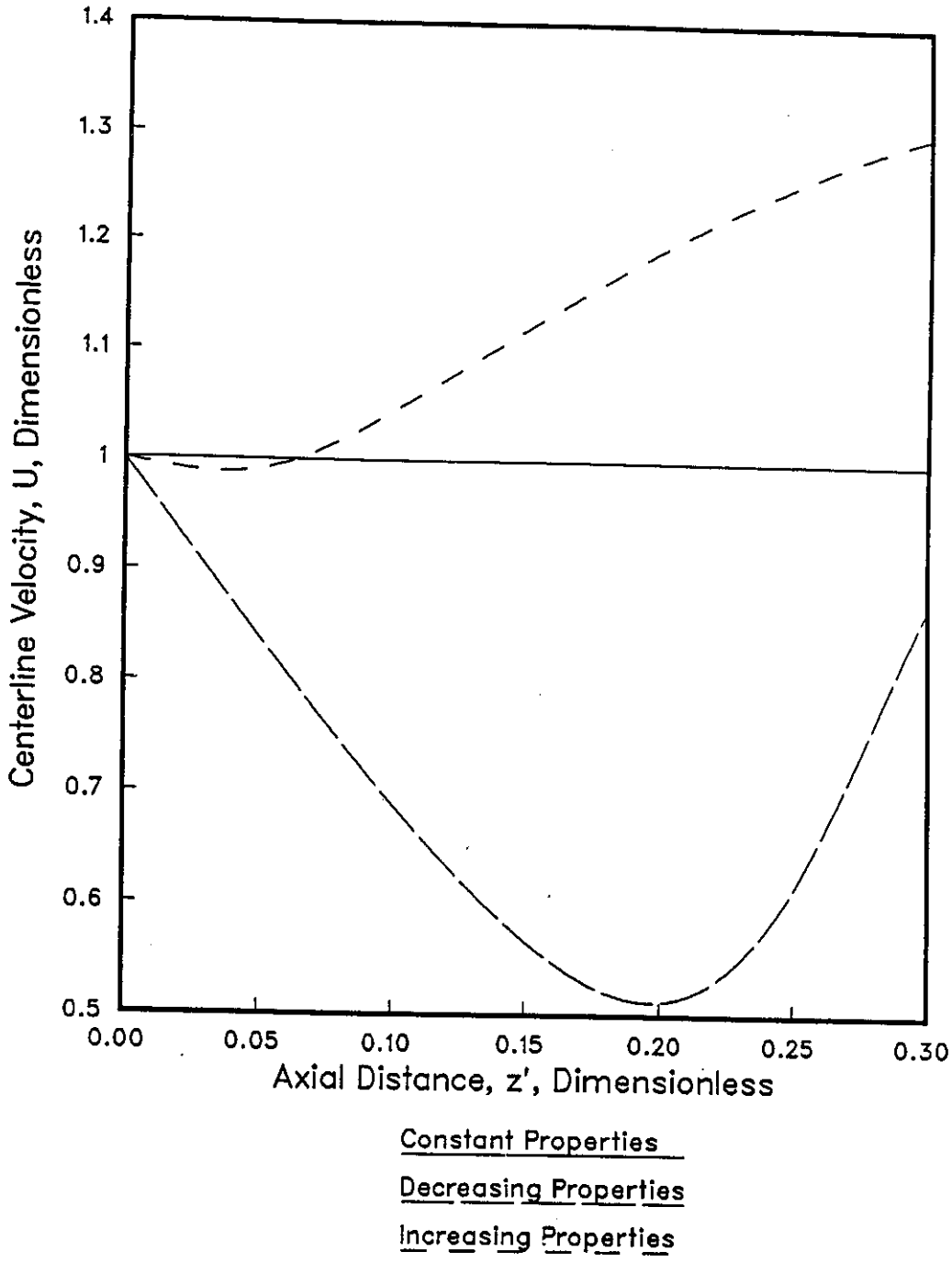

Figure A.9: Centerline Velocities for Run 17

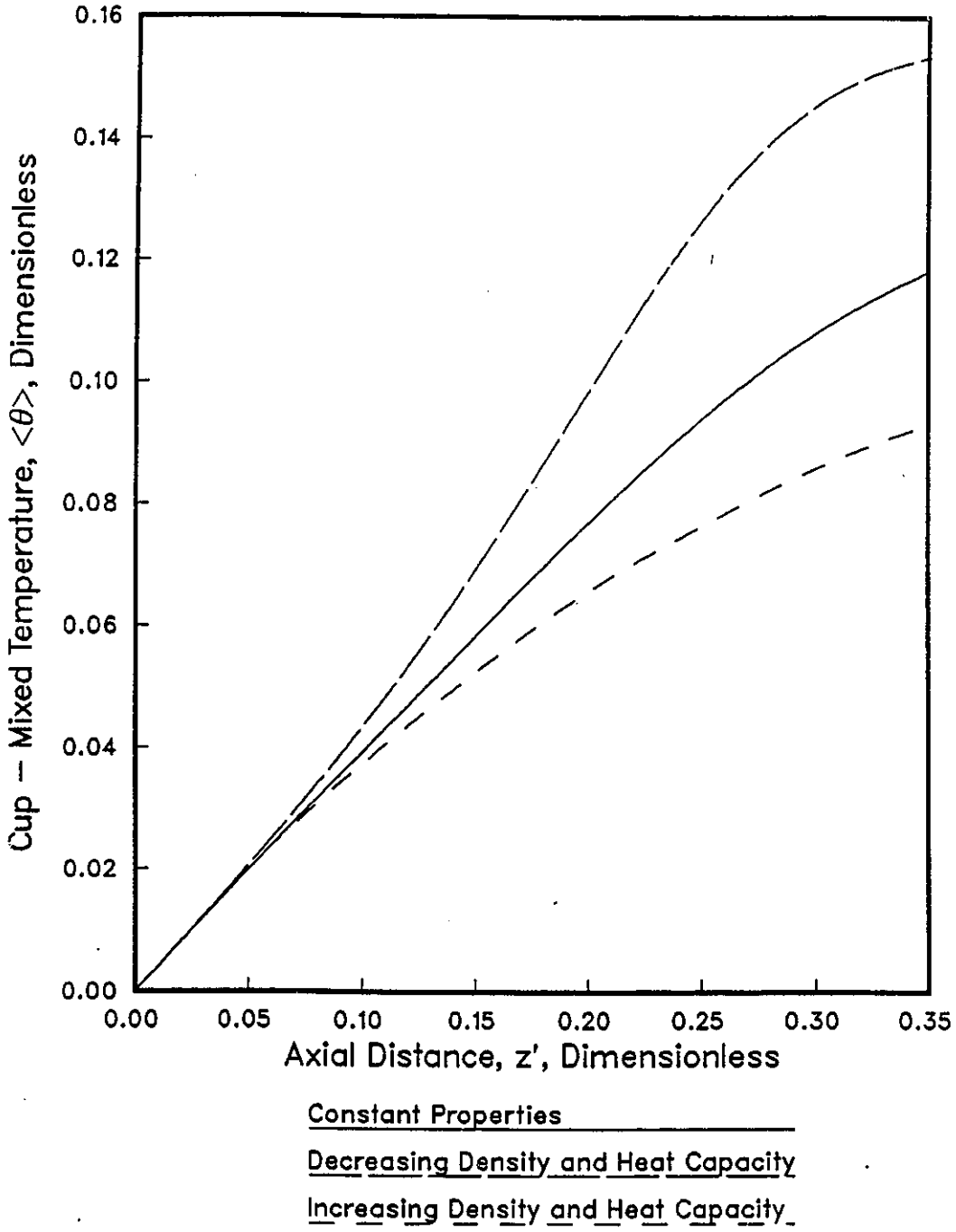

Figure A.10: Cup-mixed Temperature Profiles for Run 29

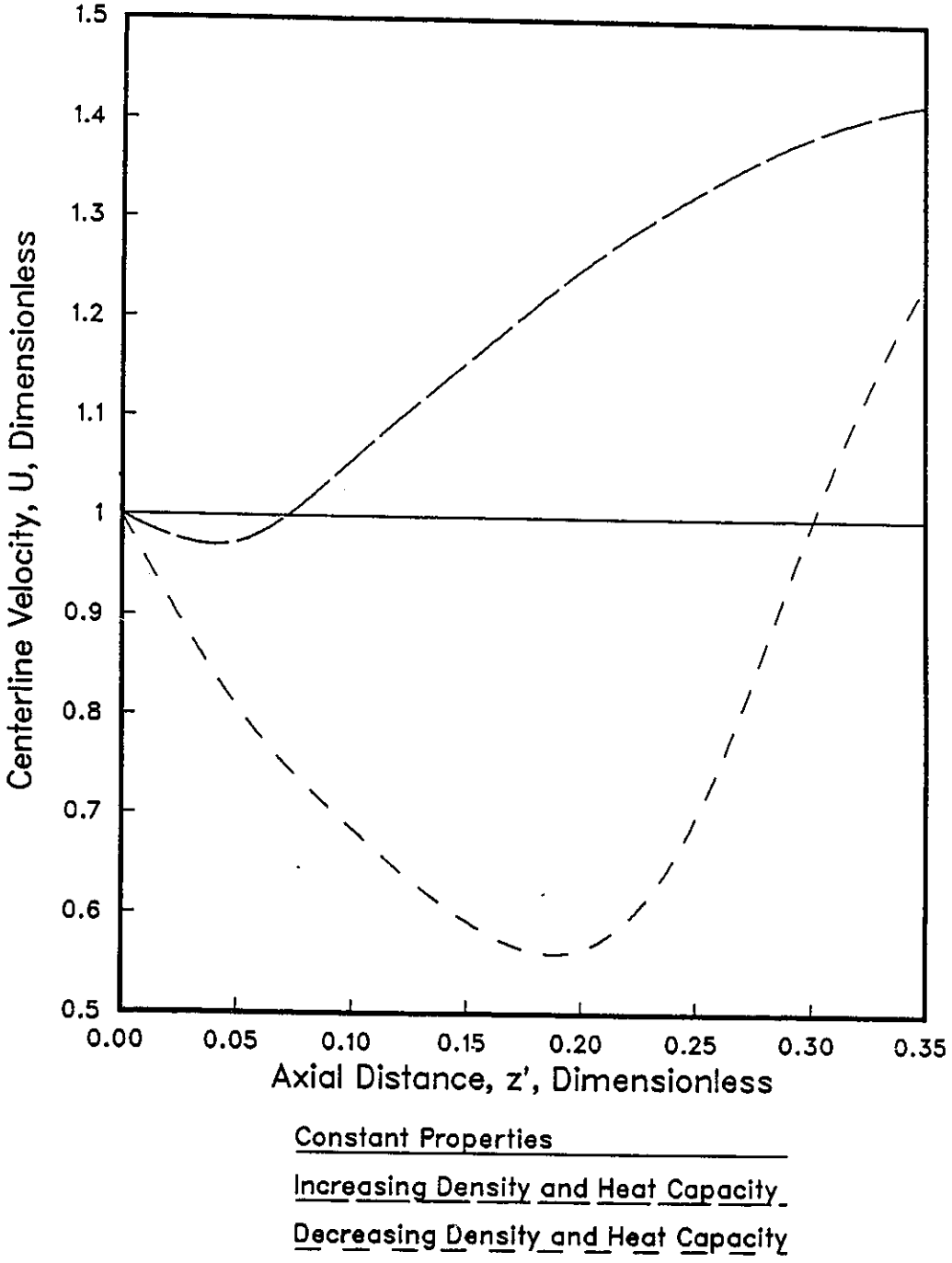

Figure A.11: Centerline Velocities for Run 29

A.3 Statistical Quantites of the Developed Regression Models

The models that were developed through the regression analysis had some terms associated with them that were used to quantitatively evaluate the significance of the regression. These terms have been given in Table A.3 given below. The model numbers given were those for their respective tables given in the main body of the thesis.

Table A.3: Statistical Results of the Developed Models

Model	SSR	R^2	Runs	Degrees of Freedom	Q
5.1	10.93	.866	89	81	64.63
5.2	4.11	.908	89	84	163.8
5.3	2.44	.937	26	20	47.10
5.5	2.12	.901	49	39	34.58
5.7	0.21	.935	26	22	75.52
5.9	.009	.986	16	12	193.68
5.11	.257	.728	89	76	15.44
5.12	.367	.515	89	81	10.62
5.13	.338	.437	89	80	6.81
5.14	.008	.693	26	21	9.03
5.15	.008	.577	26	21	5.46
5.16	.009	.470	26	22	4.66
5.17	.081	.658	49	42	11.27
5.18	.089	.592	49	43	10.16
5.19	.060	.579	49	43	9.63
5.20	.107	.794	26	20	12.21
5.21	.091	.838	26	20	16.38
5.22	.129	.702	26	20	7.46
5.23	28.24	.622	712	696	71.48
5.25	7.47	.659	208	200	48.07
5.26	11.71	.745	392	380	138.41
5.28	6.78	.799	208	199	87.45
5.30	32.74	.637	288	276	40.22
5.31	15.10	.515	320	309	29.73

A.4 Residual Plots for Constant Property Models

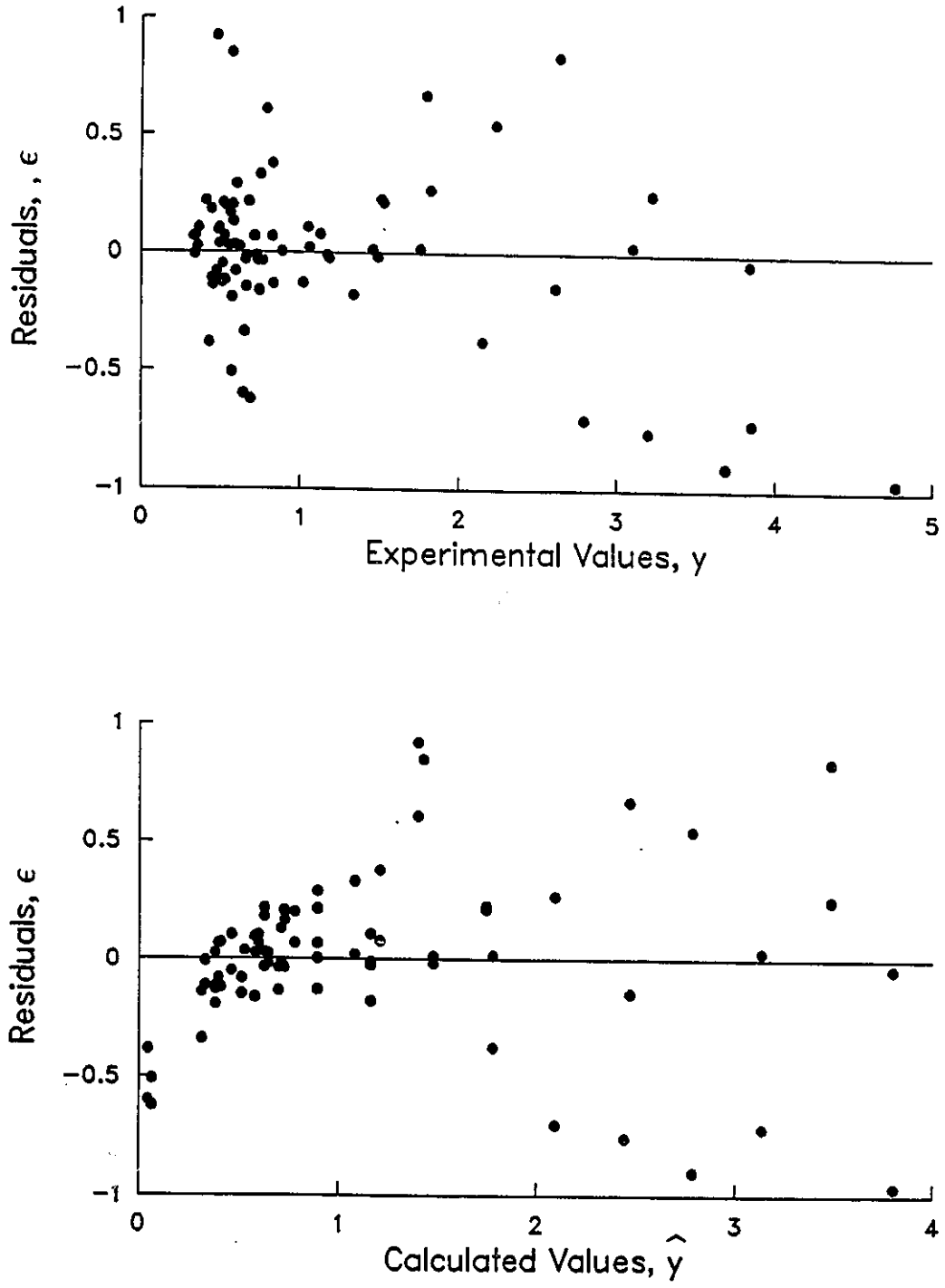

Figure A.12: Residual Plots for Length as a Function of Dimensionless Groups

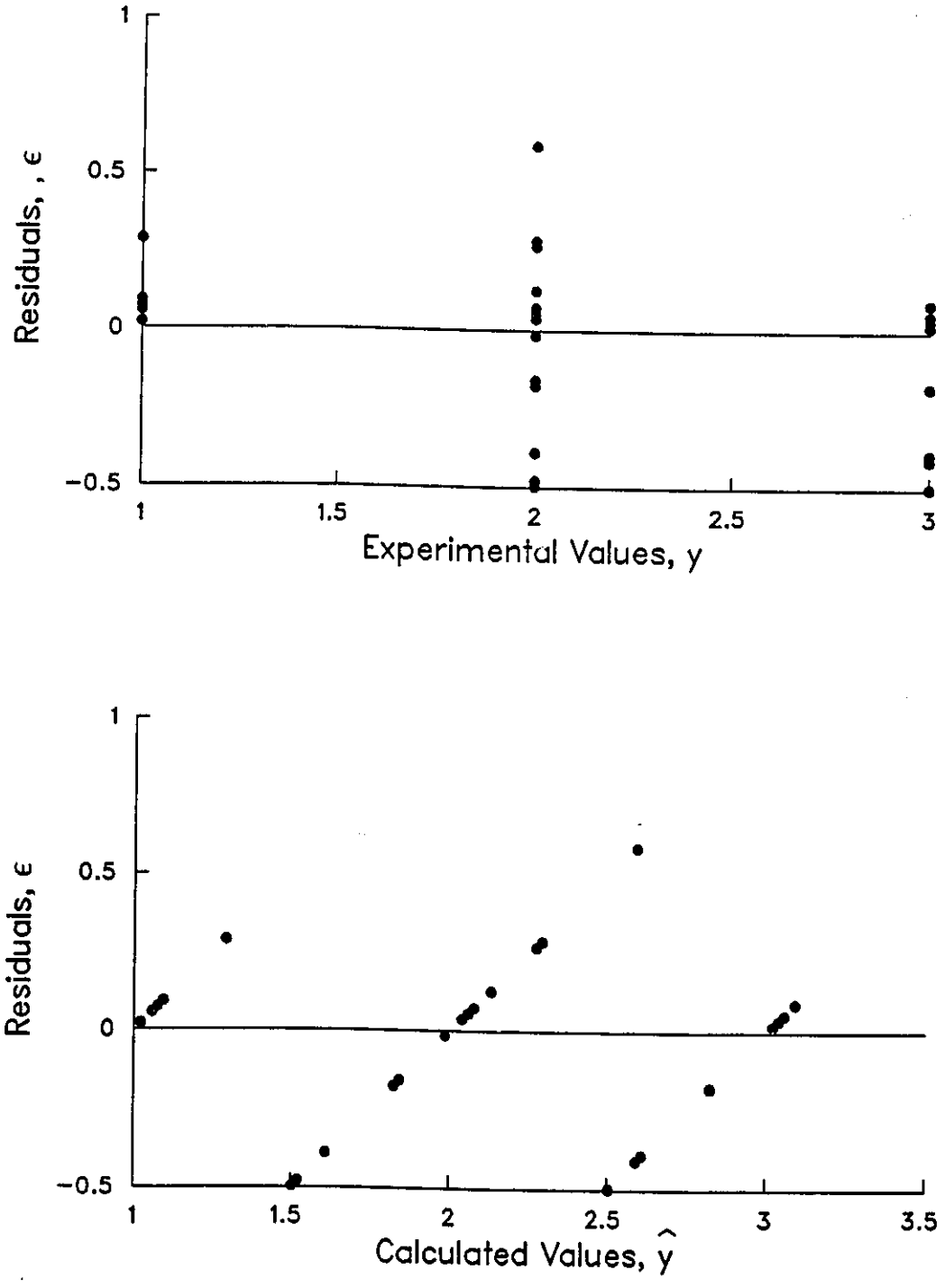

Figure A.13: Residual Plots for Determining the Heat Transfer Regime

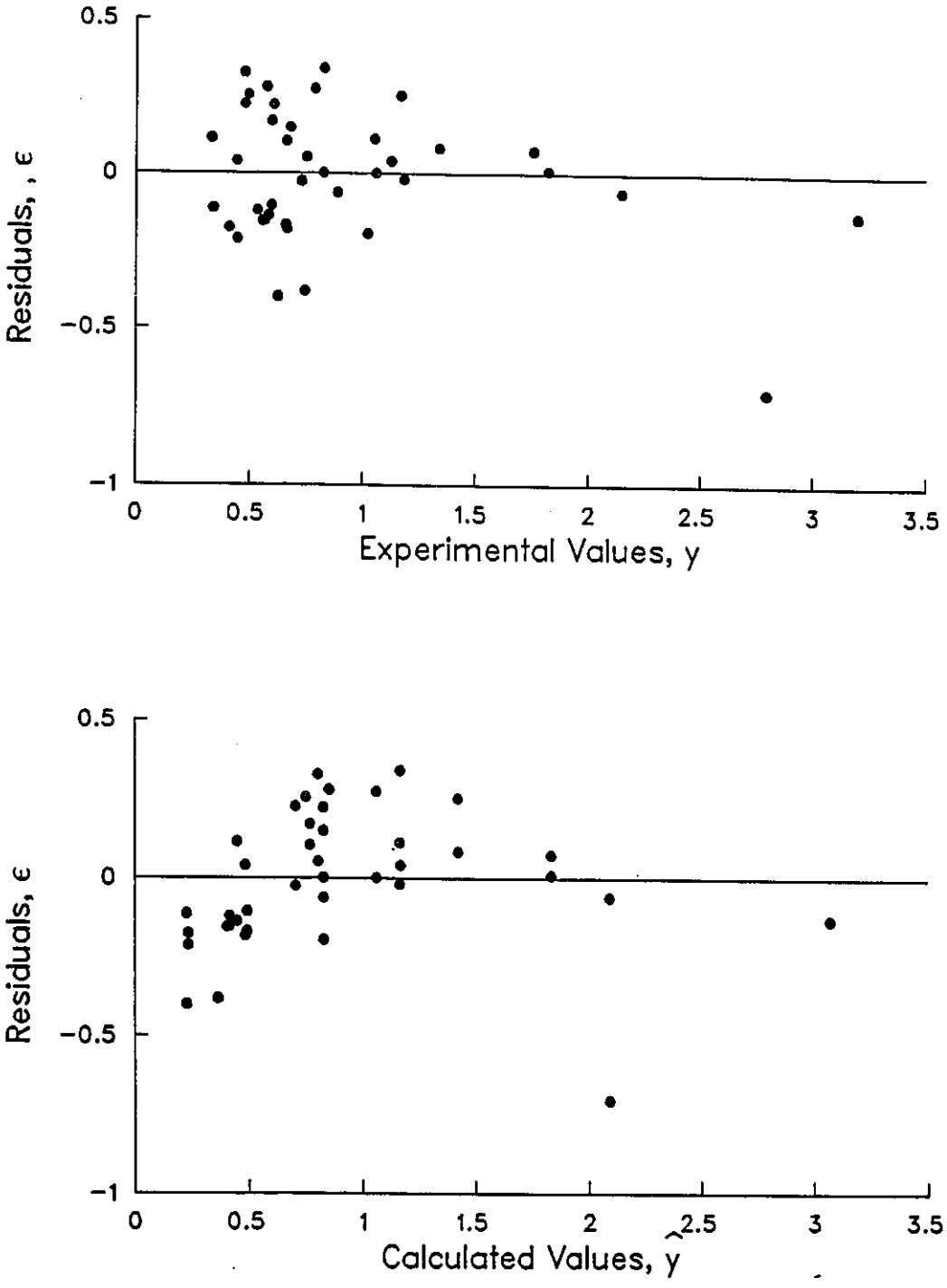

Figure A.14: Residual Plots for Length as a Function of Dimensionless Groups in the High Heat Transfer Regime

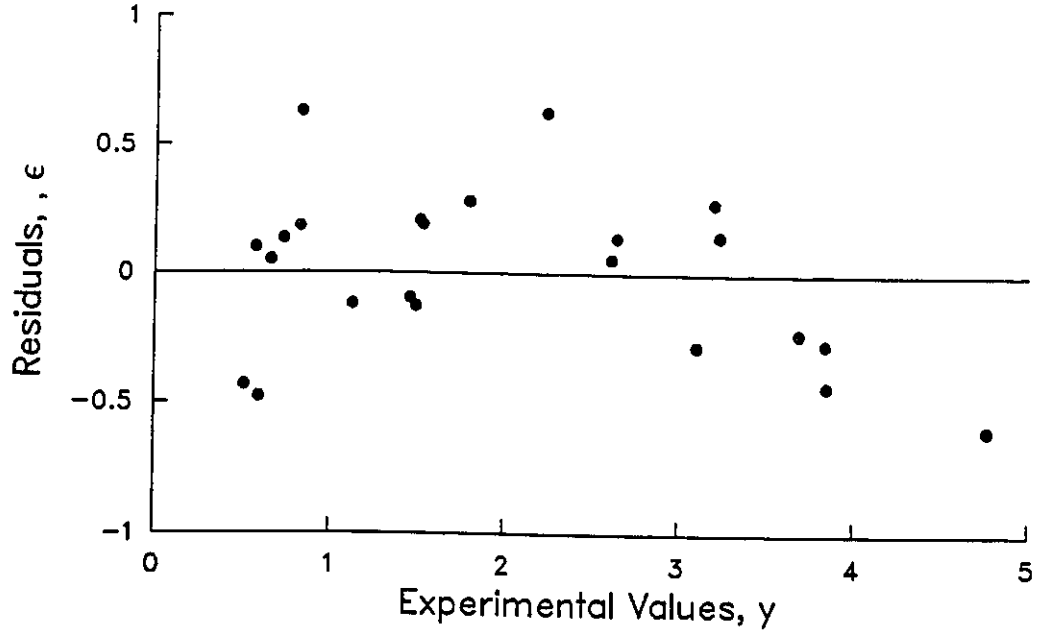

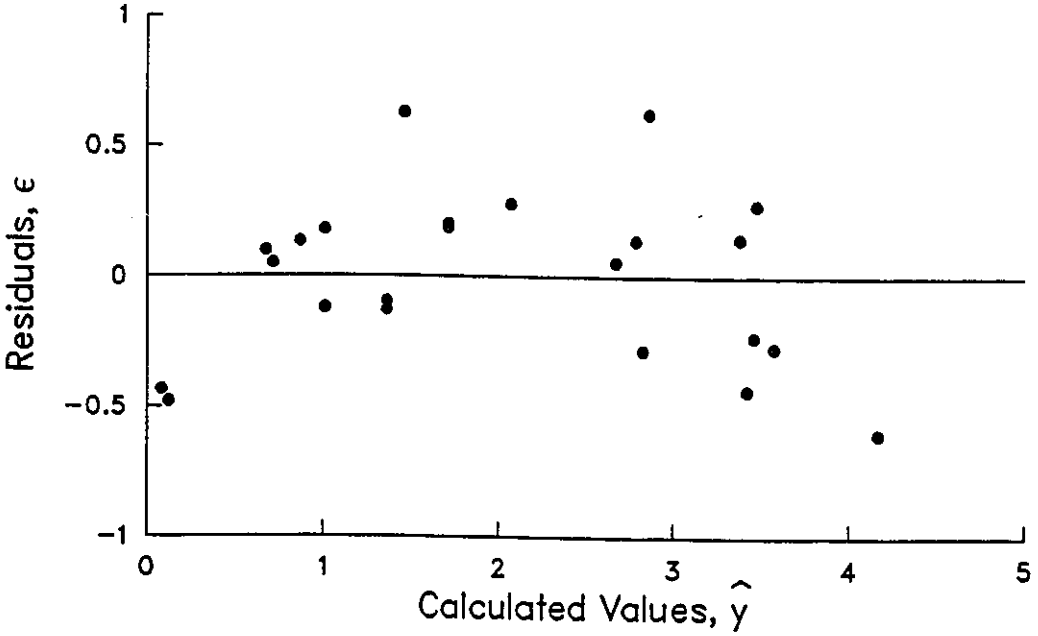

Figure A.15: Residual Plots for Length as a Function of Dimensionless Groups in the Medium Heat Transfer Regime

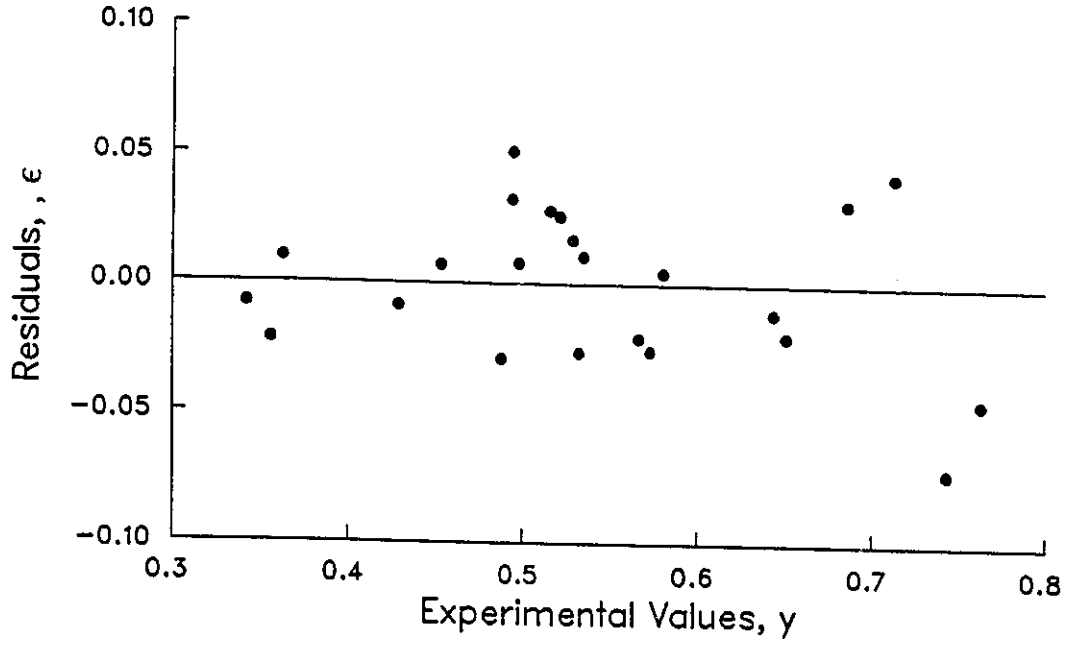

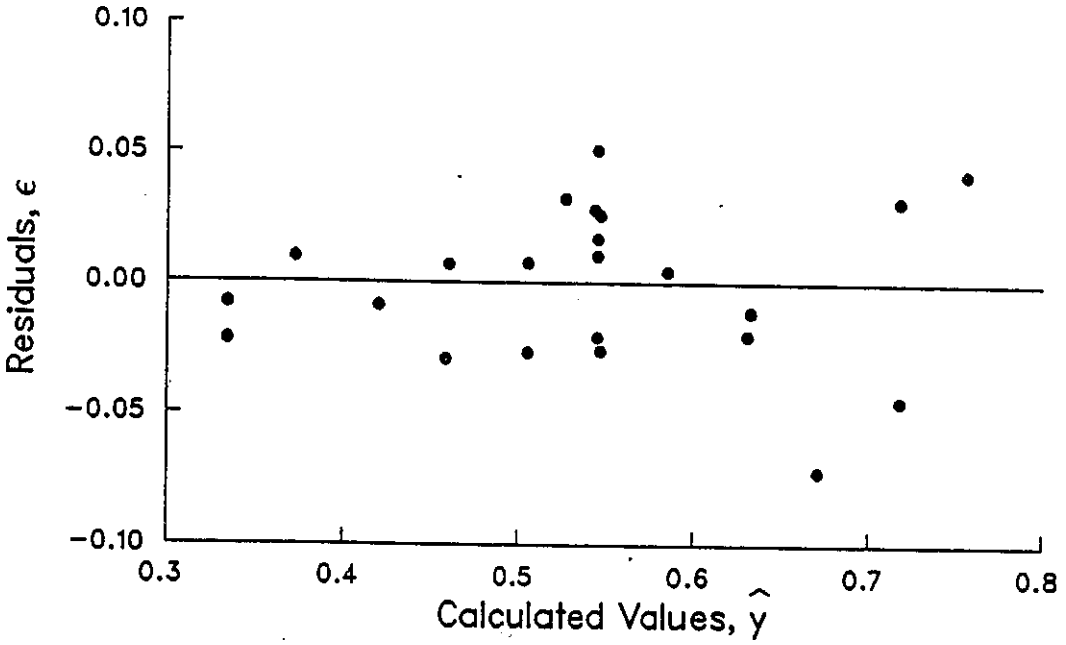

Figure A.16: Residual Plots for Length as a Function of Dimensionless Groups in the Low Heat Transfer Regime

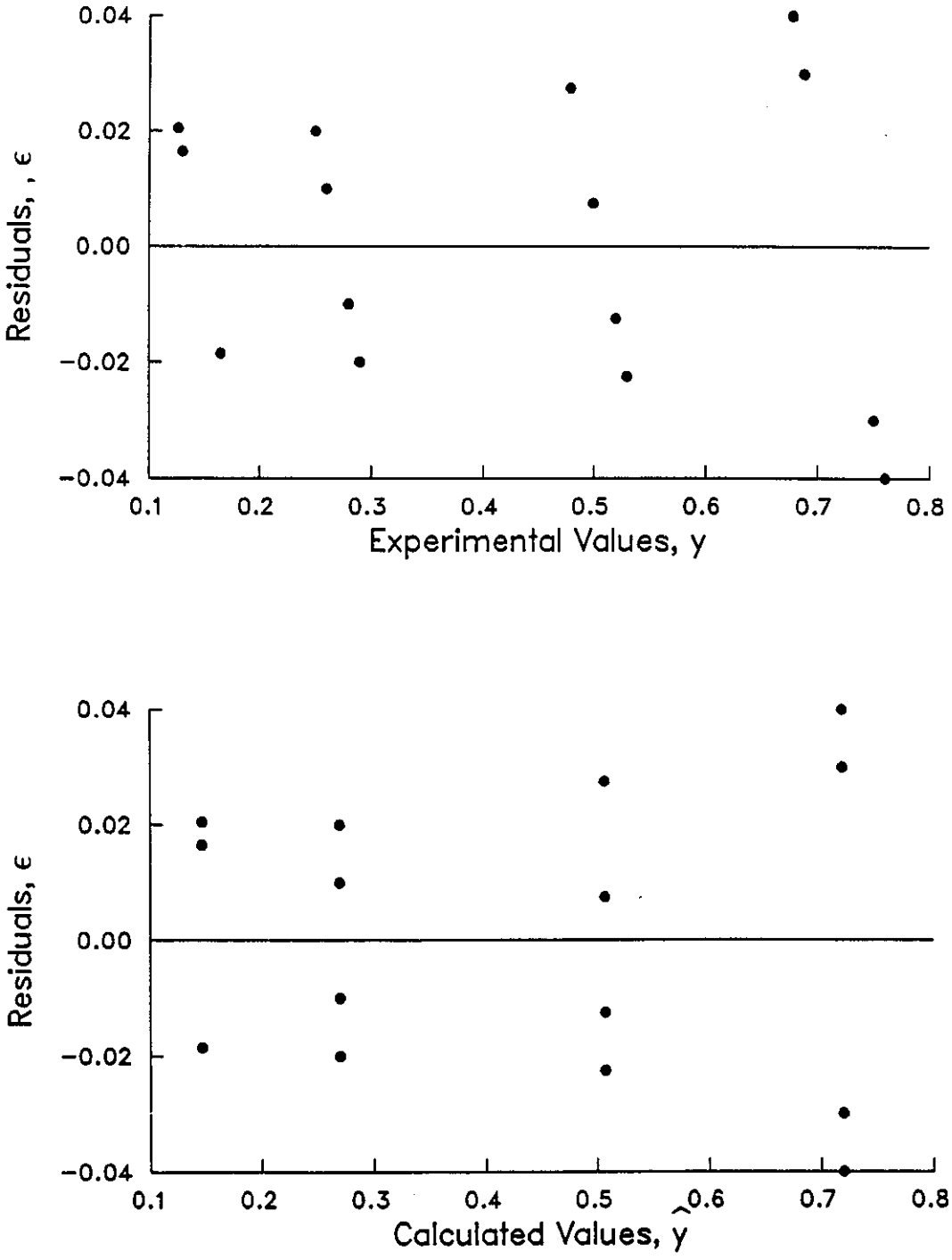

Figure A.17: Residual Plots for Length as a Function of Dimensionless Groups in an Adiabatic Reactor

A.5 Residual Plots for Temperature Dependent Property Models

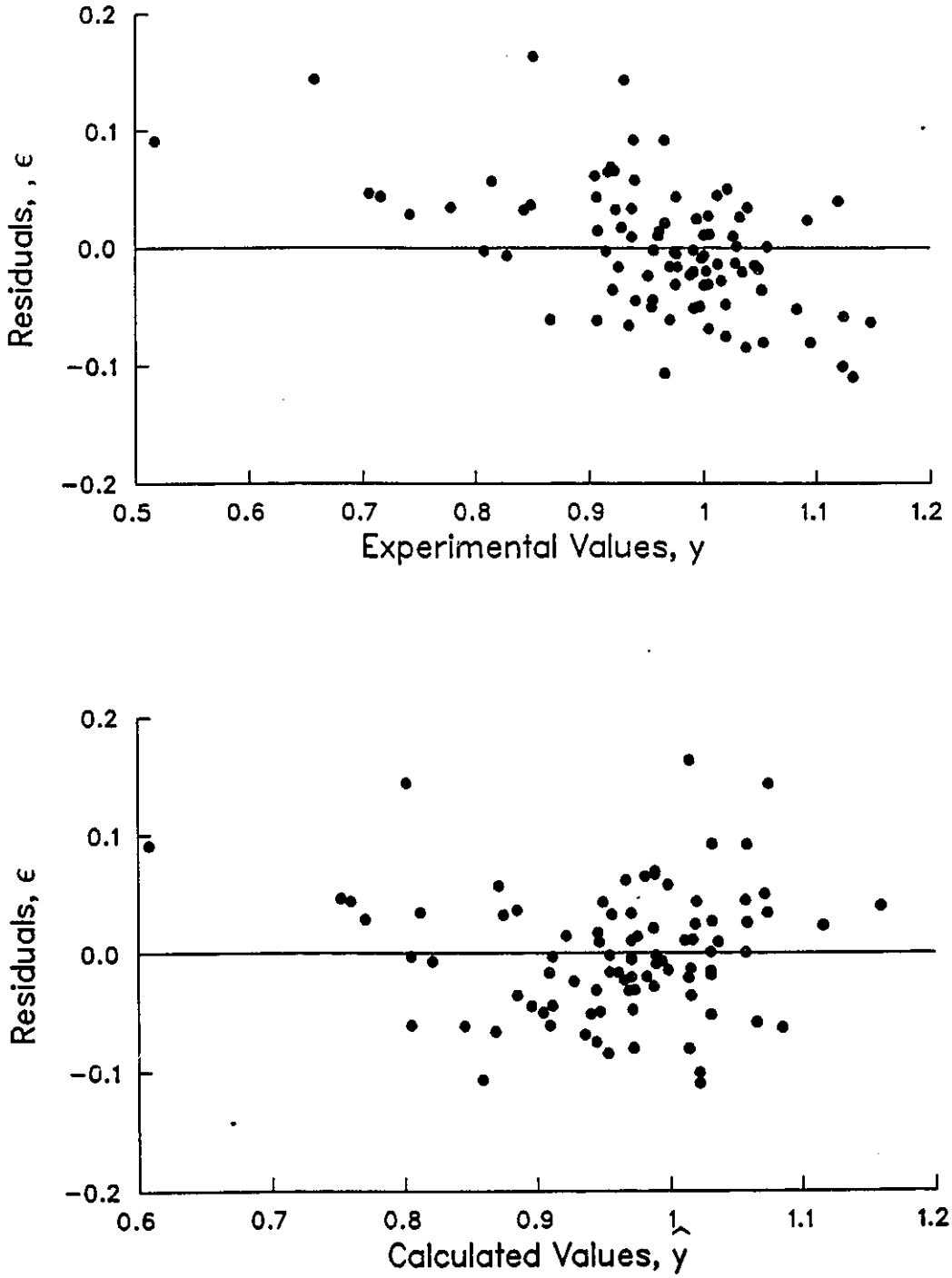

Figure A.18: Residual Plots for Deviations as a Function of Dimensionless Groups: Water

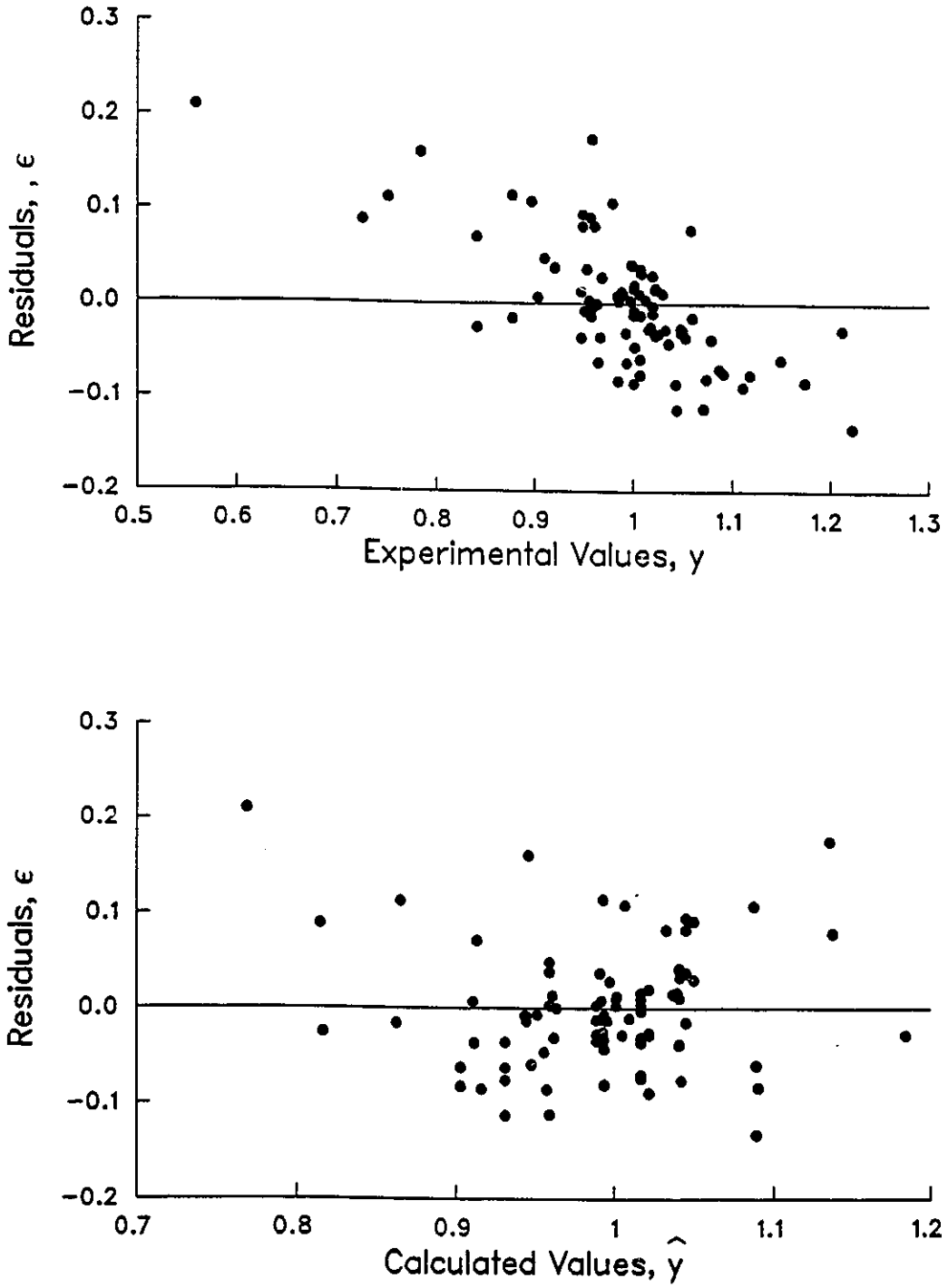

Figure A.19: Residual Plots for Deviations as a Function of Dimensionless Groups: Ethanol

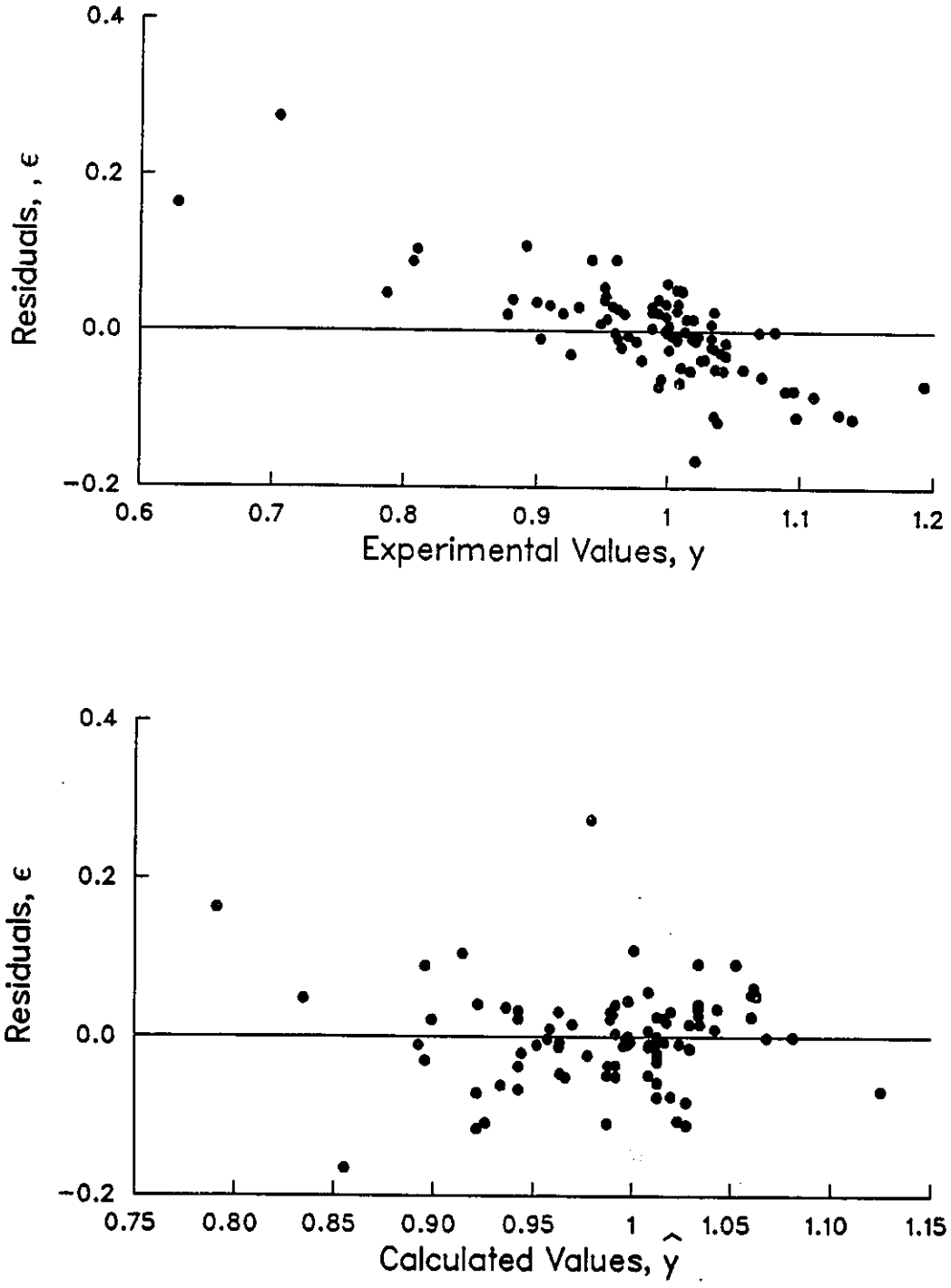

Figure A.20: Residual Plots for Deviations as a Function of Dimensionless Groups: Benzene

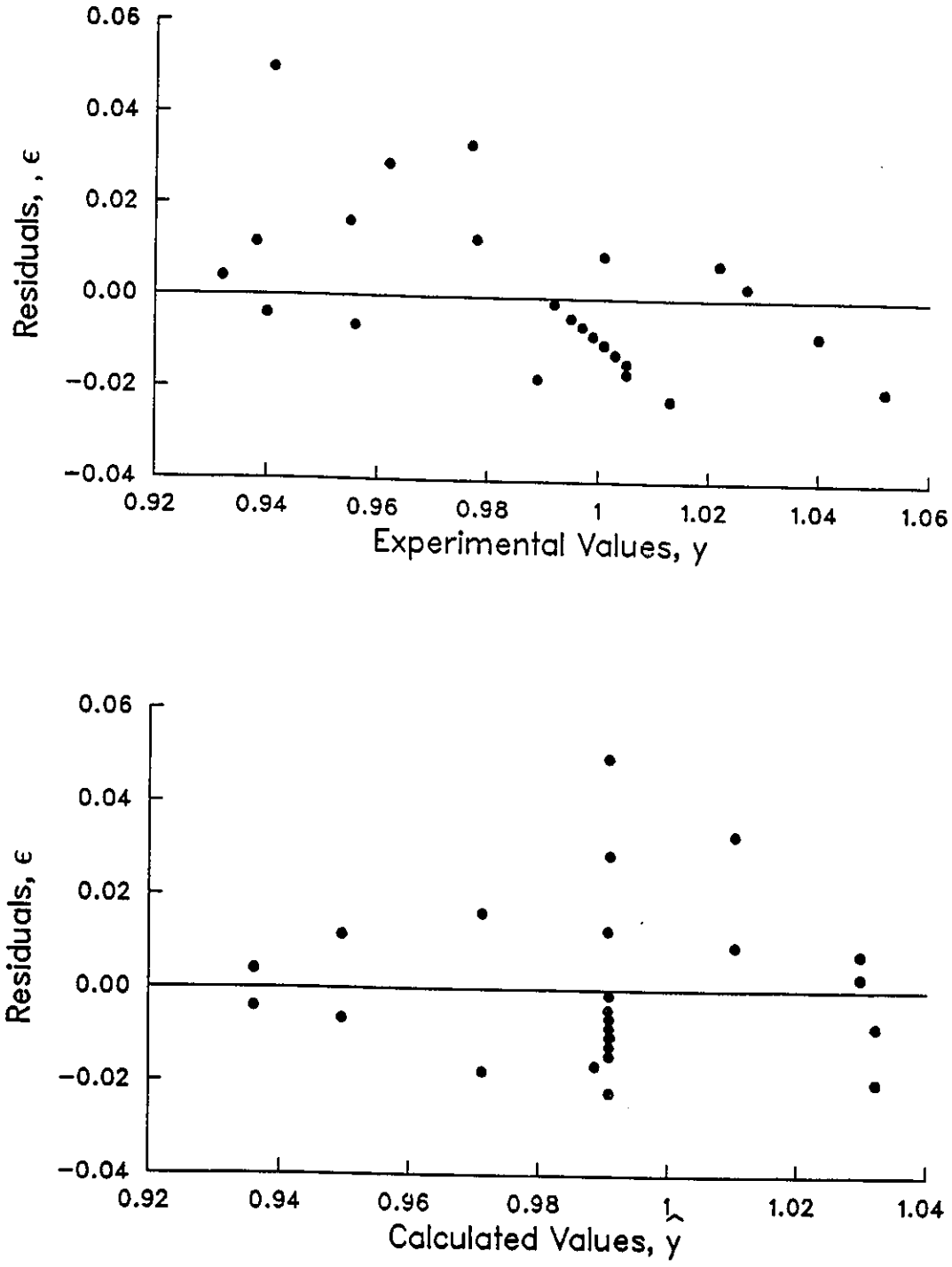

Figure A.21: Residual Plots for Deviations as a Function of Dimensionless Groups in the High Heat Transfer Regime: Water

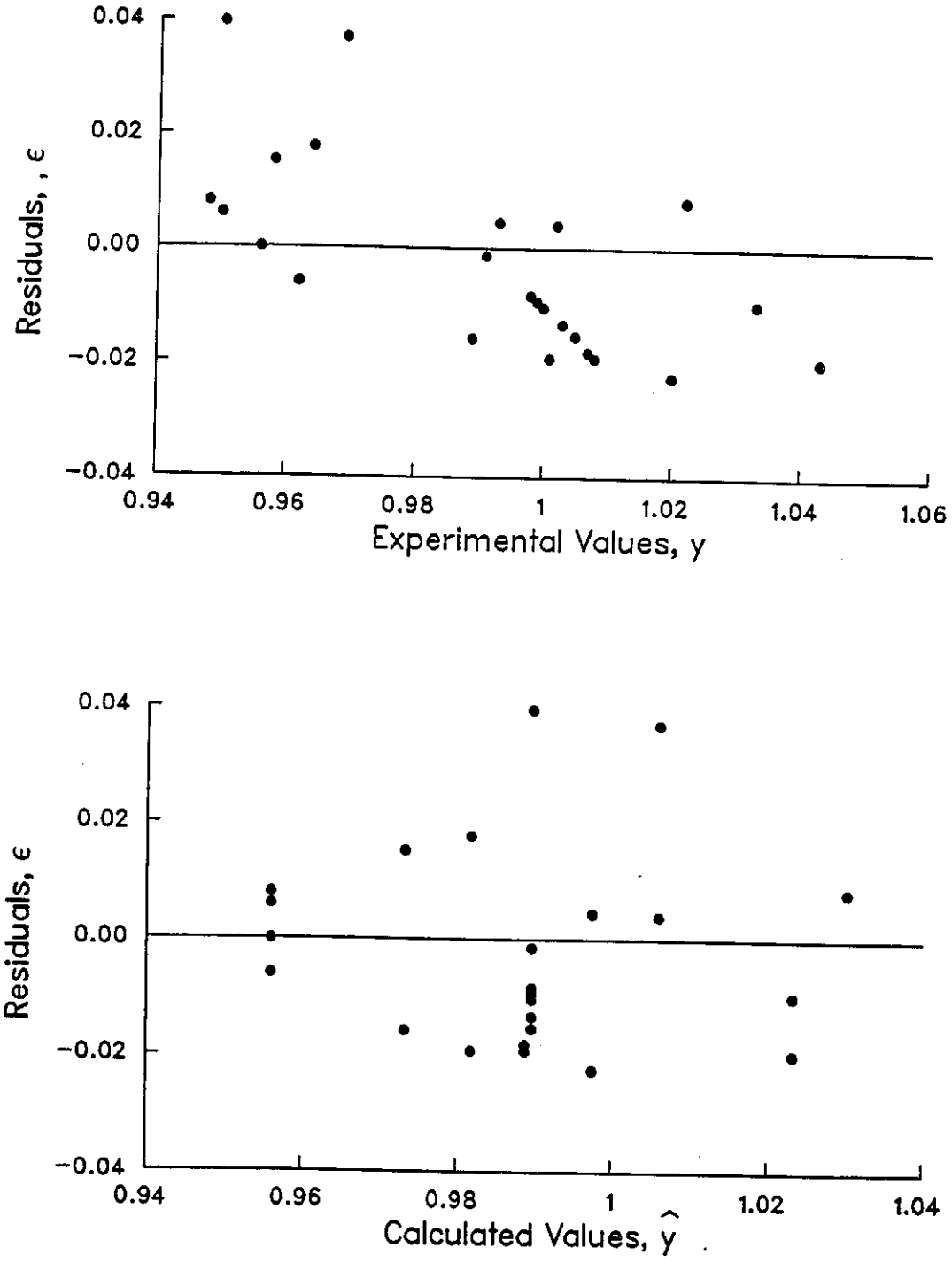

Figure A.22: Residual Plots for Deviations as a Function of Dimensionless Groups in the High Heat Transfer Regime: Ethanol

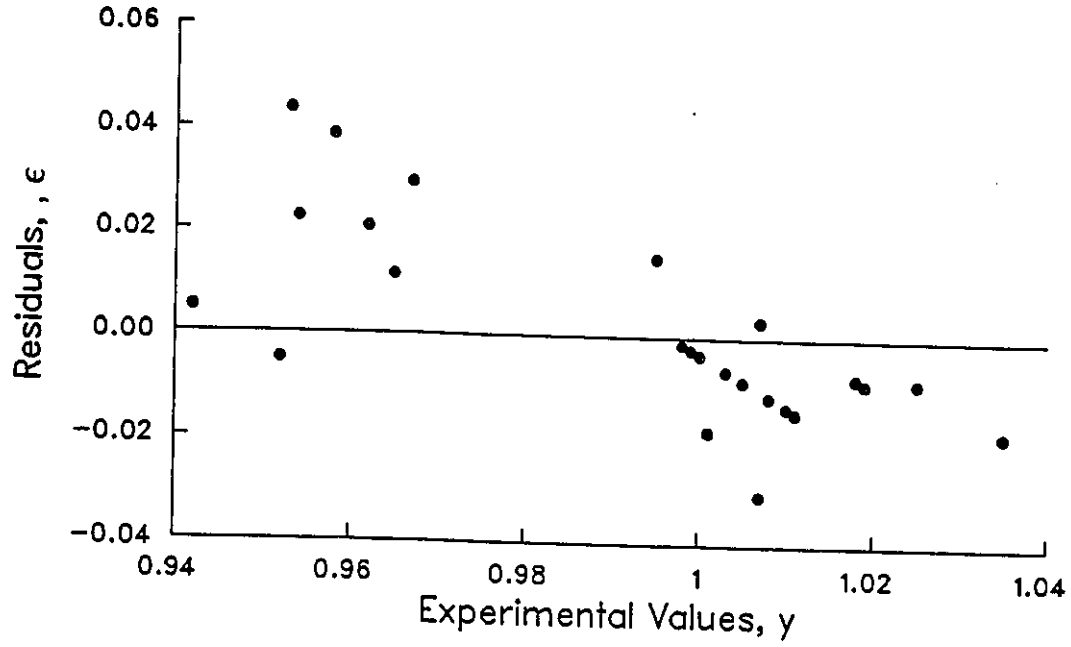

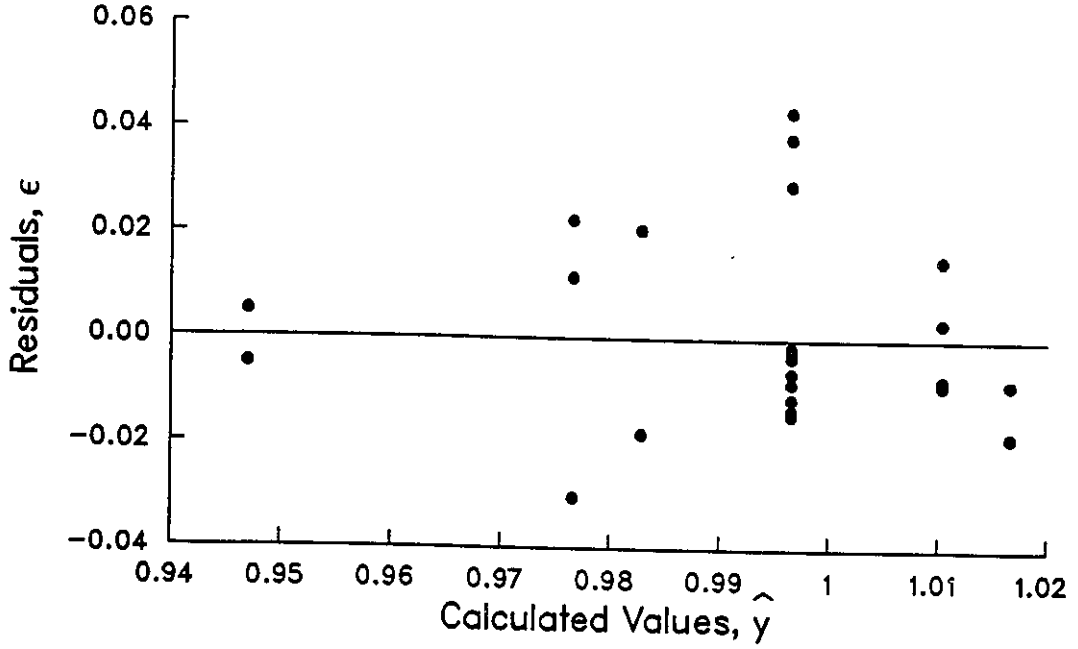

Figure A.23: Residual Plots for Deviations as a Function of Dimensionless Groups in the High Heat Transfer Regime: Benzene

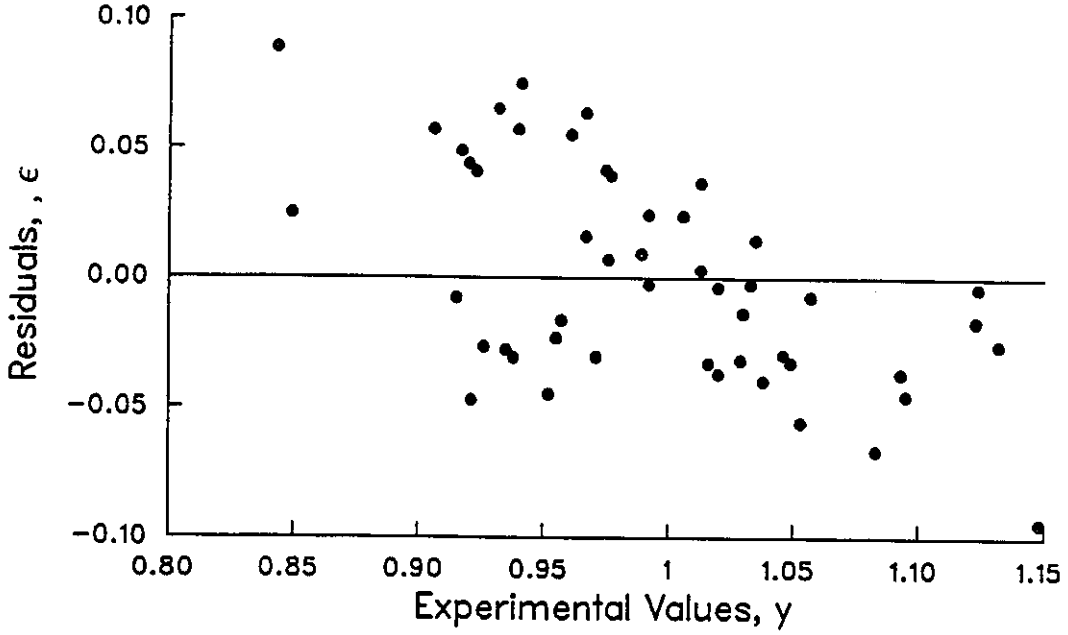

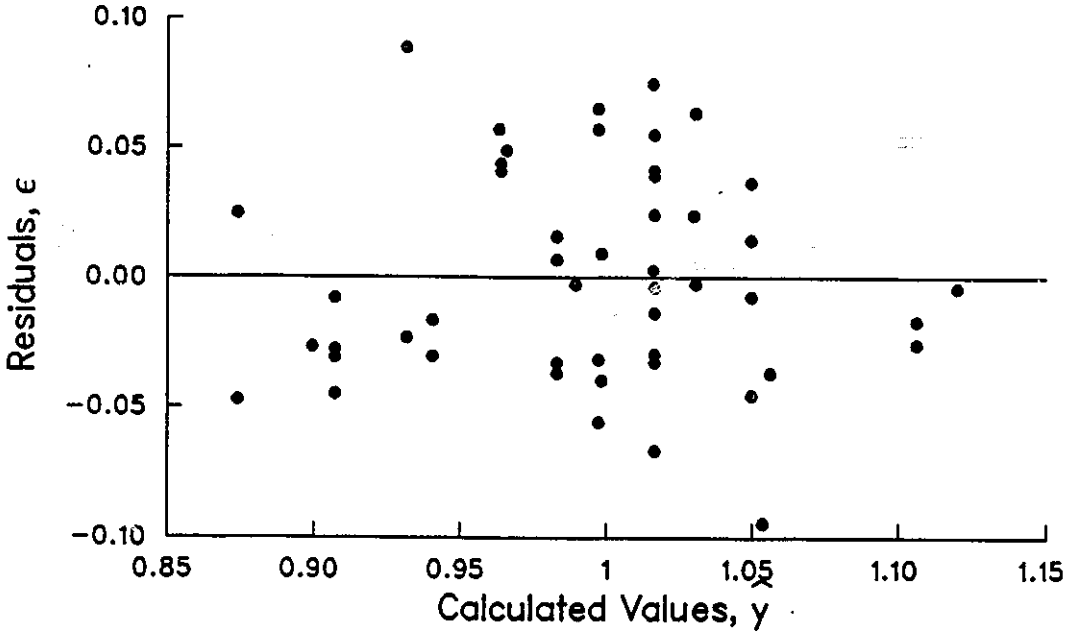

Figure A.24: Residual Plots for Deviations as a Function of Dimensionless Groups in the Medium Heat Transfer Regime: Water

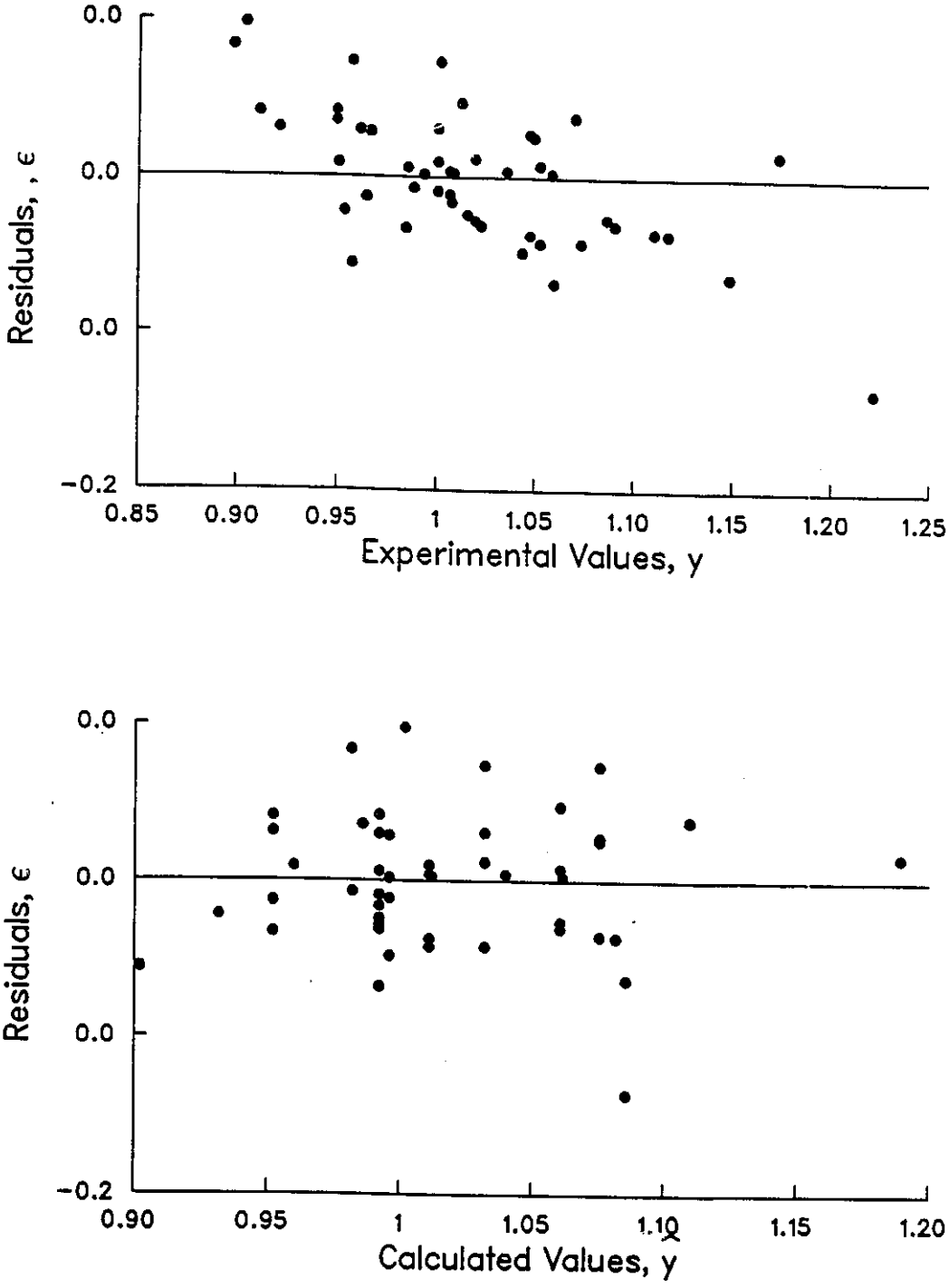

Figure A.25: Residual Plots for Deviations as a Function of Dimensionless Groups in the Medium Heat Transfer Regime: Ethanol

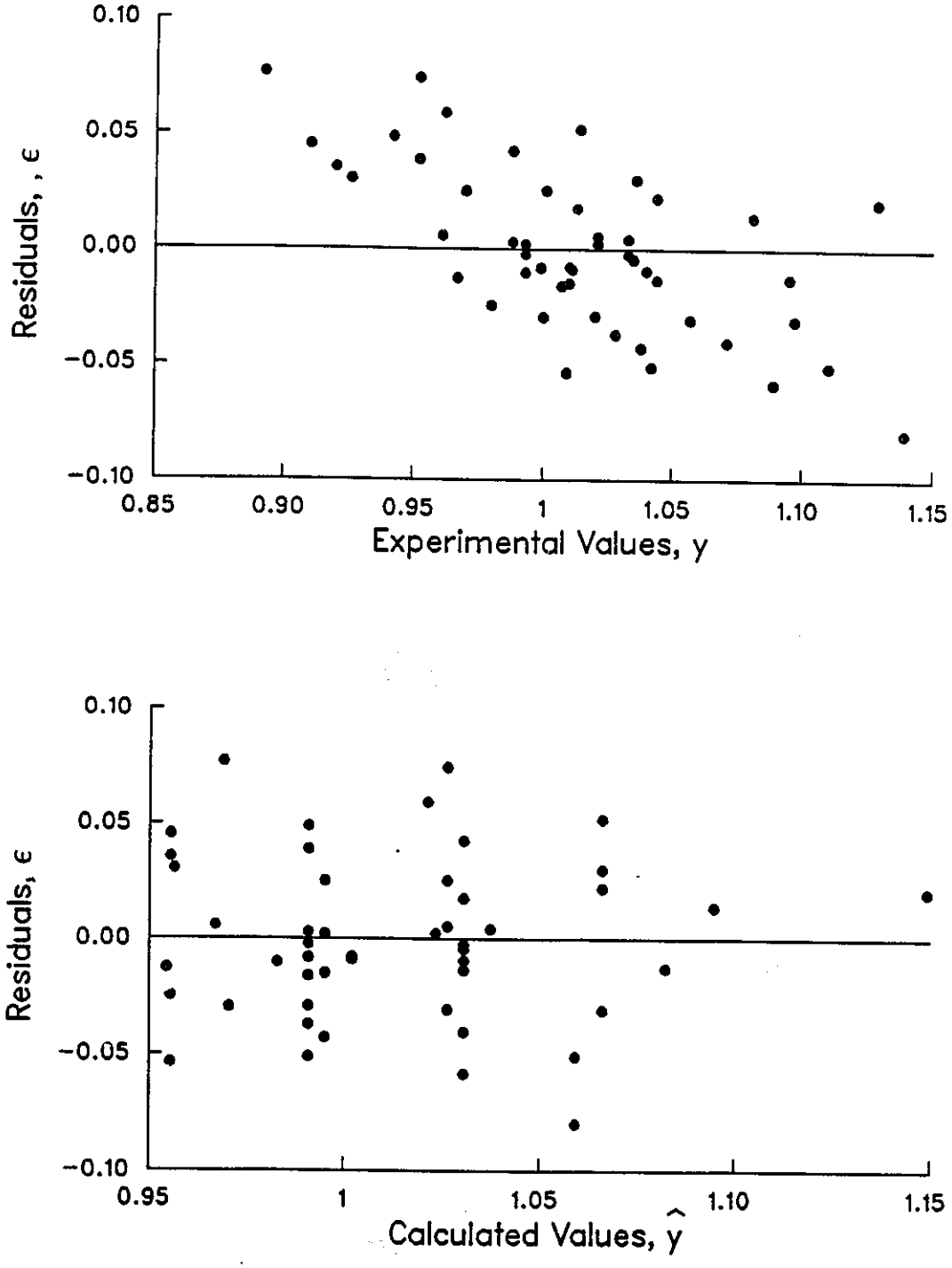

Figure A.26: Residual Plots for Deviations as a Function of Dimensionless Groups in the Medium Heat Transfer Regime: Benzene

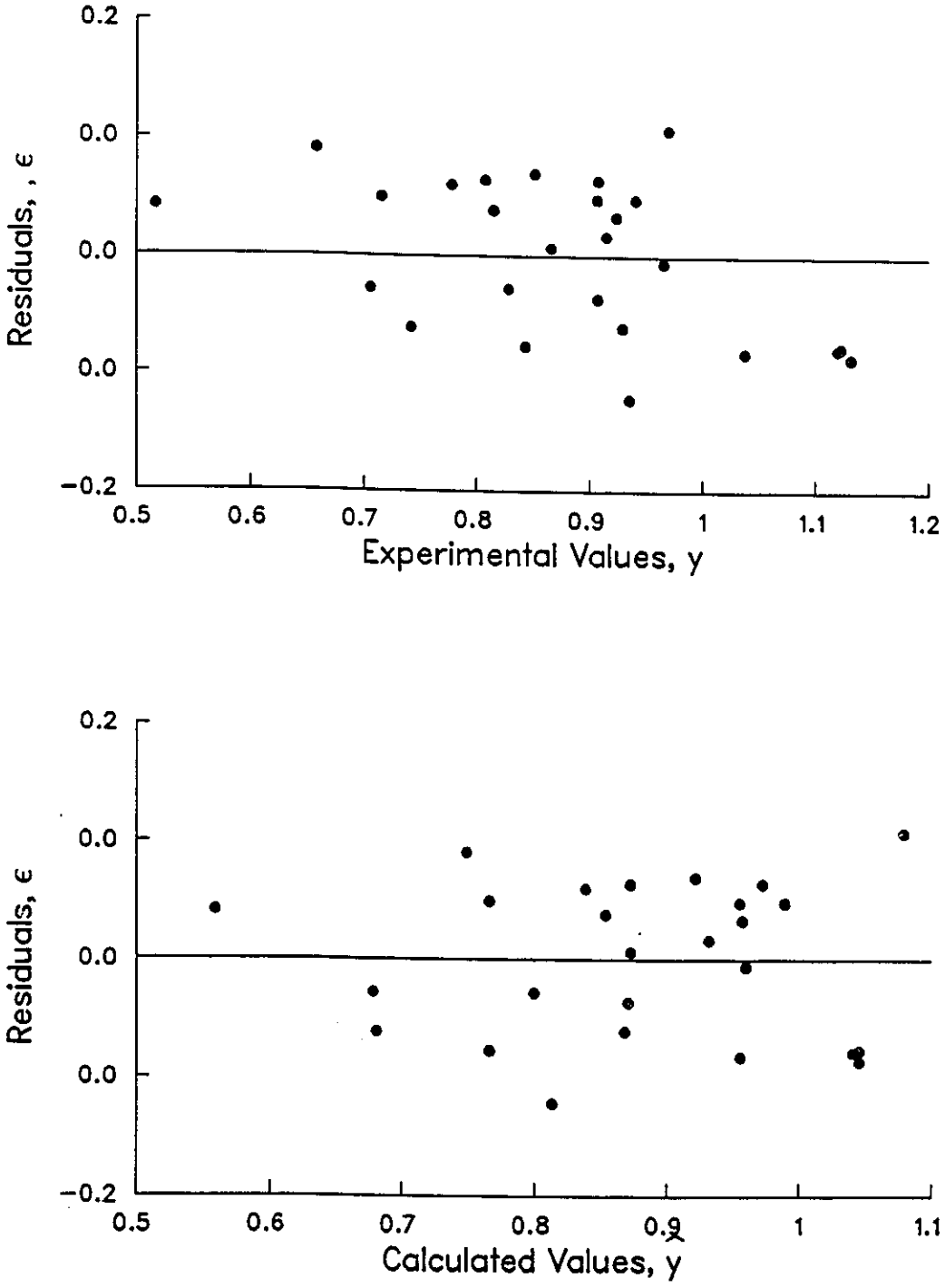

Figure A.27: Residual Plots for Deviations as a Function of Dimensionless Groups in the Low Heat Transfer Regime: Water

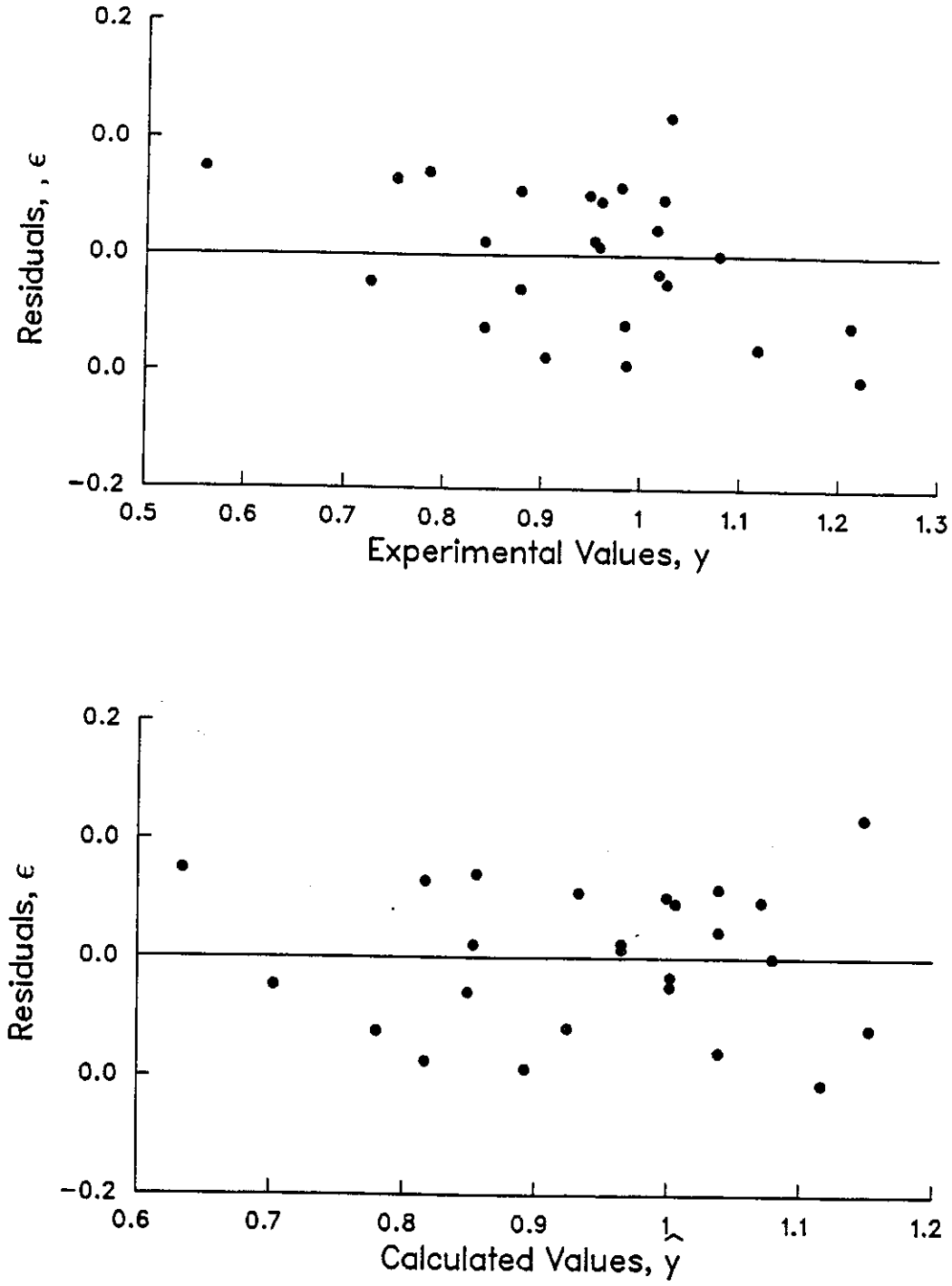

Figure A.28: Residual Plots for Deviations as a Function of Dimensionless Groups in the Low Heat Transfer Regime: Ethanol

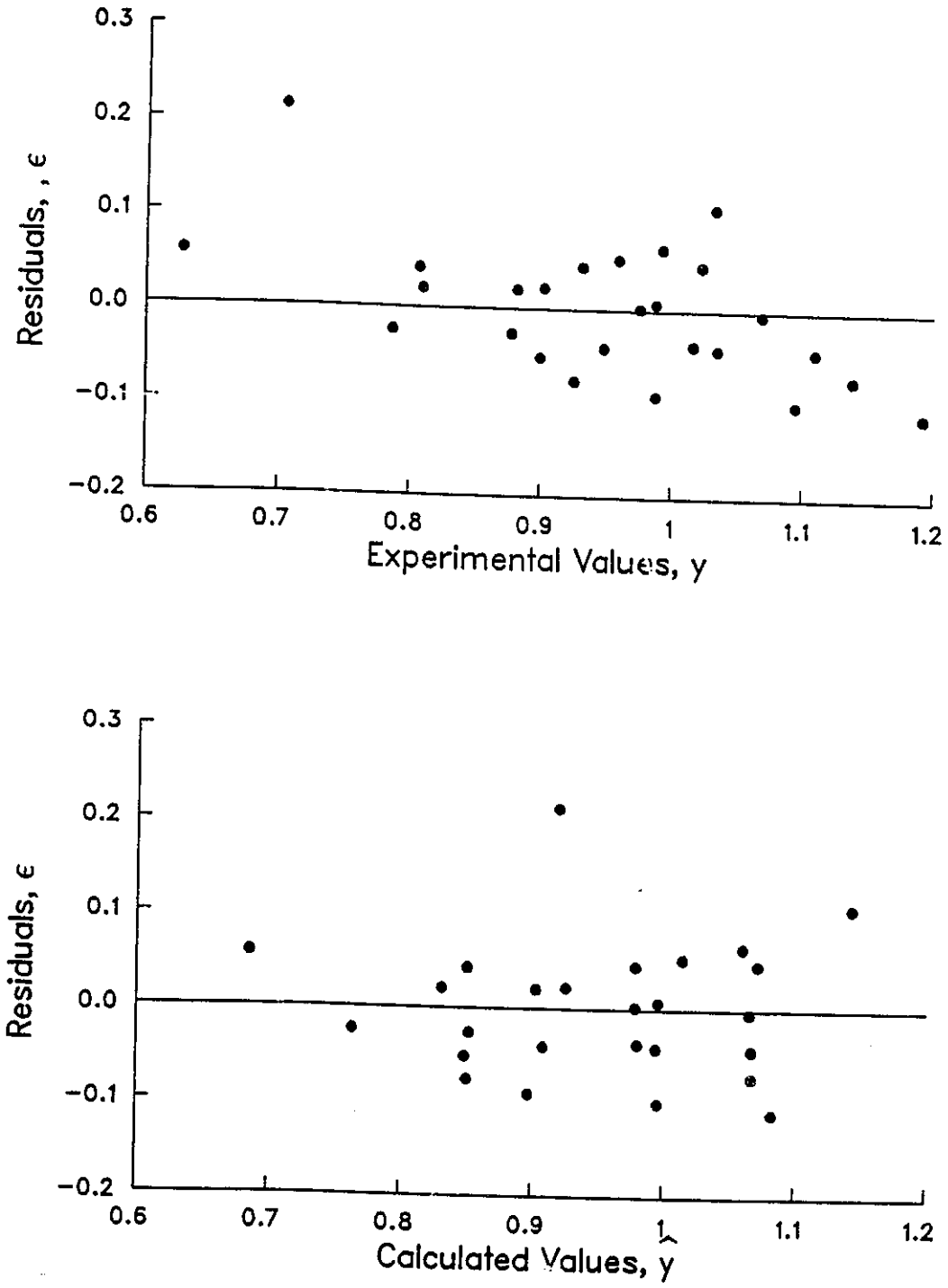

Figure A.29: Residual Plots for Deviations as a Function of Dimensionless Groups in the Low Heat Transfer Regime: Benzene

A.6 Residual Plots for Composition Dependent Property Models

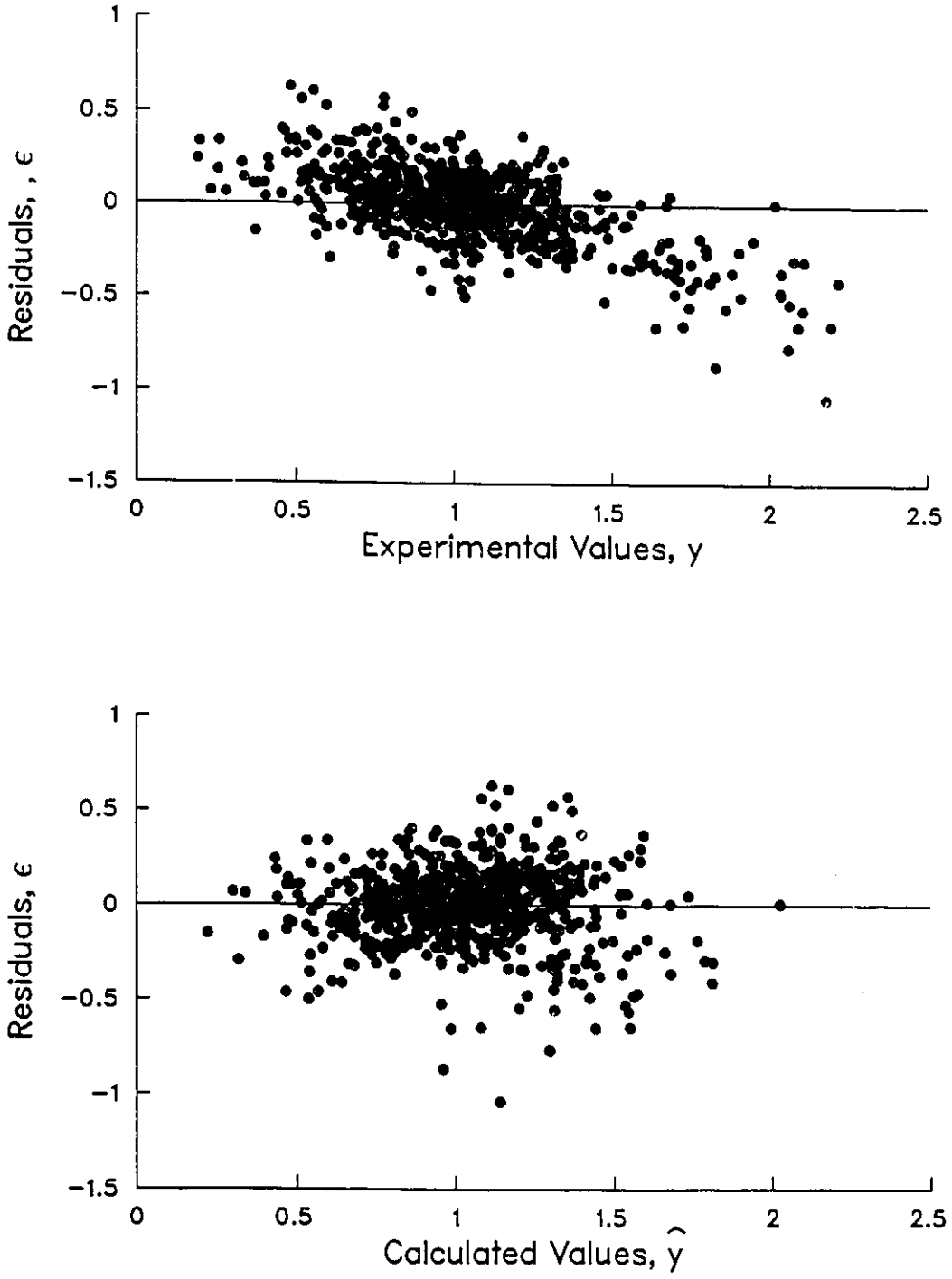

Figure A.30: Residual Plots for Deviations with Composition Dependent Physical Properties for the Overall Design

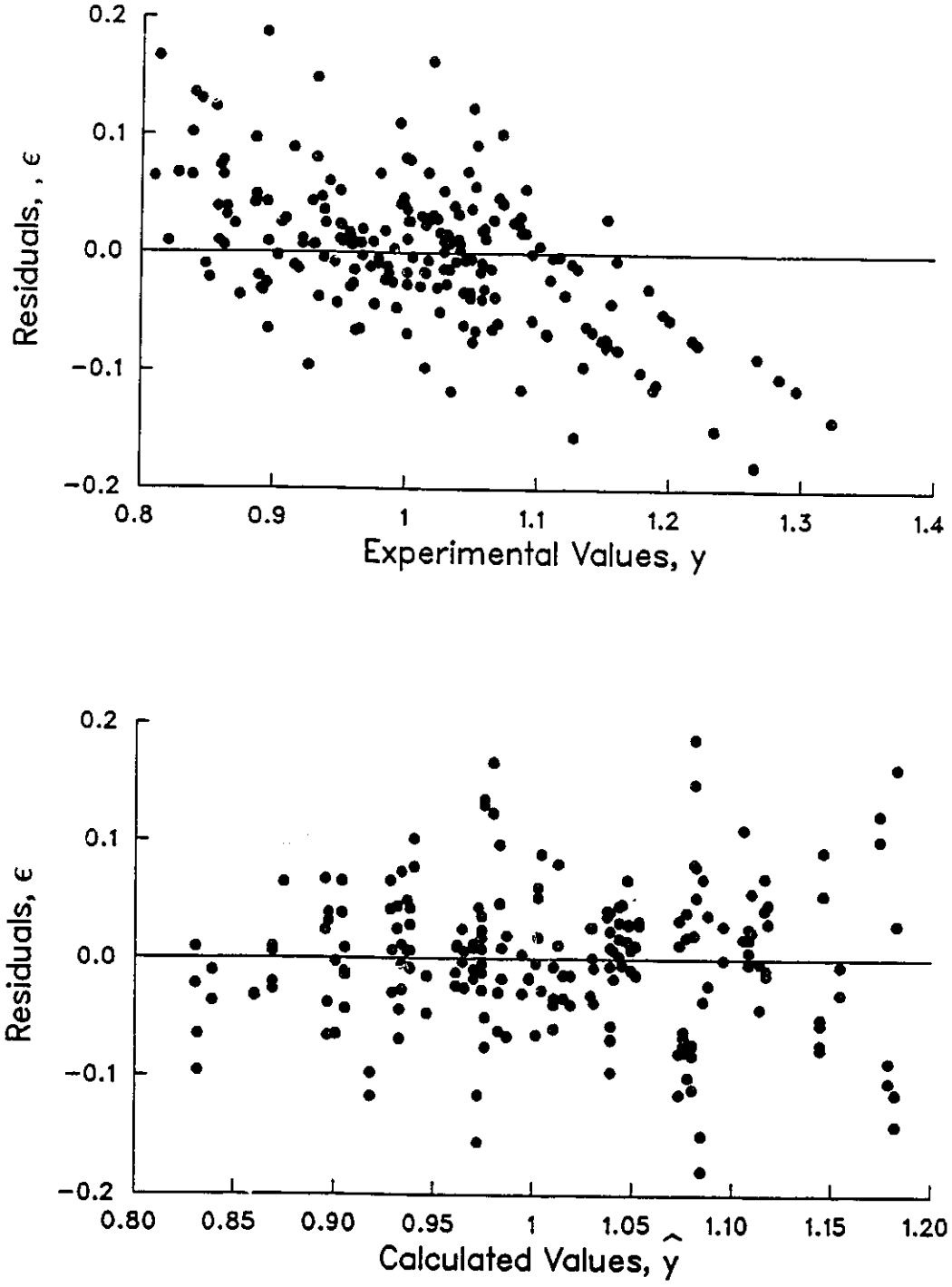

Figure A.31: Residual Plots for Deviations with Composition Dependent Physical Properties in the High Heat Transfer Regime

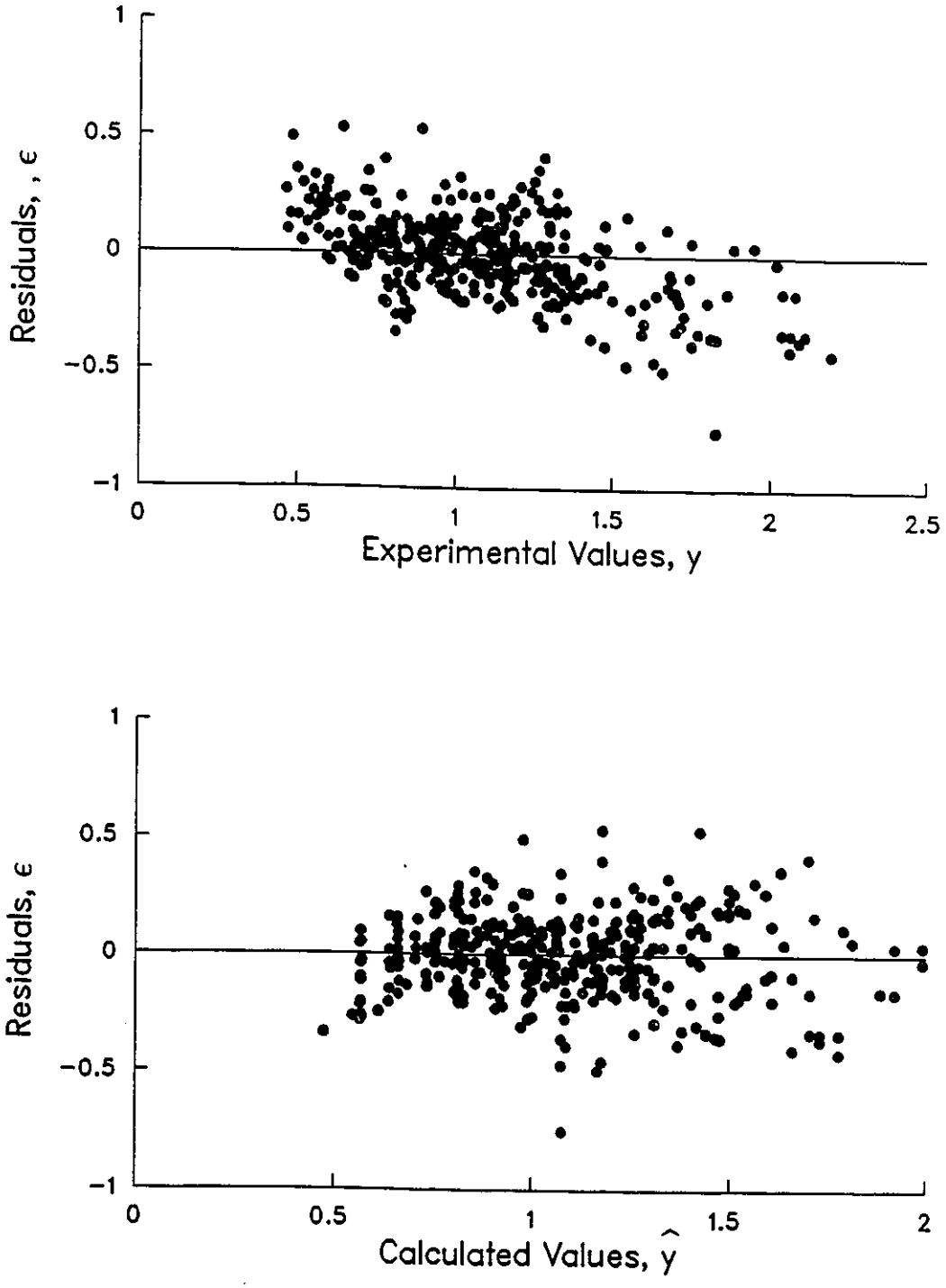

Figure A.32: Residual Plots for Deviations with Composition Dependent Physical Properties in the Medium Heat Transfer Regime

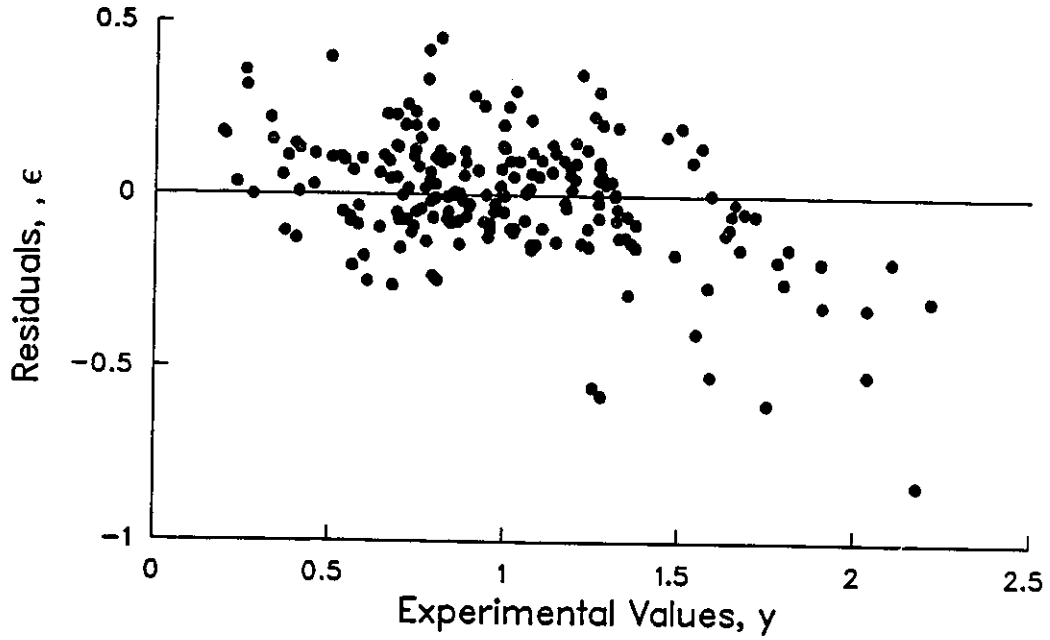

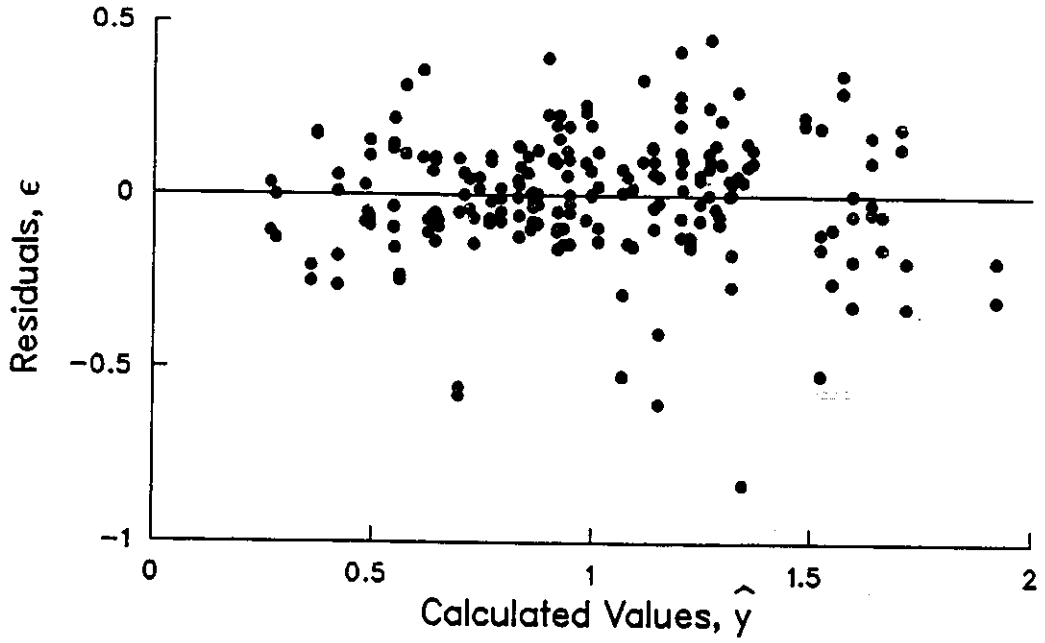

Figure A.33: Residual Plots for Deviations with Composition Dependent Physical Properties in the Low Heat Transfer Regime

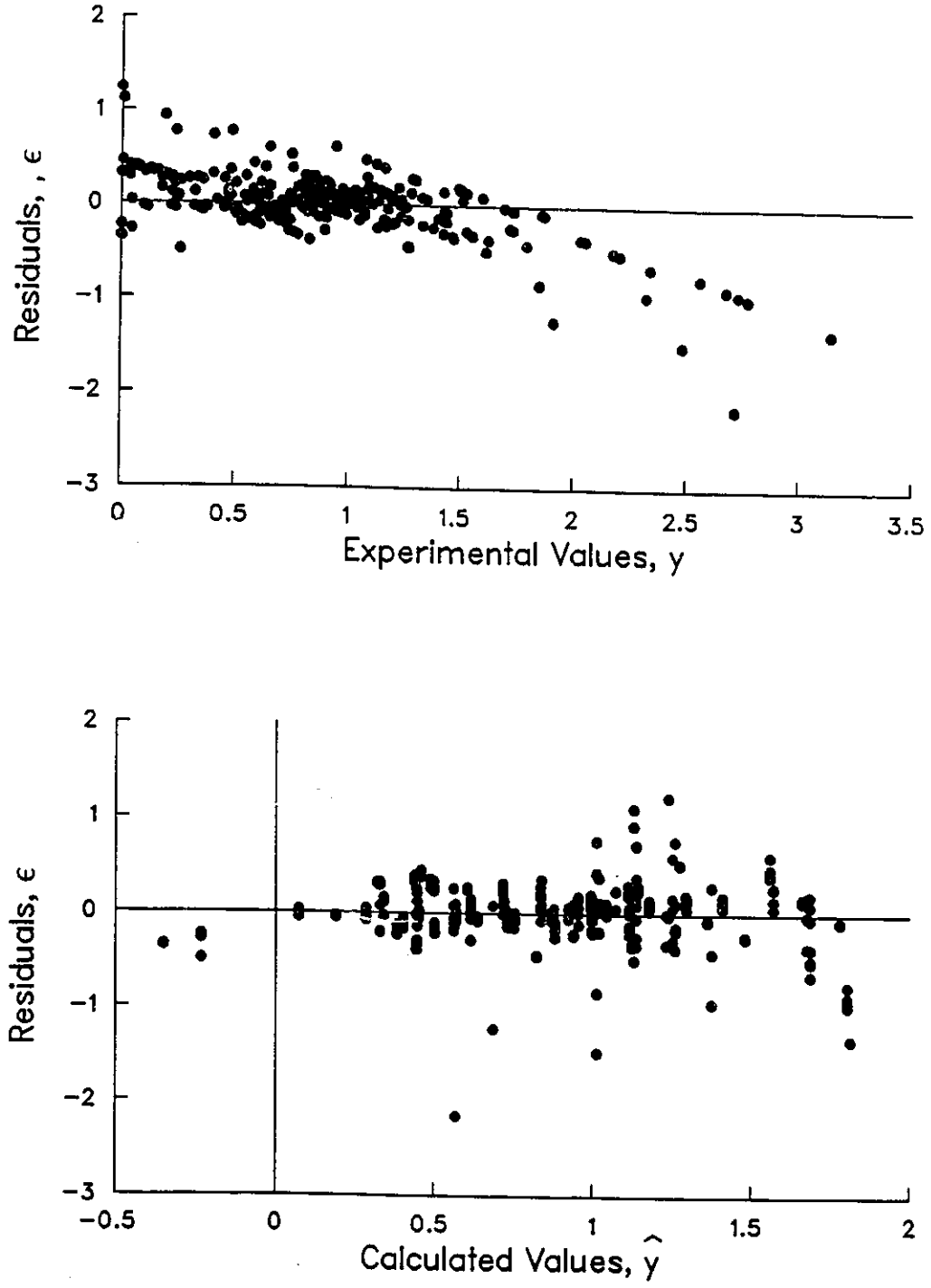

Figure A.34: Residual Plots for Deviations with Composition Dependent Physical Properties in an Adiabatic Reactor

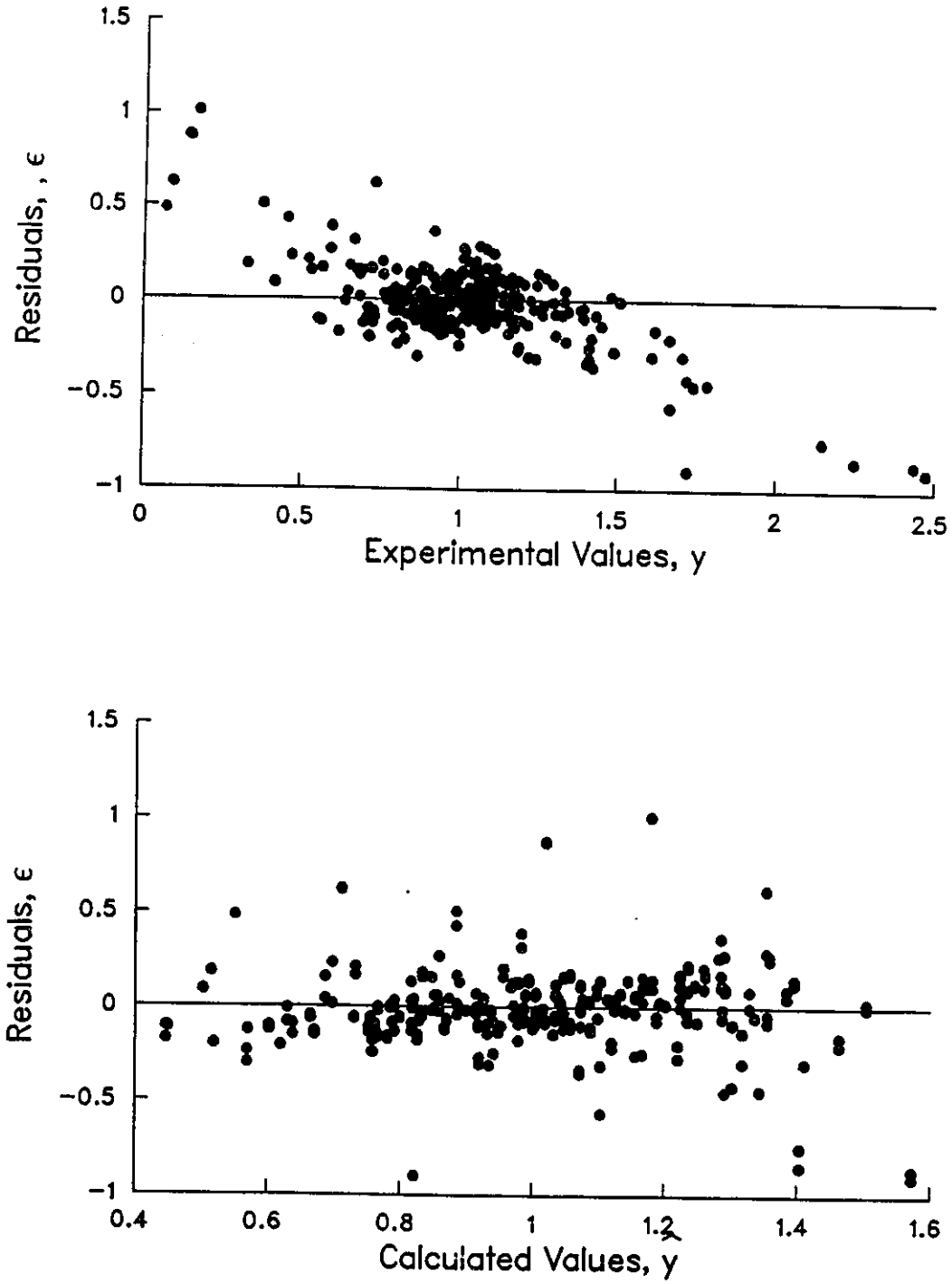

Figure A.35: Residual Plots for Deviations with Composition Dependent Physical Properties in an Adiabatic Reactor: Second Order Reaction

Appendix B

Experimental Details

B.1 Calculated Experimental Dimensionless Groups and Properties

Table B.1: Dimensionless Groups calculated from the Inlet Conditions

Run	α_x	α_T	β_T	γ
1	.0812	14.07	.177	23.51
2	.1199	21.85	.143	23.72
3	.0803	14.43	.247	23.61
4	.0780	14.86	.360	23.77
5	.0817	15.22	.265	23.71
6	.0853	15.81	.216	23.73
7	.0863	15.91	.243	23.68
8	.0918	16.75	.197	23.70
9	.0811	14.24	.239	23.50
10	.0903	16.17	.240	23.60
11	.0850	15.27	.194	23.63

Table B.2: Other Parameters Required by the Program

Run	z'	C_{B_o}/C_{A_o}	C_{C_o}/C_{A_o}	$T_o(K)$
1	.0578	4.31	1.99	292.45
2	.0370	5.11	2.33	289.95
3	.0554	3.74	0.83	291.25
4	.0626	1.72	0.50	289.25
5	.0468	2.98	0.85	290.05
6	.0599	3.79	1.34	289.75
7	.0539	3.31	0.89	290.35
8	.0512	4.55	1.36	290.15
9	.0617	2.68	0.93	292.65
10	.0537	3.90	0.73	291.35
11	.0569	3.85	1.67	291.05

B.2 The Aniline-Water Method

The aniline-water method has long been used to determine the amount of acetic anhydride in an aqueous solution [51]. It is a titration technique that utilizes the fact that the anhydride will react with aniline preferentially to water and also very rapidly.

The method was used as follows:

1. A sample was withdrawn and immediately added to an excess of aniline. The anhydride reacted with the aniline to form acetanilide in the following reaction.

$$(CH_3CO)_2 + C_6H_5NH_2 \rightarrow CH_3COOH + C_6H_5NHCOCH_3 \quad \text{(B.1)}$$

2. Simultaneously another sample was taken and allowed to continue the hydrolysis reaction

$$(CH_3CO)_2 + H_2O \rightarrow 2CH_3COOH \quad \text{(B.2)}$$

3. After sufficient time had passed to complete the hydrolysis reaction the two samples were titrated using a standard $NaOH$ solution. In the case of this study a solution of approximately 2M was employed. The differences in the titration values was used to The $NaOH$ solution was prepared daily and standardized using potassium acid phthalate. The caustic solution was also checked periodically to ensure that there was not an appreciable amount of CO_2 absorption occurring.

   The differences in the titration values were used to determine the concentration of anhydride as follows:

   (a) Let A be the number of moles of anhydride in the sample at time, t. Let x be the number of moles of acid present in the sample.

   (b) From Reaction B.1 the total amount of acid present after the reaction was;

$$A + x \quad \text{(B.3)}$$

   according to the stoichiometry.

(c) The amount of acid present in the sample allowed to hydrolyze completely was;

$$2A + x \tag{B.4}$$

again according to the stoichiometry.

(d) Subtracting B.3 from B.4 yielded A, the amount of anhydride in the system at time, t.

(e) Once A was known the amount of acid could be determined.

(f) The samples were weighed such that upon determining the acid and anhydride concentrations, the rest of the sample was assumed to be water.

Two samples for each reaction were taken from both the reactor inlet and outlet. The average composition of the system was then determined for the inlet and outlet. The quantity $\langle x \rangle$ was calculated by dividing $(C_A)_{outlet}$ by $(C_A)_{inlet}$. Where C_A represented the concentration of anhydride.

B.3 Reagent Specifications

Acetic Anhdride	
Manufacturer:	BDH
Grade:	Laboratory Reagent
Lots:	105886/2233S and 106500/23815
Minimum Assay:	98%
Non-volatile matter:	.01%
Chloride:	.005%
Sulphate:	.005%
Lead:	.002%

Aniline	
Manufacturer:	BDH
Grade:	Analar analytical reagent
Lot:	100761/4863
Minimum Assay:	99.5%
Water:	.2%
Non-volatile Matter:	.005%
Hydrocarbons:	Passes test
Nitrobenzene:	.0002%
Copper:	.00005%
Iron:	.0001%
Lead:	.00005%

B.4 Equipment List

Pump	
Manufacturer:	Milton Roy
Model:	Duplex D4 17 and Mo DO 117
Specifications:	Both sides positive displacement
	Rated at 1000 psi
	Maximum Flow Rates 1.5 and 5.0 cm^3/sec

(Note: Calibration of pumps indicated linear flow rate with respect to stroke percentage and also verified maximum flow rates.)

Temperature Indicator	
Manufacturer:	Thermo Electric
Model:	31641-00-113
Serial Number:	60087-1-1
Range:	$77K$ - $672K$

Thermocouples	
Manufacturer:	Thermo Electric
Model:	T116G-316-0-12-24-1A
Specifications:	1/16" 316 stainless steel sheath around ceramic insulated copper-constantan
	Type T calibration